arXiv:hep-ph/9907448v1 21 Jul 1999

Applications of Chiral Perturbation Theory in Reactions with Heavy Particles

Thesis by

Iain W. Stewart

In Partial Fulfillment of the Requirements
for the Degree of
Doctor of Philosophy

1891

California Institute of Technology
Pasadena, California

2008
(Submitted May 25, 1999)
CALT-68-2233

Acknowledgements

I would like to thank the people on the fourth floor of Lauritsen, S. Frautschi, D. Politzer, J. Preskill, J. Schwarz, M. Wise, M. Aganagic, M. Becker, K. Becker, O. Bergman, S. Cherkis, H. Davoudiasl, E. Gimon, W. Goldberger, M. Gremm, P. Horava, E. Keski-Vakkuri, P. Kraus, A. Kapustin, A. Leibovich, Z. Ligeti, D. Lowe, T. Mehen, S. Ouellette, C. Popescu, K. Rajagopal, K. Scaldeferri, H. Tuck, and E. Westphal for providing a friendly atmosphere in which to work. I am particularly grateful to my advisor Mark Wise and to people with whom I collaborated during my stay at Caltech: Martin Gremm, Mark Wise, Adam Leibovich, Zoltan Ligeti, Tom Mehen, and Sean Fleming. Special thanks go to my wife Susan and parents for their constant love and support. This work was supported in part by the Department of Energy under grant number DE-FG03-92-ER 40701.

Abstract

Effective field theory techniques are used to describe the interaction of heavy hadrons in a model independent way. Predictability is obtained by exploiting the symmetries of QCD. Heavy hadron chiral perturbation theory is reviewed and used to describe D^* decays. The phenomenologically important $D^* D\pi$ coupling is extracted from data working to first order in the chiral and heavy quark symmetry breaking parameters. A method is described for determining $|V_{ub}|$ from exclusive semileptonic B and D decays with 10% uncertainty. An effective field theory for two-nucleon systems is then discussed. The large S-wave scattering lengths necessitate expanding around a non-trivial fixed point. A detailed discussion of the interplay between renormalization and the power counting is given. In power counting pion interactions with nucleons it is useful to consider three classes of pion: potential, radiation, and soft. A power counting for massive radiation is developed. Finally, it is shown that the leading terms in the effective theory for nucleon-nucleon interactions are invariant under Wigner's SU(4) spin-isospin symmetry in the infinite scattering length limit.

Contents

Acknowledgements **ii**

Abstract **iii**

1 Introduction **1**

2 Theoretical Background **6**

2.1 Chiral symmetry and chiral perturbation theory 8

2.2 Dynamics with one heavy particle 12

2.2.1 The $D^{(*)}$ and $B^{(*)}$ and heavy quark symmetry 12

2.2.2 The heavy-vector meson chiral Lagrangian 14

2.3 Dynamics with two heavy particles 16

2.3.1 Two nucleon effective field theory 16

2.3.2 Power counting and ultraviolet fixed points 21

3 Extraction of the $D^*D\pi$ coupling from D^* decays **27**

3.1 $D_a^* \to D_a\ \pi$ decays 30

3.2 $D_a^* \to D_a\ \gamma$ decays 37

3.3 Extraction of the couplings g and β 41

3.4 Summary 48

4 V_{ub} from Exclusive Semileptonic B and D Decays **51**

4.1 Chiral perturbation theory for the form factor ratio 55

4.2 Long distance effects and extracting $S^{(B\to K^*)}$ 57

4.3 Nearer term prospects 61

5 NN Scattering **64**

5.1 Introduction 64

5.2 Power counting and renormalization schemes 70

5.2.1 The PDS scheme 75

5.2.2 The OS scheme 76

5.3 Theory with pions integrated out 79

5.4 Reproducing the pole in the amplitude 83

5.5 Loop integrals with a momentum cutoff regulator 85

5.6 Theory with nucleons and pions 87

5.6.1 PDS 91

5.6.2 OS 93

5.7 The coupling $D_2(\mu_R)$ 96

5.8 Schemes and amplitudes 98

5.9 Determining the range Λ_π 106

5.10 Summary 109

6 Radiation and Soft Pions **111**

6.1 Radiation pions 112

6.2 Soft pions 126

7 Wigner's SU(4) Symmetry from Effective Field Theory **133**

8 Predictions for the $^3S_1 -^3 D_1$ Mixing Parameter, ϵ_1 **141**

9 Conclusion **146**

Bibliography **149**

List of Figures

2.1 The leading order contribution to the NN scattering amplitude. . . . 22

2.2 Fixed point structure of the beta function for $C_0(\mu_R)$ in the PDS renormalization scheme. 26

3.1 D and D^* wavefunction renormalization graphs. The dashed line represents a pseudo-Goldstone boson. 34

3.2 Nonzero one-loop vertex corrections for the decays $D^{*0} \to D^0\pi^0$ and $D^{*+} \to D^+\pi^0$ (a,b,c) and the pseudo-Goldstone boson wave function renormalization graph (d). 35

3.3 Nonzero vertex corrections for the decay $D_s^* \to D_s\pi^0$ which involve π^0–η mixing. The cross denotes leading order mixing while the triangle denotes mixing at next to leading order. 36

3.4 Nonzero vertex corrections for the decays $D^* \to D\gamma$. 39

3.5 Solution contours in the g-β plane for the situation in row 5 of Table 3.1. The solid, dashed, and dotted lines correspond to solution lines for the D^{*0}, D^{*+}, and D_s^* decay rate ratios respectively. The stars correspond to the minimal χ^2 solutions and the shaded regions correspond to the 68% confidence level of experimental error in the fit. The hatched region is excluded by the experimental limit $\Gamma(D^{*+}) < 0.13\,\mathrm{MeV}$ [1]. . 44

3.6 Effect of the order m_q counterterms ($\tilde{\kappa}_1$, κ_5, $\tilde{\alpha}_1$, and α_5) on the solutions in Eq. (3.30). The counterterms are taken to be randomly distributed with $-1 < \tilde{\kappa}_1, \kappa_5 < 1$, $-2 < \alpha_1, \alpha_5 < 2$. For each set of counterterms g and β were determined at the new minimal χ^2. 5000 sets were generated near each of the two solutions. 46

4.1 Feynman diagram that gives the leading contribution to $R(1)-1$, where R is defined in Eq. (4.6). The dashed line is a π or an η. The black square indicates insertion of the weak current. 57

4.2 An estimate of long distance corrections to the $B \to K^*\ell\bar{\ell}$ rate using $d(y)$ defined in Eq. (4.16). The solid curve takes into account all six 1^{--} $c\,\bar{c}$ resonances according to Eq. (4.15), whereas the dashed curve is obtained including only the three lightest ones. 60

4.3 $\mathrm{d}\Gamma(B \to K^*\ell\,\bar{\ell})/\mathrm{d}y$ as given in Eq. (4.11). The solid curve takes into account all six 1^{--} $c\,\bar{c}$ resonances, the dashed curve includes only the three lightest ones, and the dotted curve is the perturbative result. . . 61

5.1 Renormalization conditions for $C_0(\mu_R)$ and $C_2(\mu_R)$ in the OS scheme. $i\,A^{(-1)}$ is the four point function with $C_0(\mu_R)$ and $\delta^n C_0(\mu_R)$ vertices, evaluated between incoming and outgoing ${}^1S_0$ or ${}^3S_1$ states. The amplitude $A^{(0)}$ contains graphs with one C_2 or one potential pion dressed with C_0 bubbles. 78

5.2 One and two loop counterterms for C_0 and C_2. The solid lines are nucleon propagators, and symmetry factors are shown explicitly. The generalization to higher loops is straightforward. 79

5.3 Zero, one, and two-loop graphs with C_0 and $\delta^n C_0$ vertices and potential pion exchange. The dashed lines denote potential pion propagators. . 88

5.4 The basic order Q graphs in the ${}^3S_1$ channel whose loop integrals do not factorize even for $m_\pi = 0$. 89

5.5 Fit to the phase shift data emphasizing the low momentum region. The solid line is the Nijmegen fit to the data [2], the long dashed line is the order $1/Q$ result, and the short dashed line is the order Q^0 result. 102

5.6 The effective field theory and Nijmegen Partial Wave analysis [2] values of $p\cot\delta$ are compared. The solid lines use $p\cot(\delta^{(0)}+\delta^{(1)})$, the dashed lines use Eq. (5.73) with the v_i from Ref. [3], and the dotted lines use the values of v_i from the low-energy theorems. 104

5.7 Error analysis for the phase shifts in the $^1S_0$ and $^3S_1$ channels. $\Delta\delta$ is the difference between the the effective field theory prediction and the Nijmegen partial wave analysis[2]. The long and short dashed lines use the $\mathcal{O}(Q^0)$ and $\mathcal{O}(Q)$ theoretical phase shifts respectively. 107

6.1 Leading order radiation pion graphs for NN scattering. The solid lines are nucleons, the dashed lines are pions and δM, δZ are the mass and field renormalization counterterms. The filled dot denotes the $C_0(\mu_R)$ bubble chain. There is a further field renormalization contribution that is calculated in text, but not shown. 115

6.2 Examples of order Q_r^4 radiation pion graphs for NN scattering. . . . 126

6.3 Examples of one-loop graphs which have soft pion contributions. Graphs a)-d) also have a radiation pion contribution, while in addition graph a) has a potential pion contribution. 128

7.1 Graphs contributing to $NN \rightarrow NN$ axion at leading order. The solid lines denote nucleons and the dashed lines are axions. 137

8.1 The two order Q^0 diagrams that contribute to ϵ_1 [4]. The solid lines are nucleons and the dashed lines are potential pions. 142

8.2 Order Q diagrams for ϵ_1. The filled circle is defined in Fig. 8.1, and the diamonds in c) denote insertions of the $^3S_1$ operators with $C_0^{(0)}$, C_2 or D_2 coefficients. 143

8.3 Predictions for the $^3S_1 - ^3D_1$ mixing parameter ϵ_1 in degrees. The solid line is the multi-energy Nijmegen partial wave analysis [5]. The long and short dashed lines are the LO and NLO predictions in the theory without pions [6]. The dotted line is the LO prediction in the theory with pions from Ref. [4]. The dash-dotted line is the NLO prediction in the theory with pions. The stars are data from Virginia Tech [7] and the open circles are Nijmegen single energy data [5] whose quoted errors are invisible on the scale shown. 144

List of Tables

3.1 Solutions for g and $\beta(\mathrm{GeV}^{-1})$ which minimize the χ^2 associated with a fit to the three ratios in Eq. (3.28). There are two solutions in the region of interest. 43

3.2 Predicted widths in keV for the D^* and B^* mesons. The experimental and counterterm ranges are determined by the extremal values of g and β in Eqs. (3.30) and (3.32). For $g = 0.265$ the D_s^* width is small due to a delicate cancellation in μ_3 as explained in the text. The uncertainty in the B^* widths is large due to unknown $1/m_{c,b}$ corrections. 48

5.1 ${}^1S_0$ and ${}^3S_1$ couplings in the PDS scheme. $C_0(\mu_R)$ (in fm^2), $C_2(\mu_R)$ (in fm^4), and $D_2(\mu_R)$ (in fm^4) are fit to the Nijmegen data at different values of μ_R. 101

5.2 ${}^1S_0$ and ${}^3S_1$ couplings in the OS scheme. $C_0(\mu_R)$ (in fm^2), $C_2(\mu_R)$ (in fm^4), and $D_2(\mu_R)$ (in fm^4) are fit to the Nijmegen data at different values of μ_R. 101

5.3 Values of γ, $B_0^{(2)}$, $1/a$, and r_0 (in MeV) obtained from our fits. Three values of μ_R are shown to emphasize that the value of the extracted parameters depends weakly on μ_R. 106

Chapter 1 Introduction

The minimal standard model is an appealing theory which describes the strong, weak, and electromagnetic interactions in terms of 19 input parameters. This renormalizable quantum field theory gives quite an accurate description of nature, as shown through precision tests of QED [8, 9], the Electro-Weak sector [10, 11], and to a lesser extent QCD [12, 13, 14]. These tests examine observables for which a perturbative treatment of the couplings is applicable. For QCD, this is a valid approach for high energy processes due to asymptotic freedom [15, 16]. However, at low energy or large distance the coupling becomes strong and the quarks and gluons are confined into the observed mesons and baryons. At these energies a non-perturbative approach, such as lattice gauge theory, is necessary. Since lattice calculations are still fairly crude, it is reasonable to ask if the non-perturbative nature of QCD can be handled in another model independent fashion. In certain situations the answer is yes, because the symmetries and dynamics of QCD provide other expansion parameters besides the strong coupling. Expanding about a symmetry limit provides us with a means for describing non-perturbative effects by a series of low energy parameters (matrix elements or effective couplings) which can be determined from experimental data. This approach is predicative since there are typically several observables that depend on a given parameter. In many ways this is complimentary to lattice QCD calculations, which can then concentrate on calculating these parameters.

Effective field theory is a useful tool for implementing these ideas. We begin by writing down fields for the relevant degrees of freedom, and constructing an effective Lagrangian. The Lagrangian includes all possible terms that transform correctly under the symmetries, and is typically non-renormalizable with an infinite number of terms. These terms are organized in importance by power counting in a small parameter. Identifying a small expansion parameter usually depends on having scales which are widely separated. The low energy Lagrangian is a sum of terms of the form $\mathcal{L} \sim C(\mu)\mathcal{O}(\mu)$. The coefficients $C(\mu)$ and operators $\mathcal{O}(\mu)$ encode short and long distance physics respectively, and the renormalization point μ separates the two regimes. This is essentially a Wilsonian operator product expansion [17]. The effective field theory approach is important for several reasons. In an effective field theory different scales in the problem are separated, so that one can concentrate on the most interesting physics at a particular scale. Furthermore, the power counting gives us a way to estimate the uncertainty in working at a given order. Finally, calculations are often much simpler in the effective theory. Depending on the situation, effective field theories are used in two somewhat distinct ways, either from the *top down* or from the *bottom up*.

In a top down approach the high energy theory is understood, but we find it useful or necessary to use a simpler theory at lower energies. Since the high energy theory is known, the $C(\mu)$ couplings can be calculated by performing a perturbative matching at the high scale. The theory is then run down to the desired low energy scale using the renormalization group. Solving the renormalization group equations for the running of the coefficients, we sum potentially large logarithms between the two scales. At the low scale, matrix elements of the operators are natural in size. A standard example is the calculation of QCD corrections to weak processes at momenta $p \ll 90\,\mathrm{GeV}$ (see Ref. [18] for a review). Here integrating out the W and Z leaves four-fermion interactions and an expansion in p^2/m_W^2. A second example is non-relativistic QED (NRQED) [19], which is used in describing the electromagnetic interactions of non-relativistic leptons. NRQED is especially useful in describing Coulombic bound states such as positronium, where a pure coupling constant expansion is inappropriate. Instead, a dual expansion is performed in the electromagnetic coupling and the velocity of the non-relativistic leptons. This effective theory is especially tractable since both the coefficients and matrix elements can be calculated. In QCD the quark masses are such that $\Lambda_{\rm QCD} \ll m_{c,b} = m_Q$. In the limit $m_Q \to \infty$, QCD exhibits additional flavor and spin symmetries, called heavy quark symmetry (HQS) [20, 21]. Heavy Quark Effective Theory (HQET) uses these symmetries and an expansion in $\Lambda_{\rm QCD}/m_Q$ to make predictions for processes involving hadrons containing one heavy quark. At high energies this effective field theory is matched onto QCD. In this case the matrix elements are typically not calculable, but are still related by HQS. For systems with two heavy quarks, the appropriate effective theory is called non-relativistic QCD (NRQCD) [22].

A second approach to effective field theory is from the bottom up. In this case the high energy theory is either unknown or not calculable. A well known example is SU(3) chiral perturbation theory, which exploits the pattern of dynamical chiral symmetry breaking observed in QCD. In the limit $m_q \to 0$, QCD has additional chiral symmetries, giving enhanced predictive power. Approximate chiral symmetry is a result of the small light quark masses, $m_q = m_{u,d,s} \ll \Lambda_{\rm QCD}$. Phenomenologically, this approach is valid for energy and momenta $\ll \Lambda$ where $\Lambda \sim 1.2\,{\rm GeV}$ is the chiral symmetry breaking scale. The relevant degrees of freedom here are the pions, kaons, and eta which are the pseudo-Goldstone bosons of the $SU(3)_L \times SU(3)_R \to SU(3)_V$ breaking. At low energy, matching onto QCD is not possible, so the couplings $C(\mu)$ in this low energy theory must be determined from experimental data. However, because our fields correspond to the asymptotically observed particles, the matrix elements are calculable. Processes involving a single heavy hadron can also be incorporated in this approach by combining the power counting in HQET and chiral perturbation theory into heavy hadron chiral perturbation theory [23, 24, 25, 26]. The effective field theory approach has also been extended to processes with two or more heavy particles, such as nucleon-nucleon interactions [27, 28, 29, 30, 31, 4, 32]. The latter theory will be discussed in some detail.

In the modern view, the standard model itself is a low energy effective theory. As an effective field theory it includes the usual Lagrangian as well as operators of dimension five and higher built out of standard model fields. Such operators are suppressed by powers of a scale Λ, where Λ is a measure of the energy at which the new physics becomes relevant. At energies $\sim \Lambda$ the standard model effective field theory must be replaced by something more fundamental. The fact that the standard model is renormalizable is significant since it implies that the scale Λ is not generated by standard model interactions, and is therefore, in principal, unconstrained. Large values of Λ then explain several of the beautiful features of the standard model, such as baryon and lepton number conservation and the absence of flavor changing neutral currents.

In this thesis several applications of effective field theory are discussed. The focus will be on using chiral perturbation theory for processes with heavy particles. Much of this material has now been published [33, 34, 35, 36, 37, 38], but unpublished material appears in sections 2.3.2 and chapter 8. Chapter 2 reviews the necessary theoretical tools and establishes notation. In chapter 3, D^* decays are investigated. The D^{*0}, D^{*+}, and D^*_s branching fractions are used to extract the $D^*D\pi$ and $D^*D\gamma$ couplings working to first order in the symmetry breaking parameters, m_q and $1/m_c$. Important effects due to the heavy meson mass splittings and unknown order m_q couplings are included. Predictions for the D^* and B^* widths are given. Chapter 4 discusses a method for determining $|V_{ub}|$ from exclusive B semileptonic decay. The calculable deviation from unity of the double ratio of form factors $(f^{(B\to\rho)}/f^{(B\to K^*)})/$ $(f^{(D\to\rho)}/f^{(D\to K^*)})$ is determined using chiral perturbation theory and is found to be small. It is shown that combining experimental data from $B \to \rho\,\ell\,\bar\nu_\ell$, $B \to K^*\ell\,\bar\ell$ and $D \to \rho\,\bar\ell\,\nu_\ell$ can lead to a model independent determination of $|V_{ub}|$ with an uncertainty from theory of about 10%.

In chapter 5 an effective field theory for nucleon-nucleon interactions is discussed. The power counting in this theory is controlled by the presence of a non-trivial ultraviolet fixed point or, equivalently, a bound state near threshold. Two renormalization schemes which have manifest power counting are discussed in detail, the Power Divergence Subtraction scheme (PDS)[31] and an off-shell momentum subtraction scheme which we call the OS scheme. Comparing results in these schemes gives us a method for determining if a statement about the behavior of the theory is scheme dependent. The effect of low energy poles on the organization of the perturbation series is explained. Comments are also made regarding the constraints that ultraviolet divergences make on the power counting. Theoretical and empirical arguments are then given about the range of this theory.

In chapter 6, radiative pion effects are discussed. It is shown that for the purpose of power counting the pion interactions should be divided into three classes: potential, radiation, and soft. A power counting is introduced for systematically including radiation pion effects. The leading order radiation pion graphs for nucleon-nucleon scattering are evaluated. The power counting for soft pions is also discussed.

Chapter 7 discusses the symmetries of the lowest order nucleon effective field theory. It is shown that in the limit where the NN ${}^1S_0$ and ${}^3S_1$ scattering lengths, $a^{({}^1S_0)}$ and $a^{({}^3S_1)}$, go to infinity, the leading terms in the effective field theory for strong NN interactions are invariant under Wigner's SU(4) spin-isospin symmetry. This explains why the leading effects of radiation pions on the S-wave NN scattering amplitudes vanish as $a^{({}^1S_0)}$ and $a^{({}^3S_1)}$ go to infinity. Implications of this symmetry are also discussed for $NN \rightarrow NN$ axion and $\gamma\, d \rightarrow n\, p$.

A brief discussion of predictions for the ${}^3S_1 - {}^3D_1$ mixing parameter ϵ_1 is given in chapter 8. Working in the theory with pions at NNLO gives a one parameter prediction for $\epsilon_1(p)$. The accuracy of this prediction is compared to results in the theory without pions.

Chapter 9 contains concluding remarks.

Chapter 2 Theoretical Background

This chapter introduces the chiral perturbation theory formalism for theories with zero, one or two heavy particles. We begin with the QCD Lagrangian,

$$\mathcal{L}_{\mathrm{QCD}} = -\frac{1}{4} G^A_{\mu\nu} G^{A\mu\nu} + \bar{q}(i\not{D} - m_q)q + \bar{Q}(i\not{D} - m_Q)Q + \text{g.f.} + \text{c.t.}\,, \tag{2.1}$$

where $G^A_{\mu\nu}$ is the field strength for the gluon field A^A_μ, $D^\mu = \partial^\mu + igA^A_\mu T^A$ is the color covariant derivative, g.f. stands for gauge-fixing and ghost terms, and c.t. stands for counterterms. The field q includes the three light quark fields u, d, s with masses $m_q = m_{u,d,s}$, while Q includes the three heavy quarks c, b, t with masses $m_Q = m_{c,b,t}$. The quark-gluon interaction is flavor blind so in QCD only the masses distinguish the quarks. The Lagrangian in Eq. (2.1) is renormalizable, Lorentz invariant, and is also invariant under parity, charge conjugation, and time reversal[1]. The quantum theory of QCD depends on another dynamically generated scale, $\Lambda_{\mathrm{QCD}} \sim 250\,\mathrm{MeV}$, where

$$\alpha_s(\mu) = \frac{g(\mu)^2}{4\pi} = \frac{4\pi}{\beta_0 \ln(\mu^2/\Lambda^2_{\mathrm{QCD}})} + \dots\,. \tag{2.2}$$

Here μ is the renormalization point, and $\beta_0 = 11N_c/3 - 2n_f/3$ is the lowest order coefficient of the QCD beta function for n_f flavors and $N_c(=3)$ colors. QCD is asymptotically free [15, 16], $\alpha_s(\mu \to \infty) \to 0$, making perturbation theory valid at large energies. At low energy $\alpha_s(\mu)$ becomes large, and the quarks and gluons become confined. Confinement is a non-perturbative phenomenum and a direct proof from QCD has not been given.

In the limit $m_q \to 0$ the light quark term in Eq. (2.1) is invariant under the chiral symmetry transformation

---

[1] Motivated by instanton configurations, a term of the form $\theta/(64\pi^2)\, G^A_{\mu\nu}\tilde{G}^{A\mu\nu}$ can be added to $\mathcal{L}_{\mathrm{QCD}}$. This term violates parity and time-reversal invariance. In nature θ is tiny, limits on the neutron electric dipole moment [39] give $\theta \lesssim 10^{-9}$. The occurrence of this unnaturally small value is known as the strong CP problem.

$$q_L \to L\, q_L\,, \qquad q_R \to R\, q_R\,, \qquad \text{where } L \in SU(3)_L \text{ and } R \in SU(3)_R\,. \tag{2.3}$$

Since $m_q \ll \Lambda_{\rm QCD}$ this is an approximate symmetry of QCD. This symmetry is spontaneously broken, $SU(3)_L \times SU(3)_R \to SU(3)_V$, by the vacuum expectation value

$$\langle 0|\, \bar{q}_R^a\, q_L^b\, |0\rangle = v\, \delta^{ab}\,, \qquad \text{where } v \sim \Lambda^3_{\rm QCD}\,. \tag{2.4}$$

The breaking of chiral symmetry is another non-perturbative effect, and occurs at a scale $\Lambda_\chi \sim 1\,{\rm GeV}$. The up and down quarks are much lighter than the strange quark, so $SU(2)_L \times SU(2)_R$ is an even better symmetry. In this case the unbroken $SU(2)_V$ subgroup is isospin. Chiral symmetry has important implications for the interaction of pions, kaons, and the eta with each other as well as with the heavier hadrons.

In the limit $m_Q \to \infty$ the heavy quark sector in Eq. (2.1) also exhibits additional symmetries. Consider a heavy quark with momentum $p = m_Q v$ which interacts with a gluon with momentum k, so that the final momentum of the heavy quark is $p' = m_Q v + k$. For $k \sim \Lambda_{\rm QCD}$ the velocity v of the heavy quark is conserved up to small terms of order $\Lambda_{\rm QCD}/m_Q$ and becomes a useful label for the heavy quark field. To construct a Lagrangian with a good $m_Q \to \infty$ limit we set

$$Q(x) = e^{-i m_Q v\cdot x} h_v(x) + \ldots\,, \tag{2.5}$$

where $\frac{1}{2}(1 + \not{v})\, h_v = h_v$ and $v^2 = 1$. Momenta of order $\Lambda_{\rm QCD}$ cannot produce a heavy anti-quark, so in the heavy quark sector the anti-particles can be integrated out as indicated by the ellipsis in Eq. (2.5). The number of heavy quarks is then conserved in the effective theory. After some straightforward algebra, the Lagrangian for heavy quarks with velocity v becomes[40]

$$\mathcal{L}_v = \bar{h}_v\, iv\cdot D\, h_v\, + \mathcal{O}(1/m_Q)\,. \tag{2.6}$$

At leading order this Lagrangian is independent of the spin and flavor of the heavy quark. For N heavy quarks we have an $SU(2N)_v$ symmetry, known as heavy quark symmetry[20, 21]. This symmetry has important implications for exclusive and inclusive decays involving hadrons with a heavy quark, such as the $D, D^*, B, B^*, \Lambda_b, \Lambda_c$, etc. For a more detailed discussion of the implications of heavy quark symmetry see Ref. [41].

The next few sections explain the implication of these symmetries in the formulation of the low energy effective field theories for interaction of the light pseudoscalars π, K, η, with heavy hadrons including the charm and bottom mesons D, D^*, B, B^*, vector mesons ρ, K^*, ϕ, ω, and nucleons $N = p, n$. For reviews of the formalism for zero and one heavy particle see [41, 42, 43]. For effective field theory with two heavy particles see [22, 4, 44, 45, 46, 29].

2.1 Chiral symmetry and chiral perturbation theory

In this section $SU(3)$ chiral perturbation theory is reviewed. The formalism for the more accurate but less predictive $SU(2)$ chiral perturbation theory follows in a similar manner. The eight pseudo-Goldstone bosons π^i that arise from the breaking $SU(3)_L \times SU(3)_R \to SU(3)_V$ are identified with the observed light pseudoscalar mesons, $\pi^\pm, \pi^0, K^\pm, K^0, \bar{K}^0$, and η. These will be encoded in the exponential representation

$$\Sigma = \xi^2 = \exp\left(\frac{2i\pi^i\lambda^i}{f}\right) , \tag{2.7}$$

where $\Sigma^\dagger\Sigma = \xi^\dagger\xi = 1$ and the λ^i are 3×3 matrices such that

$$\Pi = \pi^i\lambda^i = \begin{pmatrix} \pi^0/\sqrt{2} + \eta/\sqrt{6} & \pi^+ & K^+ \\ \pi^- & -\pi^0/\sqrt{2} + \eta/\sqrt{6} & K^0 \\ K^- & \bar{K}^0 & -2\eta/\sqrt{6} \end{pmatrix} . \tag{2.8}$$

In Eq. (2.7) $f \sim f_\pi = 131\,\mathrm{MeV}$, where f_π is the pion decay constant,

$$\langle 0|\, \bar{u}\, \gamma^\mu \gamma_5\, d\, |\pi^-(p)\rangle = -i f_\pi p^\mu\,. \tag{2.9}$$

Note that Π transforms as an octet under the unbroken $SU(3)_V$. The ξ field in Eq. (2.7) will become useful when we add heavy matter fields in section 2.2.1. Under an $SU(3)_L \times SU(3)_R$ transformation

$$\begin{aligned} \Sigma &\rightarrow L\Sigma R^\dagger\,, \\ \xi &\rightarrow L\xi U^\dagger = U\xi R^\dagger\,, \qquad \text{where } U = \sqrt{\Sigma} R^\dagger \sqrt{R\Sigma^\dagger L^\dagger}\,. \end{aligned} \tag{2.10}$$

The non-zero quark masses $m_q = \mathrm{diag}(m_u, m_d, m_s)$ break the chiral symmetry. To include m_q in our low energy Lagrangian we need to write a term that transforms in the same way as the light quark mass term in $\mathcal{L}_{\mathrm{QCD}}$ in Eq. (2.1). To do this we pretend that $m_q \rightarrow L m_q R^\dagger$ under a $SU(3)_L \times SU(3)_R$ transformation, and then form invariants with m_q. The Lagrangian with the fewest derivatives and powers of m_q that satisfies the symmetry constraints is

$$\mathcal{L}_\chi^{(2)} \;=\; \frac{f^2}{8} \mathrm{Tr}\, \partial^\mu \Sigma\, \partial_\mu \Sigma^\dagger + \frac{f^2 B_0}{4} \mathrm{Tr}(m_q \Sigma + m_q \Sigma^\dagger)\,, \tag{2.11}$$

where $f^2 B_0/4 = v$ in Eq. (2.4). Note that expanding the Σ fields in terms of Π gives a canonically normalized kinetic term for Π plus an infinite number of interaction terms with determined coefficients. In the interaction terms the pseudo-scalar fields are derivatively coupled, which is a general feature of chirally invariant couplings involving Π. This follows from the fact that constant goldstone boson fields π_i are a rotation of Σ, and correspond to an equivalent vacuum for the spontaneous symmetry breaking. When neglecting isospin violation it is conventional to define $\hat{m} = (m_u + m_d)/2$. In this case the meson masses are

$$m_\pi^2 = 2B_0 \hat{m}\,, \qquad m_K^2 = B_0(\hat{m} + m_s)\,, \qquad m_\eta^2 = \frac{2B_0}{3}(2m_s + \hat{m})\,. \tag{2.12}$$

Therefore, one power of a quark mass corresponds to two powers of a meson mass. This is the most general leading order behavior, given that these squared masses have a Taylor series in m_q, and that a constant term is forbidden by the fact that in the limit $m_q \to 0$ the mesons are massless Goldstone bosons.

The Lagrangian in Eq. (2.11) is not the most general one that is invariant under the desired symmetries. In particular, we can add an operator with dimension m that involves more derivatives or powers of m_q and a coupling of dimension $4-m$. After using the equations of motion[2] there are 10 linearly independent terms with dimension 0 coefficients[50, 51, 52]. For example,

$$\mathcal{L}_\chi^{(4)} = \alpha_1 \left[\mathrm{Tr}\, \partial^\mu \Sigma\, \partial_\mu \Sigma^\dagger \right]^2 + \ldots\,. \tag{2.13}$$

Couplings like α_1 encode information about the short distance physics which was integrated out, so their scale is set by short distance scales like the chiral symmetry breaking scale Λ_χ. If p is a typical momentum, then higher dimension operators are suppressed by powers of p^2/Λ_χ^2, m_π^2/Λ_χ^2, and m_K^2/Λ_χ^2. This is the chiral power counting. It is convenient to consider $p^2 \sim m_\pi^2 \sim m_K^2 \sim m_q$ and then call Eq. (2.11) the $\mathcal{O}(p^2)$ Lagrangian. Since the particles in $\mathcal{L}_\chi$ are relativistic, $E^2 = p^2 + m^2$, and counting powers of the energy and powers of momenta are equivalent here.

Along with higher dimension operators we must also consider loop corrections. These corrections are necessary, for instance, to restore unitarity to the S-matrix. The chiral power counting can also be applied to loop diagrams. Consider a graph with L loops, and n_m vertices that are $\mathcal{O}(p^m)$. Weinberg [53] proved that this diagram is $\mathcal{O}(p^D)$ where

$$D = 2(L+1) + \sum_m (m-2) n_m \ \geq\ 2\,. \tag{2.14}$$

Each additional loop adds two powers of p. Instead of remembering the formula in Eq. (2.14) we can power count an arbitrary loop graph by assigning appropriate powers of p to the vertices, a p^4 for each loop integration, and factors of $1/p^2$ for each propagator. If loop integrals are regulated in a mass independent way, then this counting is not affected by the divergences. It is convenient to use dimensional regularization where we continue the dimension of space time to $d = 4 - 2\epsilon$. At $\mathcal{O}(p^4)$ we must include the $\mathcal{O}(p^4)$ vertices at tree level and the $\mathcal{O}(p^2)$ vertices at one loop. Because of renormalization, these two contributions can not be separately specified in a unique manner. A logarithmic divergence in a loop integral induces a $1/\epsilon + \ln(\mu^2/p^2)$ dependence in the result. The $1/\epsilon$ pole is subtracted or absorbed into a $\mathcal{O}(p^4)$ coefficient, so in this sense these couplings act as counterterms. The fact that divergences are polynomial in the mass or momentum squared [54] along with the chiral power counting implies that divergences can always be absorbed in this way. This theory is said to be renormalizable order-by-order in the power counting. The finite (ϵ independent) part of the $\mathcal{O}(p^4)$ coupling depends on μ in such a way that it cancels the μ dependence from the loop. Changing μ changes the value of the loop with a compensating change in the value of the $\mathcal{O}(p^4)$ coupling. It might seem strange that the μ dependence exactly cancels (which is different than the situation in perturbative QCD where the μ dependence only cancels to a given order in $\alpha_s(\mu)$). However, this is nothing more than the statement that if we could calculate the full amplitude then it would be independent of the renormalization point. Therefore, expanding this amplitude in a power series in p^2 and m_q gives coefficients which are termwise independent of μ.

---

[2] Note that after using the equations of motion the remaining Lagrangian can also be used in loop calculations [47, 48, 49].

The μ dependence of the loops and counterterms gives us a method for determining the size of Λ_χ, called naive dimensional analysis [55]. Consider the graphs for $\pi\pi$ scattering at $\mathcal{O}(p^4)$. For simplicity we use SU(2) chiral perturbation theory. Setting constants of order unity equal to 1, the amplitude takes the form

$$\frac{p^2}{f^2} + \frac{p^4}{f^2(4\pi f)^2}\Big[\ln\Big(\frac{\mu^2}{p^2}\Big) + K\Big] + \frac{p^4}{f^4}\,\alpha_1(\mu) + \dots\,, \tag{2.15}$$

where K is a number and p is the center of mass momentum. At tree level the first term in Eq. (2.11) gives an order p^2 contribution which is the first term in Eq. (2.15).

The second term is the contribution from the loop graphs, and the factor of $1/(4\pi)^2$ arises from the loop integration. The third term in Eq. (2.15) is the contribution of the operator in Eq. (2.13). For simplicity, terms with m_π dependence have been left out as indicated by the ellipses. If the value of μ is changed then the second and third terms change in size while the sum stays the same. If there is no fine-tuning of parameters, then $\alpha_1(\mu)$ must be at least as large as the change to the loop graph induced by rescaling μ by an amount of order 1 [55]. Thus, naive dimensional analysis implies that the second and third terms will be roughly the same size, and $\alpha_1(\mu) \sim 1/(4\pi)^2 \sim 0.006$. It also implies that a natural size for the chiral symmetry breaking scale is[3] $\Lambda_\chi \sim 4\pi f$. When the $\mathcal{O}(p^4)$ couplings are fit to data, they are found to be $\sim 10^{-3}$ with $\mu = m_\rho$, which agrees with the dimensional analysis argument. The choice of μ reflects the fact that $\alpha_1(\mu)$ knows only about short distance scales (and in particular is independent of m_π) so

$$\alpha_1(\mu) \sim -\frac{1}{(4\pi)^2}\left[\ln\left(\frac{\mu^2}{\Lambda^2}\right) + K'\right], \tag{2.16}$$

where K' is a constant and $\Lambda \sim m_\rho$ or Λ_χ. To avoid large logarithms in the coefficients we pick $\mu \sim \Lambda$. This leaves potentially large logarithms in the matrix elements, $\ln(\mu^2/m_\pi^2)$. However since the theory is finite in the chiral limit $m_\pi \to 0$ these come multiplied by a power of m_π^2, so although they are enhanced relative to other $\mathcal{O}(m_\pi^2)$ terms, they are not particularly large.

2.2 Dynamics with one heavy particle

2.2.1 The $D^{(*)}$ and $B^{(*)}$ and heavy quark symmetry

The use of heavy quark symmetry[20, 21] results in a dramatic improvement in our understanding of the spectroscopy of hadrons containing a single heavy quark. In the limit where the heavy quark mass goes to infinity, $m_Q \to \infty$, such hadrons are classified not only by their total spin J, but also by the spin of their light degrees of freedom (i.e., light quarks and gluons), s_l [56]. In this limit, hadrons containing a single heavy quark come in degenerate doublets with total spin, $J_\pm = s_l \pm \frac{1}{2}$, coming from combining the spin of the light degrees of freedom with the spin of the heavy quark, $s_Q = \frac{1}{2}$. (An exception occurs for baryons with $s_l = 0$, where there is only a single state with $J = \frac{1}{2}$.) The ground state mesons with $Q\,\bar{q}$ flavor quantum numbers contain light degrees of freedom with spin-parity $s_l^{\pi_l} = \frac{1}{2}^-$, yielding a doublet containing a spin zero and spin one meson. For $Q = c$ these mesons are the D and D^*, while $Q = b$ gives the B and B^* mesons. The observed doublets are indeed very close in mass, $m_D = 1.867\,\mathrm{GeV}$, $m_{D^*} = 2.008\,\mathrm{GeV}$, $m_B = 5.279\,\mathrm{GeV}$, and $m_{B^*} = 5.325\,\mathrm{GeV}$[57]. The heavy quark flavor symmetry gives further relations between the $D^{(*)}$ and $B^{(*)}$.

---

[3] Some authors use $F_\pi = 93\,\mathrm{MeV}$ rather than $f \simeq 131\,\mathrm{MeV}$, so $\Lambda_\chi = 4\pi F_\pi$. Dimensional analysis can not tell the difference.

The heavy mesons come in triplets under the $SU(3)_V$ symmetry, (D^0, D^+, D_s), (D^{*0}, D^{*+}, D_s^*), (B^-, B^0, B_s), and (B^{*-}, B^{*0}, B_s^*). We will use the dimension 3/2 HQET velocity dependent fields $P_a^{(Q)}(v)$ and $P_a^{*(Q)\mu}(v)$ (a=1,2,3), where $P^{(c)}(v)$ destroys a D with velocity v, etc. It is convenient to include P_a and P_a^* in a 4×4 matrix

$$H_a^{(Q)} = \frac{1+\not{v}}{2}\left[P_a^{*(Q)\mu}\gamma_\mu - P_a^{(Q)}\gamma_5\right]. \tag{2.17}$$

$H_a^{(Q)}$ transforms linearly under both a heavy quark spin transformation $D(R)$, and under a heavy quark flavor transformation $U \in SU(2)$ [41],

$$H_a^{(Q)} \to D(R) H_a^{(Q)}, \qquad H_a^{(Q_i)} \to U_{ij} H_a^{(Q_j)}, \tag{2.18}$$

and satisfies $\not{v} H_a = H_a = -H_a \not{v}$. The conjugate field is defined as $\bar{H}_a = \gamma^0 H_a^\dagger \gamma^0$. It is also convenient to define vector and axial vector currents,

$$V^\mu = \frac{1}{2}(\xi^\dagger \partial^\mu \xi + \xi \partial^\mu \xi^\dagger), \qquad \text{and} \qquad A^\mu = \frac{i}{2}(\xi^\dagger \partial^\mu \xi - \xi \partial^\mu \xi^\dagger), \tag{2.19}$$

which contain an even and odd number of Π fields respectively. Under a $SU(3)_L \times$

$SU(3)_R$ transformation

$$H_a \to H_b U^\dagger_{ba}\,, \qquad V^\mu \to U V^\mu U^\dagger + i\, U \partial^\mu U^\dagger\,, \qquad \text{and} \qquad A^\mu \to U A^\mu U^\dagger\,. \tag{2.20}$$

The lowest order Lagrangian invariant under these symmetries is

$$\mathcal{L}_H^{(1)} \;=\; -\mathrm{Tr}\, \bar{H}_a i v\cdot D_{ba} H_b + g\, \mathrm{Tr}\, \bar{H}_a H_b \gamma_\mu \gamma_5 A^\mu_{ba}\,, \tag{2.21}$$

where the chiral covariant derivative is $D^\mu_{ab} = \delta_{ab}\,\partial^\mu - V^\mu_{ab}$. The H_a propagator derived from the kinetic term in Eq. (2.21) is often referred to as static, since in the rest frame $v = (1, \vec{0})$ the equations of motion give zero energy for an onshell particle. (Recall that analagous to Eq. (2.5), the v dependent fields already have a factor of m_H subtracted from their energy.) Like $\mathcal{L}_\chi$ in Eq. (2.11), $\mathcal{L}_H$ is organized by an expansion in derivatives and powers of m_q. $\mathcal{L}_H$ also involves an expansion in powers of $1/m_Q$, where terms at order $1/m_Q$ break heavy quark symmetry.

Since $D^\mu \sim A^\mu \sim p$ the Lagrangian in Eq. (2.21) is $\mathcal{O}(p)$. It contains one coupling g for $P^{(Q)*}P^{(Q)}\Pi$ and $P^{(Q)*}P^{(Q)*}\Pi$. This coupling will be discussed in greater detail in Chapter 3. The propagators for the heavy pseudo-scalar and vector mesons,

$$\frac{i\,\delta_{ab}}{2(v\cdot k + i\epsilon)}\,, \qquad \text{and} \qquad \frac{-i\,\delta_{ab}\,(g_{\mu\nu} - v_\mu v_\nu)}{2(v\cdot k + i\epsilon)}\,, \tag{2.22}$$

are $\mathcal{O}(1/p)$. When power counting graphs, the meson propagators give $1/p^2$ and the loop measure gives a p^4 as before. Because of the form of the heavy propagators and couplings, the power counting involves powers of p and m_π. Higher order corrections to the Lagrangian in Eq. (2.21) are discussed in chapter 3.

2.2.2 The heavy-vector meson chiral Lagrangian

In this section we extend the heavy matter formalism to the vector mesons, $\rho^\pm$, ρ^0, ϕ, ω, $K^{*\pm}$, K^{*0}, and $\bar{K}^{*0}$, following the presentation in Ref. [58]. One might ask if these mesons should be treated relativistically; the lightest has mass $m_\rho = 770\,\mathrm{MeV}$

which is starting to approach the low momentum regime of interest. However, if these particles are not treated as heavy then predictive power is lost. Unlike the pion, the vector mesons are not pseudo-Goldstone bosons, so they do not have to be derivatively coupled and their self-interactions are not constrained by chiral symmetry. When they are treated as heavy, the interaction terms in the Lagrangian can be expanded in derivatives giving an expansion in powers of p/m_ρ.

The vector meson fields are introduced as a 3×3 octet matrix and a singlet

$$\begin{aligned} \mathcal{O}_\mu &= \phi^i_\mu \lambda^i = \begin{pmatrix} \rho^0_\mu/\sqrt{2} + \phi^{(8)}_\mu/\sqrt{6} & \rho^+_\mu & K^{*+}_\mu \\ \rho^-_\mu & -\rho^0_\mu/\sqrt{2} + \phi^{(8)}_\mu/\sqrt{6} & K^{*0}_\mu \\ K^{*-}_\mu & \bar{K}^{*0}_\mu & -2\phi^{(8)}_\mu/\sqrt{6} \end{pmatrix} , \\ S_\mu &= \phi^{(0)}_\mu , \end{aligned} \tag{2.23}$$

where $v \cdot \mathcal{O} = v \cdot S = 0$. The dependence of these fields on the fixed four-velocity v has been suppressed. Under $SU(3)_L \times SU(3)_R$ the fields in Eq. (2.23) transform as

$$\mathcal{O}_\mu \to U \mathcal{O}_\mu U^\dagger , \qquad S_\mu \to S_\mu . \tag{2.24}$$

The $\mathcal{O}(p)$ Lagrangian is [58]

$$\begin{aligned} \mathcal{L}_V &= - S^\dagger_\mu \, iv \cdot \partial \, S^\mu - \mathrm{Tr} \mathcal{O}^\dagger_\mu \, iv \cdot D \, \mathcal{O}^\mu \qquad (2.25) \\ & \quad + i g_1 \, S^\dagger_\mu \, \mathrm{Tr}(\mathcal{O}_\nu A_\lambda) \, v_\sigma \epsilon^{\mu\nu\lambda\sigma} + h.c. + i g_2 \, \mathrm{Tr}(\{\mathcal{O}^\dagger_\mu, \mathcal{O}_\nu\} A_\lambda) \, v_\sigma \epsilon^{\mu\nu\lambda\sigma} , \end{aligned}$$

where the chiral covariant derivative is $D^\nu \mathcal{O}^\mu = \partial^\nu \mathcal{O}^\mu + [V^\nu, \mathcal{O}^\mu]$ and A^μ and V^μ are given in Eq. (2.19). The octet and singlet originally have masses μ_0 and μ_8. When the velocity dependent fields are constructed we rescale both $\mathcal{O}^\mu$ and S^μ by a common factor, $\sqrt{2\mu_8}\, e^{i\mu_8 v \cdot x}$. This leaves a term involving the mass difference, $\Delta\mu = \mu_0 - \mu_8 < 200\,\mathrm{MeV}$ which may be treated as order m_q. Corrections to Eq. (2.25) involving the quark mass matrix m_q induce mass differences between the vector mesons. The mass eigenstates of the $\phi^{(0)} - \phi^{(8)}$ mass matrix are

$$|\phi\rangle = \sin\theta\,|\phi^{(0)}\rangle - \cos\theta\,|\phi^{(8)}\rangle\,, \qquad |\omega\rangle = \cos\theta\,|\phi^{(0)}\rangle + \sin\theta\,|\phi^{(8)}\rangle\,, \tag{2.26}$$

where the $SU(3)_V$ prediction for the mixing angle is $\tan\theta \simeq \pm 0.76$.

Further predictive power can be obtained by considering the limit of large N_c [58]. In this limit $\Delta\mu = 0$, $\tan\theta = 1/\sqrt{2}$ and the octet and singlet mesons can be combined into a single *nonet* matrix

$$N_\mu \;=\; \mathcal{O}_\mu + \frac{\mathbb{I}}{\sqrt{3}} S_\mu = \begin{pmatrix} \rho^0_\mu/\sqrt{2} + \omega_\mu/\sqrt{2} & \rho^+_\mu & K^{*+}_\mu \\ \rho^-_\mu & -\rho^0_\mu/\sqrt{2} + \omega_\mu/\sqrt{2} & K^{*0}_\mu \\ K^{*-}_\mu & \bar{K}^{*0}_\mu & \phi_\mu \end{pmatrix}. \tag{2.27}$$

At leading order in N_c the Lagrangian in Eq. (2.25) becomes

$$\mathcal{L}_V \;=\; -\mathrm{Tr} N^\dagger_\mu\, iv\cdot D\, N^\mu + ig_2\, \mathrm{Tr}(\{N^\dagger_\mu, N_\nu\} A_\lambda)\, v_\sigma \epsilon^{\mu\nu\lambda\sigma}\,. \tag{2.28}$$

Chiral and heavy quark symmetries can be used to relate the form factors describing the semileptonic decays: $D \to K^*\,\bar{\ell}\,\nu_\ell$, $D \to \rho\,\bar{\ell}\,\nu_\ell$, $B \to K^*\ell\,\bar{\ell}$, and $B \to \rho\,\ell\,\bar{\nu}_\ell$. In chapter 4 the heavy vector meson formalism described in this section will be used to estimate symmetry breaking corrections to the heavy quark and chiral symmetry relations between these form factors.

2.3 Dynamics with two heavy particles

2.3.1 Two nucleon effective field theory

This section considers an effective field theory for two heavy particles. The application in chapter 5 involves nucleon-nucleon scattering, so the particles are taken to be nucleons. For processes with one nucleon a formalism similar to that in Section 2.2.1 may be used. For simplicity, pion-nucleon interactions will not be considered in this section, but will be considered in chapter 5. This simplification will allow us to emphasize the qualitatively new features of the two-nucleon theory. Without pions the effective field theory is a valid description of nucleon interactions for momenta $p \ll m_\pi$.

Below the scale m_π, the pion can be integrated out, leaving a theory of non-relativistic nucleons interacting via contact interactions. The nucleon field N is a doublet under isospin. The full Lagrangian in the two nucleon sector is given by:

$$\mathcal{L}_{NN} = N^\dagger \Big[i\partial_t + \overrightarrow{\nabla}^2/(2M) + \dots \Big] N - \sum_s \sum_{m=0}^{\infty} C_{2m}^{(s)} \mathcal{O}_{2m}^{(s)} + \dots\,, \tag{2.29}$$

where M is the nucleon mass, and the ellipsis refers to relativistic corrections. The transformation to non-relativistic fields is analogous to Eq. (2.5) where here it is convenient to choose $v = (1, \vec{0})$. In Eq. (2.29), $\mathcal{O}_{2m}^{(s)}$ is an operator with $2m$ spatial derivatives and four-nucleon fields. We will work in a basis in which these operators mediate transitions between ingoing and outgoing two-nucleon states of definite total angular momentum. The superscript s will give the angular momentum quantum numbers of these states in the standard spectroscopic notation, ${}^{2S+1}L_J$. States with $(-1)^{S+L}$ even are isospin triplets, while those with $(-1)^{S+L}$ odd are isosinglets. If we denote the incoming and outgoing orbital angular momentum by L and L', then any operator mediating a transition between these states must contain at least $L+L'$ derivatives. For states with $S = 0$, $|L - L'| = 0$, while for states with $S = 1$, $|L - L'| = 0$ or 2.

In this section only S-wave transitions ($L = L' = 0$) will be discussed. For $s = {}^1S_0$ or ${}^3S_1$ the first two terms in the series are

$$\begin{aligned} &\sum_{s,m} C_{2m}^{(s)} \mathcal{O}_{2m}^{(s)} \qquad (2.30)\\ &= C_0^{(s)} (N^T P_i^{(s)} N)^\dagger (N^T P_i^{(s)} N) - \frac{C_2^{(s)}}{8} \Big[(N^T P_i^{(s)} N)^\dagger (N^T P_i^{(s)} \overleftrightarrow{\nabla}^2 N) + h.c. \Big] + \dots\,, \end{aligned}$$

where the matrices $P_i^{(s)}$ project onto the correct spin and isospin states

$$P_i^{({}^1S_0)} = \frac{1}{\sqrt{8}}\,(i\sigma_2)\,(i\tau_2\tau_i)\,, \qquad P_i^{({}^3S_1)} = \frac{1}{\sqrt{8}}\,(i\sigma_2\sigma_i)\,(i\tau_2)\,. \tag{2.31}$$

The Galilean invariant derivative in Eq. (2.30) is $\overleftrightarrow{\nabla}^2 = \overleftarrow{\nabla}^2 - 2\overleftarrow{\nabla}\cdot\overrightarrow{\nabla} + \overrightarrow{\nabla}^2$, and the ellipsis denote contributions with more derivatives. The normalization in Eq. (2.30) implies that between S-wave states the Feynman rules are

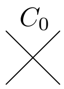

$$= \; -i\,C_0\,, \tag{2.32}$$

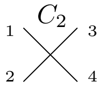

$$= \; -i\,\frac{C_2}{8}\,\left[(p_1-p_2)^2+(p_3-p_4)^2\right] = -i\,C_2\,p^2\,,$$

where the last equality is true when the nucleons are onshell in the center of mass frame, and p is the magnitude of the center of mass momentum.

In a theory with two heavy particles using a static propagator is problematic. The loop graph

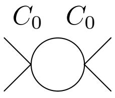

$$= (-iC_0)^2 \int \frac{d^dq}{(2\pi)^d}\,\frac{i}{q_0+i\epsilon}\,\frac{i}{-q_0+i\epsilon} \tag{2.33}$$

has a pinch-singularity in the q_0 integration at small q_0. This infrared singularity indicates that the static propagator is missing some essential physics. In theories with two heavy particles the kinetic energy term in Eq. (2.29) becomes a relevant operator of the same order as the ∂_t term. Including this term removes the singularity. The equations of motion for external nucleons are then $p_0 = p^2/(2M)$, so for power counting, the nucleon energies and momentum are not equal in size. In dimensional regularization the loop graph in Eq. (2.33) is finite

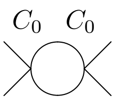

$$\begin{aligned} &= (-iC_0)^2 \int \frac{d^dq}{(2\pi)^d}\,\frac{i}{\frac{E}{2}+q_0-\frac{\vec{q}^{\,2}}{2M}+i\epsilon}\,\frac{i}{\frac{E}{2}-q_0-\frac{\vec{q}^{\,2}}{2M}+i\epsilon} \\ &= i\,(C_0)^2 \int \frac{d^{d-1}q}{(2\pi)^{d-1}}\,\frac{M}{\vec{q}^{\,2}-ME-i\epsilon} \end{aligned} \tag{2.34}$$

$$= \quad -i\,(C_0)^2\,\frac{M\sqrt{-ME-i\epsilon}}{4\pi} = -i\,(C_0)^2\left(\frac{-iMp}{4\pi}\right).$$

Here $E = p^2/M$ is the center of mass energy. In the second line of Eq. (2.34) the q_0 integration was done by contour integration. To power count this graph note that $q_0 \sim p^2/M$, $\vec{q} \sim p$, so $d^4q \sim p^5/M$, and each of the nucleon propagators gives an M/p^2. The graph is therefore order p in agreement with Eq. (2.34).

The result in Eq. (2.34) has a factor of the nucleon mass M in the numerator. Since each loop with two nucleons gives an additional factor of M one might worry that these large factors will spoil the power counting. The reason for using a non-relativistic expansion in the first place was that each graph scales as a definite power of M, so we can keep track of these large factors[4]. From Eq. (2.29) the coupling C_0 has dimension -2. To count factors of M we must determine how the C_{2m} couplings scale[5] with M. To determine this, rescale all energies, $q^0 \to \tilde{q}^0/M$, and time coordinates, $t \to M\tilde{t}$, so that dimensionful quantities have the same size (ie., are measured in units of p). If we demand that the action is independent of M, then since the measure $d^4x \sim M$, the Lagrange density $\mathcal{L} \sim 1/M$. The kinetic term determines that our nucleon fields scale as $N(x) \sim M^0$, so from Eq. (2.29) the coupling

$$C_{2m} \sim 1/M\,. \tag{2.35}$$

With the M scaling for the couplings determined, the scaling of any Feynman graph can be found. A nucleon propagator gives one power of M, and each momentum space loop integration gives a $1/M$. For bubble graphs that have insertions of the four-nucleon operators, $N_P = N_L + N_V - 1$, where N_P, N_L, N_V are the number of propagators, loops and vertices. Thus, when relativistic corrections are neglected any graph built out of the interactions in Eq. (2.29) scales as M^{-1} since $N_P - N_L - N_V = -1$. Therefore, the $2 \rightarrow 2$ scattering amplitude $\mathcal{A} \sim 1/M$. With the definition of $\mathcal{A}$ used here, this scaling gives a finite cross-section in the $M \rightarrow \infty$ limit which is physically sensible. (Note that there is a limit of QCD where $M \rightarrow \infty$ but $\Lambda_{\rm QCD}$ is finite, namely large N_c with $N_c \alpha_s$ held fixed [59].) Since all graphs scale the same way with M, M is irrelevant to the power counting. Relativistic corrections are included perturbatively[6], and are generally suppressed by p^2/M^2 relative to the leading contribution to an observable.

---

[4] What we are keeping track of is the *explicit* M dependence in the Lagrangian. The Lagrangian does have further implicit M dependence since M is a function of $\Lambda_{\rm QCD}$ and the scales that appear in the short distance couplings depend on $\Lambda_{\rm QCD}$ as well. For this reason saying we know the M dependence of an amplitude is not as strong a statement as saying we know the m_π dependence.

[5] If the contact interactions were replaced with Coulombic photon exchange then the interaction would not involve any powers of M. In this case the graph in Eq. (2.34) would scale as $\alpha^2 M/p^3 \sim \alpha^2/(p^2 v)$ where $\alpha = e^2/4\pi$ is the fine structure constant. This is a factor of α/v times a single photon exchange. For a Coulombic bound state $\alpha/v \sim 1$. Summing the most singular α/v terms is equivalent to solving the Schroedinger equation in a Coulomb potential.

Applying dimensional analysis to the short distance coupling constants now gives

$$C_0 \sim \frac{1}{M\Lambda}\,, \qquad C_2 \sim \frac{1}{M\Lambda^3}\,, \qquad C_{2m} \sim \frac{1}{M\Lambda^{2m+1}}\,, \tag{2.36}$$

where Λ denotes the scale of short distance physics that was not included explicitly (and we are assuming $\Lambda < M$). Treating the C_{2m} couplings perturbatively gives an expansion in p/Λ. In the current case we expect that $\Lambda \sim m_\pi$.

In nature, however, the dimensional analysis in Eq. (2.36) fails. This is because the nucleon-nucleon system is fine tuned to have bound states near threshold[27, 60, 61]. In the ${}^3S_1$ channel this bound state is the deuteron with binding energy $B = 2.2245 \pm 0.0002\,\mathrm{MeV}$. This energy corresponds to the momentum $\gamma = \sqrt{MB} = 45.7\,\mathrm{MeV} \ll \Lambda_{\rm QCD}$. This bound state gives a pole in the two-to-two scattering amplitude which can not be reproduced perturbatively and therefore limits the range of the momentum expansion to $p < \gamma$. In the ${}^1S_0$ channel the situation is even worse. In this case there is a pseudo-bound state sitting $8\,\mathrm{MeV}$ above threshold which limits the momentum expansion to $p < 8\,\mathrm{MeV}$. These bound states are related to the occurrence of unnaturally large scattering lengths. Recall that low energy scattering can be described by an effective range expansion

$$p \cot \delta^{(s)} = -\frac{1}{a^{(s)}} + \frac{1}{2}\, r_0^{(s)}\, p^2 + \dots\,, \tag{2.37}$$

where $\delta^{(s)}$ is the phase shift, $a^{(s)}$ is the scattering length and $r_0^{(s)}$ is the effective range.

In quantum mechanics, with a well-behaved potential, it can be shown that $r_0^{(s)}$ is of order the range of the interaction, $r_0 \sim 1/\Lambda$, but $a^{(s)}$ can differ from Λ by orders of magnitude[62]. From the formula for the amplitudes[6]

$$\mathcal{A}^{(s)} = \frac{4\pi}{M} \frac{1}{p \cot \delta^{(s)} - ip}\,, \tag{2.38}$$

it is straightforward to show that large negative or positive scattering lengths correspond to bound states just above or below threshold. Experimentally[63],

$$a^{({}^1S_0)} \;=\; -23.714 \pm 0.013\,\mathrm{fm}\,, \qquad \text{and} \qquad a^{({}^3S_1)} = 5.425 \pm 0.001\,\mathrm{fm}, \tag{2.39}$$

or $1/a^{({}^1S_0)} = -8.3\,\mathrm{MeV}$ and $1/a^{({}^3S_1)} = 36\,\mathrm{MeV}$. These values of $1/a$ are small relative to m_π and Λ_{QCD}.

If the scale for the bound states or scattering lengths were set by Λ then the scaling in Eq. (2.36) would be correct. The next section will discuss how the C_{2m} coefficients scale for a theory with large scattering lengths. This power counting was worked out by Kaplan, Savage, and Wise [31, 4] (KSW).

2.3.2 Power counting and ultraviolet fixed points

In this section we will examine how unnaturally large scattering lengths affect the importance of four-nucleon operators. We also explain how linear ultraviolet divergences play a role in determining the KSW power counting, and why it is useful to recast this in the framework of the renormalization group.

Treating the effective range term and higher powers of p^2 in Eq. (2.37) as perturbations, the amplitude is

$$\mathcal{A}^{(s)} = -\frac{4\pi}{M} \frac{1}{1/a^{(s)} + ip}\,, \tag{2.40}$$

---

[6] Strictly speaking Eq. (2.38) only holds in the ${}^1S_0$ channel. The ${}^3S_1$ channel is more complicated because of ${}^3S_1 - {}^3D_1$ mixing, but this mixing is a small effect which we will ignore for the time being, but discuss it in Chapter 8.

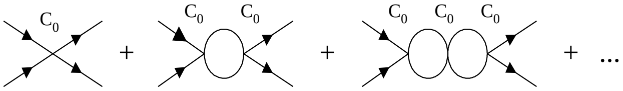

Figure 2.1: The leading order contribution to the NN scattering amplitude.

and has a good $a \to \infty$ limit. The pole at $p = i/a^{({}^3S_1)}$ corresponds to the deuteron bound state. The amplitude in Eq. (2.40) is reproduced in the effective field theory by summing the loop graphs in Fig. 2.1 using the result in Eq. (2.34)

$$i\mathcal{A} = -i\,\bar{C}_0 \sum_{m=0}^{\infty} \left(\frac{-ipM\bar{C}_0}{4\pi}\right)^m = \frac{-i\,\bar{C}_0}{1 + \frac{ipM}{4\pi}\,\bar{C}_0}\,. \tag{2.41}$$

Matching onto the effective range expansion then gives the values

$$\bar{C}_0{}^{(s)} = \frac{4\pi a^{(s)}}{M}\,. \tag{2.42}$$

Thus, the C_0 coupling must be fine tuned to a large value to reproduce the observed scattering length[28]. This result depends on our definition for the renormalized coupling constant C_0, or in other words our choice of renormalization scheme (which is distinct from choosing a regularization method). The bars in Eqs. (2.41) and (2.42) indicate that only divergent terms have been subtracted, which is the Minimal Subtraction (MS) scheme. The sum in Eq. (2.41) only converges for $p < 1/a$. Each loop graph in the sum grows with p, and the radius of convergence is $1/a$. For $p > 1/a$ we analytically continue and use the result on the right hand side of Eq. (2.41).

Looking back at Eq. (2.34), this one-loop graph is linearly divergent with $d = 4$, however in dimensional regularization this power divergence is not present. If we had calculated this loop graph with a finite momentum cutoff L then we would have

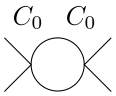

$$= i\,(C_0)^2 \int_0^L \frac{d^3q}{(2\pi)^3}\frac{M}{\vec{q}^{\,2} - p^2 - i\epsilon} = \frac{i\,M(C_0)^2}{4\pi}\left(ip + \frac{2L}{\pi} + \ldots\right), \tag{2.43}$$

where the ellipses denote terms that vanish as $L \to \infty$. Defining a counterterm to cancel the term proportional to L, and taking $L \to \infty$ gives back the result in Eq. (2.34). Note that the limit $p \to \infty$ and the integral over q do not commute because the integral is divergent. The growth of Eq. (2.43) with p is tied to this linear ultraviolet divergence. It is useful to use our freedom in defining the renormalization scheme to keep track of this. In the power divergence subtraction scheme (PDS)[31] additional finite subtractions are made in one-to-one correspondence with the linear divergences. In this scheme the coupling constants depend on the renormalization point μ_R and the value of the loop in Eq. (2.43) becomes[7]

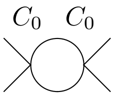

$$= \frac{i\,M}{4\pi}\,[C_0(\mu_R)]^2\left(ip + \mu_R\right). \tag{2.44}$$

In fact, the same result is obtained in a more physical scheme where the renormalized coupling is defined to be the value of the four point function evaluated at $p = i\mu_R$ [27, 64, 35, 36]. These renormalization schemes will be discussed in greater detail in Chapter 5.

In PDS, the renormalized coupling is [31, 4]

$$C_0^{(s)}(\mu_R) = -\frac{4\pi}{M}\frac{1}{\mu_R - 1/a^{(s)}}\,. \tag{2.45}$$

In this scheme the fine tuning as $a \to \infty$, is that $C_0(\mu_R)$ gets closer to its $\mu_R \to \infty$ value. $C_0(\mu_R)$ has the beta function

$$\beta_0 = \mu_R\frac{\partial}{\partial\mu_R}C_0(\mu_R) = \frac{M\mu_R}{4\pi}\,C_0(\mu_R)^2\,. \tag{2.46}$$

The renormalization group scaling gives us information about the behavior of the theory at the scale μ_R. For $\mu_R \sim p \ll 1/a$, $C_0(\mu_R)$ behaves like a constant and $p\,C_0(\mu_R)$ can be treated perturbatively. For $\mu_R \sim p > 1/a$, $p\,C_0(\mu_R) \sim 1$ and the sum in Eq. (2.41) must be done. The factors of μ_R make each term in the sum roughly the same size which is good from the point of view of power counting. For $\mu_R \sim p \gg 1/a$ the summation of C_0 bubble graphs is always necessary and should be considered to be infrared physics that has been built into the theory. In Ref. [65] it was shown that the scaling in Eq. (2.45) is also reproduced with a Wilsonian renormalization group approach.

---

[7] The notation μ_R is used for the renormalization point in this section to agree with the notation used in chapter 5.

The significance of the beta function in Eq. (2.46) is shown more clearly in Fig. 2.2[8]. To make the beta function dimensionless it has been rescaled by $M\Lambda/(4\pi)$,

$$\hat{\beta}_0 \;=\; \frac{M\Lambda}{4\pi}\,\beta_0 = a\Lambda\,\frac{a\,\mu_R}{(1-a\,\mu_R)^2}\,. \qquad (2.47)$$

The prefactor $a\Lambda$ can be safely ignored. The important dependence is in $a\,\mu_R$ since this factor measures the scale of interest relative to the scattering length. To study values of $a\,\mu_R$ from $-\infty$ to ∞, a variable x is defined to map this range onto a compact interval,

$$a\,\mu_R \;=\; \tan\left(\frac{\pi\,x}{2}\right). \qquad (2.48)$$

The dependence of $\hat{\beta}(C_0)$ on x is plotted in Fig. 2.2. Consider fixing the value of $\mu_R > 0$ and varying the value of a. The points $a = -\infty, 0,$ and ∞ are fixed points of the beta function. Classically this makes sense since the scattering length is a measure of the interaction size. For $a \simeq 0$ or $\pm\infty$ the size is so small or big that the interaction looks the same at all scales. In fact $a = 0$ is a trivial non-interacting fixed point, whereas $a = \pm\infty$ are non-trivial interacting fixed points where the theory is scale invariant at lowest order. Another feature in Fig. 2.2 is that $\beta \to \infty$ for $\mu_R = 1/a > 0$. This corresponds to the deuteron bound state. Performing perturbation theory about $a = 0$ we can never describe this bound state, so we are limited to describing the region $\mu_R < 1/a$. If perturbation theory is performed near $a = \infty$, then the deuteron is a physical state in the spectrum of the theory. If we are interested in physics at $\mu_R \simeq m_\pi$ then the observed ${}^1S_0$ and ${}^3S_1$ scattering lengths place us at the location of the stars in Fig. 2.2. Looking at the distance along the x axis we are much closer to the $a = \pm\infty$ fixed points than to $a = 0$.

---

[8] This figure was inspired by a similar plot shown by David B. Kaplan in a physics colloquium.

For $p \gg 1/a$ powers $Q \sim p \sim \mu_R$ are counted instead of just powers of momenta. The graphs in Fig. (2.1) are leading order and all scale as $1/Q$. In the PDS renormalization scheme this power counting is manifest. By solving the beta functions for the coefficients of operators with more derivatives it can be shown that [4]

$$C_{2m}(\mu_R)\, p^{2m} \sim \frac{4\pi}{M}\frac{p^{2m}}{\Lambda^m \mu_R^{m+1}} \sim \frac{Q^{(m-1)}}{M\Lambda^m}\,, \tag{2.49}$$

for $p \sim \mu_R \gg 1/a$. Since insertions of these operators scale with non-negative powers of Q, they may be treated perturbatively. This renormalization group scaling is also important in determining the power counting of operators that involve four nucleon fields and fields like the photon[32, 66] and pion. Note that since the deuteron corresponds to the pole in our scattering amplitude, deuteron properties can be systematically calculated in this field theory[32].

When pion interactions are included they enter at order Q^0, which is one higher order than insertions of C_0. Therefore, the discussion in this section is also relevant to the leading order theory with pions. In the theory with pions the physics encoded in the scale Λ in Eq. (2.2) changes. However, the power counting for the C_{2m} coefficients remains the same because pion effects are subleading corrections to the running of these operators. Pion interactions in the two-nucleon theory will be discussed in more detail in chapter 5.

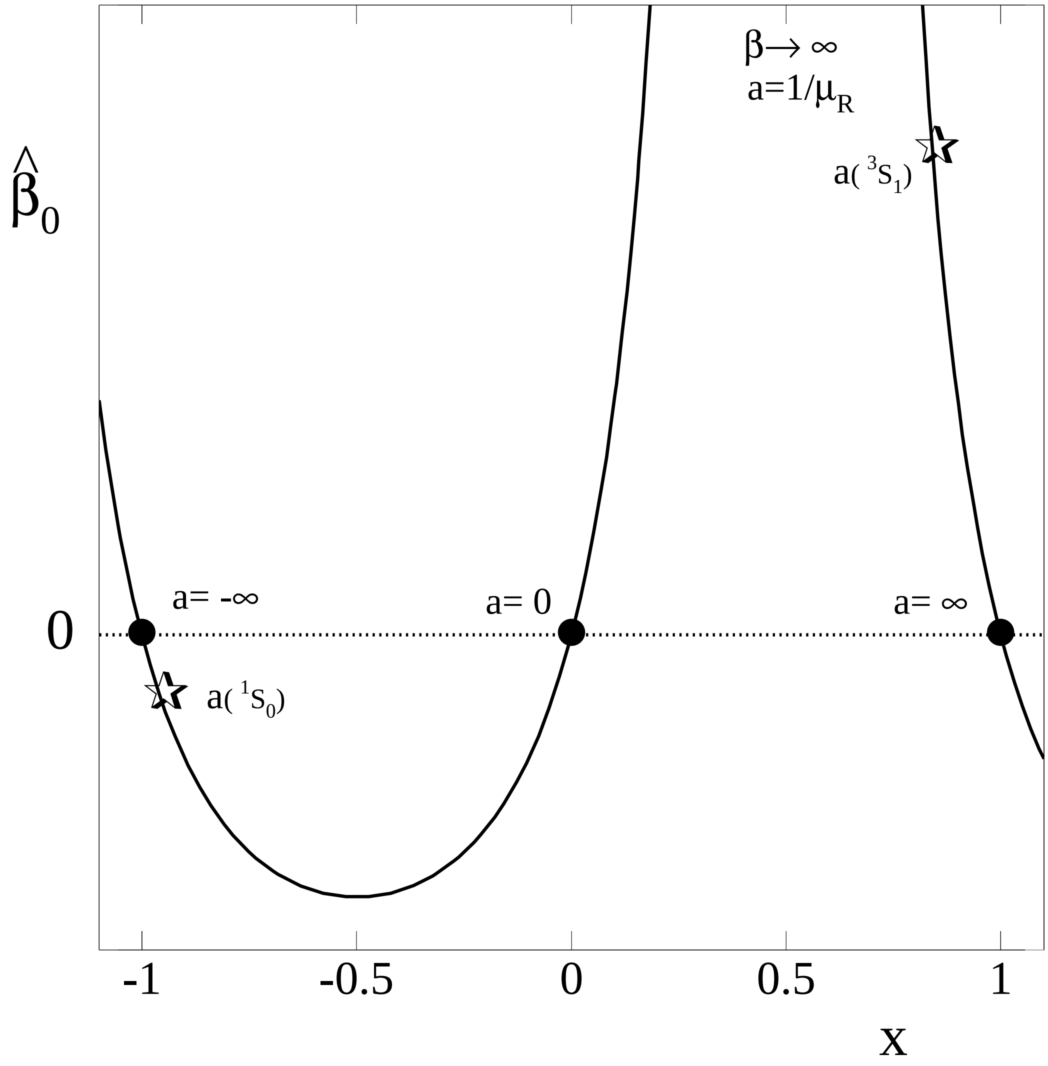

Figure 2.2: Fixed point structure of the beta function for $C_0(\mu_R)$ in the PDS renormalization scheme.

Chapter 3 Extraction of the $D^*D\pi$ coupling from D^* decays

Combining chiral perturbation theory with heavy quark effective theory (HQET) gives a good description of the low energy strong interactions between the pseudo-Goldstone bosons and mesons containing a single heavy quark. In this chapter we extend the formalism in Chapter 2 to describe D^* and B^* decays at subleading order. Due to heavy quark symmetry there is one coupling, g, for $D^*D\pi$, $D^*D^*\pi$, $B^*B\pi$, and $B^*B^*\pi$, and one coupling, β, for $D^*D\gamma$, $D^*D^*\gamma$, $B^*B\gamma$, and $B^*B^*\gamma$ at leading order[1]. The value of the coupling g is important, since it appears in the expressions for many measurable quantities at low energy. These include the rate $B \to D^{(*)}\pi\ell\bar{\nu}_\ell$ [67, 68, 69, 70, 71], form factors for weak transitions between heavy and light pseudoscalars [23, 24, 25, 72, 73, 74, 75, 76, 77], decay constants for the heavy mesons [78, 79, 80, 81, 82], weak transitions to vector mesons [83], form factors for $B \to D^{(*)}\ell\bar{\nu}_\ell$ [84, 85, 86], and heavy meson mass splittings [87, 88, 89] (for a review see [90]). However, the value of g has remained somewhat elusive, with values in the literature ranging from ~ 0.2 to 1.0. Recently, a CLEO measurement [91] of $D^{*+} \to D^+\gamma$ brought the experimental uncertainties down to a level where a model independent extraction of g is possible from D^* decays.

As a consequence of HQS, the mass splitting between D^* and D mesons is small (of order $\Lambda_{\rm QCD}^2/m_c$), leaving only a small amount of phase space for D^* decays. In the dominant modes, $D^* \to D\pi$, and $D^* \to D\gamma$, the outgoing pion and photon are soft, making the chiral expansion a valid framework. The branching ratios for D^{*+} decay are $D^0\,\pi^+$ (67.6%), $D^+\,\pi^0$ (30.7%) and $D^+\,\gamma$ (1.7%) [91]. A D^{*0} can only decay into $D^0\,\pi^0$ (61.9%) and $D^0\gamma$ (38.1%) [57] since there is not enough phase space for

---

[1] Where it is meaningful we use π to denote any member of the pseudo-Goldstone boson SU(3) octet, and D^* and D for any member of the triplets (D^{*0}, D^{*+}, D_s^*) and (D^0, D^+, D_s) with a similar notation for B^* and B.

$D^+\,\pi^-$. The D_s^* decays predominantly to $D_s\,\gamma$ (94.2%) with a small amount going into the isospin violating mode $D_s\,\pi^0$ (5.8%) [57]. Since a measurement of the widths of the D^* mesons has not yet been made, it is only possible to compare the ratios of branching fractions with theoretical predictions. The ratio

$$R_\pi^+ = \mathcal{B}(D^{*+} \to D^0\pi^+)/\mathcal{B}(D^{*+} \to D^+\pi^0) \tag{3.1}$$

is fixed by isospin to be $R_\pi^+ = 2|\vec{k}_{\pi^+}|^3/|\vec{k}_{\pi^0}|^3 = 2.199 \pm 0.064$ [91] (where $\vec{k}_{\pi^{+,0}}$ are three momenta for the outgoing pions in the D^* rest frame). This constraint is often used in experimental extractions of the branching ratios to reduce systematic errors.

It is interesting to note that the quark model predictions[92, 93] for D^{*0} and D^{*+} decays agree qualitatively with the data. One can understand, for instance, why the branching ratio $\mathcal{B}(D^{*+} \to D^+\gamma)$ is small compared to $\mathcal{B}(D^{*0} \to D^0\gamma)$. In the quark model the photon couples to the meson with a strength proportional to the sum of the magnetic moments of the two quarks, $\mu_2 = 2/(3\,m_c) - 1/(3\,m_d)$ for $D^{*+} \to D^+\gamma$ and $\mu_1 = 2/(3\,m_c) + 2/(3\,m_u)$ for $D^{*0} \to D^0\gamma$. The rate for the former is then suppressed by a factor

$$\left|\frac{\mu_2}{\mu_1}\right|^2 = (m_u/m_d)^2\frac{(m_d/m_c - 1/2)^2}{(m_u/m_c + 1)^2} \simeq 0.04\,, \tag{3.2}$$

where mass ratios appropriate for constituent quarks have been used, $m_u/m_d \simeq 1$, $m_d/m_c \simeq m_u/m_c \simeq 1/4$. This suppression results from the opposite signs in μ_1 and μ_2, which in turn follow from the (quark) charge assignments and spin wavefunctions for the heavy mesons.

In the quark model $g = 1$ and $\beta \simeq 3\,\mathrm{GeV}^{-1}$, while for the chiral quark model $g = 0.75$ [55]. Relativistic quark models tend to give smaller values, $g \sim 0.4$ [94, 95], as do QCD sum rules, $g \sim 0.2 - 0.4$ [96, 97, 98].

Our purpose here is to use heavy meson chiral perturbation theory at one-loop to extract the couplings g and β from D^* decays. In other words, we wish to examine the sensitivity of a model independent extraction of g and β to higher order corrections. For $D^* \to D\gamma$, analyses beyond leading order have included the heavy quark's magnetic moment which arises at $1/m_c$ [99, 100], and the leading non-analytic effects from chiral loops proportional to $\sqrt{m_q}$ [99]. $\sqrt{m_q}$ terms proportional to both m_K and m_π were found to be important. These effects do not introduce any new unknown quantities into the calculation of the decay rates. For $D^* \to D\gamma$ and the isospin conserving $D^* \to D\pi$ decays the effect of chiral logarithms, $m_q \ln(\mu/m_q)$, have also been considered [101]. These are formally enhanced over other m_q corrections in the chiral limit, $m_q \to 0$, however, the choice of the scale μ leads to some ambiguity in their contribution. (This scale dependence is cancelled by unknown couplings which arise at order m_q in the chiral Lagrangian.) The isospin violating decay $D_s^* \to D_s\pi^0$ has only been considered at leading order, where it occurs through $\eta - \pi^0$ mixing[102].

Here the investigation of all D^* decays is extended to one-loop, including symmetry breaking corrections to order m_q and $1/m_c$. Further $1/m_c$ and m_q contributions considered here include the effect of nonzero D^*–D and D_s–D^0 mass splittings, and the exact kinematics corresponding to nonzero outgoing pion or photon energy in the loop diagrams. (Their inclusion is motivated numerically since $m_{\pi^0} \sim m_{D^*} - m_D \sim m_{D_s} - m_D$, and the decay $D^* \to D\pi^0$ only occurs if $m_{D^*} - m_D > m_{\pi^0}$.) To simplify the organization of the calculation these splittings will be included as residual mass terms in our heavy meson propagators. This gives new non-analytic contributions to the $D^* \to D\pi^0$ and $D^* \to D\gamma$ decay rates. (To treat the mass splittings as perturbations one can simply expand these non-analytic functions.) At order m_q there are also analytic contributions due to new unknown couplings which are discussed. These new couplings can, in principle, be fixed using other observables. We estimate the effect these unknown couplings have on the extraction of g and β.

The calculation of the decay rates to order m_q and $1/m_c$ is taken up in sections 3.1 and 3.2. In section 3.3 we compare the theoretical partial rates with the data to extract the $D^*D\pi$ and $D^*D\gamma$ couplings and discuss the uncertainty involved. Predictions for the widths of the D^* and B^* mesons are also given. Conclusions can be found in section 3.4.

3.1 $D_a^* \to D_a\ \pi$ decays

In this section we construct the effective chiral Lagrangian that describes the decays $D^* \to D\pi$ to first order in the symmetry breaking parameters m_q and $1/m_c$. Going beyond leading order also involves including loops with the pseudo-Goldstone bosons. From Chapter 2 section 2 recall that the lowest order Lagrangian is

$$\begin{aligned}\mathcal{L}_0 \;&=\; \frac{f^2}{8}\mathrm{Tr}\, \partial^\mu \Sigma\, \partial_\mu \Sigma^\dagger + \frac{f^2 B_0}{4}\mathrm{Tr}(m_q \Sigma + m_q \Sigma^\dagger) \\ &\quad -\mathrm{Tr}\, \bar{H}_a iv \cdot D_{ba} H_b + g\, \mathrm{Tr}\, \bar{H}_a H_b \gamma_\mu \gamma_5 A^\mu_{ba}\,. \end{aligned} \tag{3.3}$$

The last term in Eq. (3.3) couples $P^*P\pi$ and $P^*P^*\pi$ with strength g (where $P = D, B$) and determines the decay rate $D^* \to D\pi$ at lowest order. At order $m_q \sim 1/m_c$ the following mass correction terms appear

$$\mathcal{L}_m = \frac{\lambda_2}{4\, m_Q}\mathrm{Tr}\, \bar{H}_a \sigma^{\mu\nu} H_a \sigma_{\mu\nu} + 2\lambda_1 \mathrm{Tr}\, \bar{H}_a H_b m^\xi_{ba} + 2\lambda_1' \mathrm{Tr}\, \bar{H}_a H_a m^\xi_{bb}, \tag{3.4}$$

where $m^\xi = \frac{1}{2}(\xi m_q \xi^\dagger + \xi^\dagger m_q \xi)$. The λ_1' term can be absorbed into the definition of m_H by a phase redefinition of H. The λ_2 term is responsible for the D^*-D mass splitting at this order,

$$\Delta = m_{D^*} - m_D = -2\lambda_2/m_c\,. \tag{3.5}$$

The term involving λ_1 splits the mass of the triplets of D and D^* states. Ignoring isospin violation this splitting is characterized by

$$\delta = m_{D_s^*} - m_{D^*} = m_{D_s} - m_D = 2\lambda_1(m_s - \hat{m}) \tag{3.6}$$

where $\hat{m} = m_u = m_d$. For the purpose of our power counting $\delta \sim m_q \sim 1/m_c \sim \Delta$. The effect of these mass splitting terms can be taken into account by including a residual mass term in each heavy meson propagator. Since we are interested in decay rates we choose the phase redefinition for our heavy fields to scale out the decaying particle's mass. For D^{*0} and D^{*+} decays the denominator of our propagators are: $2v\cdot k$ for D^{*0} and D^{*+}, $2(v\cdot k-\delta)$ for D_s^*, $2(v\cdot k+\Delta)$ for D^0 and D^+, and $2(v\cdot k+\Delta-\delta)$ for D_s. For the D_s^* decays the denominators are the above factors plus 2δ. (If we had scaled out a different mass then the calculation in the rest frame of the initial particle would involve a residual 'momentum' for the initial particle, but would yield the same results.) This results in additional non-analytic contributions from one-loop diagrams which are functions of the quantities Δ/m_{π_i} and δ/m_{π_i}, where $m_{\pi_i} \in \{m_\pi, m_K, m_\eta\}$. Formally, $m_{\pi_i}^2 \sim m_q \sim \Delta \sim \delta$ and one can expand these contributions to get back the result of treating the terms in Eq. (3.4) as perturbative mass insertions.

Another type of $1/m_c$ corrections are those whose coefficients are fixed by velocity reparameterization invariance [103, 82]

$$\delta\mathcal{L}_v = -\frac{1}{2m_Q}\mathrm{Tr}\,\bar{H}_a(i\vec{D})^2_{ba}H_b + \frac{g}{m_Q}\mathrm{Tr}\bar{H}_c(i\overleftarrow{D}^\mu_{ac}v\cdot A_{ba} - iv\cdot A_{ac}\overrightarrow{D}^\mu_{ba})H_b\gamma_\mu\gamma_5\,. \tag{3.7}$$

The first term here is analogous to the HQET kinetic operator, $O_{\rm kin} = \frac{1}{2m_Q}\bar{h}_v\,(i\vec{D})^2\,h_v$, but written in terms of the interpolating fields P_a and $P_a^{*\mu}$. In Eq. (3.7) the derivatives give powers of the heavy meson's momentum. There are also contributions from $O_{\rm kin}$ that break the flavor symmetry where the derivatives are order $\Lambda_{\rm QCD}$. In conjunction with the HQET chromomagnetic operator, $O_{\rm mag} = \frac{1}{2m_Q}\bar{h}_v\,\frac{g_s}{2}\,\sigma_{\alpha\beta}G^{\alpha\beta}\,h_v$, these contributions to the Lagrangian modify the dynamics of the heavy meson states. They give $\Lambda_{\rm QCD}/m_Q$ corrections in the form of time ordered products with the leading order current [104], which induce spin and flavor symmetry violating corrections to the form of the $D^*D\pi$ coupling. We account for these corrections by introducing the couplings g_1 and g_2 in Eq. (3.8) below. The last term in Eq. (3.7) contributes at higher order in our power counting since it is suppressed by both a derivative and a power of $1/m_c$.

Further terms that correct the Lagrangian in Eq. (3.3) at order $m_q \sim 1/m_c$ include

[82][2]

$$
\begin{aligned}
\delta\mathcal{L}_g &= \frac{g\kappa_1\,B_0}{\Lambda_\chi^2}\mathrm{Tr}\,\bar{H}_a H_b\gamma_\mu\gamma_5 A^\mu_{bc} m^\xi_{ca} + \frac{g\kappa_1'\,B_0}{\Lambda_\chi^2}\mathrm{Tr}\,\bar{H}_a H_b\gamma_\mu\gamma_5 m^\xi_{bc} A^\mu_{ca} \\
&+ \frac{g\kappa_3\,B_0}{\Lambda_\chi^2}\mathrm{Tr}\,\bar{H}_a H_b\gamma_\mu\gamma_5 A^\mu_{ba} m^\xi_{cc} + \frac{g\kappa_5\,B_0}{\Lambda_\chi^2}\mathrm{Tr}\,\bar{H}_a H_a\gamma_\mu\gamma_5 A^\mu_{bc} m^\xi_{cb} \\
&+ \frac{\delta_2}{\Lambda_\chi}\mathrm{Tr}\,\bar{H}_a H_b\gamma_\mu\gamma_5 iv\cdot D_{bc} A^\mu_{ca} + \frac{\delta_3}{\Lambda_\chi}\mathrm{Tr}\,\bar{H}_a H_b\gamma_\mu\gamma_5 iD^\mu_{bc} v\cdot A_{ca} \\
&+ \frac{g_1}{m_Q}\mathrm{Tr}\,\bar{H}_a H_b\gamma_\mu\gamma_5 A^\mu_{ba} + \frac{g_2}{m_Q}\mathrm{Tr}\,\bar{H}_a\gamma_\mu\gamma_5 H_b A^\mu_{ba} + \ldots\,, \qquad (3.8)
\end{aligned}
$$

where $D^\alpha_{bc}A^\beta_{ca} = \partial^\alpha A^\beta_{ba} + [V^\alpha, A^\beta]_{ba}$ and $\Lambda_\chi = 4\pi f$. The ellipses here denote terms linear in $m^\xi_- = \frac{1}{2}(\xi m_q \xi^\dagger - \xi^\dagger m_q \xi)$ which contribute to processes with more than one pion, as well as terms with $(iv\cdot D)$ acting on an H. For processes with at most one pion and H on-shell the latter terms can be eliminated at this order, regardless of their chiral indices, by using the equations of motion for H. The κ_i coefficients contain infinite and scale dependent pieces which cancel the corresponding contributions from the one-loop $D^* \to D\pi$ diagrams. For the κ_1 and κ_1' terms only the combination $\tilde{\kappa}_1 = \kappa_1 + \kappa_1'$ will enter in an isospin conserving manner here. (The combination $\kappa_1 - \kappa_1'$ will contribute an isospin violating correction to R^+_π.) At a given scale μ, the finite part of κ_3 can be absorbed into the definition of g. The decays $D^* \to D\pi$ have analytic contributions from $\tilde{\kappa}_1$ and κ_5 at order m_q.

For $m_Q = m_c$ the term in Eq. (3.8) involving g_1 can be absorbed into g (this term only enters into a comparison with B^* decays). The term g_2 breaks the equality of the $D^*D\pi$ and $D^*D^*\pi$ couplings. Since we only need the coupling $D^*D^*\pi$ in loops we can also absorb g_2 into the definition of g. Thus, our g is defined as the $D^*D\pi$ coupling with $1/m_Q$ corrections arising in relating it to the couplings for $D^*D^*\pi$ and $B^{(*)}B^*\pi$.

The terms in Eq. (3.8) involving δ_2 and δ_3 contribute to $D^* \to D\pi^0$, entering in a fixed linear combination with the tree level coupling g of the form $g - (\delta_2 + \delta_3)v\cdot k/\Lambda_\chi$. These are $\sim 10\%$ corrections for the decays $D^* \to D\pi$. The energy of the outgoing pion is roughly the same for all three decays, $v \cdot k \sim .144\,\mathrm{GeV}$. Therefore, it is impossible to disentangle the contribution of $\delta_{2,3}$ from that of g for these decays, and the extraction of g presented here will implicitly include their contribution. For other processes involving pions with different $v \cdot k$ these counterterms can give a different contribution. This should be kept in mind when this value of g is used in a different context.

---

[2] The κ_1' term was not present in [82]. The factor B_0/Λ_χ^2 is introduced here for later convenience.

Techniques for one-loop calculations in heavy hadron chiral perturbation theory are well known and will not be discussed here. Dimensional regularization is used and the renormalized counterterms are defined by subtracting the pole terms $1/\epsilon - \gamma + \log(4\pi)$. In doing this type of one-loop calculation an important integral is

$$\int \frac{d^{4-2\epsilon}q}{(2\pi)^{4-2\epsilon}} \frac{\mu^{2\epsilon}}{(q^2 - m^2 + i\varepsilon)\, 2(q \cdot v - b + i\varepsilon)} = \frac{-i\, b}{(4\pi)^2} \left[\frac{1}{\hat{\epsilon}} + \ln(\frac{\mu^2}{m^2}) + 2 - 2F(\frac{m}{b}) \right] , \tag{3.9}$$

where $1/\hat{\epsilon} = 1/\epsilon - \gamma + \log(4\pi)$. F is needed for both positive and negative b, so

$$F\left(\frac{1}{x}\right) = \begin{cases} -\frac{\sqrt{1-x^2}}{x} \left[\frac{\pi}{2} - \tan^{-1}\left(\frac{x}{\sqrt{1-x^2}} \right) \right] & |x| \le 1 \\ \frac{\sqrt{x^2-1}}{x} \ln\left(x + \sqrt{x^2-1} \right) & |x| \ge 1 \end{cases} . \tag{3.10}$$

For $b > 0$ the function F was derived in [105, 77] and agrees with the above formula[3]. For $x = b/m < -1$ the logarithm in Eq. (3.10) has an imaginary part. This corresponds to the physical intermediate state where a heavy meson of mass m_H produces particles of mass $m_H + b$ and m. For the calculation here the imaginary part only contributes from $F(m_\pi/(d_0 - \Delta))$, and was found to always be numerically insignificant. Note that the real part of $x\, F(1/x)$ is continuous everywhere, and differentiable everywhere except $x = -1$. Also $F(1) = F(-1) = 0$.

The decays $D^{*0} \to D^0\pi^0$ and $D^{*+} \to D^+\pi^0$, and $D_s^* \to D_s\pi^0$ have decay rates Γ_π^1,

---

[3] Eq. (3.10) for F disagrees with [82] for $x < 0$. Their $F(1/x)$ is even under $x \to -x$ making Eq. (3.9) discontinuous at $\Delta = 0$. Furthermore, their F has no imaginary part corresponding to the physical intermediate state.

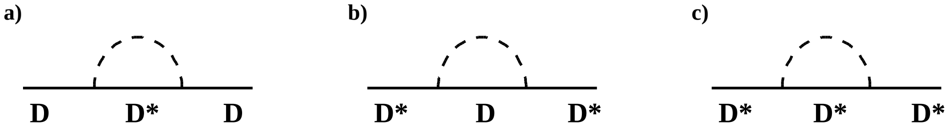

Figure 3.1: D and D^* wavefunction renormalization graphs. The dashed line represents a pseudo-Goldstone boson.

Γ_π^2, and Γ_π^3 given by

$$\Gamma_\pi^a = \frac{g^2}{12\,\pi\,f^2}\left|\frac{Z_{\rm wf}^a}{Z_\pi^a}\right|^2 |\vec{k}_\pi^{\,a}|^3\,. \qquad (3.11)$$

Here $\vec{k}_\pi^{\,a}$ is the three momentum of the outgoing pion, Z_π^a contains the vertex corrections, and $Z_{\rm wf}^a = \sqrt{Z_{D^*}^a Z_D^a}$ contains the wavefunction renormalization for the D^* and D. When the ratio of Γ_π^a to the $D^* \to D\gamma$ rate is taken $Z_{\rm wf}^a$ will cancel out. However, $Z_{\rm wf}^a$ does contribute to our predictions for the D^* widths, where the ratio $Z_{\rm wf}^a/Z_\pi^a$ will be kept to order g^2. The graphs in Fig. 3.1 give

$$\begin{aligned} Z_D^a &= 1+\frac{g^2}{(4\pi f)^2}(\lambda^i_{ab}\lambda^{i\dagger}_{ba})\Big\{[3m_i^2-6(\Delta+d_0)^2]\log(\frac{\mu^2}{m_i^2})+\,3\,G_1(m_i,\Delta+d_0)\Big\}\,,\\ Z_{D^*}^a &= 1+\frac{g^2}{(4\pi f)^2}(\lambda^i_{ab}\lambda^{i\dagger}_{ba})\Big\{[3m_i^2-4d_0^2-2(d_0-\Delta)^2]\log(\frac{\mu^2}{m_i^2})+2\,G_1(m_i,d_0)\\ &\qquad +G_1(m_i,d_0-\Delta)\Big\}\,, \end{aligned} \qquad (3.12)$$

where m_i is the mass of π^i, $d_0 = \delta^{b3}\delta$ for D^{*0} and D^{*+} decays and $d_0 = (\delta^{b3}-1)\delta$ for D_s^* decays. The notation in Eq. (3.12) assumes that we sum over $b = 1,2,3$ and $i = 1,\ldots,8$. The logarithms agree with [101], except that we have kept terms of order $\Delta^2 \sim d_0^2$ in the prefactor since these terms are enhanced for $m_q \to 0$. Analytic terms of order $\Delta^2 \sim d_0^2$ are neglected since they are higher order in our power counting. The function $G_1(a,b)$ in Eq. (3.12) has mass dimension 2,

$$G_1(a,b) = \frac{5}{3}\,a^2+(4b^2-\frac{4}{3}a^2)F(a/b)+\frac{4}{3}(a^2-b^2)\frac{a}{b}F'(a/b)\,. \qquad (3.13)$$

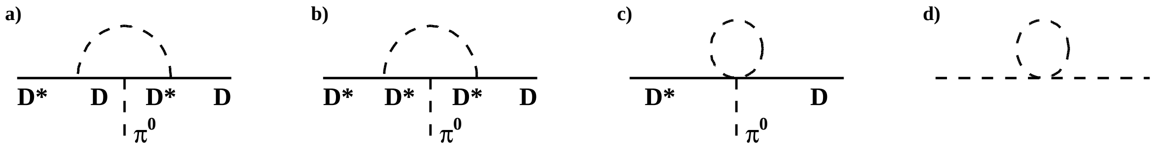

Figure 3.2: Nonzero one-loop vertex corrections for the decays $D^{*0} \to D^0\pi^0$ and $D^{*+} \to D^+\pi^0$ (a,b,c) and the pseudo-Goldstone boson wave function renormalization graph (d).

It contains an analytic part proportional to a^2, and a non-analytic part which is a function of the ratio b/a. In the limit $\Delta \to 0$ Eq. (3.12) gives $Z_D = Z_{D^*}$ in agreement with HQS. To obtain HQS in the finite part of the dimensionally regularized calculation of the graphs in Fig. 3.1 it was necessary to continue the D^* fields to $d = 4-2\epsilon$ dimensions (so the D^* polarization vector $\epsilon_\alpha = (1-\frac{\epsilon}{3})\tilde{\epsilon}_\alpha$ where $\sum \tilde{\epsilon}^*_\alpha \tilde{\epsilon}^\alpha = -3$).

For $a = 1, 2$ the decay proceeds directly so that at tree level $Z^{1,2}_{\rm wf}/Z^{1,2}_\pi = 1$. At one loop we have non-zero vertex corrections from the graphs in Fig. 3.2a,b,c. As noted in [101], the two one-loop graphs that contain a $D^{(*)}D^*\pi\pi$ vertex (not shown) vanish, and the graph in Fig. 3.2c cancels with the π^0 wavefunction renormalization in Fig. 3.2d (this is also true for $D^{*+} \to D^0\pi^+$ and $D_s^* \to D_s\pi^0$). For $a = 1, 2$ the vertex corrections are

$$\begin{aligned}\frac{1}{Z^a_\pi} &= 1 + \frac{g^2}{(4\pi f)^2}\frac{\lambda^i_{ab}\lambda^1_{bb}\lambda^{i\dagger}_{ba}}{\lambda^1_{aa}}\Big\{ \log\big(\frac{\mu^2}{m_i^2}\big)\Big[m_i^2 + \frac{2}{3}(-d_1^2 + d_1\, d_2 + d_2^2 - 2d_1\, d_0 - 2\, d_0^2)\Big] \\ &\quad +2\, F_1(m_i, d_1, d_2) - 4\, F_1(m_i, d_1, d_0)\Big\} + \varrho^a_\pi(\tilde{\kappa}_1, \kappa_5)\,, \qquad (3.14)\end{aligned}$$

where here $d_0 = \delta^{b3}\delta$, $d_1 = k\cdot v + d_0$, $d_2 = -\Delta + d_0$, and k is the outgoing momentum of the π^0. The coefficient of the $m_i^2 \log(\mu^2/m_i^2)$ term agrees with [101]. The function F_1 in Eq. (3.14) has mass dimension 2 and contains both analytic and non-analytic parts. $\varrho^a_{\pi\, ct}$ contains the dependence of the rate on the (renormalized) counterterms $\tilde{\kappa}_1(\mu)$ and $\kappa_5(\mu)$.

$$F_1(a,b,c) \;=\; -\frac{7}{6}a^2 + \frac{2}{3(b-c)}\left[b(a^2-b^2)F(a/b) - c(a^2-c^2)F(a/c)\right]\,,$$

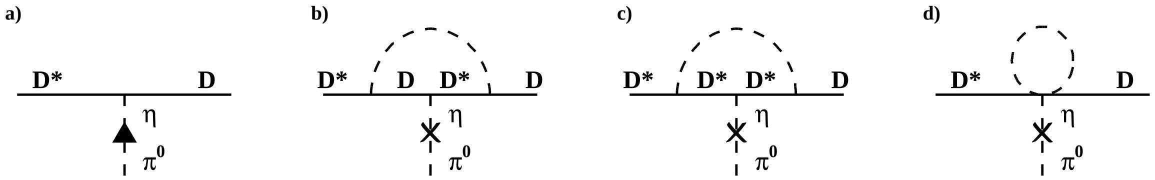

Figure 3.3: Nonzero vertex corrections for the decay $D_s^* \to D_s\pi^0$ which involve $\pi^0 - \eta$ mixing. The cross denotes leading order mixing while the triangle denotes mixing at next to leading order.

$$\varrho_\pi^{a=1,2} \;=\; \frac{m_\pi^2}{(4\pi f)^2}\frac{\tilde{\kappa}_1(\mu)}{2}\,. \tag{3.15}$$

We have ignored isospin violating counterterm corrections in $\varrho_\pi^{1,2}$. In this case $\varrho_\pi^{1,2}$ do not depend on κ_5, and furthermore are proportional to $m_\pi^2/(4\pi f)^2$, so these counterterms are small.

The decay $D_s^* \to D_s\pi^0$ is isospin violating, and the leading contribution occurs through $\eta - \pi^0$ mixing[102]. To first order in the isospin violation the decay is suppressed at tree level by the mixing angle $\theta = (1.00 \pm 0.05) \times 10^{-2}$ [50]

$$\frac{1}{Z_\pi^3} = \frac{(m_u - m_d)}{2\,(m_s - \hat{m})} = -\frac{2}{\sqrt{3}}\theta \simeq -\frac{1}{87.0}\,. \tag{3.16}$$

Beyond tree level we have corrections to the $\eta - \pi^0$ mixing angle parameterized by $\delta_{mix} = 0.11$ [52] (Fig. 3.3a), loop corrections to the $\eta{-}\pi^0$ mixing graph (Figs. 3.3b,c,d), as well as loop graphs with decay directly to π^0 that occur in an isospin violating combination (Figs. 3.2a,b). The contribution of Fig. 3.3d is again cancelled by the pseudo-Goldstone boson wave function renormalization graph (Fig. 3.2d). Note that the decay $D_s^* \to D_s\pi^0$ cannot occur via a single virtual photon in the effective theory. In the quark model, decay to the spin and color singlet π^0 can occur if the single photon is accompanied by at least two gluons (with suppression $\alpha/\pi \simeq 1/430$ [102]). We will neglect the possibility of such a single photon mediated transition here. Thus,

$$\frac{1}{Z_\pi^3} \;=\; \frac{(m_u - m_d)}{2\,(m_s - \hat{m})}\Bigg[1 + \delta_{mix} + \frac{g^2}{(4\pi f)^2}\frac{\lambda^i_{3b}\lambda^8_{bb}\lambda^{i\dagger}_{b3}}{\lambda^8_{33}}\Bigg\{\log\big(\frac{\mu^2}{m_i^2}\big)\Big[m_i^2 + \frac{2}{3}(-d_1^2 + d_1\,d_2$$

$$
\begin{aligned}
& \quad +d_2^2 - 2d_1\, d_0 - 2\, d_0^2)\Big] + 2\, F_1(m_i, d_1, d_2) - 4\, F_1(m_i, d_1, d_0)\Big\}\Big] \\
& + \frac{g^2}{(4\pi f)^2} \frac{\lambda^i_{3b}\lambda^1_{bb}\lambda^{i\dagger}_{b3}}{(1/\sqrt{2})} \left[\tilde{m}_i^2 \log(\frac{\mu^2}{\tilde{m}_i^2}) + 2\, F_1(\tilde{m}_i, d_1, d_2) - 4\, F_1(\tilde{m}_i, d_1, d_0)\right] \\
& + \varrho^3_\pi(\tilde{\kappa}_1, \kappa_5)\,, \qquad (3.17)
\end{aligned}
$$

where for D^*_s decay $d_0 = (\delta^{b3} - 1)\delta$, $d_1 = k \cdot v + d_0$, and $d_2 = -\Delta + d_0$. The tilde on the mass, $\tilde{m}_i$, indicates that isospin violation is taken into account. Also note that $\sqrt{2}\, \sum_{i,b} \lambda^i_{3b}\lambda^1_{bb}\lambda^{i\dagger}_{b3}\tilde{m}_i^2 = m^2_{K^\pm} - m^2_{K^0}$. In Eq. (3.17), the function ϱ^3_π depends on $\tilde{\kappa}_1$ and κ_5, and at leading order in the isospin violation is

$$
\varrho^3_\pi \;=\; \frac{1}{(4\pi f)^2} \frac{(m_u - m_d)}{2(m_s - \hat{m})} \left[(m_K^2 - \frac{m_\pi^2}{2})\, \tilde{\kappa}_1 + (m_K^2 - m_\pi^2)\, \kappa_5\right] + \frac{(m^2_{K^\pm} - m^2_{K^0})}{(4\pi f)^2}\, \kappa_5\,. \qquad (3.18)
$$

In deriving this equation use has been made of $m_\pi^2 = 2B_0 m_u = 2B_0 m_d = 2B_0 \hat{m}$, $m_K^2 - m_\pi^2/2 = B_0 m_s$, and $m^2_{K^\pm} - m^2_{K^0} = (m_u - m_d)B_0$.

3.2 $D^*_a \to D_a\ \gamma$ decays

To describe $D^* \to D\gamma$, electromagnetic effects must be included, so the Lagrangian in Eq. (3.3) is gauged with a $U(1)$ photon field B^μ. With octet and singlet charges, $Q = \mathrm{diag}(\frac{2}{3}, -\frac{1}{3}, -\frac{1}{3})$ and $Q' = \frac{2}{3}$ (for the c), the covariant derivative $\mathcal{D}_\mu$ is [106]

$$
\begin{aligned}
\mathcal{D}_\mu\, \xi &= \partial_\mu \xi + ieB_\mu[Q, \xi]\,, \qquad (3.19) \\
\mathcal{D}_\mu\, H &= \partial_\mu H + ieB_\mu(Q'H - HQ) - \mathcal{V}_\mu H\,,
\end{aligned}
$$

where the vector and axial vector currents are now

$$
\begin{aligned}
\mathcal{V}_\mu &= \frac{1}{2}(\xi^\dagger \mathcal{D}_\mu \xi + \xi \mathcal{D}_\mu \xi^\dagger)\,, \qquad (3.20) \\
\mathcal{A}_\mu &= \frac{i}{2}(\xi^\dagger \mathcal{D}_\mu \xi - \xi \mathcal{D}_\mu \xi^\dagger)\,.
\end{aligned}
$$

However, this procedure does not induce a coupling between D^*, D and B_μ without additional pions. Gauge invariant contact terms should also be included, and it is one of these that gives rise to the $D^*D\gamma$ coupling (and a $D^*D^*\gamma$ coupling)

$$\mathcal{L}_\beta = \frac{\beta\, e}{4} \mathrm{Tr}\, \bar{H}_a H_b \sigma^{\mu\nu} F_{\mu\nu} Q^\xi_{ba} . \tag{3.21}$$

Here β has mass dimension -1, $Q^\xi = \frac{1}{2}(\xi^\dagger Q \xi + \xi Q \xi^\dagger)$, and $F_{\mu\nu} = \partial_\mu B_\nu - \partial_\nu B_\mu$. The terms which correct this Lagrangian at order $m_q \sim 1/m_c$ have a similar form to those in Eq. (3.8)

$$\begin{aligned} \delta\mathcal{L}_\beta \;=\; & \frac{\alpha_1\, B_0}{\Lambda_\chi^2}\frac{\beta\, e}{4} \mathrm{Tr}\, \bar{H}_a H_b \sigma^{\mu\nu} F_{\mu\nu} Q^\xi_{bc} m^\xi_{ca} + \frac{\alpha_1'\, B_0}{\Lambda_\chi^2}\frac{\beta\, e}{4} \mathrm{Tr}\, \bar{H}_a H_b \sigma^{\mu\nu} F_{\mu\nu} m^\xi_{bc} Q^\xi_{ca} \\ + \; & \frac{\alpha_3\, B_0}{\Lambda_\chi^2}\frac{\beta\, e}{4} \mathrm{Tr}\, \bar{H}_a H_b \sigma^{\mu\nu} F_{\mu\nu} Q^\xi_{ba} m^\xi_{cc} + \frac{\alpha_5\, B_0}{\Lambda_\chi^2}\frac{\beta\, e}{4} \mathrm{Tr}\, \bar{H}_a H_a \sigma^{\mu\nu} F_{\mu\nu} Q^\xi_{bc} m^\xi_{cb} \\ + \; & \frac{\tau_2\, e}{4\Lambda_\chi^2} \mathrm{Tr}\, \bar{H}_a H_b \sigma^{\mu\nu} Q^\xi_{bc} iv\cdot D_{ca} F_{\mu\nu} + \frac{\tau_3\, e}{4\Lambda_\chi^2} \mathrm{Tr}\, \bar{H}_a H_b \sigma^{\mu\nu} Q^\xi_{bc} i D^\mu_{ca} v^\lambda F_{\nu\lambda} \\ + \; & \frac{\beta_1}{m_Q}\frac{e}{4} \mathrm{Tr}\, \bar{H}_a H_b \sigma^{\mu\nu} F_{\mu\nu} Q^\xi_{ba} + \frac{\beta_2}{m_Q}\frac{e}{4} \mathrm{Tr}\, \bar{H}_a \sigma^{\mu\nu} H_b F_{\mu\nu} Q^\xi_{ba} \\ - \; & \frac{e}{4\, m_Q} Q'\, \mathrm{Tr}\, \bar{H}_a \sigma^{\mu\nu} H_a F_{\mu\nu} + \ldots\,. \end{aligned} \tag{3.22}$$

The ellipses denote terms that do not contribute for processes without additional pions and/or can be eliminated using the equations of motion for H. For our purposes Q^ξ and m^ξ in Eq. (3.22) are diagonal so only $\tilde{\alpha} = \alpha_1 + \alpha_1'$ contributes. The finite part of α_3 will be absorbed into the definition of β. For $m_Q = m_c$, the β_1 term can be absorbed, and we absorb the part of the β_2 term that contributes to $D^*D\gamma$ since $D^*D^*\gamma$ only contributes in loops for us. Thus, β is defined to be the $D^*D\gamma$ coupling at order $1/m_c$. The last term in Eq. (3.22) is the contribution from the photon coupling to the c quark and has a coefficient which is fixed by heavy quark symmetry [100, 99]. This term is numerically important. However, here the leading order contribution to $D^*_a \to D_a\gamma$ is taken to be the $m_Q \to \infty$, $m_q \to 0$ effect from Eq. (3.21), so this $1/m_c$ term is part of the first order corrections. The $\tau_{1,2}$ terms are similar to the $\delta_{2,3}$ terms in Eq. (3.8), and appear with β in the combination $\beta - (\tau_1 + \tau_2) v\cdot k/\Lambda_\chi^2$. Here $\tau_1 + \tau_2$ will have an infinite part necessary for the one-loop renormalization. Again it is not

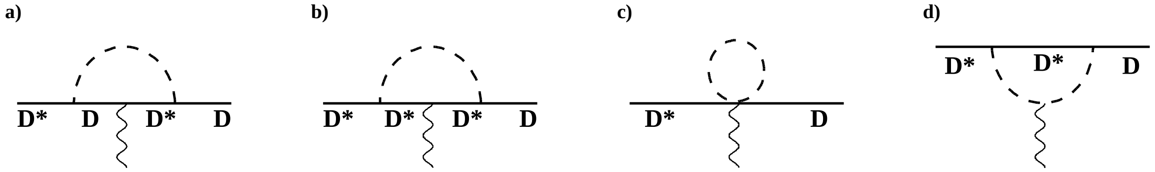

Figure 3.4: Nonzero vertex corrections for the decays $D^* \to D\gamma$.

possible to isolate the finite part of the $(\tau_1 + \tau_2)$ contribution from that of β, so the extraction at this order includes the renormalized $\tau_{1,2}$ with $v \cdot k \sim 0.137\,\mathrm{GeV}$.

The decays $D^{*0} \to D^0\gamma$, $D^{*+} \to D^+\gamma$, and $D_s^* \to D_s\gamma$ have decay rates Γ_γ^1, Γ_γ^2, and Γ_γ^3 given by

$$\Gamma_\gamma^a \;=\; \frac{\alpha}{3}\,|\mu_a|^2\,|\vec{k}_\gamma^{\,a}|^3, \qquad\qquad \mu_a = Z_{\mathrm{wf}}^a\left(\beta\,\frac{Q_{aa}}{Z_\gamma^a} + \frac{Q'}{m_c}\right)\,, \tag{3.23}$$

where $\alpha \simeq 1/137$, $\vec{k}_\gamma^{\,a}$ is the three momentum of the outgoing photon, and the wave-function renormalization, Z_{wf}^a, is given by Eq. (3.12). To predict the D^* widths, $Z_{\mathrm{wf}}^a/Z_\gamma^a$ is kept to order g^2 and we take $Z_{\mathrm{wf}}^a \times 1/m_c = 1/m_c$. The vertex correction factor Z_γ^a has nonzero contributions from the graphs in Fig. 3.4. Note that the two one-loop graphs that contain a $D^{(*)}D^*\pi\gamma$ vertex (not shown) do not contribute [101]. Furthermore, the graph in Fig. 3.4b has no contribution from the $D^*D^*\gamma$ coupling which arises from gauging the lowest order Lagrangian in Eq. (3.3). Thus

$$\begin{aligned}
\frac{1}{Z_\gamma^a} \;=\;& 1 + \frac{g^2}{(4\pi f)^2}\frac{\lambda^i_{ab}Q_{bb}\lambda^{i\dagger}_{ba}}{Q_{aa}}\bigg\{ \log\big(\frac{\mu^2}{m_i^2}\big)\Big[m_i^2 + \frac{2}{3}(-d_1^2 + d_1\,d_2 + d_2^2 - 2d_1\,d_0 - 2\,d_0^2)\Big] \\
&\qquad\qquad\qquad + 2\,F_1(m_i, d_1, d_2) - 4\,F_1(m_i, d_1, d_0)\bigg\} \\
&- \frac{1}{(4\pi f)^2}\frac{[\lambda^{i\dagger},[Q,\lambda^i]]_{aa}}{2\,Q_{aa}}\Big[m_i^2\,\log\big(\frac{\mu^2}{m_i^2}\big) + m_i^2\Big] \\
&+ \frac{4\,g^2}{(4\pi f)^2}\frac{(\lambda^i_{ab}\lambda^{i\dagger}_{ba})\,q^i}{\beta Q_{aa}}\Big[-\log\big(\frac{\mu^2}{m_i^2}\big)(d_0 + \frac{k\cdot v}{2}) + F_2(m_i, d_0, k\cdot v)\Big] \\
&+ \varrho_\gamma^a(\tilde{\alpha}_1, \alpha_5)\,,
\end{aligned} \tag{3.24}$$

where q^i is the charge of meson π^i, k is now the outgoing photon momentum, and the d_i are as above (again they differ depending on whether it is D_s^* or one of D^{*0}, D^{*+} that is decaying). The coefficients of the $m_i^2 \log(\mu^2/m_i^2)$ terms agree with [101]. The new function F_2 has mass dimension 1,

$$\begin{aligned} F_2(a,b,c) &= -2\,b - c - \frac{2a^2}{c}\int_{a/b}^{a/(b+c)} dt \frac{F(t)}{t^3} \\ &= -2\,b - c - \frac{2a^2}{c}\left[\frac{1}{4x^2} - \frac{F(x)}{2\,x^2} - \frac{F(x)^2}{4\,(x^2-1)}\right]\Bigg|_{x=a/b}^{x=a/(b+c)} . \end{aligned} \tag{3.25}$$

It contains an analytic part proportional to $2d_0 + v\cdot k$, and a non-analytic part which is a function of δ/m_i and $v\cdot k/m_i$. In Eq. (3.24) ϱ_γ^a contains the dependence of the rate on the (renormalized) counterterms $\tilde{\alpha}_1(\mu)$ and $\alpha_5(\mu)$. Assuming isospin to be conserved we have

$$\begin{aligned} \varrho_\gamma^{a=1,2} &= \frac{m_\pi^2\,\tilde{\alpha}_1}{2\,(4\pi f)^2} - \frac{(m_K^2 - m_\pi^2)\,\alpha_5}{3\,Q_{aa}\,(4\pi f)^2}, \\ \varrho_\gamma^3 &= \frac{(2\,m_K^2 - m_\pi^2)\,\tilde{\alpha}_1}{2\,(4\pi f)^2} + \frac{(m_K^2 - m_\pi^2)\,\alpha_5}{(4\pi f)^2}. \end{aligned} \tag{3.26}$$

By examining Eqs. (3.12), (3.14), (3.17), and (3.24) we can get an idea of the size of the various one-loop corrections to Γ_π^a and Γ_γ^a. With our power counting $\Delta \sim \delta \sim v\cdot k \sim m_q \sim m_i^2$ so we can consider expanding in Δ/m_i, δ/m_i, and $v\cdot k/m_i$

$$\begin{aligned} G_1(m_i,b) &= \frac{m_i^2}{3}\left[1 - \frac{6\pi b}{m_i} + \frac{16b^2}{m_i^2} + \dots\right], \\ F_1(m_i,b,c) &= -\frac{m_i^2}{2}\left[1 - \frac{\pi(b+c)}{m_i} + \frac{16(b^2+bc+c^2)}{9m_i^2} + \dots\right], \\ F_2(m_i,d_0,k\cdot v) &= -\pi m_i\left[1 - \frac{3d_0^2 + 3d_0 k\cdot v + (k\cdot v)^2}{6m_i^2} + \dots\right]. \end{aligned} \tag{3.27}$$

The leading terms in G_1 and F_1 are m_q corrections to the rates. The second terms are order $m_q^{3/2}$ and $\sqrt{m_q}/m_c$, and can be kept since they are unambiguously determined at the order we are working. The third and remaining terms in G_1 and F_1 are subleading in our power counting. The term $-\pi m_i$ in F_2 is the formally enhanced contribution discovered in [99]. Note that there are no contributions to F_2 proportional to δ or

$k \cdot v$. The second term in F_2 in Eq. (3.27) has contributions of order $m_q^{3/2}$, $\sqrt{m_q} k \cdot v$, and $(k \cdot v)^2/\sqrt{m_q}$ which again can be kept since they are unambiguously determined.

The above power counting is sensible when m_i is m_K or m_η. We know that numerically $m_\pi \sim \Delta \sim \delta \sim k \cdot v$, so for $m_i = m_\pi$ the series in Eq. (3.27) are not sensible. In [99] the term $-\pi m_\pi$ in F_2 was found to be important, so we want to keep corrections with m_π dependence. Therefore, instead of expanding the non-analytic functions we choose to keep them in the non-analytic forms given in the Appendix. Numerically the one-loop corrections to Γ_π^1 and Γ_π^2 are very small; with $g = 1$ they are of order $\sim 2\%$. For Γ_π^3, δ_{mix} is a 11% correction to the tree level result in Eq. (3.16). Individually the terms proportional to $g^2 F_1$ and $g^2 \log(\mu/m_q)$ in Eq. (3.17) are $\sim 10\%$ corrections for $g = 1$. However, the loops graphs with $\eta - \pi^0$ mixing tend to cancel those without $\eta - \pi^0$ mixing leaving a $\sim 2\%$ correction. The one-loop corrections to Γ_γ^a are larger, for instance the graph in Fig. 3.4c gives sizeable corrections that are not suppressed by g^2. Corrections to the coefficient of the leading g^2/β term range from $\sim 3\%$ for D_s^* and $\sim 20\%$ for D^{*0} decay, to $\sim 50\%$ for the D^{*+}. (The latter percentage is large because the only contribution for this decay comes from a charged pion in the loop of Fig. 3.4d.) Corrections proportional to g^2 are only sizeable for $D_s^* \to D_s \gamma$ where they are $\sim 10\%$ for $g = 1$.

3.3 Extraction of the couplings g and β

Using the calculation of the decay rates from the previous section, the couplings g and β can be extracted from a fit to the experimental data. Input parameters include $m_c = 1.4\,\mathrm{GeV}$ [107, 108], the meson masses from [57], $\Delta = m_{D^*} - m_D = 0.142\,\mathrm{GeV}$, $\delta = m_{D_s^{(*)}} - m_{D^{(*)}} = 0.100\,\mathrm{GeV}$, and $v \cdot k$ which is determined from the masses. When isospin is assumed we use $m_K = 0.4957\,\mathrm{GeV}$ and $m_\pi = 0.1373\,\mathrm{GeV}$. f is extracted from π^- decays. At tree level we use $f = f_\pi = 0.131\,\mathrm{GeV}$ [57], while when loop contributions are included we use the one-loop relation between f and f_π [52] to get $f = 0.120\,\mathrm{GeV}$. The ratio of the decay rates Γ_γ^a and Γ_π^a are fit to the experimental numbers

$$\begin{aligned}
\mathcal{B}(D^{*0} \to D^0\gamma)/\mathcal{B}(D^{*0} \to D^0\pi^0) &= 0.616 \pm 0.076 \text{ [57]}\,, \\
\mathcal{B}(D^{*+} \to D^+\gamma)/\mathcal{B}(D^{*+} \to D^+\pi^0) &= 0.055 \pm 0.017 \text{ [91]}\,, \\
\mathcal{B}(D_s^* \to D_s\pi^0)/\mathcal{B}(D_s^* \to D_s\gamma) &= 0.062 \pm 0.029 \text{ [57]}\,, \qquad (3.28)
\end{aligned}$$

where the errors combine both statistical and systematic. Using the masses $m_{D^{*0}}$, $m_{D^{*+}}$, $m_{D_s^*}$, and mass splittings $m_{D^{*0}} - m_{D^0}$, $m_{D^{*+}} - m_{D^+}$, $m_{D_s^*} - m_{D_s}$ from [57] gives the momentum ratios that appear in $\Gamma_\gamma^a/\Gamma_\pi^a$:

$$\frac{|\vec{k}_\gamma^1|^3}{|\vec{k}_\pi^1|^3} = 32.65 \pm 0.44, \qquad \frac{|\vec{k}_\gamma^2|^3}{|\vec{k}_\pi^2|^3} = 45.2 \pm 1.0, \qquad \frac{|\vec{k}_\gamma^3|^3}{|\vec{k}_\pi^3|^3} = 24.4 \pm 1.5\,. \qquad (3.29)$$

The errors here are clearly dominated by those in Eq. (3.28). Equating the numbers in Eq. (3.28) to the ratio of rates from Eqs. (3.11) and (3.23) gives a set of three nonlinear equations for g and β (where we ignore for the moment the unknown counterterms). In general any pair of these equations will have several possible solutions. To find the best solution we take the error from Eq. (3.28) and minimize the χ^2 for the fit to the three measurements. We will restrict ourselves to the interesting range of values, $0 < g < 1$ and $0 < \beta < 6$, discarding any solutions that lie outside this range. (The sign of g will not be determined here since it only appears quadratically in Γ_π^a and Γ_γ^a.)

To test the consistency of the chiral expansion we will first check how the extraction of g and β differs at various orders. The results are given in Table 3.1. At tree level only the ratio β/g is determined, and the χ^2 is rather large. We might next consider adding the contribution from the chiral loop corrections to $D^* \to D\gamma$ which go as $\sqrt{m_q}$. However, this does not lead to a consistent solution between the three data points unless β is negative. This signals the importance of the Q'/m_c contribution in Eq. (3.23) corresponding to a nonzero heavy quark magnetic moment. Adding this contribution gives the results in the second row of Table 3.1, where there are now two solutions with similar χ^2 in the region of interest. Adding the chiral

Order	g	β	χ^2	g	β	χ^2
tree level	$\beta/g = 3.6$		30.			
$+Q'/m_c$ + one-loop with $\sqrt{m_q}$	0.23	0.89	4.3	0.45	2.8	3.7
+ chiral logs	0.25	0.78	4.1	0.56	3.2	1.4
one-loop with nonzero Δ,δ,$v \cdot k$, without analytic m_q terms	0.25	0.86	3.9	0.83	6.0	2.5
order $m_q \sim 1/m_c$ with $\tilde{\kappa}_1 = \kappa_5 = \tilde{\alpha}_1 = \alpha_5 = 0$	0.265	0.85	3.0	0.756	4.9	3.9

Table 3.1: Solutions for g and $\beta(\mathrm{GeV}^{-1})$ which minimize the χ^2 associated with a fit to the three ratios in Eq. (3.28). There are two solutions in the region of interest.

logarithms, $m_q \log(\mu/m_q)$, at scale $\mu = 1\,\mathrm{GeV}$ gives the solutions in the third row. Taking nonzero δ, Δ, and $v \cdot k$ in the non-analytic functions F_1 and F_2 gives the solutions in the fourth row of Table 3.1, where the value of g in the second solution has increased by $\sim$ 50%. For these two solutions only the analytic m_i^2 dependence has been neglected. Finally, the solutions in row five include the analytic m_i^2 dependence with the counterterms set to zero (at $\mu = 1\,\mathrm{GeV}$). The uncertainty associated with these counterterms will be investigated below. It is interesting to note that the extracted value of g in the second column of Table 3.1 changes very little with the addition of the various corrections.

One can see more clearly how these solutions are determined by looking at Fig. 3.5. The central value for each ratio of decay rates in Eq. (3.28) gives a possible contour in the g-β plane, as shown by the solid (D^{*0}), dashed (D^{*+}), and dotted (D_s^*) lines. An exact solution for two of the ratios occurs at the intersection of two of these contour lines. However, a good solution for all three ratios requires a point that is close to all three lines. The solutions in the fifth row of Table 3.1 are indicated by stars in Fig. 3.5. The size of the experimental uncertainties can be seen in the 68% confidence level ellipses which are shown as shaded regions in the figure (for two degrees of freedom they correspond to $\chi^2 \leq \chi^2_{min} + 2.3$). These regions are centered on the solid line since the D^{*0} ratio has the smallest experimental error. The errors in Eq. (3.28) give

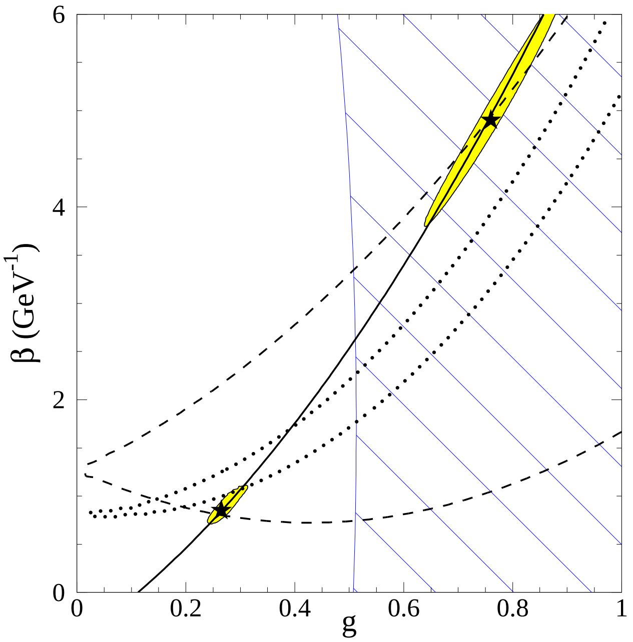

Figure 3.5: Solution contours in the g-β plane for the situation in row 5 of Table 3.1. The solid, dashed, and dotted lines correspond to solution lines for the D^{*0}, D^{*+}, and D_s^* decay rate ratios respectively. The stars correspond to the minimal χ^2 solutions and the shaded regions correspond to the 68% confidence level of experimental error in the fit. The hatched region is excluded by the experimental limit $\Gamma(D^{*+}) < 0.13\,\mathrm{MeV}$ [1].

the following one sigma errors on the two solutions

$$\begin{aligned} g &= 0.265^{+.036}_{-.018} \quad \beta = 0.85^{+.21}_{-.10}\,\mathrm{GeV}^{-1} \,, \\ g &= 0.756^{+0.028}_{-0.027} \quad \beta = 4.90^{+.27}_{-.26}\,\mathrm{GeV}^{-1} \,. \end{aligned} \tag{3.30}$$

Both solutions fit the first two ratios in Eq. (3.28), but do not do as well for the third. Minimizing the χ^2 has biased against the third ratio as a result of its large experimental error. For this ratio the $g = 0.265$ and $g = 0.76$ solutions give values which are 4 and 13 times too small respectively. For the first solution it is possible to improve the fit to the third ratio with reasonably sized counterterms. For instance, simply taking $\tilde{\alpha}_1 = 2$ gives $\mathcal{B}(D_s^* \to D_s\pi^0)/\mathcal{B}(D_s^* \to D_s\gamma) = 0.036$. As we will see below, a large g solution with $\chi^2 \lesssim 1$ is only possible if g increases to ~ 0.9 and β increases to $\sim 6.0\,\mathrm{GeV}^{-1}$ (c.f. Fig. 3.6).

The experimental limit $\Gamma(D^{*+}) < 0.13\,\mathrm{MeV}$ [1] translates into an upper bound on the value of g. Since $\mathcal{B}(D^{*+} \to D^+\gamma)$ is small, this bound is almost β independent and to a good approximation is

$$g < 0.52\sqrt{\sqrt{1+3.01\,x}-1} \qquad\qquad x = \Gamma(D^{*+})^{\,\mathrm{limit}}/(0.13\,\mathrm{MeV})\,. \qquad (3.31)$$

For the situation in row five of Table 3.1 this excludes the hatched region in Fig. 3.5. The limit on $\Gamma(D^{*+})$ therefore eliminates the $g \simeq 0.76$ solution at the two sigma level. Since this limit has not been confirmed by other groups it would be useful to have further experimental evidence that could exclude this solution.

The central values in Eq. (3.30) have uncertainty associated with the parameter m_c. Taking $m_c = 1.4 \pm 0.1\,\mathrm{GeV}$ gives $0.25 < g < 0.28$ and $0.79\,\mathrm{GeV}^{-1} < \beta < 0.93\,\mathrm{GeV}^{-1}$ for the first solution, and $0.72 < g < 0.80$ and $4.6\,\mathrm{GeV}^{-1} < \beta < 5.3\,\mathrm{GeV}^{-1}$ for the second solution (in both cases the χ^2 changes very little). There is also ambiguity in the solution in Eq. (3.30) due to the choice of scale μ (ie., the value of the counterterms α_1, α_5, $\tilde{\kappa}_1$ and κ_5). Increasing μ to $1.3\,\mathrm{GeV}$ gives solutions ($g = 0.28, \beta = 0.91\,\mathrm{GeV}^{-1}, \chi^2 = 1.4$) and ($g = 0.78, \beta = 5.0\,\mathrm{GeV}^{-1}, \chi^2 = 4.1$), while decreasing μ to $0.7\,\mathrm{GeV}$ gives solutions ($g = 0.25, \beta = 0.83\,\mathrm{GeV}^{-1}, \chi^2 = 3.7$) and ($g = 0.72, \beta = 4.7\,\mathrm{GeV}^{-1}, \chi^2 = 3.1$). Note that the χ^2 of the second solution remains large, while the χ^2 of the first solution is reduced significantly by an increased scale.

Another method of testing the effect of the unknown counterterms $\tilde{\alpha}_1$, α_5, $\tilde{\kappa}_1$ and κ_5 is to take their values at $\mu = 1\,\mathrm{GeV}$ to be randomly distributed within some reasonable range of values. We take $-1 < \tilde{\kappa}_1, \kappa_5 < 1$ and $-2 < \tilde{\alpha}_1, \alpha_5 < 2$, with the motivation that the counterterms change the tree level value of Z_π^a and Z_γ^a by less than 30%, and give corrections that are not much bigger than those from the one-loop graphs. Near each of the two solutions 5000 values of g and β were then generated by minimizing the χ^2. This gives the distributions in Fig. 3.6. The solution with $g = 0.265$ and $\beta = 0.85\,\mathrm{GeV}^{-1}$ has fairly small uncertainty from the counterterms. The $g = 0.76$, $\beta = 4.9\,\mathrm{GeV}^{-1}$ solution has much larger uncertainty because the corresponding contour lines in Fig. 3.5 are almost parallel. For this solution the upper

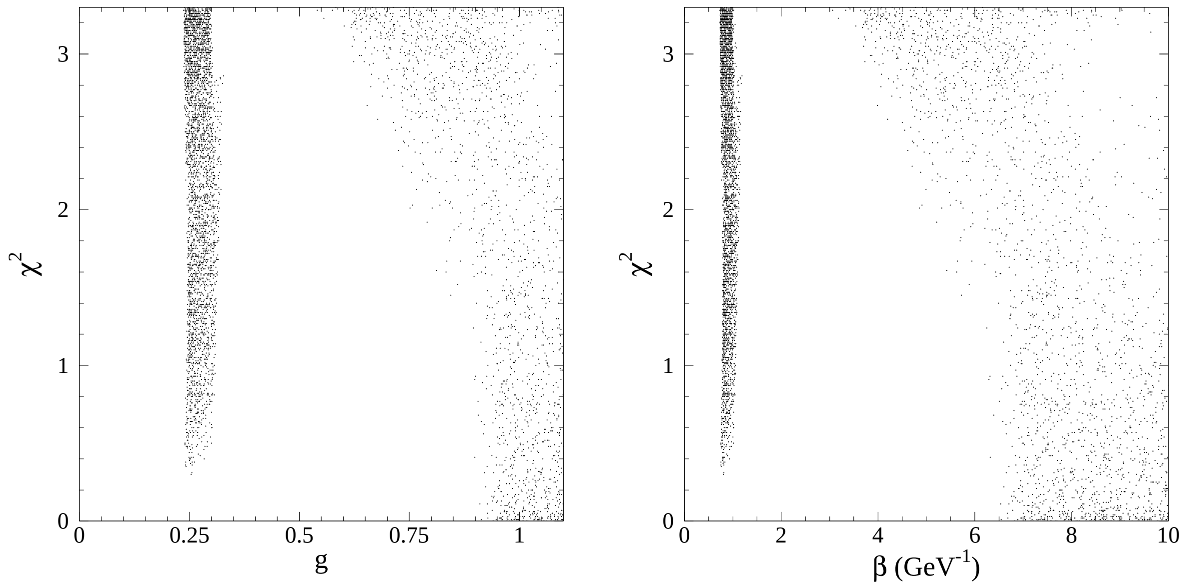

Figure 3.6: Effect of the order m_q counterterms ($\tilde{\kappa}_1$, κ_5, $\tilde{\alpha}_1$, and α_5) on the solutions in Eq. (3.30). The counterterms are taken to be randomly distributed with $-1 < \tilde{\kappa}_1, \kappa_5 < 1$, $-2 < \alpha_1, \alpha_5 < 2$. For each set of counterterms g and β were determined at the new minimal χ^2. 5000 sets were generated near each of the two solutions.

bounds are determined by the limits of a few MeV [57] on the D^* widths. From this analysis we estimate the theoretical uncertainty of the solutions in Eq. (3.30) to be roughly

$$\begin{aligned} g &= 0.265^{+0.05}_{-0.02} \quad \beta = 0.85^{+0.3}_{-0.1}\,\mathrm{GeV}^{-1}\,, \\ g &= 0.76^{+0.2}_{-0.1} \quad \beta = 4.9^{+5.0}_{-0.7}\,\mathrm{GeV}^{-1}\,, \end{aligned} \tag{3.32}$$

at this order in chiral perturbation theory. The errors on g and β are positively correlated since the values of g and β are constrained in one direction by the small error on the D^{*0} rate ratio in Eq. (3.28).

From Eq. (3.31) and Fig. 3.6, we see that if the error in

$$\frac{\mathcal{B}(D_s^* \to D_s\pi^0)}{\mathcal{B}(D_s^* \to D_s\gamma)} \tag{3.33}$$

can be decreased by a factor of two, in conjunction with a limit of $\Gamma(D^{*+}) \lesssim 0.6\,\mathrm{MeV}$ then this could provide strong evidence that the $g = 0.76$ solution is excluded. On the other hand if the central values of the second and third ratios in Eq. (3.28) decrease, then a width measurement or stronger limit on $\Gamma(D^{*+})$ will be needed to distinguish the two solutions.

Using the extracted values of g and β gives the widths shown in Table 3.2. The couplings were extracted at one-loop and order $m_q \sim 1/m_c$, so the predictions for the D^* widths are made at this order. The experimental uncertainty in the D^* widths is estimated by setting g and β to the extremal values in Eq. (3.30), which gives the range shown in the second and fourth rows of the Table. The uncertainty from the unknown counterterms in the third and fifth rows is estimated in the same way using the uncertainties from Eq. (3.32). Note that for the $g = 0.265$ solution the D_s^* width is small due to a delicate cancellation in μ_3 resulting from setting $Z^a_{\rm wf} \times 1/m_c = 1/m_c$. Keeping $Z^a_{\rm wf}/m_c$ to order m_q gives a D_s^* width of $0.28\,{\rm keV}$ with a range of $0.1 - 0.4\,{\rm keV}$ for both the experimental and the counterterm uncertainties.

Making use of HQS allows us to predict the width of the B^* mesons from their dominant mode $B^* \to B\gamma$. Eq. (3.23) gives the rate for $B^* \to B\gamma$ with $Q' = -1/3$ and $m_c \to m_b$. Since the couplings β_1 and β_2 are unknown these rates can not be determined at order $1/m_{c,b}$, but we can include the order m_q corrections. The B meson masses are taken from [57] and we use $m_b = 4.8\,{\rm GeV}$ [107]. We set $\delta = 0.047\,{\rm GeV}$ and $\Delta = k \cdot v = 0$, but since the contribution Q'/m_b in Eq. (3.23) is numerically important it is kept in our estimate. For comparison the widths obtained with the $g = 0.76$ and $\beta = 4.9\,{\rm GeV}^{-1}$ solution are also shown.

As a final comment, we note that heavy meson chiral perturbation theory can also be used to examine excited $D^{(*)}$ mesons, such as the p-wave states, D_0^*, D_1^*, D_1, and D_2^* [109, 110, 111, 90]. To do so, explicit fields for these particles may be added to the Lagrangian giving a new effective theory. For interactions without external excited mesons (such as the ones considered here) these new particles can then contribute as virtual particles. However, since we have not included these heavier particles they are assumed to be 'integrated out', whereby such contributions are absorbed into the definitions of our couplings.

Widths (keV)	D^{*0}	D^{*+}	D^*_s	B^{*+}	B^{*0}	B^*_s
$g = 0.265$, $\beta = 0.85\,\mathrm{GeV}^{-1}$	18	26	0.06	~ 0.06	~ 0.03	~ 0.04
uncertainty from experiment	16 - 24	23 - 35	0.01 - 0.13	–	–	–
uncertainty from counterterms	16 - 27	22 - 39	0.04 - 0.13	–	–	–
$g = 0.76$, $\beta = 4.9\,\mathrm{GeV}^{-1}$	323	448	103	~ 2.1	~ 2.0	~ 1.6
uncertainty from experiment	285 - 367	396 - 508	83 - 128	–	–	–
uncertainty from counterterms	215 - 1318	281 - 1157	53 - 1078	–	–	–

Table 3.2: Predicted widths in keV for the D^* and B^* mesons. The experimental and counterterm ranges are determined by the extremal values of g and β in Eqs. (3.30) and (3.32). For $g = 0.265$ the D^*_s width is small due to a delicate cancellation in μ_3 as explained in the text. The uncertainty in the B^* widths is large due to unknown $1/m_{c,b}$ corrections.

3.4 Summary

For the D^{*0}, D^{*+}, and D^*_s, the decays $D^* \to D\pi$ and $D^* \to D\gamma$ are well described by heavy meson chiral perturbation theory. Using the recent measurement of $\mathcal{B}(D^{*+} \to D^+\gamma)$ [91], the ratios of the $D\gamma$ and $D\pi^0$ branching fractions were used to extract the couplings g and β. Here g and β are the $D^*D\pi$ and $D^*D\gamma$ couplings since order m_q and $1/m_Q$ corrections have been absorbed into their definitions. Two solutions were found

$$
\begin{aligned}
g &= 0.265\,{}^{+.04}_{-.02}\,{}^{+.05}_{-.02} \quad \beta = 0.85^{+.2}_{-.1}{}^{+.3}_{-.1}\,\mathrm{GeV}^{-1} \\
g &= 0.76\,{}^{+.03}_{-.03}\,{}^{+.2}_{-.1} \quad \beta = 4.9^{+.3}_{-.3}{}^{+5.0}_{-.7}\,\mathrm{GeV}^{-1}\,.
\end{aligned}
\tag{3.34}
$$

The first error here is the one sigma error associated with a minimized χ^2 fit to the three experimental branching fraction ratios (see Fig. 3.5). The second error is our estimate of the uncertainty in the extraction due to four unknown counterterms $\tilde{\alpha}_1$, α_5, $\tilde{\kappa}_1$ and κ_5 that arise at order m_q (see Fig. 3.6).

It is possible that the uncertainty from these counterterms can be reduced by determining them from other processes. For these corrections to contribute at low enough order in the chiral expansion we need processes with outgoing photons or pseudo-Goldstone bosons, such as semileptonic D decays to K, η, or π. Here there are also SU(3) corrections to the left handed current which involve an unknown parameter η_0 [82]. Information on κ_1 and κ_1' can be determined from the pole part of the $D_s \to K\ell\nu_\ell$ form factor [82]. In a similar manner $D_s \to \eta\ell\nu_\ell$ can constrain $\tilde{\kappa}_1$ and κ_5, and a comparison of the form factors for $D^+ \to \bar{K}^0\ell\nu_\ell$ and $D_s \to \eta\ell\nu_\ell$ gives information on κ_1' and κ_5. These investigations were beyond the scope of this study. In principle, information about the constants $\tilde{\alpha}_1$, and α_5 could be obtained from a measurement of $B \to \gamma\ell\nu_\ell$. The CLEO experimental bound on $B \to \ell\nu_\ell$ $(\ell = e, \mu)$[112] is roughly two orders of magnitude above the theoretical prediction, but due to the helicity suppression for $B \to \ell\nu_\ell$ the branching ratio for $B \to \gamma\ell\nu_\ell$ may be up to an order of magnitude bigger[113, 114].

Another possible approach would be to use large N_c scaling for the counterterms in $\delta\mathcal{L}_g$ and $\delta\mathcal{L}_\beta$. Terms that have two chiral traces are suppressed by a power of N_c compared to those with only one trace. In the large N_c limit the counterterms $\tilde{\kappa}_1$ and $\tilde{\alpha}_1$ would dominate, and κ_5 and α_5 could be neglected, thus reducing the theoretical uncertainty.

The smaller solution for g in Eq. (3.34) is fairly insensitive to the addition of the one-loop corrections (see Table 3.1). However, corrections at order $m_q \sim 1/m_c$, including the heavy meson mass splittings, were important in determining the solution with larger g. The limit $\Gamma(D^{*+}) < 0.13\,\mathrm{MeV}$ [1] gives an upper bound on the coupling g (see Eq. (3.31) and Fig. 3.5), and eliminates the $g = 0.76$, $\beta = 4.9\,\mathrm{GeV}^{-1}$ solution. Experimental confirmation of this limit is therefore desirable. Note that the largest experimental uncertainty in our extraction comes from the measurement of $\mathcal{B}(D_s^* \to D_s\pi^0)$, and dominates the theoretical uncertainty due to decay via single photon exchange. A better measurement of $\mathcal{B}(D_s^* \to D_s\pi^0)/\mathcal{B}(D_s^* \to D_s\gamma)$ along with a limit $\Gamma(D^{*+}) \lesssim 0.6\,\mathrm{MeV}$ could provide further evidence that the $g = 0.76$ solution is excluded. However, if the central values of the second and third ratios in Eq. (3.28) decrease then a width measurement or stronger limit on $\Gamma(D^{*+})$ will be needed to distinguish the two solutions. An improved measurement of $\mathcal{B}(D_s^* \to D_s\pi^0)$ may also give valuable information on the unknown couplings $\tilde{\kappa}_1$, κ_5, $\tilde{\alpha}_1$, and α_5.

The extraction of g has important consequences for other physical quantities [2-11]. For example[4], for the $B \to \pi\ell\bar{\nu}_\ell$ form factors with $E_\pi < 2\,m_\pi$, analyticity bounds combined with chiral perturbation theory give $g\,f_B \lesssim 50\,\mathrm{MeV}$ [115]. The solution $g = 0.265$ gives $f_B \lesssim 190\,\mathrm{MeV}$ for the B decay constant. However, for $g = 0.76$ we have $f_B \lesssim 66\,\mathrm{MeV}$, which is roughly a factor of three smaller than lattice QCD values, $f_B \simeq 160 - 205$ [116, 117, 118, 119, 120, 121, 122].

---

[4] Glenn Boyd and Ben Grinstein, private communication.

Chapter 4 V_{ub} from Exclusive Semileptonic B and D Decays

The next generation of B decay experiments will test the flavor sector of the standard model at high precision. The basic approach is to determine the elements of the CKM matrix using different methods and then check for the consistency of these results. At the present time CP non-conservation has only been observed in kaon decay arising from $K^0 - \bar{K}^0$ mixing. Many extensions of the minimal standard model (e.g., models with several Higgs doublets or low energy supersymmetry) have new particles with weak scale masses that contribute to flavor changing neutral current processes like $K^0 - \bar{K}^0$ mixing, $B^0 - \bar{B}^0$ mixing, $B \to K^* \gamma$, etc., at a level comparable to the standard model.

At the present time, the magnitude of the $b \to u$ CKM matrix element is determined by comparing experimental results on the inclusive electron spectrum in the endpoint region with phenomenological models [123], or by comparing experimental results on $B \to \rho\, \ell\, \bar{\nu}_\ell$ and $B \to \pi\, \ell\, \bar{\nu}_\ell$ with phenomenological models and lattice QCD results [124]. These two approaches yield remarkably consistent determinations of $|V_{ub}|$, but have large uncertainties.

In this chapter we discuss the proposal to determine $|V_{ub}|$ [125, 126] using a combination of heavy quark symmetry [20, 21] and $SU(3)$ flavor symmetry. The basic idea is to compare $D \to K^*\, \bar{\ell}\, \nu_\ell$ with the Cabibbo suppressed decay $D \to \rho\, \bar{\ell}\, \nu_\ell$. Using heavy quark symmetry the $SU(3)$ violations in the form factors that occur in these decays are related to those that occur in a comparison of $B \to K^* \ell\, \bar{\ell}$ (or $B \to K^*\, \nu_\ell\, \bar{\nu}_\ell$) with $B \to \rho\, \ell\, \bar{\nu}_\ell$. Therefore, experimental data on $B \to K^* \ell\, \bar{\ell}$ in conjunction with data on $D \to \rho\, \bar{\ell}\, \nu_\ell$ and $D \to K^*\, \bar{\ell}\, \nu_\ell$ can be used to determine $|V_{ub}|$. This proposal is complementary to other approaches for determining $|V_{ub}|$, since it relies on the standard model correctly describing the rare flavor changing neutral current process

$B \to K^* \ell\, \bar{\ell}$.

In this chapter we compute corrections to these form factor relations which violate both chiral and heavy quark symmetry, and are non-analytic in the symmetry breaking parameters. We also reconsider the influence of long distance effects on the extraction of the $B \to K^*$ form factors from $B \to K^* \ell\, \bar{\ell}$.

We denote the form factors relevant for semileptonic transitions between a pseudoscalar meson $P^{(Q)}$, containing a heavy quark Q, and a member of the lowest lying multiplet of vector mesons, V, by $g^{(H\to V)}$, $f^{(H\to V)}$ and $a_\pm^{(H\to V)}$, where

$$\begin{aligned} \langle V(p',\epsilon)|\, \bar{q}\, \gamma_\mu\, Q\, |H(p)\rangle &= i\, g^{(H\to V)}\, \varepsilon_{\mu\nu\lambda\sigma}\, \epsilon^{*\nu}\, (p+p')^\lambda\, (p-p')^\sigma\,, \\ \langle V(p',\epsilon)|\, \bar{q}\, \gamma_\mu \gamma_5\, Q\, |H(p)\rangle &= f^{(H\to V)}\, \epsilon^*_\mu + a_+^{(H\to V)}\, (\epsilon^*\cdot p)\, (p+p')_\mu \\ &\quad + a_-^{(H\to V)}\, (\epsilon^*\cdot p)\, (p-p')_\mu\,, \end{aligned} \tag{4.1}$$

and $\varepsilon^{0123} = -\varepsilon_{0123} = 1$. We view the form factors g, f and $a_\pm$ as functions of the dimensionless variable $y = v\cdot v'$, where $p = m_H\, v$, $p' = m_V\, v'$, and $q^2 = (p-p')^2 = m_H^2 + m_V^2 - 2 m_H\, m_V\, y$. (Although we are using the variable $v\cdot v'$, we are not treating the quarks in V as heavy.) The experimental values for the $D \to K^*\, \bar{\ell}\, \nu_\ell$ form factors assuming nearest pole dominance for the q^2 dependences are [127]

$$\begin{aligned} f^{(D\to K^*)}(y) &= \frac{(1.9 \pm 0.1)\,\mathrm{GeV}}{1+0.63\,(y-1)}\,, \\ a_+^{(D\to K^*)}(y) &= -\frac{(0.18 \pm 0.03)\,\mathrm{GeV}^{-1}}{1+0.63\,(y-1)}\,, \\ g^{(D\to K^*)}(y) &= -\frac{(0.49 \pm 0.04)\,\mathrm{GeV}^{-1}}{1+0.96\,(y-1)}\,. \end{aligned} \tag{4.2}$$

The shapes of these form factors are beginning to be probed experimentally [127]. The form factor a_- is not measured because its contribution to the $D \to K^*\, \bar{\ell}\, \nu_\ell$ decay amplitude is suppressed by the lepton mass. The minimal value of y is unity (corresponding to the zero recoil point) and the maximum value of y is $(m_D^2 + m_{K^*}^2)/(2 m_D\, m_{K^*}) \simeq 1.3$ (corresponding to $q^2 = 0$). Note that $f(y)$ changes by less than 20% over the whole kinematic range $1 < y < 1.3$. In the following analysis we will extrapolate the measured form factors to the larger region $1 < y < 1.5$. The full kinematic region for $B \to \rho\,\ell\,\bar{\nu}_\ell$ is $1 < y < 3.5$.

The differential decay rate for semileptonic B decay (neglecting the lepton mass, and not summing over the lepton type ℓ) is

$$\frac{\mathrm{d}\Gamma(B \to \rho\,\ell\,\bar{\nu}_\ell)}{\mathrm{d}y} = \frac{G_F^2\,|V_{ub}|^2}{48\,\pi^3}\,m_B\,m_\rho^2\,S^{(B\to\rho)}(y)\,. \tag{4.3}$$

Here $S^{(H\to V)}(y)$ is the function

$$\begin{aligned} S^{(H\to V)}(y) &= \sqrt{y^2-1}\,\Big[\Big|f^{(H\to V)}(y)\Big|^2\,(2+y^2-6yr+3r^2) \\ &\quad + 4\mathrm{Re}\Big[a_+^{(H\to V)}(y)\,f^{(H\to V)}(y)\Big]m_H^2\,r\,(y-r)(y^2-1) \\ &\quad + 4\Big|a_+^{(H\to V)}(y)\Big|^2 m_H^4\,r^2(y^2-1)^2 \\ &\quad + 8\Big|g^{(H\to V)}(y)\Big|^2 m_H^4\,r^2(1+r^2-2yr)(y^2-1)\,\Big] \\ &= \sqrt{y^2-1}\,\Big|f^{(H\to V)}(y)\Big|^2\,(2+y^2-6yr+3r^2)\,[1+\delta^{(H\to V)}(y)]\,, \end{aligned} \tag{4.4}$$

with $r = m_V/m_H$. The function $\delta^{(H\to V)}$ depends on the ratios of form factors $a_+^{(H\to V)}/f^{(H\to V)}$ and $g^{(H\to V)}/f^{(H\to V)}$. $S^{(B\to\rho)}(y)$ can be estimated using combinations of $SU(3)$ flavor symmetry and heavy quark symmetry. $SU(3)$ symmetry implies that the $\bar{B}^0 \to \rho^+$ form factors are equal to the $B \to K^*$ form factors and the $B^- \to \rho^0$ form factors are equal to $1/\sqrt{2}$ times the $B \to K^*$ form factors. Heavy quark symmetry implies the relations [125]

$$\begin{aligned} f^{(B\to K^*)}(y) &= \left(\frac{m_B}{m_D}\right)^{1/2}\left[\frac{\alpha_s(m_b)}{\alpha_s(m_c)}\right]^{-6/25} f^{(D\to K^*)}(y)\,, \\ a_+^{(B\to K^*)}(y) &= \left(\frac{m_D}{m_B}\right)^{1/2}\left[\frac{\alpha_s(m_b)}{\alpha_s(m_c)}\right]^{-6/25} a_+^{(D\to K^*)}(y)\,, \\ g^{(B\to K^*)}(y) &= \left(\frac{m_D}{m_B}\right)^{1/2}\left[\frac{\alpha_s(m_b)}{\alpha_s(m_c)}\right]^{-6/25} g^{(D\to K^*)}(y)\,. \end{aligned} \tag{4.5}$$

The second relation is obtained using $a_-^{(D\to K^*)} = -a_+^{(D\to K^*)}$, valid in the large m_c limit.

Using Eq. (4.5) and $SU(3)$ to get $\bar{B}^0 \to \rho^+ \, \ell \, \bar{\nu}_\ell$ form factors (in the region $1 < y < 1.5$) from those for $D \to K^* \bar{\ell} \, \nu_\ell$ given in Eq. (4.2) yields $S^{(B\to\rho)}(y)$ plotted in Fig. 4.1 of Ref. [126]. The numerical values in Eq. (4.2) differ slightly from those used in Ref. [126]. This makes only a small difference in $S^{(B\to\rho)}$, but changes $\delta^{(B\to\rho)}$ more significantly. In the region $1 < y < 1.5$, $|\delta^{(B\to\rho)}(y)|$ defined in Eq. (4.4) is less than 0.06, indicating that $a_+^{(B\to\rho)}$ and $g^{(B\to\rho)}$ make a small contribution to the differential rate in this region.

This prediction for $S^{(B\to\rho)}$ can be used to determine $|V_{ub}|$ from a measurement of the $B \to \rho \, \ell \, \bar{\nu}_\ell$ semileptonic decay rate in the region $1 < y < 1.5$. This method is model independent, but cannot be expected to yield a very accurate value of $|V_{ub}|$. Typical $SU(3)$ violations are at the $10 - 20\%$ level and one expects similar violations of heavy quark symmetry.

Ref. [126] proposed a method for getting a value of $S^{(B\to\rho)}(y)$ with small theoretical uncertainty. They noted that the "Grinstein-type" [81] double ratio

$$R(y) = \Big[f^{(B\to\rho)}(y) / f^{(B\to K^*)}(y) \Big] \Big/ \Big[f^{(D\to\rho)}(y) / f^{(D\to K^*)}(y) \Big] \tag{4.6}$$

is unity in the limit of $SU(3)$ symmetry or in the limit of heavy quark symmetry. Corrections to the prediction $R(y) = 1$ are suppressed by $m_s/m_{c,b}$ ($m_{u,d} \ll m_s$) instead of $m_s/\Lambda_{\rm QCD}$ or $\Lambda_{\rm QCD}/m_{c,b}$. Since $R(y)$ is very close to unity, the relation

$$S^{(B\to\rho)}(y) = S^{(B\to K^*)}(y) \left| \frac{f^{(D\to\rho)}(y)}{f^{(D\to K^*)}(y)} \right|^2 \left(\frac{m_B - m_\rho}{m_B - m_{K^*}} \right)^2 , \tag{4.7}$$

together with measurements of $|f^{(D\to K^*)}|$, $|f^{(D\to\rho)}|$, and $S^{(B\to K^*)}$ will determine $S^{(B\to\rho)}$ with small theoretical uncertainty. The last term on the right-hand-side makes Eq. (4.7) equivalent to Eq. (4.6) in the $y \to 1$ limit. The ratio of the $(2 + y^2 - 6yr + 3r^2)\,[1 + \delta^{(B\to V)}(y)]$ terms makes only a small and almost y-independent contribution to $S^{(B\to\rho)}/S^{(B\to K^*)}$ in the range $1 < y < 1.5$. Therefore, corrections to Eq. (4.7) are at most a few percent larger than those to $R(y) = 1$.

$|f^{(D\to K^*)}|$ has already been determined. $|f^{(D\to\rho)}|$ may be obtainable in the future, for example from experiments at B factories, where improvements in particle identification help reduce the background from the Cabibbo allowed decay. The measurement $\mathcal{B}(D \to \rho^0\, \bar{\ell}\, \nu_\ell)/\mathcal{B}(D \to \bar{K}^{*0}\, \bar{\ell}\, \nu_\ell) = 0.047 \pm 0.013$ [128] already suggests that $|f^{(D\to\rho)}/f^{(D\to K^*)}|$ is close to unity. Assuming $SU(3)$ symmetry for the form factors, but keeping the explicit m_V-dependence in $S^{(D\to V)}(y)$ and in the limits of the y integration, the measured form factors in Eq. (4.2) imply $\mathcal{B}(D \to \rho^0\, \bar{\ell}\, \nu_\ell)/\mathcal{B}(D \to \bar{K}^{*0}\, \bar{\ell}\, \nu_\ell) = 0.044$.[1] $S^{(B\to K^*)}$ is obtainable from experimental data on $B \to K^*\, \nu_\ell\, \bar{\nu}_\ell$ or $B \to K^* \ell\, \bar{\ell}$. While the former process is very clean theoretically, it is very difficult experimentally. A more realistic goal is to use $B \to K^* \ell\, \bar{\ell}$, since CDF expects to observe $400-1100$ events in the Tevatron run II (if the branching ratio is in the standard model range) [129]. There are some uncertainties associated with long distance nonperturbative strong interaction physics in this extraction of $S^{(B\to K^*)}(y)$. To use the kinematic region $1 < y < 1.5$, the form factor ratio $f^{(D\to\rho)}/f^{(D\to K^*)}$ in Eq. (4.7) must be extrapolated to a greater region than what can be probed experimentally. For this ratio, the uncertainty related to this extrapolation is likely to be small.

The main purpose of this study is to examine the deviation of R from unity using chiral perturbation theory. We find that it is at the few percent level. The uncertainty from long distance physics in the extraction of $S^{(B\to K^*)}$ is also reviewed. On average, in the region $1 < y < 1.5$, this is probably less than a 10% effect on the $B \to K^* \ell\, \bar{\ell}$ decay rate. Consequently, a determination of $|V_{ub}|$ from experimental data on $D \to K^* \bar{\ell}\, \nu_\ell$, $D \to \rho\, \bar{\ell}\, \nu_\ell$, $B \to K^* \ell\, \bar{\ell}$ and $B \to \rho\, \ell\, \bar{\nu}_\ell$ with an uncertainty from theory of about 10% is feasible.

4.1 Chiral perturbation theory for the form factor ratio

The leading deviation of R from unity can be calculated using a combination of heavy hadron chiral perturbation theory for the mesons containing a heavy quark

---

[1] This prediction would be $|V_{cd}/V_{cs}|^2/2 \simeq 0.026$ with $m_\rho = m_{K^*}$. Phase space enhances $D \to \rho$ compared to $D \to K^*$ to yield the quoted prediction.

(section 2.2.1) and for the lowest lying vector mesons (section 2.2.2). We adopt the notations and conventions of Refs. [79, 58]. The weak current transforms as $(\bar{3}_L, 1_R)$, and at the zero recoil kinematic point there are two operators that are relevant for $P^{(Q)} \to V$ transition matrix elements (where $P^{(b)} = B$, $P^{(c)} = D$, and V is one of the lowest lying vector mesons ρ, ω, K^*, ϕ). Demanding that the Zweig suppressed $D_s \to \omega\, \bar{\ell}\, \nu_\ell$ process vanishes relates the two operators, yielding [83]

$$\bar{q}_a\, \gamma_\mu (1-\gamma_5)\, Q = \beta\, \mathrm{Tr}[\not{N}^\dagger_{cb} \gamma_\mu (1-\gamma_5) H_c^{(Q)} \xi^\dagger_{ba}]\,, \tag{4.8}$$

where N_{cb} is given in Eq. (2.27). Here repeated $SU(3)$ indices are summed and the trace is over Lorentz indices. $H^{(Q)}$ contains the ground state heavy meson doublet, N is the nonet vector meson matrix [58], and β is a constant. The leading contribution to $R(1)-1$ arises from the Feynman diagrams in Fig. 4.1. Diagrams with a virtual kaon cancel in the double ratio R. Neglecting the vector meson widths,[2] these diagrams yield

$$R(1)-1 = -\frac{g\, g_2}{12\, \pi^2 f^2} \Big[G(m_\pi, \Delta^{(b)}) - G(m_\eta, \Delta^{(b)}) - G(m_\pi, \Delta^{(c)}) + G(m_\eta, \Delta^{(c)}) \Big]\,, \tag{4.9}$$

where $\Delta^{(b)} = m_{B^*} - m_B$, $\Delta^{(c)} = m_{D^*} - m_D$, and for $m \geq \Delta$,

$$G(m, \Delta) = \frac{\pi\, m^3}{2\,\Delta} - \frac{(m^2-\Delta^2)^{3/2}}{\Delta}\, \arctan\left(\frac{\sqrt{m^2-\Delta^2}}{\Delta} \right) - \Delta^2 \ln m\,. \tag{4.10}$$

Here g_2 is the $\rho\,\omega\,\pi$ coupling, g is the $DD^*\pi$ coupling, and $f \simeq 131\,\mathrm{MeV}$ is the pion decay constant. In the nonrelativistic constituent quark model $g = g_2 = 1$ [79], while in the chiral quark model [55] $g = g_2 = 0.75$. Experimental data on $\tau \to \omega\,\pi\,\nu_\tau$ in the region of low $\omega\,\pi$ invariant mass gives $g_2 \simeq 0.6$ [130]. In chapter 3 we saw that the measured branching ratios for D^* decays give $g = 0.27$ or $g = 0.76$.

For small Δ, Eq. (4.9) for $R(1)-1$ has a non-analytic $\sqrt{m_q}$ dependence on the light quark masses. This cannot arise from corrections to the current in Eq. (4.8) or

---

[2] The only significant width is that of the ρ meson. Since it occurs in the loop graph involving an η, neglecting the ρ width amounts to treating $\Gamma_\rho/2m_\eta \ll 1$, which is a reasonable approximation.

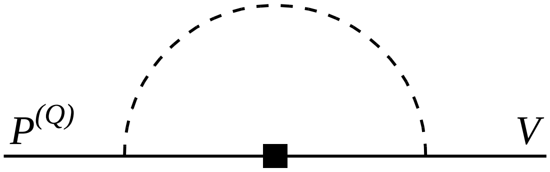

Figure 4.1: Feynman diagram that gives the leading contribution to $R(1)-1$. The dashed line is a π or an η. The black square indicates insertion of the weak current.

to the chiral Lagrangian, and must come from 1-loop diagrams involving the pseudo-Goldstone bosons π, K, η. Using the measured values of the pion and eta masses, Eqs. (4.9) and (4.10) imply $R(1) = 1 - 0.035\, g\, g_2$. There may be significant corrections from analytic terms of order $m_s/m_c \sim 1/10$ or from higher orders in chiral perturbation theory. However, the smallness of our result lends support to the expectation that $R(1)-1$ is very close to zero. There is no reason to expect any different conclusion over the kinematic range $1 < y < 1.5$.

4.2 Long distance effects and extracting $S^{(B\to K^*)}$

The decay rate for $B \to K^*\, \nu_\ell\, \bar\nu_\ell$ could determine $S^{(B\to K^*)}$ free of theoretical uncertainties. However, experimental study of this decay is very challenging. A more practical approach to extracting this quantity is to use $B \to K^* \ell\, \bar\ell$. The differential decay rate is

$$\begin{aligned} \frac{\mathrm{d}\Gamma(B\to K^*\ell\,\bar\ell)}{\mathrm{d}y} &= \frac{G_F^2\, |V_{ts}^* V_{tb}|^2}{24\,\pi^3} \left(\frac{\alpha}{4\pi}\right)^2 m_B\, m_{K^*}^2 \left[|\widetilde{C}_9(y)|^2 + |C_{10}|^2\right] [1+\Delta(y)] \\ &\quad \times S^{(B\to K^*)}(y)\, [1+d(y)]\,. \end{aligned} \tag{4.11}$$

This and Eq. (4.7) allow us to rewrite Eq. (4.3) as

$$\begin{aligned} \frac{\mathrm{d}\Gamma(B\to \rho\,\ell\,\bar\nu_\ell)}{\mathrm{d}y} &= \frac{|V_{ub}|^2}{|V_{ts}^* V_{tb}|^2}\, \frac{8\,\pi^2}{\alpha^2}\, \frac{1}{|\widetilde{C}_9(y)|^2 + |C_{10}|^2}\, \frac{1}{1+\Delta(y)}\, \frac{1}{1+d(y)}\, \frac{m_\rho^2}{m_{K^*}^2} \\ &\quad \times \left(\frac{m_B - m_\rho}{m_B - m_{K^*}}\right)^2 \left|\frac{f^{(D\to\rho)}(y)}{f^{(D\to K^*)}(y)}\right|^2 \frac{\mathrm{d}\Gamma(B\to K^*\ell\,\bar\ell)}{\mathrm{d}y}\,. \end{aligned} \tag{4.12}$$

which can be directly used to extract $|V_{ub}|$. Unitarity of the CKM matrix implies that $|V_{ts}^* V_{tb}| \simeq |V_{cs}^* V_{cb}|$ with less than a 3% uncertainty. The fine structure constant, $\alpha = 1/129$, is evaluated at the W-boson mass. $d(y)$ parameterizes long distance effects, and will be discussed below. $\Delta(y)$ takes into account the contribution of the magnetic moment operator, $O_7 = (e/16\pi^2)\, m_b\, (\bar{s}_L\, \sigma_{\mu\nu}\, b_R)\, F^{\mu\nu}$ (a factor of $-4G_F V_{ts}^* V_{tb}/\sqrt{2}$ has been extracted out in the definition of operator coefficients). Ref. [126] (see also Ref. [131]) found using heavy quark symmetry that $\Delta(y) \simeq -0.14 - 0.08(y-1)$ in the region $1 < y < 1.5$. Corrections to this are expected to be small since there are no $1/m_c$ corrections to $\Delta(1)$. C_{10} is the Wilson coefficient of the operator $O_{10} = (e^2/16\pi^2)\, (\bar{s}_L\, \gamma_\mu\, b_L)(\bar{\ell}\, \gamma^\mu \gamma_5\, \ell)$. $\widetilde{C}_9(y)$ takes into account the contribution of the four-quark operators, $O_1 - O_6$, and the operator $O_9 = (e^2/16\pi^2)\, (\bar{s}_L\, \gamma_\mu\, b_L)\, (\bar{\ell}\, \gamma^\mu\, \ell)$. In perturbation theory using the next-to-leading logarithmic approximation [132, 133]

$$\begin{aligned} \widetilde{C}_9(y) &= C_9 + h(z,y)\,(3C_1 + C_2 + 3C_3 + C_4 + 3C_5 + C_6) - \frac{1}{2}\, h(0,y)\,(C_3 + 3C_4) \\ &\quad - \frac{1}{2}\, h(1,y)\,(4C_3 + 4C_4 + 3C_5 + C_6) + \frac{2}{9}\,(3C_3 + C_4 + 3C_5 + C_6)\,, \end{aligned} \tag{4.13}$$

where $z = m_c/m_b$. Here

$$h(u,y) = -\frac{8}{9}\ln u + \frac{8}{27} + \frac{4}{9}\,x - \frac{2}{9}\,(2+x)\sqrt{|1-x|}\begin{cases} \ln\dfrac{1+\sqrt{1-x}}{1-\sqrt{1-x}} - i\pi\,; & x<1 \\ 2\arctan(1/\sqrt{x-1})\,; & x>1\,, \end{cases} \tag{4.14}$$

where $x \equiv 4u^2 m_b^2/(m_B^2 + m_{K^*}^2 - 2m_B\, m_{K^*}\, y)$. Using $m_t = 175\,\mathrm{GeV}$, $m_b = 4.8\,\mathrm{GeV}$, $m_c = 1.4\,\mathrm{GeV}$, $\alpha_s(m_W) = 0.12$, and $\alpha_s(m_b) = 0.22$, the numerical values of the Wilson coefficients are $C_1 = -0.26$, $C_2 = 1.11$, $C_3 = 0.01$, $C_4 = -0.03$, $C_5 = 0.008$, $C_6 = -0.03$, $C_7 = -0.32$, $C_9 = 4.26$, and $C_{10} = -4.62$. Of these, C_9 and C_{10} are sensitive to m_t (quadratically for $m_t \gg m_W$).

In Eq. (4.13) the second term on the right-hand-side, proportional to $h(z,y)$ comes from charm quark loops. Since the kinematic region we are interested in is close to $q^2 = 4m_c^2$, a perturbative calculation of the $c\,\bar{c}$ loop cannot be trusted. Threshold effects which spoil local duality are important. It is these long distance effects that give rise to the major theoretical uncertainty in the extraction of $|V_{ub}|$ from the $B \to K^* \ell \, \bar{\ell}$ differential decay rate using Eq. (4.12).[3] The influence of this long distance physics on the differential decay rate is parameterized by $d(y)$ in Eq. (4.11), where setting $d(y) = 0$ gives the perturbative result.

For the part of the $c \, \bar{c}$ loop where the charm quarks are not far off-shell, a model for $h(z, y)$ which sums over 1^{--} $c \, \bar{c}$ resonances is more appropriate than the perturbative calculation. Consequently, we model the part of $h(z, y)$ with explicit q^2-dependence in Eq. (4.14) with a sum over resonances [134, 135, 136, 137] calculated using factorization

$$h(z, y) \to -\frac{8}{9} \ln z + \frac{8}{27} - \frac{3\pi\kappa}{\alpha^2} \sum_n \frac{\Gamma_{\psi^{(n)}} \, \mathcal{B}(\psi^{(n)} \to \ell \, \bar{\ell})}{(q^2 - M^2_{\psi^{(n)}})/M_{\psi^{(n)}} + i\Gamma_{\psi^{(n)}}} \, . \tag{4.15}$$

The resonances $\psi^{(n)}$ have masses 3.097 GeV, 3.686 GeV, 3.770 GeV, 4.040 GeV, 4.160 GeV, and 4.415 GeV, respectively, and their widths $\Gamma_{\psi^{(n)}}$ and leptonic branching ratios $\mathcal{B}(\psi^{(n)} \to \ell \, \bar{\ell})$ are known [57]. The factor $\kappa = 2.3$ takes into account the deviation of the factorization model [138] parameter a_2 from its perturbative value. Denoting the value of $\widetilde{C}_9(y)$ in this model by $\widetilde{C}_9'(y)$, its influence on the differential decay rate is given by $d(y)$ defined as

$$|\widetilde{C}_9'(y)|^2 + |C_{10}|^2 = (|\widetilde{C}_9(y)|^2 + |C_{10}|^2) \, [1 + d(y)] \, . \tag{4.16}$$

$d(y)$ is plotted in Fig. 4.2 (solid curve). The physical interpretation of the 1^{--} resonances above 4 GeV is not completely clear. It might be more appropriate to treat them as $D\bar{D}$ resonances than as $c \, \bar{c}$ states. It is possible that for these resonances factorization as modeled by Eq. (4.15) with $\kappa = 2.3$ is not a good approximation. Including only the first three 1^{--} resonances in Eq. (4.15), yields $d(y)$ plotted with the dashed curve in Fig. 4.2.

This estimate of $d(y)$ based on factorization and resonance saturation differs from that in Ref. [126] in two respects. Firstly, the phase of κ is viewed as fixed because

---

[3] The four-quark operators involving light u, d, and s quarks also have uncertainty from long distance physics. However, this is expected to have a very small effect on the $B \to K^* \ell \, \bar{\ell}$ rate.

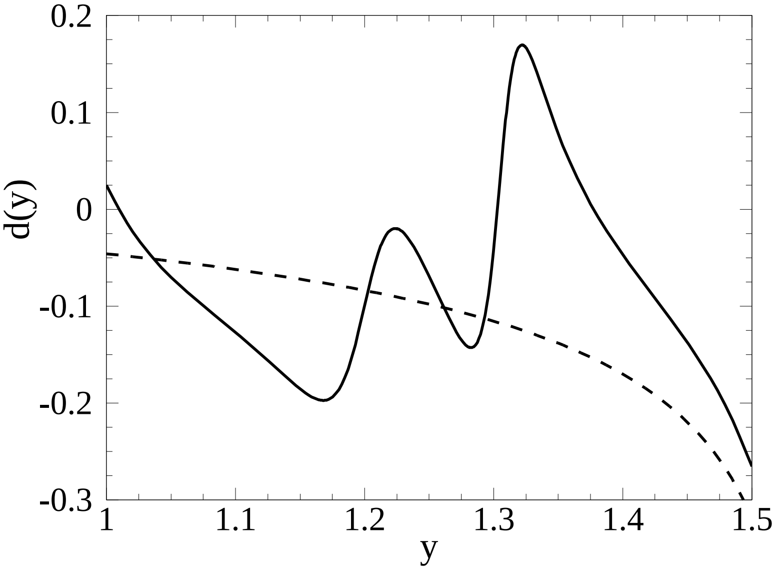

Figure 4.2: $d(y)$ defined in Eq. (4.16). The solid curve takes into account all six 1^{--} $c\,\bar{c}$ resonances according to Eq. (4.15), whereas the dashed curve is obtained including only the three lightest ones.

recent data has determined the sign of the ratio of factorization model parameters, a_2/a_1, and the phase of a_1 is expected to be near its perturbative value [139]. Secondly, since the resonance saturation model only represents the $c\,\bar{c}$ loop for charm quarks that are not far off-shell, we have only used it for the part of $h(z,y)$ in Eq. (4.14) with explicit q^2 dependence, retaining the perturbative expression for the first two terms, $-(8/9)\ln z + 8/27$. The $\ln z$ term has dependence on m_b, which is clearly short distance in origin. This reduces somewhat the magnitude of $d(y)$ and makes it more symmetric about zero (compare Fig. 4.2 with Fig. 6 of Ref. [126]). It would be interesting to have a more physical separation between the long and short distance parts of the amplitude.

Whether it is reasonable to use factorization for the resonances above 4 GeV can be tested experimentally, since these states cause a very distinctive pattern in $\mathrm{d}\Gamma/\mathrm{d}y$. In Fig. 4.3 the shape of $\mathrm{d}\Gamma/\mathrm{d}y$ is plotted in the region $1 < y < 1.5$ using the resonance saturation model for $d(y)$ (solid curve). Experimental support for this shape would provide evidence that this model correctly describes the long distance physics parameterized by $d(y)$. Although $d(y)$ gets as large as ± 0.2, since it oscillates, its influence

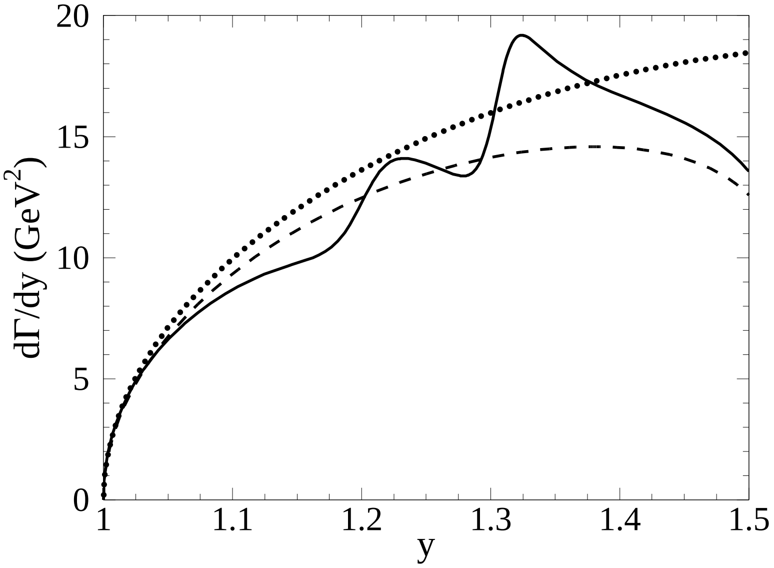

Figure 4.3: $\mathrm{d}\Gamma(B \to K^*\ell\,\bar\ell)/\mathrm{d}y$ in units of $[|\widetilde{C}_9(1)|^2 + |C_{10}|^2]\, m_B\, m_{K^*}^2\, G_F^2\, \alpha^2 \times |V_{ts}^* V_{tb}|^2/(384\pi^5)$ as given in Eq. (4.11). The solid curve takes into account all six 1^{--} $c\,\bar c$ resonances, the dashed curve includes only the three lightest ones, and the dotted curve is the perturbative result (i.e., $d(y) = 0$).

on the $B \to K^*\ell\,\bar\ell$ decay rate in the region $1 < y < 1.5$ is about -8% compared to the perturbative result (which is plotted with the dotted curve in Fig. 4.3). Even if our estimates of this long distance physics based on factorization and resonance saturation has a 100% uncertainty (a prospect that we do not consider particularly unlikely), it will only cause about a 4% uncertainty in this determination of $|V_{ub}|$. Including only the first three 1^{--} resonances in the sum in Eq. (4.15) yields the dashed curve in Fig. 4.3. In this case $d(y)$ causes a -13% change in the $B \to K^*\ell\,\bar\ell$ decay rate in the region $1 < y < 1.5$.

4.3 Nearer term prospects

Without information on the y spectrum for the B decay rates in Eq. (4.12), it is still possible to determine $|V_{ub}|$ by comparing the branching ratios for $B \to \rho\,\ell\,\bar\nu_\ell$ and $B \to K^*\ell\,\bar\ell$ in the region $1 < y < 1.5$. Integrating Eq. (4.12) over $1 < y < 1.5$ we can write

$$\Gamma(\bar{B}^0 \to \rho^+\,\ell\,\bar{\nu}_\ell)\Big|_{y<1.5} \;=\; \frac{|V_{ub}|^2}{|V_{ts}^*V_{tb}|^2}\,\frac{8\pi^2}{\alpha^2}\,\frac{1}{\overline{C}_9^2 + C_{10}^2}\,\frac{1}{(1+\overline{\Delta})}\,\frac{1}{(1+\overline{d})} \qquad (4.17)$$

$$\times\,\frac{m_\rho^2}{m_{K^*}^2}\left(\frac{m_B - m_\rho}{m_B - m_{K^*}}\right)^2 \left|\frac{f^{(D\to\rho)}(1)}{f^{(D\to K^*)}(1)}\right|^2 \Gamma(B \to K^*\ell\,\bar{\ell})\Big|_{y<1.5}\,.$$

Here the barred quantities, $\overline{C}_9^2$, $\overline{\Delta}$, and $\overline{d}$ denote the averages of $|\widetilde{C}_9(y)|^2$, $\Delta(y)$, and $d(y)$ weighted with $S^{(B\to K^*)}(y)$. Using the shape for $S^{(B\to K^*)}$ predicted from heavy quark symmetry, we find $\overline{C}_9 = 4.58$, $\overline{\Delta} = -0.16$, and $\overline{d} = -0.08$. Note that the y-dependence of $\widetilde{C}_9$ is small and $\overline{C}_9$ is close to C_9. In Eq. (4.17) the y-dependence of the ratio $f^{(D\to\rho)}(y)/f^{(D\to K^*)}(y)$ has been neglected. If the shape of these form factors can be approximated with a pole form, then the pole masses of 2.56 GeV for $f^{(D\to K^*)}$ and 2.45 GeV for $f^{(D\to\rho)}$ (corresponding to D_s^{**} and to D^{**}) imply that $|f^{(D\to\rho)}(y)/f^{(D\to K^*)}(y)|^2$ varies by less than 1% over the range $1 < y < 1.5$. $SU(3)$ symmetry and the measured $D \to K^*$ form factors imply that $\delta^{(D\to\rho)}$ contributes only about 23% of the $D \to \rho\,\bar{\ell}\,\nu_\ell$ decay rate. Using this prediction for $\delta^{(D\to\rho)}$, and assuming that $f^{(D\to\rho)}$ and $f^{(D\to K^*)}$ have the same y-dependence, yields $\mathcal{B}(D \to \rho^0\,\bar{\ell}\,\nu_\ell)/\mathcal{B}(D \to \bar{K}^{*0}\,\bar{\ell}\,\nu_\ell) = 0.044\,|f^{(D\to\rho)}(1)/f^{(D\to K^*)}(1)|^2$.

In the region $q^2 = (p_\ell + p_{\bar{\ell}})^2 < m_{J/\psi}^2$ (corresponding roughly to $y > 2$), one cannot use the double ratio and Eq. (4.12). Moreover, the O_7 contribution to the $B \to K^*\ell\,\bar{\ell}$ rate is large and proportional to $1/q^2$, so the (leading order) heavy quark symmetry relations between the tensor and (axial-)vector form factors[4] introduce a significant uncertainty. For $q^2 < m_{J/\psi}^2$, one can do better using $SU(3)$ flavor symmetry alone to predict $\mathrm{d}\Gamma(B \to \pi\,\ell\,\bar{\nu}_\ell)/\mathrm{d}q^2$ from a measurement of $\mathrm{d}\Gamma(B \to K\ell\,\bar{\ell})/\mathrm{d}q^2$. Since this region is far from $q_{\max}^2$, the B^* pole contribution [72, 23, 24, 141, 25, 73] is unlikely to upset the $SU(3)$ relations. The O_7 contribution to $\mathrm{d}\Gamma(B \to K\ell\,\bar{\ell})/\mathrm{d}q^2$ is at the $10 - 15\%$ level, fairly independent of q^2. In the region $(1-2)\mathrm{GeV}^2 < q^2 < m_{J/\psi}^2$, neglecting $m_{K,\pi}^2/m_B^2$,

---

[4] It was argued in Ref. [140] that heavy quark symmetry can be used even at small q^2.

$$\frac{\mathrm{d}\Gamma(\bar{B}^0 \to \pi^+ \,\ell\, \bar{\nu}_\ell)}{\mathrm{d}q^2} = \frac{|V_{ub}|^2}{|V_{ts}^* V_{tb}|^2}\, \frac{8\pi^2}{\alpha^2}\, \frac{1}{|\widetilde{C}_9(q^2) + 2C_7|^2 + |C_{10}|^2}\, \frac{\mathrm{d}\Gamma(B \to K \,\ell\, \bar{\ell})}{\mathrm{d}q^2}\,. \qquad (4.18)$$

A similar relation also holds for integrated rates.

A measurement of the $B \to K^*\ell\,\bar{\ell}$ decay rate is unlikely before the Tevatron run II. Without this measurement, one has to rely on predicting the $B \to \rho$ form factors from $D \to \rho$ using heavy quark symmetry, or from $D \to K^*$ using both chiral and heavy quark symmetries. As discussed following Eq. (4.7), recent experimental data [128] suggests that the $SU(3)$ relation between $f^{(D\to K^*)}$ and $f^{(D\to\rho)}$ is not violated by more than 15%. Furthermore, a prediction for $B \to K^*\gamma$ can be made using heavy quark symmetry and extrapolating the $D \to K^*\bar{\ell}\nu$ form factors [142]. The surprising agreement of this prediction with data may indicate that heavy quark symmetry violation in the form factor relations is smaller than anticipated. Heavy quark symmetry and the measured $D \to K^*$ form factors in Eq. (4.2) imply that the $\bar{B}^0 \to \rho^+\ell\,\bar{\nu}_\ell$ branching ratio in the region $1 < y < 1.5$ is $5.9\,|V_{ub}|^2$. The measured decay rate $\mathcal{B}(\bar{B}^0 \to \rho^+\ell\,\bar{\nu}_\ell) = (2.5 \pm 0.4^{+0.5}_{-0.7} \pm 0.5) \times 10^{-4}$ [124] together with $|V_{ub}| \sim 0.003$ imply that about 20% of $\bar{B}^0 \to \rho^+\ell\,\bar{\nu}_\ell$ decays are in the range $1 < y < 1.5$.

Despite the presence of long distance effects associated with the $c\,\bar{c}$ resonance region, the $B \to K^*\ell\,\bar{\ell}$ rate can be used in Eq. (4.12) to determine $|V_{ub}|$ with a theoretical uncertainty that is about 10%. Experimental verification of the distinctive y-dependence of the differential rate associated with the 1^{--} resonances above 4 GeV (see Fig. 4.3) would reduce the theoretical uncertainty from long distance effects. A precise value of $|V_{ub}|$ may be available from other processes, e.g., the hadronic invariant mass spectrum in inclusive $\bar{B} \to X_u\ell\,\bar{\nu}_\ell$ decay [143, 144] or from lattice QCD results on exclusive form factors [145] before the $B \to K^*\ell\,\bar{\ell}$ decay rate is measured. In that case, Eq. (4.12) gives an accurate standard model prediction for the $B \to K^*\ell\,\bar{\ell}$ decay rate in the region $1 < y < 1.5$. Comparison with data may signal new physics or provide stringent constraints on extensions of the standard model.

Chapter 5 NN Scattering

5.1 Introduction

Effective field theory is a useful tool for studying nuclear interactions. To describe low energy processes involving nucleons and pions in a model independent way, all possible operators consistent with the symmetries of QCD are included in an effective Lagrangian. A further advantage of effective field theory over potential models is that theoretical errors can be estimated in a systematic way. Contributions to an observable are organized by a power counting in Q/Λ, where Q is a momentum scale which characterizes the process under consideration, and Λ is the range of validity of the effective theory. A disadvantage of the effective field theory method is that the expansion parameter may not be very small, so that the description is not precise at low orders.

In an effective field theory, ultraviolet divergences must be regulated and a renormalization scheme defined. The ultraviolet divergences give a constraint on the power counting, because when a divergent loop graph occurs a contact operator that can absorb the divergence must be included at the same or lower order in Q. This is familiar from pion chiral perturbation theory as discussed in section 2.1. The choice of regulator cannot affect physical results, but may make implementing a renormalization scheme easier. The renormalization scheme and power counting are also tied together. In a natural scheme, the renormalized coefficients of the operators in the Lagrangian are normal in size based on dimensional analysis with Λ. Once a power counting is established one can translate between different renormalization schemes at a given order in Q without changing the physical predictions. Recall from section 2.3 that counting powers of Q/Λ in the nuclear effective theory is a subtle issue because of the large S-wave scattering length, a. In Refs. [31, 4] Kaplan, Savage, and Wise (KSW) devised a power counting to take this into account.

Two different calculational techniques for the effective theory of nucleons are used in the literature. In one approach, the power counting is applied to regulated N-nucleon potentials and the Schroedinger equation is solved [27, 28, 146, 147, 148, 149, 30, 150]. Solving the Schroedinger equation is equivalent to including all ladder graphs with the potential as the two-particle irreducible kernel (see, for e.g., [61]). The second approach, advocated by KSW, is like ordinary chiral perturbation theory in that the power counting is applied directly to the Feynman graphs which contribute to the amplitude. As discussed in section 2.3.1, a non-relativistic propagator is used which includes the kinetic energy term to regulate the infrared divergence at zero kinetic energy. In the Feynman diagram approach, dimensional regularization is the most convenient regulator, and analytic results are readily obtained. In the potential method, the Schroedinger equation is usually solved numerically. In practice, divergences are regulated and renormalized couplings are defined using a finite cutoff scheme. In Ref. [151], it has been explicitly shown that without pions the potential method can deal with large scattering lengths, and gives an expansion in Q/Λ.

An important aspect of the KSW analysis is the use of a novel renormalization scheme, power divergence subtraction (PDS). In PDS, loop integrals in Feynman graphs are regulated using dimensional regularization, and poles in both $d = 3$ and $d = 4$ are subtracted. The subtraction of $d = 3$ poles gives a power law dependence on the renormalization point, μ_R, to the coefficients of four-nucleon operators. Choosing $\mu_R \sim Q$, graphs with an arbitrary number of $C_0^{(s)}(\mu_R)$ ($s =^1 S_0$, or $^3S_1$) vertices scale as $1/Q$ and must be summed to all orders. This is precisely the set of graphs that sums corrections that scale like $(Qa)^n$. Higher order contributions form a series in Q/Λ. In Ref. [60], it is emphasized that it is possible to phrase the power counting in a scheme independent manner. The choice of scheme is simply to give natural sized coefficients which make the power counting manifest. PDS is one example of such a scheme. In Ref. [152], it is shown how the KSW power counting can be implemented by solving the Schroedinger equation in a finite cutoff scheme.

Pions can be added to the effective field theory by identifying them as the pseudo-Goldstone bosons of the spontaneously broken chiral symmetry of QCD. All operators with the correct transformation properties are added to the effective Lagrangian. This includes operators with insertions of the light quark mass matrix and derivatives, whose coefficients are needed to cancel ultraviolet divergences from loop graphs. In dimensional regularization, these ultraviolet divergences are of the form $p^{2n} m_\pi^{2m}/\epsilon$. For instance, for nucleons in the ${}^3S_1$ channel, the two loop graph with three pions and a two loop graph with two pions and one C_0 have ultraviolet divergences of the form p^2/ϵ. This pole must be cancelled by a counterterm involving a four-nucleon operator with 2 derivatives. Because divergences of the form p^{2n}/ϵ must be cancelled by local counterterms, pion exchange can only be calculated in a model independent way if higher derivative contact interactions are included at the same order that these divergence occur[45, 153]. In Weinberg's [27] power counting, pion exchange is included in the leading order potential. Therefore, graphs with arbitrary numbers of pions are leading order, while the counterterms necessary to cancel the ultraviolet divergences in these graphs are subleading. However, the potential method can still be used. As higher order derivative operators are added to the potential the accuracy is systematically improved, because the onset of the model dependence of the pion summation appears at higher order in Q/Λ. For example, the cutoff dependence of the two pion graph with one C_0 will be cancelled by cutoff dependence in C_2. At a given order, the left over cutoff dependence in this method is a measure of the size of higher order corrections.

Different estimates of the range, Λ_π, of an effective theory of nucleons with perturbative pions exist in the literature. Some authors [154, 155, 3] argue that Λ_π is as small as m_π, so that including perturbative pions is superfluous. One estimate of the range is given by KSW who conclude that $\Lambda_\pi \sim 300\,\mathrm{MeV}$. They point out that in PDS the renormalization group equation for the coefficient $C_0(\mu_R)$ is modified by the inclusion of pions in such a way that for $\mu_R \gtrsim 300\,\mathrm{MeV}$, $C_0(\mu_R)$ scales like μ_R^0 instead of μ_R^{-1}. Since the power counting is no longer manifest above this scale, KSW conclude that the effective theory breaks down at this point. In Ref. [155] different renormalized couplings are obtained. Here a breakdown of the power counting for $C_2(\mu_R)$ at $\mu_R \sim m_\pi$ is observed. A crucial question is whether a breakdown in the running of the coupling constants is a physical effect or simply an artifact of the renormalization scheme. It is dangerous to draw conclusions based on the large momentum behavior of the coupling constants because the beta functions of the couplings are scheme dependent[1]. In section 5.2, a momentum subtraction scheme is introduced where the power law dependence of the coupling constants persists even in the presence of pions, and for all values of $\mu_R > 1/a$. This scheme is called the OS scheme, since in a relativistic theory it might be called an off-shell momentum subtraction scheme. In Ref. [64], a similar scheme is applied to the spin singlet channel in the theory without pions, where it is shown to give results identical to the PDS scheme. The OS scheme is a natural scheme that works with arbitrary partial waves and with pions. Thus, the range of validity of the effective theory is not limited by the large μ_R behavior of the couplings. PDS is still a useful scheme in which to calculate observables. If one splits $C_0(\mu_R)$ into a non-perturbative and perturbative part, $C_0(\mu_R) = C_0^p(\mu_R) + C_0^{np}(\mu_R)$, then $C_0^{np}(\mu_R) \sim 1/\mu_R$ for all $\mu_R > 1/a$. We will see that this split is also necessary if we wish to avoid having the location of the pole in the amplitude shifted by chiral m_π/Λ corrections. Once this split has been performed, it is straightforward to establish relations between the OS and PDS schemes order by order in perturbation theory, and any prediction for an observable will be identical in the two schemes up to the order in Q/Λ_π to which it is calculated. Since in both schemes there is no scale where the power counting breaks down, it is possible that $\Lambda_\pi > 300\,\mathrm{MeV}$. The importance of looking at results in several schemes is that it allows us to disentangle which results are physical and which are scheme dependent.

Physically, one expects the effective theory to be valid up to a threshold where new degrees of freedom can be created on-shell. For elastic nucleon scattering, the relevant physical threshold is production of Δ resonances which occurs at $p = \sqrt{M_N(M_\Delta - M_N)} = 525$ MeV (the S-wave channels couple only to the $\Delta\,\Delta$ intermediate state so $p = \sqrt{2M_N(M_\Delta - M_N)} = 740$ MeV [156]). Above this scale, the Δ must be included as an explicit degree of freedom. Below this scale, the Δ can be integrated out leaving an effective theory of pions and nucleons. Rho exchange becomes relevant at a scale, $p \sim m_\rho = 770\,\mathrm{MeV}$. There is also a $N^*(1440)N$ intermediate state with a threshold of $p = 685\,\mathrm{MeV}$. One might expect Λ_π to be of order these thresholds. However, there is an intermediate scale of 300 MeV associated with short distance contributions from potential pion exchange[2]. Using dimensional analysis, a graph with the exchange of $n+1$ potential pions is suppressed by $p/300\,\mathrm{MeV}$ relative to a graph with n potential pions. Comparison of the size of individual graphs is scheme dependent (for example the size of graphs differ in MS and in $\overline{\mathrm{MS}}$). The 300 MeV scale applies only to a subset of graphs, and may change once all graphs at a given order in Q are included in the estimate. Therefore, 300 MeV can be taken as an order of magnitude estimate for the range of the theory, but the actual range may be enhanced or suppressed by an additional numerical factor.

---

[1] This is in contrast with dimensionless coupling constants like g in QCD. In that case the first two coefficients of the beta function are scheme independent, so conclusions based on the behavior of the running coupling constant at small coupling (e.g., asymptotic freedom) are physical.

This then motivates the important question: How does one determine the range of the effective field theory? This is obviously a question of great practical importance. Theoretical arguments can only give an approximate estimate for the range. A good example comes from SU(3) chiral perturbation theory. In this strong coupling theory, it is natural to expect that the range of the theory is the chiral symmetry breaking scale $\Lambda_\chi \sim 2\sqrt{2} f_\pi = 1200\,\mathrm{MeV}$ [55, 157, 158]. However, the convergence of the momentum expansion will depend on the particular process under consideration. For instance, in $\pi - \pi$ scattering the range of the expansion is set by the threshold for ρ production, $m_\rho = 770\,\mathrm{MeV}$. In this chapter, the range of the two nucleon effective theory will be estimated using nucleon-nucleon scattering data. Our results are consistent with $\Lambda_\pi \sim 500\,\mathrm{MeV}$. As we will explain in section 5.9, the error analysis is applied to δ rather than to $p \cot \delta$ as in Ref. [155]. This range does not depend on the value of the renormalization point chosen, and is found in both the OS and PDS schemes. However, only next-to-leading order calculations have been used so it is hard to estimate the error in this value. When higher order corrections are computed, it should be possible to obtain a reasonably accurate estimate of the range of the two nucleon effective field theory with perturbative pions. This 500 MeV estimate is based solely on the phase shift data. The accuracy of predictions for deuteron observables [159] indicates $Q/\Lambda \sim 1/3$, which for $Q \sim m_\pi$ is $\Lambda \sim 400\,\mathrm{MeV}$.

---

[2] The phrase "potential pion exchange" will be used for a perturbative pion with energy independent propagator. This is sometimes called static pion exchange.

In section 5.2, we review the power counting method of KSW [31, 4], and the PDS scheme. The importance of being able to count factors of the large nucleon mass in a non-relativistic effective field theory is discussed. We review the OS scheme, which is compatible with the KSW power counting. We describe the procedure for defining the renormalized couplings using local counterterms for each of these schemes.

In section 5.3, we discuss the theory with only nucleons, where $\Lambda \sim m_\pi$. Local counterterms for both the PDS and OS schemes are computed. These counterterms are used to obtain the beta functions for the four-nucleon operators, and we explain why the beta functions for the most relevant operators in this theory are one-loop exact. In section 5.4 we explain how treating part of C_0 perturbatively allows us to reproduce the effective range expansion with an amplitude that has its pole in the physical location at every order in perturbation theory. In section 5.5 we show how calculations with a cutoff regulator reproduce the dimensional regularization results.

The theory with nucleons and pions is analyzed in section 5.6. In the ${}^3S_1$ channel, there are corrections to the PDS beta functions at all orders in Q. As examples, we compute the PDS beta functions for $C_0^{({}^3S_1)}(\mu_R)$ to order Q, and for $C_2^{({}^3S_1)}(\mu_R)$ to order Q^0. In this channel, even in the limit $m_\pi \to 0$, there are logarithmic divergences (poles of the form p^2/ϵ in dimensional regularization). In the OS scheme, the ${}^3S_1$ beta functions can be calculated exactly. We compute the exact beta functions for $C_0(\mu_R)$, $C_2(\mu_R)$, and $C_4(\mu_R)$ in the OS scheme in the ${}^1S_0$ and ${}^3S_1$ channels. In section 5.7, the counterterms for the coupling constant $D_2(\mu_R)$ are derived in the OS and PDS schemes.

In section 5.8, we discuss why it is important to have μ_R independent amplitudes order by order in the expansion. In the OS scheme amplitudes are μ_R independent, while in PDS μ_R independent amplitudes can be obtained by treating part of $C_0(\mu_R)$ perturbatively. If this is not done then the sensitivity to μ_R is larger than one might expect [154], for reasons we explain. Fits to the data are presented for different values of μ_R and the coupling constants in both OS and PDS are shown to evolve according to the renormalization group equations.

In section 5.9, an error analysis similar to a method due to Lepage [30] is used to investigate the range of the effective field theory with perturbative pions at next-to-leading order. Weighted fits are performed for the scattering data in both the ${}^1S_0$ and ${}^3S_1$ channels. Our results rule out $\Lambda_\pi \sim m_\pi$, and are consistent with $\Lambda_\pi \sim 500\,\mathrm{MeV}$.

5.2 Power counting and renormalization schemes

In this section, the KSW power counting and compatible renormalization schemes are discussed. The theory containing only nucleon fields is considered first. The renormalized couplings are then defined in terms of local counterterms, and the KSW power counting for coefficients of four-nucleon operators is reviewed. Next, we consider the theory including pions. We review the power counting for potential pions, and explain the origin of the 300 MeV scale associated with potential pion exchange. The PDS renormalization scheme is then discussed and we introduce the OS momentum subtraction scheme, which is also compatible with the power counting.

Recall from section 2.3.1 that the Lagrangian in the two nucleon sector is given by:

$$\mathcal{L}_{NN} = N^\dagger \Big[i\partial_t + \overleftrightarrow{\nabla}^2/(2M) + \ldots \Big] N - \sum_s \sum_{m=0}^{\infty} C_{2m}^{(s)}\, \mathcal{O}_{2m}^{(s)} \,. \tag{5.1}$$

The C_{2m} appearing in Eq. (5.1) are bare parameters. To renormalize the theory, the bare coupling is separated into a renormalized coupling and counterterms as follows:

$$C_{2m}^{\mathrm{bare}} \;=\; C_{2m}^{\mathrm{finite}} - \delta^{\mathrm{uv}} C_{2m}\,, \qquad\qquad C_{2m}^{\mathrm{finite}} = C_{2m}(\mu_R) - \sum_{n=0}^{\infty} \delta^n C_{2m}(\mu_R)\,. \tag{5.2}$$

Note that we divide the counterterms into two classes. The first, which have the superscript uv, contain all genuine ultraviolet divergences. These include $1/\epsilon$ poles, if dimensional regularization is used, or powers and logarithms of the cutoff if a hard cutoff is used. We will also include some finite constants (e.g., the $-\gamma + \ln(4\pi)$ that is subtracted in $\overline{MS}$) if this proves to be convenient for keeping expressions compact. By construction, these counterterms are μ_R independent, but will depend on $C_{2m}^{\rm finite}$. The renormalized coupling is denoted $C_{2m}(\mu_R)$. The remaining counterterms, $\delta^n C_{2m}(\mu_R)$, contain no ultraviolet divergences and will be referred to as the finite counterterms. The choice of the finite counterterms differentiates between the schemes studied here. An infinite number of finite counterterms are needed because an infinite number of loop graphs are included at leading order. The renormalization is carried out order by order in the loop expansion. The superscript n indicates that $\delta^n C_{2m}$ is included at tree level for a graph with n loops. When higher loop graphs are considered, the $\delta^n C_{2m}$ counterterm takes the place of n loops [54]. For example, at three loops we have three loop diagrams with renormalized couplings at the vertices, two loop diagrams with a $\delta^1 C$ counterterm, one loop diagrams with either one $\delta^2 C$ or two $\delta^1 C$'s, and a tree level diagram with $\delta^3 C$. Examples are given in section 5.3.

For the nucleon theory, the kinematic part of the power counting is very simple [27, 32]. Q is identified with a typical external momentum characterizing the process under consideration. For instance, in elastic nucleon-nucleon scattering $Q \sim p$, where p is the center of mass momentum[3]. Each nucleon propagator gives a Q^{-2}, each spatial derivative a Q, each time derivative a Q^2, and each loop integration a Q^5.

In the theory with only nucleons, the only graphs relevant to 2 → 2 scattering are bubble chains. Consider a graph $\mathcal{G}$ with L loops in the non-relativistic limit. In dimensional regularization, each loop will give a factor $Mp/4\pi$, and there are $L+1$ vertices, each giving a factor $-iC_{2m}^{\rm finite} p^{2m}$. If the operator O_{2m} appears n_m times in the graph ($L+1 = \sum_m n_m$) the result is:

$$\mathcal{G} \;=\; \frac{4\pi}{M} \prod_{m=0}^{\infty} \left(\frac{-iMC_{2m}^{\rm finite}}{4\pi} \right)^{n_m} p^j, \qquad \text{where} \quad j = \sum_{m=0}^{\infty} 2\, m\, n_m + L\,. \tag{5.3}$$

---

[3] For the scattering $N(\vec{q}+\vec{p}) + N(\vec{q}-\vec{p}) \to N(\vec{q}+\vec{p}\,') + N(\vec{q}-\vec{p}\,')$ it is useful to define $p = \sqrt{ME_{tot} - \vec{q}^{\,2} + i\epsilon}$, where E_{tot} is the total incoming energy, and M is the nucleon mass. To simplify the notation we will work in the center of mass frame, $\vec{q} = 0$, where $p^2 = \vec{p}^{\,2} = \vec{p}\,'^{\,2} = ME$, and E is the center of mass energy. For external particles, one can always translate between E and p using the equations of motion.

If one matches onto the effective range expansion in $\overline{\mathrm{MS}}$ one finds [61]

$$C_{2m}^{\rm finite} \sim 4\pi\, a^{m+1}/(M\,\Lambda^m)\,. \tag{5.4}$$

Note that all graphs $\mathcal{G}$ are proportional to $1/M$ in agreement with the discussion in section 2.3.1. The large S-wave scattering lengths enhance the importance of some graphs compared to the p power counting. This affects the power counting for S-wave couplings, and through the mixing, couplings with L and/or $L' = 2$ and $S = 1$. For other channels we have the usual chiral power counting of p's. The power counting for insertions of four-nucleon operators is [32]

$$C_{2m}^{(s)}(\mu_R) \quad \mathcal{O}_{2m}^{(s)} \;\sim C_{2m}^{(L-L')}(\mu_R)\, p^{2m} \sim Q^{\,q(s,m)}\ , \qquad\qquad \text{where}$$

$$q(s,m) \quad = \quad \begin{cases} m-1 & \text{for } L = L' = 0 \\ m & \text{for } S=1 \text{ and } (L,L'=0,2)\,,\ \text{or}\ \ (L,L'=2,0) \\ m+1 & \text{for } S=1 \text{ and } L,L'=2,2 \\ 2m & \text{for all other } S, L, \text{ and } L' \end{cases} \tag{5.5}$$

With the coefficients C_{2m} scaling as in Eq. (5.5), the graph $\mathcal{G}$ scales as

$$\mathcal{G} \sim Q^{\,i} \qquad\qquad \text{where} \quad i = \sum_m n_m\, q(s,m) \;+\; L\,. \tag{5.6}$$

Note that the power of Q is less than or equal to the power of p, $i \leq j$. A useful mnemonic for this power counting is $1/a \sim Q$, however, the power counting is still valid for $Qa \gg 1$.

This Q power counting will be manifest in any renormalization scheme[4] in which the $C_{2m}(\mu_R)$ scale with $\mu_R \sim Q$ in such a way that Eq. (5.5) is true. At leading order the counterterms $\delta^n C_{2m}(\mu_R)$ will have the same Q scaling as the coefficient $C_{2m}(\mu_R)$. These schemes may differ by contributions in $C_{2m}(\mu_R)$ that scale with a larger power of μ_R/Λ, since this will not change the power counting at low momentum.

---

[4] Although the power counting can be implemented in different schemes, the PDS scheme introduced in Ref. [31] was very useful for initially working out the power counting.

Let us now discuss the theory with pions. To add pions, we identify them as the three pseudo-Goldstone bosons which arise from the breaking of chiral symmetry, $SU(2)_L \times SU(2)_R \rightarrow SU(2)_V$. With the pions included in this way, we are doing an expansion in m_π/Λ_π and p/Λ_π. Note that in this theory, no matter how small p is made the expansion parameter will never be smaller than m_π/Λ_π. This theory still includes the four-nucleon operators in Eq. (2.30), but the short distance physics parameterized by the coefficients C_{2m} is different because the pion is no longer integrated out. In the pion theory, the short distance C_{2m} coefficients should be independent of the scale m_π. All the m_π dependence is now contained explicitly in powers of the light quark mass matrix in the Lagrangian.

Pions will be encoded in the representation, $\Sigma = \xi^2 = \exp\left(2i\Pi/f\right)$, where

$$\Pi = \begin{pmatrix} \pi^0/\sqrt{2} & \pi^+ \\ \pi^- & -\pi^0/\sqrt{2} \end{pmatrix} , \tag{5.7}$$

and $f = 130\,\mathrm{MeV}$ is the pion decay constant. Under $SU(2)_L \times SU(2)_R$ the fields transform as $\Sigma \rightarrow L\Sigma R^\dagger$, $\xi \rightarrow L\xi U^\dagger = U\xi R^\dagger$, and $N \rightarrow UN$. The chiral covariant derivative is $D^\mu = \partial^\mu + \frac{1}{2}(\xi\partial^\mu\xi^\dagger + \xi^\dagger\partial^\mu\xi)$. With pions we have the following Lagrangian with terms involving 0, 1 and 2 nucleons:

$$\begin{aligned} \mathcal{L}_\pi &= \frac{f^2}{8}\mathrm{Tr}\left(\partial^\mu\Sigma\,\partial_\mu\Sigma^\dagger\right) + \frac{f^2 w}{4}\,\mathrm{Tr}(m_q\Sigma + m_q\Sigma^\dagger) \\ &+ \frac{ig_A}{2}\,N^\dagger\sigma_i(\xi\partial_i\xi^\dagger - \xi^\dagger\partial_i\xi)N + N^\dagger\Big(iD_0 + \frac{\vec{D}^2}{2M}\Big)N \\ &- \sum_{s,m} C_{2m}^{(s)}\,\mathcal{O}_{2m}^{(s)} - D_2^{(s)}\omega\mathrm{Tr}(m^\xi)(N^T P_i^{(s)} N)^\dagger (N^T P_i^{(s)} N) + \ldots\,. \end{aligned} \tag{5.8}$$

Here $m^\xi = \frac{1}{2}(\xi m_q \xi + \xi^\dagger m_q \xi^\dagger)$, $m_q = \mathrm{diag}(m_u, m_d)$ is the quark mass matrix, $m_\pi^2 = w(m_u + m_d)$ where w is a constant, and $g_A = 1.25$ is the nucleon axial-vector coupling. The ellipsis in Eq. (5.8) denote terms with more derivatives and more powers of m^ξ.

With pions there are additional complications to the power counting [45, 46, 153] which are similar to those encountered in Non-Relativistic QED and QCD [19, 22, 44]. The complications arise because there are two relevant energy scales for the pions,

$E_\pi \sim Q^2/M$ for potential pions, and $E_\pi \sim Q$ for radiation pions. When the energy integral in loops is performed via contour integration, the graphs with potential pions come from terms in which one keeps the residue of a nucleon propagator pole. In these loops, the energy of the loop momentum is $\sim Q^2/M$ and the energy dependent pieces of the pion propagator are suppressed by an additional Q^2/M^2. Nucleon propagators give a Q^{-2} and the loop integrals give Q^5. There are also radiative pion graphs, in which the residue of the pion pole is kept. The power counting for these graphs is discussed in Chapter 6. In general graphs with radiation pions are higher order than those with potential pions. The combined propagator and vertices for a single pion exchange give Q^0, so the pions can be treated perturbatively [4].

In general, pion exchange gives both long and short distance contributions. The short distance contributions from potential pions are important since they may limit the range of the effective field theory. A single potential pion exchange gives

$$i\frac{g_A^2}{2f^2}\,\frac{\vec{q}\cdot\vec{\sigma}_{\alpha\beta}\;\vec{q}\cdot\vec{\sigma}_{\gamma\delta}}{\vec{q}^{\,2}+m_\pi^2}\;\vec{\tau}_1\,\cdot\,\vec{\tau}_2 = i\frac{g_A^2}{2f^2}\left[\frac{\vec{q}\cdot\vec{\sigma}_{\alpha\beta}\;\vec{q}\cdot\vec{\sigma}_{\gamma\delta}}{\vec{q}^{\,2}} - \frac{m_\pi^2\;\vec{q}\cdot\vec{\sigma}_{\alpha\beta}\;\vec{q}\cdot\vec{\sigma}_{\gamma\delta}}{\vec{q}^{\,2}\,(\vec{q}^{\,2}+m_\pi^2)}\right]\vec{\tau}_1\,\cdot\,\vec{\tau}_2\ , \tag{5.9}$$

where the spin indices connect to nucleon fields $N_\alpha^\dagger N_\beta N_\gamma^\dagger N_\delta$ which belong to external lines or propagators. The first term dominates for $\vec{q}^{\,2} \gg m_\pi^2$, and can be isolated by taking the limit $m_\pi \to 0$. To study the dominant short distance contribution of pion exchange the m_π dependence can be neglected. Graphs with radiation pions are suppressed by powers of $(m_\pi/M)^{1/2}$. In the non-relativistic limit, with only potential pions, the only loop diagrams are ladders. Consider an arbitrary graph $\mathcal{G}$ with n_m four point vertices, $C_{2m}^{\rm finite}$, and k potential pions. For L loops, this graph has a total of $L+1 = k + \sum_m n_m$ vertices, and with $m_\pi = 0$

$$\begin{aligned}
\mathcal{G} \;&\propto\; \left(\frac{M}{4\pi}\right)^L \left(\frac{-ig_A^2}{2\,f^2}\right)^k p^j \prod_{m=0}^{\infty}(-iC_{2m}^{\rm finite})^{n_m} \qquad (5.10)\\
&=\; \frac{4\pi}{M}\left(\frac{-iMg_A^2}{8\,\pi f^2}\right)^k p^j \prod_{m=0}^{\infty}\left(\frac{-iMC_{2m}^{\rm finite}}{4\pi}\right)^{n_m}, \quad \text{where} \quad j = \sum_{m=0}^{\infty} 2\,m\,n_m + L\,.
\end{aligned}$$

In the $^1S_0$ channel, the relation in Eq. (5.10) becomes an equality. The graph $\mathcal{G} \sim Q^i$ where i is given in Eq. (5.6). The power counting of the $\delta^{\rm uv}C_{2m}$ counterterms is determined by the need to cancel ultraviolet divergences, and will not spoil the scaling for the renormalized coefficients, since $i \leq j$. For graphs with only potential pions ($n_m = 0$), it appears that our expansion is in $p/(300\,\mathrm{MeV})$ since

$$\frac{1}{\Lambda_{NN}} \equiv \frac{M g_A^2}{8\pi f^2} \sim (300\,\mathrm{MeV})^{-1}\,. \tag{5.11}$$

Comparing the size of potential pion graphs therefore predicts a range of 300 MeV, but the size of these graphs may change depending on the renormalization scheme (i.e., the finite subtractions). As mentioned in section 2.1 the value of the loop graphs and contact interactions separately do not have unique values. It is not known *a priori* how the contact interactions will affect the range of the effective theory. The scale 300 MeV is therefore an approximate estimate for the range of the effective field theory with perturbative pions. A further discussion of this issue will be taken up in section IV.

Next, consider the power counting for coefficients that multiply operators with powers of m_q. If we are interested in momenta of order m_π, then one counts $m_q \sim m_\pi^2 \sim Q^2$. Therefore, any interaction term that has an operator with a total of $2m$ powers of p and m_π will scale as $Q^{\,q(s,m)}$ where $q(s,m)$ is given in Eq. (5.5). For example, $D_2^{(^1S_0)} m_\pi^2 \sim Q^0$. It is important to understand that in the KSW power counting D_2 should be treated perturbatively even though the structure of the operator it multiplies is similar to that of the leading four nucleon operator with no derivatives. Graphs with radiation pions will also give contributions with powers of m_π^2.

5.2.1 The PDS scheme

PDS is one scheme in which the KSW power counting is manifest. In PDS, we first let $d = 4$ and take the $\delta^{\rm uv}C_{2m}$ counterterms to subtract $1/\epsilon$ poles as in $\overline{\rm MS}$. We use the notation μ_R for the renormalization point, and μ for the dimensional regularization parameter. In PDS, like in the $\overline{\rm MS}$ scheme, one takes $\mu = \mu_R$. In a momentum subtraction scheme this is not necessary. The next step in PDS is to take $d = 3$ and define the finite counterterms, $\delta^n C_{2m}(\mu_R)$, to subtract the $1/(d-3)$ poles in the amplitude. Graphs which contribute to $\delta^n C_{2m}(\mu_R)$ are those whose *vertices* have a total of $2m$ derivatives. When calculating the $\delta^n C_{2m}(\mu_R)$ we can take $m_\pi = 0$ since, for instance, counterterms proportional to m_π^2 renormalize coefficients like $D_2(\mu_R)$. After making these subtractions everything is continued back to four dimensions. It is this second set of finite subtractions that gives the right power law dependence on μ_R. To define the coefficients that multiply operators with powers of m_q, a similar procedure is followed except we count the powers of m_π^2 at the vertices. In PDS with just nucleons, all the graphs that affect the running of $C_{2m}(\mu_R)$ are order $Q^{\,q(s,m)}$, except for those with intermediate states of different orbital angular momentum. For example, the beta function for $C_4^{(^3S_1)}$ has contributions $\sim Q$ ($q(^3S_1, 4) = 1$), as well as contributions $\sim Q^3$ from graphs with two $C_2^{(^3S_1-{}^3D_1)}$ vertices. When pions are included there are additional graphs that are sub-leading in the power counting and affect the running of the couplings. In fact, in section 5.6 we will show that there will be corrections to the PDS beta function for $C_0^{(^3S_1)}(\mu_R)$ at all orders in Q.

5.2.2 The OS scheme

Another renormalization scheme that can be used to reproduce the power counting in Eq. (5.5) is a momentum subtraction scheme. A simple physical definition for the renormalized couplings can be made by relating the couplings to the amplitude evaluated at the unphysical momentum $p = i\mu_R$. This scheme will be called the OS scheme, since in a relativistic field theory this would be referred to as an off-shell momentum subtraction scheme. We start by dividing up the full amplitude as

$$i\,\mathcal{A}^s = i\sum_{m=0}^{\infty} \mathcal{A}^s_{2m} + \ldots\,. \tag{5.12}$$

Here $\mathcal{A}^s_{2m}$ contains the Feynman diagrams that will be used to define the coupling $C^{(s)}_{2m}(\mu_R)$ (or equivalently the counterterms $\delta^n C_{2m}$). The ellipsis in Eq. (5.12) denotes pieces that vanish as $m_\pi \to 0$ which are not needed to define $C_{2m}(\mu_R)$. A^s_{2m} is defined to contain the remaining graphs that scale as $Q^{\,q(s,m)}$, where $q(s,m)$ is defined in Eq. (5.5). The definition for the renormalized coupling is then

$$i\,\mathcal{A}^{s}_{2m}\Big|_{\substack{p\,=\,i\mu_R\\ m_\pi\,=\,0}} = -iC^{(s)}_{2m}(\mu_R)\,(i\mu_R)^{2m}\,. \tag{5.13}$$

As we will see, this ensures that $C_{2m}(\mu_R)$ scales in the desired way. In general, there may be divergent graphs scaling as $Q^{\,i}$ and p^{2m} ($i \leq 2m$) whose $1/\epsilon$ poles need to be absorbed by a $\delta^{\rm uv}C_{2m}$ counterterm. For example, consider the graph with two pions and one C_0 shown in row four of Fig. 5.4. This graph has a p^2/ϵ pole which is cancelled by a counterterm $\delta^{\rm uv}C_2$. The finite part of this graph is used in Eq. (5.13) to define $C_4(\mu_R)$ because the graph is order Q. The key point is that since $q(s,m) \leq 2m$, an ultraviolet divergence that appears in a graph of a given order can always be absorbed into a coefficient that appeared at the same or lower order in the power counting. Therefore, we will define $\delta^{\rm uv}C_{2m}$ in $\overline{\rm MS}$ to subtract all four dimensional $1/\epsilon$ poles so that these subtractions are independent of the renormalization point. The finite counterterms are then fixed by the renormalization condition in Eq. (5.13).

In the OS scheme, the couplings $C_0(\mu_R)$ and $C_2(\mu_R)$ are defined by the renormalization condition in Fig. 5.1. This condition is to be imposed order by order in the loop expansion so that graphs with n loops determine $\delta^n C_0(\mu_R)$. The $m_\pi = 0$ part of pion graphs contribute to $C_{2m}(\mu_R)$ for $m \geq 1$ in which case the condition $m_\pi = 0$ in Eq. (5.13) is important. In the theory with pions, we also need to define couplings multiplying powers of m_q, like D_2 in Eq. (5.8). To define these couplings we will not include all the terms in the amplitude proportional to m_π^2. In particular, pion exchange graphs give long distance non-analytic contributions which will not be used to define the running of the short distance coupling $D_2(\mu_R)$. The idea that long distance physics must be excluded from the short distance coefficients is discussed in Ref. [155]. A detailed discussion of how we define $D_2(\mu_R)$ in the OS scheme will be left to section V.

Note that in the OS scheme there is another approach for calculating an amplitude in terms of renormalized couplings. One can calculate all loop graphs in $\mathcal{A}^{s}_{2m}$ in terms

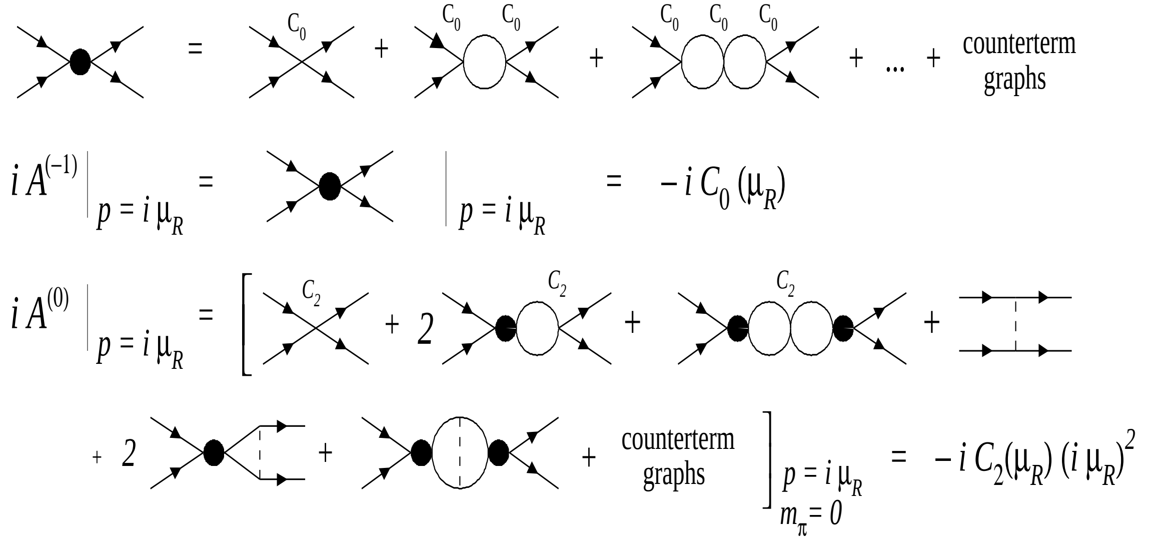

Figure 5.1: Renormalization conditions for $C_0(\mu_R)$ and $C_2(\mu_R)$ in the OS scheme. $i\,A^{(-1)}$ is the four point function with $C_0(\mu_R)$ and $\delta^n C_0(\mu_R)$ vertices, evaluated between incoming and outgoing ${}^1S_0$ or ${}^3S_1$ states. The amplitude $A^{(0)}$ contains graphs with one C_2 or one potential pion dressed with C_0 bubbles.

of the finite (or $\overline{\rm MS}$) parameters and then demand that the renormalization condition in Eq. (5.13) is satisfied. This gives expressions for the renormalized couplings in terms of the constants $C_{2m}^{\rm finite}$. The amplitude can then be written in terms of renormalized couplings by inverting these equations. This simplifies higher order calculations.

In the OS scheme, when an amplitude is written in terms of renormalized couplings it will be explicitly μ_R independent at each order in Q. The μ_R dependence in PDS with pions is cancelled by higher order terms. It is possible to obtain μ_R independent amplitudes in PDS if part of $C_0(\mu_R)$ is treated perturbatively[35]. Consequences of this μ_R dependence will be discussed in section 5.8. In section 5.3 we will see that for the theory with just nucleons the OS scheme gives very similar definitions for the renormalized couplings to those in PDS. In section 5.6, we investigate the running couplings in both schemes in the theory with pions.

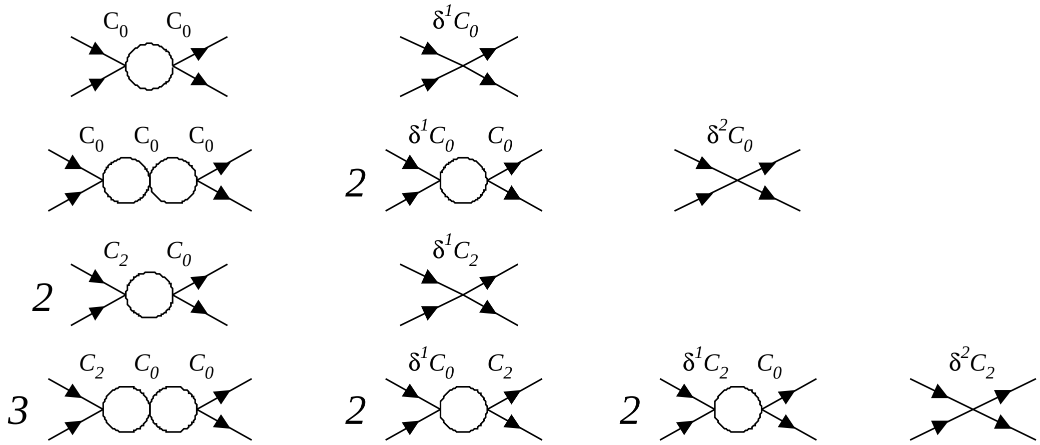

Figure 5.2: One and two loop counterterms for C_0 and C_2. The solid lines are nucleon propagators, and symmetry factors are shown explicitly. The generalization to higher loops is straightforward.

5.3 Theory with pions integrated out

In this section, we compute the renormalized couplings in the non-relativistic nucleon effective theory without pions. We expect $\Lambda \sim m_\pi$. This theory will be examined in both PDS and the OS scheme. The renormalization program is implemented by explicitly calculating the local counterterms. In Ref. [64], it is shown that the PDS and OS schemes give the same renormalized coupling constants in the $^1S_0$ channel. Here we also consider the spin-triplet channel and higher derivative operators. Divergences in loop integrals are regulated using dimensional regularization. For the OS scheme, the same renormalization program can be carried out using a momentum cutoff regulator as shown in section 5.5. Following Ref. [4], we will multiply each loop integral by $(\mu/2)^{(4-d)}$, and define $d = 4 - 2\epsilon$. Since there are no logarithmic divergences in the nucleon theory, $\delta^{\rm uv} C_{2m} = 0$ in dimensional regularization.

In both PDS and OS scheme, it is straightforward to derive the finite counterterms, $\delta^n C_{2m}(\mu_R)$. The tree level graphs with $C_0(\mu_R)$ and $C_2(\mu_R)$ satisfy the renormalization condition in Eq. (5.13). Therefore, in both PDS and OS, $\delta^0 C_0 = \delta^0 C_2 = 0$. At one and two loops we have the graphs in Fig. 5.2. In d dimensions, the two graphs in the first row give

$$(-iC_0)^2\Big(\tfrac{-iM}{4\pi}\Big)\Gamma(\tfrac{3-d}{2})\Big(\frac{\mu}{2}\Big)^{4-d}\Big(\frac{-p^2-i\varepsilon}{4\pi}\Big)^{\frac{d-3}{2}}+i\,\delta^1 C_0\,, \tag{5.14}$$

determining $\delta^1 C_0$. In PDS, we define the counterterm to cancel the $d=3$ pole in Eq. (5.14) and then continue back to four dimensions. In the OS scheme, we take $d=4$ and demand that the contribution to the amplitude in Eq. (5.14) satisfies the condition in Fig. 5.1. The counterterms calculated in each scheme are the same (with $\mu=\mu_R$ in PDS). In both schemes the counterterms determined from the graphs in Fig. 5.2 are

$$\begin{aligned}
\delta^1 C_0(\mu_R) &= \Big(\frac{M\mu_R}{4\pi}\Big)\,C_0(\mu_R)^2\ , & \delta^2 C_0(\mu_R) &= -\Big(\frac{M\mu_R}{4\pi}\Big)^2\,C_0(\mu_R)^3\ , \\
\delta^1 C_2(\mu_R) &= 2\Big(\frac{M\mu_R}{4\pi}\Big)\,C_2(\mu_R)C_0(\mu_R)\ , & \delta^2 C_2(\mu_R) &= -3\Big(\frac{M\mu_R}{4\pi}\Big)^2\,C_2(\mu_R)C_0(\mu_R)^2\ .
\end{aligned} \tag{5.15}$$

Note that it is essential that loop graphs also have vertices with insertions of the counterterms. For instance, the contribution to the amplitude from all the graphs in the second row of Fig. 5.2 is

$$-\,iC_0(\mu_R)^3\Big(\frac{M(ip+\mu_R)}{4\pi}\Big)^2\ . \tag{5.16}$$

If the one-loop graph with a $\delta^1 C_0$ counterterm had been left out then the answer would have been proportional to $(p^2+\mu_R^2)$ which is not correct. Since the loops in the nucleon theory factorize, the renormalized n-loop graph gives $(ip+\mu_R)^n$. Loop graphs will not always factorize once pions are included.

It is straightforward to extend this calculation to n loops and to include higher derivatives. In both the OS and PDS schemes, this gives the following counterterms ($s={}^1S_0, {}^3S_1$, $n\geq 1$):

${}^1S_0$:

$$\delta^n C_0^{({}^1S_0)}(\mu_R) = (-1)^{n+1}\,\left(\frac{M\mu_R}{4\pi}\right)^n\ C_0^{({}^1S_0)}(\mu_R)^{\,n+1}\,,$$

$$\delta^n C_2^{({}^1S_0)}(\mu_R) = (-1)^{n+1}\left(\frac{M\mu_R}{4\pi}\right)^n\ (n+1)\ C_0^{({}^1S_0)}(\mu_R)^n\, C_2^{({}^1S_0)}(\mu_R)\,,$$

$$\delta^n C_4^{({}^1S_0)}(\mu_R) = (-1)^{n+1}\left(\frac{M\mu_R}{4\pi}\right)^n\ (n+1)C_0^{({}^1S_0)}(\mu_R)^{n-1} \times\Big[C_4^{({}^1S_0)}(\mu_R)\, C_0^{({}^1S_0)}(\mu_R) + \frac{n}{2}C_2^{({}^1S_0)}(\mu_R)^2\Big]\,,$$

${}^3S_1, {}^3D_1$: (5.17)

$$\delta^n C_0^{({}^3S_1)}(\mu_R) = (-1)^{n+1}\left(\frac{M\mu_R}{4\pi}\right)^n\ C_0^{({}^3S_1)}(\mu_R)^{n+1}\,,$$

$$\delta^n C_2^{({}^3S_1)}(\mu_R) = (-1)^{n+1}\left(\frac{M\mu_R}{4\pi}\right)^n\ (n+1)\ C_0^{({}^3S_1)}(\mu_R)^n\, C_2^{({}^3S_1)}(\mu_R)\,,$$

$$\delta^n C_2^{({}^3S_1-{}^3D_1)}(\mu_R) = (-1)^{n+1}\left(\frac{M\mu_R}{4\pi}\right)^n\ C_0^{({}^3S_1)}(\mu_R)^n\, C_2^{({}^3S_1-{}^3D_1)}(\mu_R)\,,$$

$$\delta^n C_4^{({}^3D_1)}(\mu_R) = (-1)^{n+1}\left(\frac{M\mu_R}{4\pi}\right)^n C_0^{({}^3S_1)}(\mu_R)^{n-1}\left[C_2^{({}^3S_1-{}^3D_1)}(\mu_R)\right]^2.$$

Note that with $\mu_R \sim Q$, the counterterms have the same Q scaling as their corresponding coupling constant. In the PDS scheme, there are also subleading terms that come from the mixing of angular momentum states. In PDS

$$\delta^n C_4^{({}^3S_1)}(\mu_R) = (-1)^{n+1}\left(\frac{M\mu_R}{4\pi}\right)^n C_0^{({}^3S_1)}(\mu_R)^{n-1}\Big[(n+1)C_4^{({}^3S_1)}(\mu_R)\, C_0^{({}^3S_1)}(\mu_R) + \frac{n(n+1)}{2}C_2^{({}^3S_1)}(\mu_R)^2 + nC_2^{({}^3S_1-{}^3D_1)}(\mu_R)^2\Big]\,, \tag{5.18}$$

where the last term is suppressed by Q^2. In the OS scheme

$$\delta^n C_4^{({}^3S_1)}(\mu_R) = (-1)^{n+1}\left(\frac{M\mu_R}{4\pi}\right)^n C_0^{({}^3S_1)}(\mu_R)^{n-1} \times\Big[(n+1)C_4^{({}^3S_1)}(\mu_R)\, C_0^{({}^3S_1)}(\mu_R) + \frac{n(n+1)}{2}C_2^{({}^3S_1)}(\mu_R)^2\Big]\,, \tag{5.19}$$

which is the same as the ${}^1S_0$ channel. In the OS scheme, graphs with two $C_2^{({}^3S_1-{}^3D_1)}$ couplings and any number of $C_0^{({}^3S_1)}$'s contribute to the beta function for $C_8^{({}^3S_1)}$ since they are order Q^3. One might also ask about channels where the large scattering length does not effect the power counting. In this case $C_{2m}^{(s)}(\mu_R) \sim Q^0$, and we recover the usual chiral power counting. In our OS scheme, the counterterms $\delta^n C_{2m}^{(s)}(\mu_R)$ in these channels are either zero or a constant independent of μ_R.

From Eq. (5.2) one can derive the beta functions using

$$\beta_{2m} \equiv \mu_R \frac{\partial}{\partial \mu_R} C_{2m}(\mu_R) = \sum_{n=0}^{\infty} \mu_R \frac{\partial}{\partial \mu_R} \delta^n C_{2m}(\mu_R)\,. \tag{5.20}$$

The first few beta functions are

$$\begin{aligned}
&{}^1S_0 : \\
&\qquad \beta_0^{({}^1S_0)} = \left(\frac{M\mu_R}{4\pi}\right) C_0^{({}^1S_0)}(\mu_R)^2\,, \\
&\qquad \beta_2^{({}^1S_0)} = 2\left(\frac{M\mu_R}{4\pi}\right) C_0^{({}^1S_0)}(\mu_R)\, C_2^{({}^1S_0)}(\mu_R)\,, \\
&\qquad \beta_4^{({}^1S_0)} = \left(\frac{M\mu_R}{4\pi}\right)\left(2C_4^{({}^1S_0)}(\mu_R)\, C_0^{({}^1S_0)}(\mu_R) + C_2^{({}^1S_0)}(\mu_R)^2\right), \\
&{}^3S_1, {}^3D_1 : \\
&\qquad \beta_0^{({}^3S_1)} = \left(\frac{M\mu_R}{4\pi}\right) C_0^{({}^3S_1)}(\mu_R)^2\,, \\
&\qquad \beta_2^{({}^3S_1)} = 2\left(\frac{M\mu_R}{4\pi}\right) C_0^{({}^3S_1)}(\mu_R)\, C_2^{({}^3S_1)}(\mu_R)\,, \\
&\qquad \beta_2^{({}^3S_1-{}^3D_1)} = \left(\frac{M\mu_R}{4\pi}\right) C_0^{({}^3S_1)}(\mu_R)\, C_2^{({}^3S_1-{}^3D_1)}(\mu_R)\,,
\end{aligned} \tag{5.21}$$

in agreement with Refs. [31, 4]. For $S = 0$ states the beta functions are one loop exact in the sense that the contribution in Eq. (5.21) comes from the one-loop graphs, with the higher order graphs giving contributions which cancel. The reason for this cancellation is that the only loop corrections are in the bubble chain, and they form a geometric series. The sum of bubble graphs is just the chain of irreducible one loop bubbles for the full (point-like) propagator. An analogy would be QED, if the only possible graphs were the two point photon graphs with electron loops. In this case the beta function would also be one-loop exact because the graphs that are not 1PI do not contribute. In general, the beta functions of higher order couplings may have contributions beyond one-loop in cases where angular momentum mixing is present.

Expressions for the running coupling constants can be derived by summing the counterterms in Eq. (5.2) or by solving renormalization group equations. For $s = {}^1S_0$

or ${}^3S_1$ this gives

$$C_0^{(s)}(\mu_R) \;=\; \frac{1}{\frac{1}{C_0^{\rm finite}}-\frac{M\mu_R}{(4\pi)}}\,, \quad C_2^{(s)}(\mu_R)=\frac{C_2^{\rm finite}}{(C_0^{\rm finite})^2}\frac{1}{\left[\frac{1}{C_0^{\rm finite}}-\frac{M\mu_R}{4\pi}\right]^2}\,, \tag{5.22}$$

where $C_0^{\rm finite}$ and $C_2^{\rm finite}$ are constants which can be determined by specifying boundary conditions. Since the theory should be good for arbitrarily small momenta, one possibility is to demand that the amplitude reproduces the effective range expansion, $p\cot(\delta)=-1/a+\frac{1}{2}r_0p^2+\mathcal{O}(p^4)$. In Refs. [31, 4] this matching was done at $\mu_R=0$ giving $C_0^{\rm finite}=\frac{4\pi a}{M}$, $C_2^{\rm finite}=\frac{4\pi a}{M}\frac{a\,r_0}{2}$, etc. We could equally well have chosen a different matching point (such as $\mu_R=1/a$), and obtained the same results. For $\mu_R\sim Q$, the running couplings in Eq. (5.22) have the scaling in Eq. (5.5). Written in terms of renormalized couplings the amplitude in the ${}^1S_0$ or ${}^3S_1$ channels is [4]

$$\mathcal{A}=-\frac{4\pi}{M}\left[\frac{1}{\frac{4\pi}{MC_0(\mu_R)}+\mu_R+ip}+\frac{4\pi}{M}\frac{C_2(\mu_R)}{C_0(\mu_R)^2}\frac{p^2}{(\frac{4\pi}{MC_0(\mu_R)}+\mu_R+ip)^2}+\mathcal{O}(Q)\right], \tag{5.23}$$

and satisfies Eq. (5.13). The amplitude $\mathcal{A}$ is μ_R independent. It is interesting to note that we can choose a renormalization point where all loop corrections vanish giving

$$\begin{aligned}\mathcal{A}^s &= \sum_{m=0}^{\infty}\mathcal{A}^s_{2m}=-\sum_{m=1}^{\infty}C_{2m}^{(s)}(\mu_R=-ip)\,p^{2m}\\ &= -\frac{4\pi}{M}\frac{1}{1/a+ip}-\frac{4\pi}{M}\left(\frac{1}{1/a+ip}\right)^2\frac{r_0}{2}\,p^2+\ldots\,.\end{aligned} \tag{5.24}$$

The amplitude exactly reproduces the effective range expansion by construction. From Eq. (5.24) the range of the effective field theory can be estimated as $\Lambda\sim 2/r_0\sim m_\pi$ as expected.

5.4 Reproducing the pole in the amplitude

It is possible to choose the boundary condition for $C_0(\mu_R)$ to change the location of the pole that appears at each order in the expansion. For instance, consider the following expansion of the amplitude in the theory without pions:

$$\begin{aligned} A &= \frac{4\pi}{M}\left[\frac{1}{-1/a+\frac{r_0}{2}p^2+...-ip}\right] = \frac{4\pi}{M}\left[\frac{1}{-1/a-\Delta+\Delta+\frac{r_0}{2}p^2+...-ip}\right] \\ &= \frac{-4\pi}{M}\left[\frac{1}{1/a+\Delta+ip}+\frac{\frac{r_0}{2}p^2+\Delta}{(1/a+\Delta+ip)^2}+...\right], \end{aligned} \tag{5.25}$$

where $\Delta \lesssim 1/a$. The series with $\Delta = 0$ and with $\Delta \neq 0$ will both reproduce effective range theory, but differ in the location of the pole that appears at each order in the perturbative expansion. In the ${}^3S_1$ channel, the pole of the physical amplitude is at

$$-ip = \gamma = \sqrt{ME_d} = 45.7\,\mathrm{MeV}\,, \tag{5.26}$$

where E_d is the binding energy of the deuteron. For comparison, $1/a = 36.3\,\mathrm{MeV}$ in this channel. For $\Delta = 0$, the pole that appears at each order in the perturbative expansion will be off by 30%. For some calculations, such as processes involving the deuteron [32, 160, 161, 162, 163], a better behaved perturbation series is obtained by choosing $1/a + \Delta = \gamma$. The pole in the amplitude occurs at $p\cot\delta(p) = ip$ so

$$\Delta = \gamma - 1/a = \frac{1}{2}r_0\gamma^2\,. \tag{5.27}$$

Therefore, although the second term in Eq. (5.25) has a double pole, the residue of this unphysical double pole is zero.

If we want to reproduce the expansion in Eq. (5.25) in the theory without pions then part of $C_0(\mu_R)$ must be treated perturbatively, $C_0(\mu_R) = C_0^{np}(\mu_R) + C_0^{p}(\mu_R)$, where $C_0^{np}(\mu_R) \sim 1/Q$ and $C_0^{p}(\mu_R) \sim Q^0$. Choosing the pole to be at $p = i\gamma$ gives $C_0^{\mathrm{finite}} = 4\pi/(M\gamma)$. In this case the amplitude becomes

$$\mathcal{A}^s = -\frac{4\pi}{M}\Big[\frac{1}{\gamma+ip}+\frac{4\pi}{M}\frac{C_0^p(\mu_R)}{(C_0^{np}(\mu_R))^2}\frac{1}{(\gamma+ip)^2}+\frac{4\pi}{M}\frac{C_2(\mu_R)}{(C_0^{np}(\mu_R))^2}\frac{p^2}{(\gamma+ip)^2}\Big], \tag{5.28}$$

where the first term is order $1/Q$, and the second and third terms are order Q^0. This is simply a reorganization of the perturbative series. The RGE's are

$$\begin{aligned}\mu_R\frac{\partial}{\partial\mu_R}C_0^{np}(\mu_R) &= \frac{M\mu_R}{4\pi}C_0^{np}(\mu_R)^2\,, \\ \mu_R\frac{\partial}{\partial\mu_R}C_0^{p}(\mu_R) &= 2\,\frac{M\mu_R}{4\pi}C_0^{np}(\mu_R)C_0^{p}(\mu_R)+\mathcal{O}(Q)\,.\end{aligned} \tag{5.29}$$

These can be derived by substituting $C_0(\mu_R) = C_0^{np}(\mu_R) + C_0^{p}(\mu_R)$ into the renormalization group equation for $C_0(\mu_R)$. They can also be derived using the counterterm method described above. If we demand that the observed scattering length and effective range are reproduced at this order then we find

$$\frac{4\pi}{M}\frac{C_0^{p}(\mu_R)}{(C_0^{np}(\mu_R))^2} = \gamma - \frac{1}{a}\,, \qquad\qquad \frac{4\pi}{M}\frac{C_2(\mu_R)}{(C_0^{np}(\mu_R))^2} = \frac{r_0}{2}\,. \tag{5.30}$$

In order for the power counting of $C_0^{p}(\mu_R)$ to be consistent we must treat $\gamma - 1/a \sim Q^2$. From Eq. (5.27) we see that the first relation in Eq. (5.30) could have been derived by demanding that the residue of the double pole in the amplitude vanishes

$$\left.\frac{A^{(0)}}{[A^{(-1)}]^2}\right|_{-ip=\gamma} = 0\,. \tag{5.31}$$

At higher orders there will be order Q^n parts to C_0 whose values are fixed by conditions analogous to Eq. (5.31). These conditions ensure that the position of the pole is not shifted by perturbative corrections. This is analogous to what we do in computing perturbative corrections to the electron mass in QED.

5.5 Loop integrals with a momentum cutoff regulator

Although the analysis in section 5.3 used dimensional regularization to regulate divergent loop integrals, the results for the coefficients $C_{2m}(\mu_R)$ in our momentum subtraction scheme are independent of this choice. As an exercise we will derive the counterterms for $C_0(\mu_R)$ and $C_2(\mu_R)$ using a momentum cutoff regulator, Λ. This will give us the chance to see what type of complications can arise using a different regulator. Note that this is not the same as using a *finite* cutoff scheme. There the momentum cutoff plays a double role as both a regulator and as part of the subtraction scheme.

The graph in the first row first column of Fig. 5.2 gives

$$\begin{aligned}
&iC_0^2 M\int_0^\Lambda \frac{d^3q}{(2\pi)^3}\frac{1}{\vec{q}^{\,2}-p^2}\\
&=\frac{iM}{2\pi^2}C_0^2\Big[\Lambda+\frac{i\pi p}{2}-p\tanh^{-1}\Big(\frac{p}{\Lambda}\Big)\Big]\\
&=\frac{iM}{2\pi^2}C_0^2\Big[\Lambda+\frac{i\pi p}{2}-\frac{p^2}{\Lambda}-\frac{p^4}{3\Lambda^2}-\ldots\Big]\,.
\end{aligned} \tag{5.32}$$

An ultraviolet counterterm cancels the linear divergence,

$$\delta^{1,\mathrm{uv}}C_0=\frac{M}{4\pi}C_0^{\mathrm{finite}^2}\left(-\frac{2\Lambda}{\pi}\right)\,, \tag{5.33}$$

and the same finite counterterm, $\delta^1 C_0(\mu_R)$ in Eq. (5.17) is used to satisfy the condition in Fig. 5.1. The renormalized graph is then the same as calculated in dimensional regularization in section III. Note that contributions of order p^2 have been neglected in defining $C_0(\mu_R)$ as required by our renormalization condition. An added complication with a cutoff is that graphs with only C_0's give a contribution to the amplitude proportional to p^2. However, as $\Lambda\to\infty$, $p\tanh^{-1}(p/\Lambda)\to 0$, so these terms can be completely neglected. This will remain true even for higher loops since the counterterms will always cancel dangerous powers of Λ that appear in the numerator. At n loops we find an ultraviolet counterterm of the form

$$\delta^{n,\mathrm{uv}}C_0=-\Big(\frac{-M}{4\pi}\Big)^n C_0(\mu_R)^{n+1}\left(-\frac{2\Lambda}{\pi}\right)^n\,, \tag{5.34}$$

while the finite counterterms are given by Eq. (5.17).

The graph in the third row first column of Fig. 5.2 gives

$$2iC_0C_2\frac{M}{2}\int_0^\Lambda\frac{d^3q}{(2\pi)^3}\frac{\vec{q}^{\,2}+p^2}{\vec{q}^{\,2}-p^2}$$

$$= 2\,\frac{iM}{2\pi^2}C_0C_2\left\{\frac{\Lambda^3}{6}+p^2\left[\Lambda+\frac{i\pi p}{2}-p\tanh^{-1}\!\left(\frac{p}{\Lambda}\right)\right]\right\}. \tag{5.35}$$

Note that there are different contributions from this graph when the vertices are in the order $C_0\,C_0\,C_2$ or $C_0\,C_2\,C_0$. At order p^2, this graph gives a correction to the counterterm $\delta^{1,\mathrm{uv}}C_0$, i.e., $\delta^{1,\mathrm{uv}}C_0 \to \delta^{1,\mathrm{uv}}C_0+\delta^{1*,\mathrm{uv}}C_0$, where

$$\delta^{1*,\mathrm{uv}}C_0 \;=\; -\frac{M}{4\pi}2\,C_0^{\mathrm{finite}}\,C_2^{\mathrm{finite}}\frac{\Lambda^3}{3\pi}\,. \tag{5.36}$$

Unlike the contribution to $\delta^{1,\mathrm{uv}}C_0$ in Eq. (5.34), $\delta^{1*,\mathrm{uv}}C_0$ is to be treated perturbatively, so that at it only appears once in any graph. The justification of this fact is that this contribution to the counterterm appeared at order Q^0 (a purely formal trick to recover this counting is to take $\Lambda\sim\mu_R\sim Q$). The counterterm $\delta^{1,\mathrm{uv}}C_2$ is fixed by considering the order p^2 terms in Fig. 5.2, row 3. From Eq. (5.35) (the $\tanh^{-1}$ piece can again be thrown away) we have

$$\delta^{1,\mathrm{uv}}C_2 \;=\; \frac{M}{4\pi}2\,C_0^{\mathrm{finite}}\,C_2^{\mathrm{finite}}\left(-\frac{2\Lambda}{\pi}\right)\,. \tag{5.37}$$

The calculation for higher loops is similar and there are again corrections $\delta^{n*,\mathrm{uv}}C_0$ to $\delta^{n,\mathrm{uv}}C_0$

$$\begin{aligned}\delta^{n*,\mathrm{uv}}C_0 \;&=\; \left(\frac{-M}{4\pi}\right)^n n(n+1)\,(C_0^{\mathrm{finite}})^n\,C_2^{\mathrm{finite}}\left(-\frac{2\Lambda}{\pi}\right)^{n-1}\frac{\Lambda^3}{3\pi}\,,\\ \delta^{n,\mathrm{uv}}C_2 \;&=\; -\left(\frac{-M}{4\pi}\right)^n(n+1)\,(C_0^{\mathrm{finite}})^n\,C_2^{\mathrm{finite}}\left(-\frac{2\Lambda}{\pi}\right)^n\,.\end{aligned} \tag{5.38}$$

The finite counterterms are the same as in Eq. (5.17). Thus the running couplings and amplitudes with a cutoff are the same as found using dimensional regularization.

5.6 Theory with nucleons and pions

In this section, we study the renormalization of contact interactions in the effective field theory with pions. In the ${}^3S_1$ channel, graphs with two or more consecutive

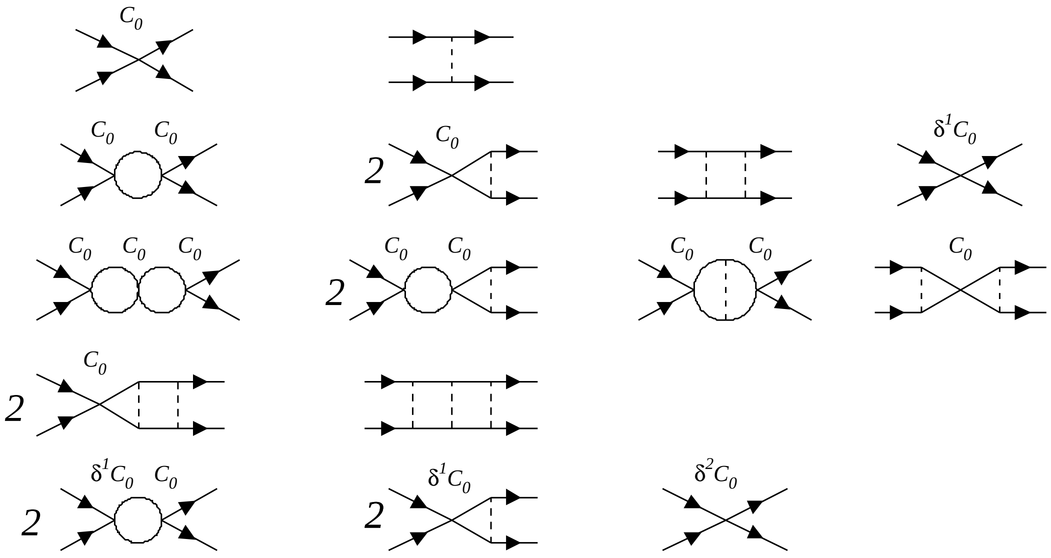

Figure 5.3: Zero, one, and two-loop graphs with C_0 and $\delta^n C_0$ vertices and potential pion exchange. The dashed lines denote potential pion propagators.

potential pions do not factorize and give poles of the form p^{2m}/ϵ where $d = 4 - 2\epsilon$. We explicitly compute these poles for two loop pion graphs. There are also m_π^2/ϵ poles in both the ${}^1S_0$ and ${}^3S_1$ channels at order Q^0 [31, 4]. Because of these $1/\epsilon$ poles, pions cannot be summed to all orders in a model independent way. The finite counterterms in PDS and OS are different in this theory. Throughout this section we will take $m_\pi = 0$, since we are only interested in the couplings $C_{2m}(\mu_R)$. The $D_2(\mu_R)$ counterterms will be considered in section V. We compute the PDS counterterms and beta functions for $C_0(\mu_R)$ and $C_2(\mu_R)$ to order Q. In PDS, $C_0(\mu_R)$ no longer obeys the Q scaling for $\mu_R \gtrsim 300\,\text{MeV}$[4]. This can be fixed by treating part of the coupling $C_0(\mu_R)$ perturbatively as discussed in Section VI. The exact expressions for $C_0(\mu_R)$, $C_2(\mu_R)$, and $C_4(\mu_R)$ are given in the OS scheme and exhibit the correct Q scaling for all $\mu_R > 1/a$. Therefore, it is no longer apparent that the power counting breaks down at 300 MeV. The 300 MeV scale does appear in the short distance contribution to the amplitude from pion exchange, however, it can only be taken as an estimate for the range of the effective field theory once pion and contact interactions are both included.

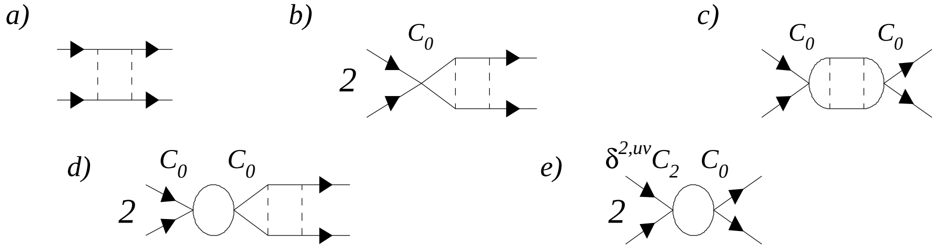

Figure 5.4: The basic order Q graphs in the ${}^3S_1$ channel whose loop integrals do not factorize even for $m_\pi = 0$.

In section VI, we will discuss how experimental data suggests that $\Lambda_\pi \gtrsim 300\,\mathrm{MeV}$.

To determine how the pions contribute to the beta functions for $C_{2m}(\mu_R)$, we use the rules in section II. Some of the pion graphs that will be needed are shown in Fig. 5.3.

In both PDS and OS, the first step is to subtract $1/\epsilon$ poles with $d = 4 - 2\epsilon$. For two nucleons in the ${}^1S_0$ channel the spinor indices in Eq. (5.9) are dotted into $\delta_{\alpha\delta}\,\delta_{\beta\gamma}$. Therefore the $m_\pi = 0$ piece of pion exchange reduces to a contact interaction and gives no $1/\epsilon$ poles. In the ${}^3S_1$ channel, graphs with two or more consecutive pions do not factorize and may have $1/\epsilon$ poles. Order Q graphs with two consecutive potential pions are shown in the first row of Fig. 5.4, and labeled a), b), and c). We find

$$\begin{aligned}
a) &= -i\,\frac{3}{2}\left(\frac{g_A^2}{2f^2}\right)^2\left(\frac{-ip\,M}{4\pi}\right), \qquad (5.39)\\
b) &= -3i\,C_0^{\mathrm{finite}}\left(\frac{g_A^2}{2f^2}\right)^2\left(\frac{-ip\,M}{4\pi}\right)^2\left[\frac{1}{\epsilon} - 2\gamma + \frac{14}{3} - 4\ln(2) + 2\,\ln\left(\frac{\pi\mu^2}{-p^2 - i\varepsilon}\right)\right],\\
c) &= -3i\,(C_0^{\mathrm{finite}})^2\left(\frac{g_A^2}{2f^2}\right)^2\left(\frac{-ip\,M}{4\pi}\right)^3\left[\frac{1}{\epsilon} - 3\gamma - 6\ln 2 + \frac{37}{6} + 3\,\ln\left(\frac{\pi\mu^2}{-p^2 - i\varepsilon}\right)\right].
\end{aligned}$$

Graphs b) and c) have been written with C_0^{finite} vertices to emphasize that the uv counterterm which cancels their divergent part is independent of μ_R. The divergence in $b)$ is cancelled by a tree level graph with the counterterm

$$\delta^{2,\,\mathrm{uv}}C_2 = -\,6\, C_0^{\mathrm{finite}}\Big(\frac{M g_A^2}{8\pi f^2}\Big)^2 \left[\frac{1}{2\epsilon} - \gamma + \ln{(\pi)} + 2 - 2\ln{(2)}\right] \,, \tag{5.40}$$

where the superscript 2 indicates that the counterterm comes in at two loops. The extra factor $2 - 2\ln{(2)}$ is included because this leads to simpler analytic expressions. Expanding the C_0 bubble graph (second row, first column of Fig. 5.3) in ϵ gives

$$-\,\frac{pM}{4\pi}(C_0)^2 \left\{1 + \epsilon\Big[2 - \gamma - 2\ln{(2)} + \ln\Big(\frac{\pi\mu^2}{-p^2 - i\epsilon}\Big)\Big]\right\} \,. \tag{5.41}$$

When graphs with $1/\epsilon$ poles are dressed with C_0 bubbles, the factors of $[2 - \gamma - 2\ln 2 + \ln{(\pi)}]$ that appear are cancelled by similar factors from the counterterms. In fact, $\delta^{2,\,\mathrm{uv}}C_2$ is the only uv counterterm we need for two potential pion exchange with $m_\pi = 0$. The $1/\epsilon$ pole in $c)$ is nonanalytic since it is proportional to p^3. When graph $c)$ is added to graphs $d)$ and $e)$ the poles cancel. These cancellations continue to occur when more C_0 bubbles are added to $b)$ and $c)$. After including graphs with $\delta^{2,\mathrm{uv}}C_2$ we find

$$\begin{aligned} b) + i\delta^{2,\,\mathrm{uv}}C_2\, p^2 &= -3i\, C_0^{\mathrm{finite}} \Big(\frac{g_A^2}{2f^2}\Big)^2 \Big(\frac{-ip\,M}{4\pi}\Big)^2 \left[\frac{2}{3} + 2\ln\Big(\frac{\mu^2}{-p^2 - i\varepsilon}\Big)\right], \\ c) + \frac{1}{2}e) &= -3i\, (C_0^{\mathrm{finite}})^2 \Big(\frac{g_A^2}{2f^2}\Big)^2 \Big(\frac{-ip\,M}{4\pi}\Big)^3 \left[\frac{1}{6} + 2\ln\Big(\frac{\mu^2}{-p^2 - i\varepsilon}\Big)\right]. \end{aligned} \tag{5.42}$$

Note that for $\mu \sim p$ there are no large numerical factors from these graphs.

In the ${}^3S_1$ channel, potential pion graphs without contact interactions also have p^2/ϵ poles. The two loop graph with three potential pions (fourth row, second column in Fig. 5.3) is equal to

$$\frac{4\pi i}{M}\Big(\frac{M g_A^2}{8\pi f^2}\Big)^3\, p^2\, \left[\frac{3}{\epsilon} + \ldots\right]. \tag{5.43}$$

In the Q power counting, this graph is order Q^2 and will not be considered here. Because of these $1/\epsilon$ poles it is not possible to sum pion ladder graphs to all orders.

Now that the ultraviolet divergences have been removed from graphs *b*) and *c*), the finite subtractions can be performed.

5.6.1 PDS

For PDS in the $^1S_0$ channel, we can compute the effect of potential pions on the $C_{2m}(\mu_R)$ counterterms to all orders in Q (neglecting relativistic corrections). For $C_0(\mu_R)$, the relevant zero, one, and two loop graphs are shown in Fig. 5.3. The $C_0(\mu_R)$ and $C_2(\mu_R)$ counterterms are

$$\begin{aligned}
\delta^n C_0^{(^1S_0)}(\mu_R) &= (-1)^{n+1}\Big(\frac{M\mu_R}{4\pi}\Big)^n\Big[C_0(\mu_R)+\frac{g_A^2}{2f^2}\Big]^{n+1}\,, \\
\delta^n C_2^{(^1S_0)}(\mu_R) &= (-1)^{n+1}(n+1)\Big(\frac{M\mu_R}{4\pi}\Big)^n\Big[C_0(\mu_R)+\frac{g_A^2}{2f^2}\Big]^{n} C_2(\mu_R)\,. \qquad (5.44)
\end{aligned}$$

The PDS counterterms in the $^3S_1$ channel will only be computed to order Q since the loop graphs with consecutive pions do not factorize. For this case it is essential to use the counterterms to carry out the PDS renormalization program. To define $C_0(\mu_R)$ at order Q, we set up the finite subtractions as in Fig. 5.3, but leave out all graphs with more than two potential pions since they are $\mathcal{O}(Q^2)$ (we also neglect relativistic corrections that are order Q but come with an additional $1/M^2$). Note that in $d=3$ only the overall divergence ($\propto 1/(d-3)^n$ for n loops) is needed since loops with counterterms will cancel the sub-divergences. Evaluating the graphs in Fig. 5.4 with $d=3$ and then continuing back to $d=4$ gives

$$\begin{aligned}
a) &= -9\,i\Big(\frac{g_A^2}{2f^2}\Big)^2\Big(\frac{\mu_R M}{4\pi}\Big), \qquad b) = -12\,i\,C_0(\mu_R)\Big(\frac{g_A^2}{2f^2}\Big)^2\Big(\frac{\mu_R M}{4\pi}\Big)^2, \\
c) &= -5\,i\,C_0(\mu_R)^2\Big(\frac{g_A^2}{2f^2}\Big)^2\Big(\frac{\mu_R M}{4\pi}\Big)^3. \qquad (5.45)
\end{aligned}$$

Using these values we find

$$\begin{aligned}
\delta^1 C_0^{(^3S_1)} &= \Big(\frac{M\mu_R}{4\pi}\Big)\Big[C_0(\mu_R)^2+2C_0(\mu_R)\frac{g_A^2}{2f^2}+9\Big(\frac{g_A^2}{2f^2}\Big)^2\Big]\,, \qquad (5.46) \\
\delta^n C_0^{(^3S_1)} &= (-1)^{n+1}\Big(\frac{M\mu_R}{4\pi}\Big)^n\Big[C_0(\mu_R)^{n+1}+(n+1)C_0(\mu_R)^n\frac{g_A^2}{2f^2}
\end{aligned}$$

$$+\frac{1}{2}(n+1)(n+4)C_0(\mu_R)^{n-1}\Big(\frac{g_A^2}{2f^2}\Big)^2\Big]\,. \qquad \text{for } n\geq 2$$

Note that for graphs with two consecutive potential pions, the μ_R dependence does not come in the linear combination μ_R+ip. For instance, adding the PDS counterterm to graph a) in Fig. 5.4 gives the linear combination $3ip/2+9\mu_R$.

In PDS, like in $\overline{\rm MS}$, the renormalized coupling $C_2(\mu_R)$ will depend on $\ln(\mu_R^2/\mu_0^2)$ in such a way that the $\ln(\mu_R^2)$ dependence in the amplitudes in Eq. (5.39) is cancelled. Here μ_0 is an arbitrary scale expected to be of order Λ_π. At order Q we find

$$\begin{aligned}
\delta^1 C_2^{(^3S_1)}(\mu_R) &= 2\Big(\frac{M\mu_R}{4\pi}\Big)\Big[C_0(\mu_R)+\frac{g_A^2}{2f^2}\Big]C_2(\mu_R)\,, \\
\delta^n C_2^{(^3S_1)}(\mu_R) &= (-1)^{n+1}\Big\{(n+1)\Big(\frac{M\mu_R}{4\pi}\Big)^n\Big[C_0(\mu_R)^n+n\frac{g_A^2}{2f^2}C_0(\mu_R)^{n-1}\Big]C_2(\mu_R) \\
&\quad +6\Big(\frac{M\mu_R}{4\pi}\Big)^{n-2}C_0(\mu_R)^{n-1}\Big(\frac{Mg_A^2}{8\pi f^2}\Big)^2\ln\Big(\frac{\mu_R^2}{\mu_0^2}\Big)\Big\} \qquad \text{for } n\geq 2\,.
\end{aligned} \tag{5.47}$$

Note that the part of $\delta^n C_2(\mu_R)$ proportional to $\ln(\mu_R^2/\mu_0^2)$ has a coefficient that sums up to $C_0^{\rm finite}$ at this order. From Eqs. (5.44), (5.46), and (5.47) we find

$$\begin{aligned}
\beta_0^{(^1S_0)} &= \frac{M\mu_R}{4\pi}\Big[C_0(\mu_R)+\frac{g_A^2}{2f^2}\Big]^2\,, \\
\beta_2^{(^1S_0)} &= 2\,\frac{M\mu_R}{4\pi}\Big[C_0(\mu_R)+\frac{g_A^2}{2f^2}\Big]C_2(\mu_R)\,, \\
\beta_0^{(^3S_1)} &= \frac{M\mu_R}{4\pi}\Big\{C_0^2+2\frac{g_A^2}{2f^2}C_0+\Big[9+4\Big(\frac{\mu_R MC_0}{4\pi}\Big)+2\Big(\frac{\mu_R MC_0}{4\pi}\Big)^2\Big]\Big(\frac{g_A^2}{2f^2}\Big)^2\Big\} \\
&\quad +\mathcal{O}(Q^2)\,, \\
\beta_2^{(^3S_1)} &= 2\,\frac{M\mu_R}{4\pi}\Big[C_0(\mu_R)+\frac{g_A^2}{2f^2}\Big]C_2(\mu_R)-12\Big(\frac{Mg_A^2}{8\pi f^2}\Big)^2C_0(\mu_R)\Big[1+\mu_R\frac{M}{4\pi}C_0(\mu_R)\Big] \\
&\quad +\mathcal{O}(Q^0)\,.
\end{aligned} \tag{5.48}$$

Note that in the $^1S_0$ channel all contributions to the beta functions beyond one-loop cancel, leaving them one-loop exact. In Ref. [4], the last two terms in $\beta_0^{(^3S_1)}$ are absent, but should be included in the complete order Q calculation. Dimensional analysis implies that the $^3S_1$ beta functions can have corrections at all higher orders in

Q, since there is nothing to prevent the dimensionless factor $(\mu_R\, g_A^2\, M)/(8\pi f^2) \sim Q$ from appearing. In Ref. [155], expressions for the beta functions are derived by demanding that $\partial\mathcal{A}/\partial\mu_R = 0$, but these are not the PDS beta functions. Since in all renormalization schemes $\partial\mathcal{A}/\partial\mu_R = 0$, this condition is not sufficient to fix the renormalization scheme uniquely.

When the beta function is not exactly known, the large μ_R behavior is ambiguous. For example, the PDS beta function for $C_0(\mu_R)$ is [4]

$$\beta_0 \;=\; \mu_R \frac{\partial C_0(\mu_R)}{\partial \mu_R} = \frac{M\mu_R}{4\pi}\left[C_0^2(\mu_R) + 2\frac{g_A^2}{2f^2}C_0(\mu_R)\right] + \mathcal{O}(Q)\,. \tag{5.49}$$

Two solutions which satisfy this equation to order Q^0 are

$$\begin{aligned} C_0(\mu_R) &= -\frac{4\pi}{M}\frac{\left[1 - 2a\mu_R - 2\mu_g - \sqrt{1 + 4\mu_g^2 - 4\mu_g(1 - a\mu_R)}\,\right]}{2\mu_R(1 - a\mu_R - \mu_g)}\,, \\ C_0(\mu_R) &= -\frac{g_A^2}{f^2}\frac{1}{1 - \left[1 + 2/(a\Lambda_{NN})\right]\exp\left(-2\mu_g\right)}\,, \end{aligned} \tag{5.50}$$

where $\mu_g = \mu_R/\Lambda_{NN}$ and we have chosen $C_0(0) = 4\pi a/M$. The first solution is obtained by computing the counterterms $\delta^n C_0(\mu_R)$ to order Q^0 and summing them. This solution falls as $1/\mu_R$ for all $\mu_R > 1/a$, and is numerically close to the $g_A \to 0$ solution. The second solution is obtained by truncating and solving Eq. (5.49). This solution approaches a constant as $\mu_R \to \infty$. The two solutions both solve the beta function to order Q^0 but have very different large μ_R behavior. Since the beta function for $C_0^{({}^3S_1)}(\mu_R)$ can have corrections at any order in Q its large μ_R behavior is unknown and not meaningful. This issue can be dealt with by expanding the C_{2m} coupling constants in a series in Q and solving the beta function for each order separately.

5.6.2 OS

In the OS scheme, there is no such ambiguity since at a given order in Q the running of all the coupling constants that enter at that order are known exactly. The coupling $C_0^{(s)}(\mu_R)$ has contributions only from the nucleon graphs discussed in section II and therefore has the same beta function. For $C_2^{(s)}(\mu_R)$, the order Q^0 graphs in $\mathcal{A}_2$ include the nucleon graphs from section II, as well as the graphs with one potential pion and any number of C_0 vertices. At tree level we add a finite counterterm to cancel the $m_\pi = 0$ part of the tree level pion interaction at $p = i\mu_R$

$$\delta^0 C_2^{(s)}(\mu_R) = -\,\frac{g_A^2}{2f^2}\,\frac{1}{\mu_R^2}\,. \tag{5.51}$$

This counterterm is order Q^{-2} like $C_2(\mu_R)$ itself. Since all the graphs in $\mathcal{A}_2$ factorize the higher loop counterterms are the same as in the theory without pions, so $\delta^n C_2$ for $n \geq 1$ are given in Eq. (5.17). The exact beta function is then

$$\beta_2^{(s)} = 2\,\frac{M\mu_R}{4\pi}\,C_0(\mu_R)C_2(\mu) + 2\,\frac{g_A^2}{2f^2}\Big(1 + \frac{M\mu_R}{4\pi}C_0(\mu_R)\Big)^2\,\frac{1}{{\mu_R}^2}\,. \tag{5.52}$$

Note that the finite $\ln(\mu^2/(-p^2 - i\epsilon))$ terms in Eq. (5.39) are order Q and in the OS scheme do not affect the running of $C_2(\mu_R)$, but rather $C_4(\mu_R)$. In terms of the finite constants $C_0^{\rm finite}$ and $C_2^{\rm finite}$ we have solutions

$$C_0^{(s)}(\mu_R) \;=\; \frac{1}{\frac{1}{C_0^{\rm finite}} - \frac{M\mu_R}{(4\pi)}}\,, \qquad\qquad C_2^{(s)}(\mu_R) = \frac{C_2^{\rm finite} - \frac{g_A^2}{2f^2\mu_R^2}}{\Big[1 - \mu_R\frac{C_0^{\rm finite}M}{4\pi}\Big]^2}\,. \tag{5.53}$$

Although it may seem that the piece of $C_2^{(s)}(\mu_R)$ that goes as $1/\mu_R^4$ will spoil the power counting for low momentum, in fact, the $1/\mu_R^2$ part dominates entirely until $\mu_R \sim 1/a$, since $C_0^{\rm finite} \sim a$, $C_2^{\rm finite} \sim a^2$. Written in terms of renormalized couplings the $m_\pi = 0$ part of the next-to-leading order OS amplitude is

$$\frac{-C_2(\mu_R)\,p^2}{\Big[1 + (\mu_R + ip)\frac{MC_0(\mu_R)}{4\pi}\Big]^2} \;-\; \frac{g_A^2}{2f^2}\,\frac{\mu_R^2 + p^2}{\mu_R^2}\,\frac{\Big[1 + \mu_R\frac{C_0(\mu_R)M}{4\pi}\Big]^2}{\Big[1 + (\mu_R + ip)\frac{C_0(\mu_R)M}{4\pi}\Big]^2}\,, \tag{5.54}$$

which is order Q^0 as desired.

One might still ask if the problem with the 300 MeV scale will reappear in higher order coefficients. To check that this is not the case we compute the running of the coupling $C_4(\mu_R)$ in the OS scheme. The easiest way to compute this running coupling constant is to compute the order Q amplitude in terms of the finite couplings, $C_{2m}^{\rm finite}$, and then demand that the amplitude satisfies the renormalization condition in Eq. (5.13). The graphs we need to compute include those with

$$\begin{array}{rl} i) & \text{one } C_4 \text{ and any number of } C_0\text{'s}\,, \\ ii) & \text{two } C_2\text{'s and any number of } C_0\text{'s}\,, \\ iii) & \text{one } C_2\text{, one potential pion and any number of } C_0\text{'s}\,, \\ iv) & \text{two potential pions and any number of } C_0\text{'s}\,. \end{array} \qquad (5.55)$$

Computing these graphs in terms of the finite couplings and then demanding that the amplitudes satisfy the renormalization condition gives the OS couplings

$$C_4^{(^1S_0)}(\mu_R) = \frac{C_4^{\rm finite}}{\left[1-\mu_R\frac{M}{4\pi}C_0^{\rm finite}\right]^2} + \frac{\mu_R M}{4\pi}\,\frac{\left[C_2^{\rm finite} - g_A^2/(2f^2)\,\frac{1}{\mu_R{}^2}\right]^2}{\left[1-\mu_R\frac{M}{4\pi}C_0^{\rm finite}\right]^3}\,, \qquad (5.56)$$

$$\begin{aligned} C_4^{(^3S_1)}(\mu_R) &= \frac{C_4^{\rm finite}}{\left[1-\mu_R\frac{M}{4\pi}C_0^{\rm finite}\right]^2} + \frac{\mu_R M}{4\pi}\,\frac{\left[C_2^{\rm finite} - g_A^2/(2f^2)\,\frac{1}{\mu_R{}^2}\right]^2}{\left[1-\mu_R\frac{M}{4\pi}C_0^{\rm finite}\right]^3} \\ &+\frac{1}{2}\left(\frac{g_A^2}{2f^2}\right)^2 \quad \frac{M}{4\pi}\,\frac{1}{\mu_R{}^3}\,\frac{\left[1-2\mu_R\frac{M}{4\pi}C_0^{\rm finite}\right]}{\left[1-\mu_R\frac{M}{4\pi}C_0^{\rm finite}\right]^2} - 6\left(\frac{Mg_A^2}{8\pi f^2}\right)^2 \frac{C_0^{\rm finite}\ln\left(\mu_R^2/\mu^2\right)}{\mu_R^2\left[1-\mu_R\frac{M}{4\pi}C_0^{\rm finite}\right]}\,, \end{aligned}$$

where here μ is an unknown scale expected to be of order Λ_π. Again the pion contributions do not spoil the μ_R scaling behavior, since they are suppressed by factors of the large scattering length. Note that at order Q the PDS coupling $C_4(\mu_R)$ [4] is the $g_A \to 0$ limit of Eq. (5.56).

In this section, expressions for the renormalized couplings $C_0(\mu_R)$, $C_2(\mu_R)$, and $C_4(\mu_R)$ were derived in the PDS and OS schemes working to order Q. For the $^3S_1$ channel, we have shown that $C_0(\mu_R)$ has corrections at all orders in Q in PDS. Unlike PDS, the OS couplings $C_{2m}(\mu_R)$ can be computed exactly because they only have contributions at one order in Q. The OS couplings exhibit the correct μ_R scaling for all $\mu_R > 1/a$.

5.7 The coupling $D_2(\mu_R)$

In this section, the OS and PDS counterterms for $D_2(\mu_R)$ are computed. To define $D_2(\mu_R)$ in the OS scheme, we take

$$i\, A^s(D_2)\Big|_{p=i\mu_R,} = -i\, D_2^{(s)}(\mu_R)\, m_\pi^2 \,, \tag{5.57}$$

where $\mathcal{A}^s(D_2)$ contains terms in the amplitude that are analytic in m_π^2 and proportional to m_π^2. Only terms that are analytic in m_π^2 are kept because it is unnatural to put long-distance nonanalytic contributions that come from pion exchange into the definition of the short distance coupling [155]. For example, one potential pion exchange gives a $m_\pi^2/p^2\ \ln(1+4p^2/m_\pi^2)$ term. Including this in $A^s(D_2)$ would give $D_2(\mu_R)$ both a branch cut at $\mu_R = m_\pi/2$ as well as explicit dependence on the scale m_π. In the OS scheme, $D_2(\mu_R)$ will be calculated as follows. First m_π^2/ϵ poles are subtracted. The finite counterterms are then determined by including graphs with a single $D_2(\mu_R)$ or potential pion and any number of $C_0(\mu_R)$ vertices in $\mathcal{A}^s(D_2)$. Contributions from these graphs that are non-analytic in m_π^2 are dropped.

There is a m_π^2/ϵ pole in the $\mathcal{O}(Q^0)$ graph in the third row and third column of Fig. 5.3 [31, 4], so we have a counterterm

$$\delta^{2,\mathrm{uv}} D_2 = -i\Big(\frac{M C_0^{\mathrm{finite}}}{4\pi}\Big)^2\, \frac{g_A^2}{4f^2}\, \left[\frac{1}{2\epsilon} - \gamma + \log(\pi)\right] . \tag{5.58}$$

Note that when this counterterm is dressed with C_0 bubbles the extra factors of $2-\ln 2$ from Eq. (5.41) will cancel without the need for an additional finite term in $\delta^{2,\mathrm{uv}} D_2$. After subtracting this counterterm the value of the two-loop graph is

$$i\Big(\frac{M C_0^{\mathrm{finite}}}{4\pi}\Big)^2\, \frac{g_A^2}{2f^2}\, \left[-(ip)^2 + \frac{m_\pi^2}{2} + \frac{m_\pi^2}{2}\ln\Big(\frac{\mu^2}{m_\pi^2}\Big) - m_\pi^2 \ln\Big(1 - \frac{2ip}{m_\pi}\Big)\right] . \tag{5.59}$$

For PDS we set $\mu = \mu_R$ and then find finite counterterms

$$\delta^1 D_2(\mu_R) \;=\; 2\Big(\frac{M\mu_R}{4\pi}\Big) C_0(\mu_R) D_2(\mu_R)\,, \tag{5.60}$$

$$\begin{aligned}\delta^n D_2(\mu_R) &= (-1)^{n+1}\Big[(n+1)\Big(\frac{M\mu_R}{4\pi}\Big)^n C_0(\mu_R)^n D_2(\mu_R) \\ &\quad -\frac{(n-1)}{2}\Big(\frac{M\mu_R}{4\pi}\Big)^{n-2} C_0(\mu_R)^n \Big(\frac{M}{4\pi}\Big)^2 \frac{g_A^2}{2f^2}\ln\Big(\frac{\mu_R^2}{\mu_0^2}\Big)\Big] \qquad \text{for } n \geq 2\,.\end{aligned}$$

Here μ_0 is an unknown scale expected to be of order Λ_π.

In the OS scheme, the $\delta^1 D_2(\mu_R)$ counterterm is the same as in PDS. In dimensional regularization logarithms of the form $\ln(\mu^2/m_\pi^2)$ will appear in loop graphs. To make the μ^2 dependent part analytic in m_π^2 we write

$$\ln\left(\frac{\mu^2}{m_\pi^2}\right) = \ln\left(\frac{\mu^2}{\mu_R^2}\right) + \ln\left(\frac{\mu_R^2}{m_\pi^2}\right)\,, \tag{5.61}$$

and then subtract the $\ln(\mu^2/\mu_R^2)$ term with the counterterms. This will give $D_2(\mu_R)$ a μ_R dependence which cancels the $\ln(\mu_R^2/m_\pi^2)$ in the amplitude. In the OS scheme, the $m_\pi^2/2$ in Eq. (5.59) gets subtracted along with the logarithm. We find

$$\begin{aligned}\delta^n D_2(\mu_R) &= (-1)^{n+1}\Big\{(n+1)\Big(\frac{M\mu_R}{4\pi}\Big)^n C_0(\mu_R)^n D_2(\mu_R) \\ &\quad -\frac{(n-1)}{2}\Big(\frac{M\mu_R}{4\pi}\Big)^{n-2} C_0(\mu_R)^n \Big(\frac{M}{4\pi}\Big)^2 \frac{g_A^2}{2f^2}\Big[-1+\ln\Big(\frac{\mu_R^2}{\mu^2}\Big)\Big]\Big\}\end{aligned} \tag{5.62}$$

for $n \geq 2$. Summing the counterterms the solutions for $D_2(\mu_R)$ are then

$$\begin{aligned}\frac{D_2^{(s)}(\mu_R)}{C_0^{(s)}(\mu_R)^2} &= \frac{D_2^{\rm finite}}{(C_0^{\rm finite})^2} + \frac{M}{8\pi}\Big(\frac{Mg_A^2}{8\pi f^2}\Big)\ln\Big(\frac{\mu_R^2}{\mu_0^2}\Big) \qquad \text{in PDS}\,, \\ \frac{D_2^{(s)}(\mu_R)}{C_0^{(s)}(\mu_R)^2} &= \frac{D_2^{\rm finite}}{(C_0^{\rm finite})^2} + \frac{M}{8\pi}\Big(\frac{Mg_A^2}{8\pi f^2}\Big)\Big[-1+\ln\Big(\frac{\mu_R^2}{\mu^2}\Big)\Big] \qquad \text{in OS}\,,\end{aligned} \tag{5.63}$$

which can be written as

$$\begin{aligned}\frac{D_2^{(s)}(\mu_R)}{C_0^{(s)}(\mu_R)^2} &= \frac{M}{8\pi}\Big(\frac{Mg_A^2}{8\pi f^2}\Big)\ln\Big(\frac{\mu_R^2}{\tilde\mu^2}\Big)\,, \\ \text{where} \qquad \tilde\mu^2 &= \mu_0^2\,\exp\Big(\frac{-64\pi^2 f^2 D_2^{\rm finite}}{M^2 g_A^2 (C_0^{\rm finite})^2}\Big) \qquad \text{in PDS}\,, \\ \tilde\mu^2 &= \mu^2\,\exp\Big(1-\frac{64\pi^2 f^2 D_2^{\rm finite}}{M^2 g_A^2 (C_0^{\rm finite})^2}\Big) \qquad \text{in OS}\,.\end{aligned} \tag{5.64}$$

The parameter $\tilde{\mu}$ must be determined by fitting to data. With $m_\pi \sim Q \sim \mu_R$, $D_2(\mu_R) m_\pi^2 \sim Q^0$ in both OS and PDS, implying that $D_2(\mu_R)$ should be treated perturbatively.

5.8 Schemes and amplitudes

In this section, the amplitudes in the ${}^1S_0$ and ${}^3S_1$ channels are presented to order Q^0, both in PDS [31, 4] and OS. Fits to the ${}^1S_0$ and ${}^3S_1$ phase shift data are done in both schemes for different values of μ_R. As pointed out in section 5.4, one has the freedom to split $C_0(\mu_R)$ into perturbative and nonperturbative pieces: $C_0(\mu_R) = C_0^{np}(\mu_R) + C_0^{p}(\mu_R)$, where $C_0^{np}(\mu_R) \sim Q^{-1}$ and $C_0^{p}(\mu_R) \sim Q^0$. This division is necessary in PDS in order to obtain μ_R independent amplitudes at each order. Furthermore, $C_0^{np}(\mu_R) \sim 1/\mu_R$ so the coefficients scale in a manner consistent with the power counting for all $\mu_R > 1/a$. For convenience we will drop the superscript np in what follows. Some issues that arise in matching the pion theory onto the effective range expansion are also discussed.

First, we give the nucleon-nucleon scattering amplitudes in the PDS and OS schemes. In PDS, the amplitudes were calculated to order Q^0 in Refs. [31, 4]. At this order, amplitudes in the ${}^1S_0$ and ${}^3S_1$ channels have the same functional form,

$$A = A^{(-1)} + A^{(0,a)} + A^{(0,b)} + \mathcal{O}(Q^1) \,. \tag{5.65}$$

In both OS and PDS we have

$$A^{(-1)} = -\frac{4\pi}{M} \frac{1}{\frac{4\pi}{MC_0(\mu_R)} + \mu_R + ip} \,, \tag{5.66}$$

$$\frac{A^{(0,a)}}{\left[A^{(-1)}\right]^2} = \frac{g_A^2 m_\pi^2}{2f^2} \left(\frac{M}{4\pi}\right)^2 \left\{ \frac{1}{2} \ln\left(\frac{\mu_R^2}{m_\pi^2}\right) - \left(\frac{4\pi}{MC_0(\mu_R)} + \mu_R\right) \frac{1}{p} \tan^{-1}\left(\frac{2p}{m_\pi}\right) \right.$$
$$\left. + \left[\left(\frac{4\pi}{MC_0(\mu_R)} + \mu_R\right)^2 - p^2\right] \frac{1}{4p^2} \ln\left(1 + \frac{4p^2}{m_\pi^2}\right) \right\} - \frac{D_2(\mu_R)\, m_\pi^2}{C_0(\mu_R)^2} \,.$$

The remaining part of the order Q^0 PDS amplitude is

$$\frac{A^{(0,b)}}{\left[A^{(-1)}\right]^2} = -\frac{C_2(\mu_R)\, p^2}{C_0(\mu_R)^2} + \frac{1}{2}\,\frac{g_A^2 m_\pi^2}{2f^2}\Big(\frac{M}{4\pi}\Big)^2 - \frac{1}{C_0(\mu_R)^2}\Big[\frac{g_A^2}{2f^2} + C_0^p(\mu_R)\Big]\,. \tag{5.67}$$

Note that since we have made a different finite subtraction than KSW the second term has a prefactor of 1/2, rather than a 1 as in Ref. [4]. In the OS scheme

$$\frac{A^{(0,b)}}{\left[A^{(-1)}\right]^2} = -\frac{C_2(\mu_R)\, p^2}{C_0(\mu_R)^2} - \frac{g_A^2}{2f^2}\Big(1+\frac{p^2}{\mu_R^2}\Big)\Big(\frac{1}{C_0(\mu_R)} + \frac{M\mu_R}{4\pi}\Big)^2 - \frac{C_0^p(\mu_R)}{C_0(\mu_R)^2}\,. \tag{5.68}$$

The OS and PDS couplings that appear at this order are related by a change of variables. Couplings on the left are in PDS while those on the right are in the OS scheme.

$$\begin{aligned}
C_0(\mu_R) &= C_0(\mu_R)\,,\\
\frac{C_2(\mu_R)}{C_0(\mu_R)^2} &= \frac{C_2(\mu_R)}{C_0(\mu_R)^2} + \frac{g_A^2}{2f^2}\frac{1}{\mu_R^2}\Big[\frac{1}{C_0(\mu_R)} + \frac{M\mu_R}{4\pi}\Big]^2,\\
\frac{D_2(\mu_R)}{C_0(\mu_R)^2} - \frac{M}{8\pi}\Big(\frac{Mg_A^2}{8\pi f^2}\Big) &= \frac{D_2(\mu_R)}{C_0(\mu_R)^2}\,,\\
\frac{C_0^p(\mu_R)}{C_0(\mu_R)^2} + \frac{g_A^2}{2f^2}\frac{1}{C_0(\mu_R)^2} &= \frac{C_0^p(\mu_R)}{C_0(\mu_R)^2} + \frac{g_A^2}{2f^2}\Big[\frac{1}{C_0(\mu_R)} + \frac{M\mu_R}{4\pi}\Big]^2.
\end{aligned} \tag{5.69}$$

In the PDS scheme, there are order Q^0 contributions to β_0 (c.f., Eq. (5.48)). If the order Q^0 contributions are separated from the order $1/Q$ pieces, the beta function for $C_0^p(\mu_R)$ is

$$\mu_R\frac{\partial C_0^p(\mu_R)}{\partial\mu_R} = 2\,\frac{M\mu_R}{4\pi}C_0(\mu_R)\Big[C_0^p(\mu_R) + \frac{g_A^2}{2f^2}\Big] + \mathcal{O}(Q)\,. \tag{5.70}$$

This equation has the solution

$$\frac{C_0^p(\mu_R)}{C_0(\mu_R)^2} = \frac{M}{4\pi}K - \frac{g_A^2}{2f^2}\frac{1}{C_0(\mu_R)^2}\,, \tag{5.71}$$

where K is a constant which must be order Q^2 for $C_0^p(\mu_R) \sim Q^0$. (Recall, from Eq. (5.30) that $K = \gamma - 1/a \lesssim 1/a$ in the pure nucleon theory.) Including $C_0^p(\mu_R)$ makes the PDS amplitudes explicitly μ_R independent. In performing fits to the data the constant K and coupling $D_2(\mu_R)$ cannot be determined independently. In what follows we will drop K when fitting and simply remember that the values of $D_2(\mu_R)$ extracted from the fits may differ from the renormalized coupling in the Lagrangian. In PDS, if $C_0^p(\mu_R)$ is omitted from our expressions then $D_2(\mu_R)$ does not follow the renormalization group equation, as we will see below.

In the OS scheme, the constant $g_A^2/(2f^2)$ in Eqs.(5.70) and (5.71) is not present, so $C_0^p(\mu_R)/C_0(\mu_R)^2$ is μ_R independent. The OS scheme amplitudes $A^{(-1)}$ and $A^{(0)}$ are therefore μ_R independent without $C_0^p(\mu_R)$ as can be seen by examining Eqs. (5.53), and (5.63). In OS the constant K will also be absorbed into $D_2(\mu_R)$ for fitting.

Using the Nijmegen phase shifts [2] between 7 and 100 MeV, we fit the coefficients $C_0(\mu_R)$, $C_2(\mu_R)$ and $D_2(\mu_R)$. We took $m_\pi = 137\,\mathrm{MeV}$. Clearly we would like to bias the fit towards the low momentum points since that is where the theoretical error is smallest. This can be accomplished by assigning a percent error, $\simeq p/(300\,\mathrm{MeV})$, to the data and then minimizing the χ^2 function. In Tables 5.1 and 5.2 we show the values[5] of $C_0(\mu_R)$, $C_2(\mu_R)$ and $D_2(\mu_R)$ extracted from the fits for $\mu_R = 70, 100, 137, 160, 280\,\mathrm{MeV}$. These values exhibit the μ_R dependence predicted by the RGE's to $\sim 1\%$ in the $^1S_0$ channel and $\sim 4\%$ in the $^3S_1$ channel. Since the amplitudes are explicitly μ_R independent this deviation is a measure of the accuracy of the fitting routine. In Fig. 5.5 the results of the fits are shown. The results of the fits shown in the figure are identical in both schemes. Higher order corrections will give contributions to δ of the form p^2/Λ_π^2. The error in δ at $p = 300\,\mathrm{MeV}$ is consistent with $\Lambda_\pi \gtrsim 500\,\mathrm{MeV}$.

For processes involving the deuteron it is convenient to fix $C_0(\mu_R)$ using the deuteron binding energy, $C_0(m_\pi) = -5.708\,\mathrm{fm}^2$. Fitting with this constraint we

---

[5] The coefficients extracted from our fits differ from those in Ref.[4] because we have emphasized the low energy data as opposed to doing a global fit. It is interesting to note that using our PDS value $C_2(\mu_R = 137\,\mathrm{MeV}) = 11.5\,\mathrm{fm}^4$, the prediction for the RMS charge radius of the deuteron [32] becomes 1.966 fm which is within 1% of the experimental result.

	Fit to $^1S_0$			Fit to $^3S_1$		
μ_R(MeV)	$C_0(\mu_R)$	$C_2(\mu_R)$	$D_2(\mu_R)$	$C_0(\mu_R)$	$C_2(\mu_R)$	$D_2(\mu_R)$
70	−6.48	10.11	−0.532	−22.73	171.	−70.41
100	−4.71	5.36	1.763	−9.93	32.7	−4.157
137	−3.53	3.01	2.000	−5.88	11.5	1.500
160	−3.05	2.25	1.869	−4.69	7.32	1.897
280	−1.79	0.772	1.105	−2.19	1.57	1.004

Table 5.1: $^1S_0$ and $^3S_1$ couplings in the PDS scheme. $C_0(\mu_R)$ (in fm^2), $C_2(\mu_R)$ (in fm^4), and $D_2(\mu_R)$ (in fm^4) are fit to the Nijmegen data at different values of μ_R.

	Fit to $^1S_0$			Fit to $^3S_1$		
μ_R(MeV)	$C_0(\mu_R)$	$C_2(\mu_R)$	$D_2(\mu_R)$	$C_0(\mu_R)$	$C_2(\mu_R)$	$D_2(\mu_R)$
70	−6.50	9.75	−6.047	−24.1	121.	−170.1
100	−4.73	5.33	−1.143	−10.0	27.3	−20.18
137	−3.54	3.00	0.378	−5.92	10.5	−4.124
160	−3.06	2.25	0.658	−4.74	6.89	−1.671
280	−1.80	0.779	0.692	−2.23	1.61	0.2985

Table 5.2: $^1S_0$ and $^3S_1$ couplings in the OS scheme. $C_0(\mu_R)$ (in fm^2), $C_2(\mu_R)$ (in fm^4), and $D_2(\mu_R)$ (in fm^4) are fit to the Nijmegen data at different values of μ_R.

find $C_2(m_\pi) = 10.80\,\mathrm{fm}^4$ and $D_2(m_\pi) = 1.075\,\mathrm{fm}^4$ in the PDS scheme. The fit to the phase shift data with these values is as good as that in Fig. 5.5.

In PDS, it is necessary to break $C_0(\mu_R)$ into perturbative and non-perturbative parts to obtain amplitudes that are μ_R independent order-by-order. If $C_0^p(\mu_R)$ is omitted then the values of $D_2(\mu_R)$ determined from the fit will not follow the RGE. To see this we define the μ_R independent quantity

$$R = c\Big[\frac{-D_2(\mu_R)}{C_0(\mu_R)^2} + \frac{M}{8\pi}\Big(\frac{Mg_A^2}{8\pi f^2}\Big)\ln\Big(\frac{\mu_R^2}{\mu_0^2}\Big)\Big]\,, \tag{5.72}$$

and choose the constant c so that $R = 1$ for $\mu_R = 137\,\mathrm{MeV}$. For other values of μ_R the deviation of R from 1 gives the discrepancy between the values predicted by the RGE and those extracted from the fit. For $\mu_R = 70, 280\,\mathrm{MeV}$ we find $R = -0.53,\ 7.25$ in the $^1S_0$ channel and $R = -0.52,\ 11.4$ in the $^3S_1$ channel. These large deviations disappear

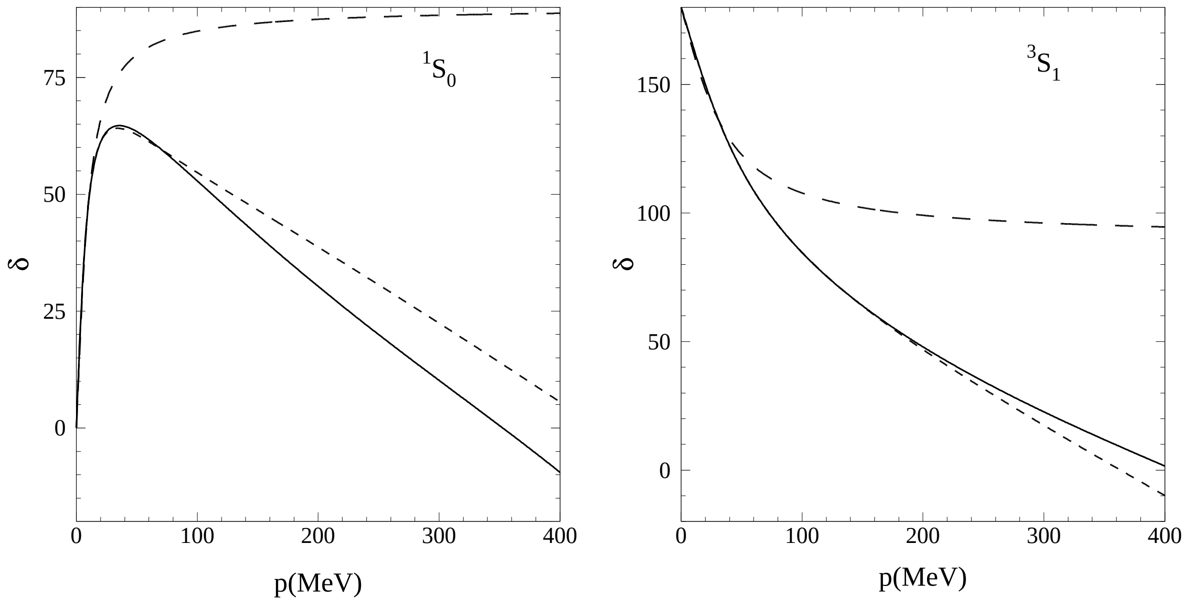

Figure 5.5: Fit to the phase shift data emphasizing the low momentum region. The solid line is the Nijmegen fit to the data [2], the long dashed line is the order $1/Q$ result, and the short dashed line is the order Q^0 result.

if $C_0^p(\mu_R)$ is included. Without $C_0^p(\mu_R)$, the PDS amplitude is μ_R independent to the order that one is working. However, this residual μ_R dependence gives larger corrections than expected [154]. The reason for this (as explained below) is that the residual μ_R dependence makes the tuning that was setup to give the large scattering length μ_R dependent.

Integrating out the pion gives low-energy theorems for the coefficients v_i in the effective range expansion[3],

$$p\cot(\delta) = -\frac{1}{a} + \frac{r_0}{2}\,p^2 + v_2\,p^4 + v_3\,p^6 + v_4\,p^8 + \ldots\,. \tag{5.73}$$

Performing a matching calculation between the two theories gives expressions for a, r_0 and the v_i in terms of the parameters in the pion theory. Since the theory with pions is an expansion in Q these predictions take the form of Taylor series in Q/Λ_π

$$\frac{1}{a} = \gamma + \sum_{i=2}^{\infty} B_0^{(i)}\,, \qquad \frac{r_0}{2} = \sum_{i=0}^{\infty} B_1^{(i)}\,, \qquad v_n = \sum_{i=2-2n}^{\infty} B_n^{(i)}\,, \tag{5.74}$$

where $B_n^{(i)} \sim Q^i$. At this time only the first coefficient in each series is known since $p\cot\delta$ has only been calculated[6] to order Q^2. The notation

$$\gamma = \frac{4\pi}{MC_0(\mu_R)} + \mu_R \tag{5.75}$$

will be used to denote the location of the perturbative pole in the amplitudes. In PDS

$$\begin{aligned} B_0^{(2)} &= \Big(\frac{-4\pi}{M}\Big)\frac{m_\pi^2 D_2(\mu_R)}{C_0(\mu_R)^2} + \frac{m_\pi^2\, Mg_A^2}{8\pi f^2}\Big[\frac{1}{2}+\frac{1}{2}\ln\Big(\frac{\mu_R^2}{m_\pi^2}\Big) - \frac{2\gamma}{m_\pi} + \frac{\gamma^2}{m_\pi^2}\ \Big] - K\,, \\ B_1^{(0)} &= \Big(\frac{4\pi}{M}\Big)\frac{C_2(\mu_R)}{\Big[C_0(\mu_R)\Big]^2} + \frac{Mg_A^2}{8\pi f^2}\Big[1 - \frac{8\gamma}{3\,m_\pi} + \frac{2\gamma^2}{m_\pi^2}\Big]\,. \end{aligned} \tag{5.76}$$

Note that if $C_0^p(\mu_R)$ had been neglected then $B_0^{(2)}$ would not be μ_R independent. With $\mu_R = m_\pi$ Eq. (5.76) agrees with Ref. [4] if their definition of $D_2(\mu_R)$ is adopted. In the OS scheme we have

$$\begin{aligned} B_0^{(2)} &= \Big(\frac{-4\pi}{M}\Big)\frac{m_\pi^2 D_2(\mu_R)}{C_0(\mu_R)^2} + \frac{m_\pi^2\, Mg_A^2}{8\pi f^2}\Big[\frac{1}{2}\ln\Big(\frac{\mu_R^2}{m_\pi^2}\Big) - \frac{2\gamma}{m_\pi}\Big] - K\,, \\ B_1^{(0)} &= \Big(\frac{4\pi}{M}\Big)\frac{C_2(\mu_R)}{C_0(\mu_R)^2} + \frac{Mg_A^2}{8\pi f^2}\Big[\frac{\gamma^2}{\mu_R^2} + 1 - \frac{8\gamma}{3\,m_\pi} + \frac{2\gamma^2}{m_\pi^2}\Big]\,. \end{aligned} \tag{5.77}$$

The value of the remaining $B_n^{(i)}$ determined at this order are the same in both schemes

$$B_n^{(2-2n)} = -\frac{Mg_A^2}{8\pi f^2}\Big(\frac{-4}{m_\pi^2}\Big)^n \Big[\frac{1}{4n} - \frac{2\gamma}{(2n+1)m_\pi} + \frac{\gamma^2}{(n+1)m_\pi^2}\Big]\, m_\pi^2\,. \tag{5.78}$$

For $n = 2, 3, 4$, Eq. (5.78) gives the low-energy theorems derived in Ref. [3].

The v_i in Eq. (5.73) can be predicted in terms of one parameter, $C_0^{np}(\mu_R)$, which is fixed in Ref. [3] by the condition $4\pi/[MC_0^{np}(\mu_R)] + \mu_R = 1/a$. Corrections to these predictions are expected to be $30 - 50\%$ due to higher order Q/Λ terms. The v_i extracted from the phase shift data [3, 165] disagree with the low-energy theorems

---

[6] A calculation of the low energy theorems at order Q^3 in the ${}^1S_0$ channel was presented at the INT Workshop on Nuclear Physics with Effective Field Theory, Seattle, WA, 25-26 Feb 1999 (S. Fleming, T. Mehen, and I.W. Stewart) [164]. This result will not be discussed here.

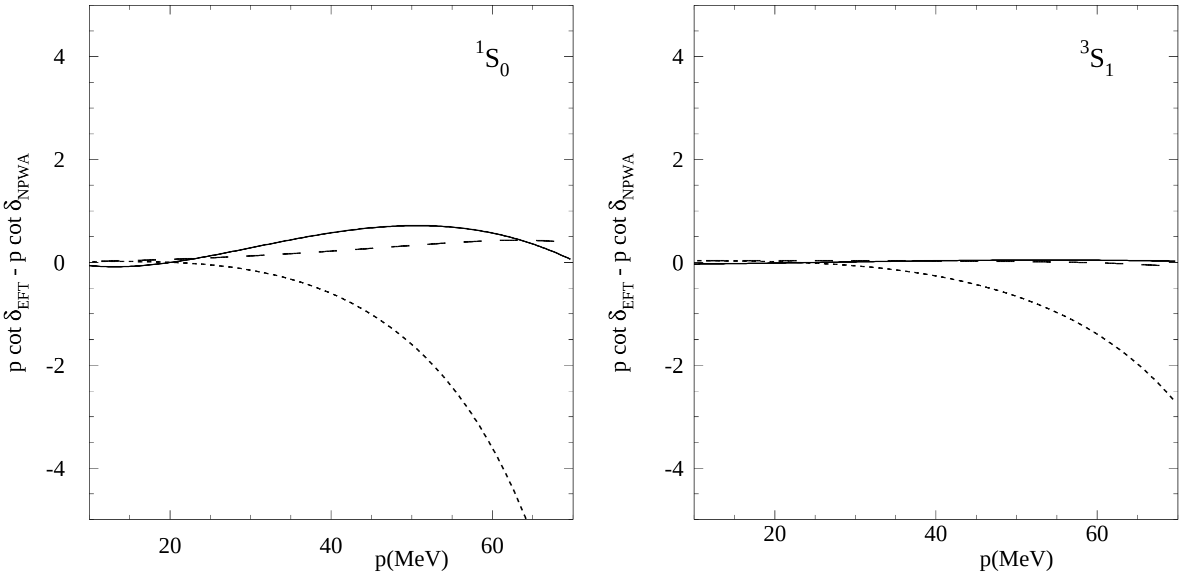

Figure 5.6: The effective field theory and Nijmegen Partial Wave analysis [2] values of $p\cot\delta$ are compared. The solid lines use $p\cot(\delta^{(0)}+\delta^{(1)})$, the dashed lines use Eq. (5.73) with the v_i from Ref. [3], and the dotted lines use the values of v_i from the low-energy theorems.

by factors of order 5. In Fig. 5.6, we see that the agreement of $p\cot(\delta^{(0)}+\delta^{(1)})$ (solid lines)[7] with the Nijmegen partial wave analysis is comparable to that of the effective range expansion with the v_i from the fits in Refs. [3, 165] (dashed lines). Note that our fit is more accurate at low momentum than the global fit in Ref. [4]. However, keeping only the first five terms from the low-energy theorems (dotted lines) gives larger disagreement at 70 MeV. This is not surprising since the pion introduces a cut at $p = i\,m_\pi/2$, so the radius of convergence of the series expansion of $p\cot(\delta)$ in Eq (5.73) is $\simeq 70\,\mathrm{MeV}$. At $p = 70\,\mathrm{MeV}$, one expects large corrections from the next term in the series. However, the fit values of v_i give good agreement with the data even at 70 MeV. It is possible that uncertainty from higher order terms in the Taylor series has been absorbed into v_2, v_3, and v_4 in the process of performing the fits. For this reason, the uncertainty in the values of v_i that were found from fitting to the data may be considerable.

---

[7] Note that when expanded in Q, $p\cot\delta = ip + 4\pi/[MA^{(-1)}] - 4\pi A^{(0)}/[M(A^{(-1)})^2] + \mathcal{O}(Q^3)$, which differs from $p\cot(\delta^{(0)}+\delta^{(1)})$ by terms of order Q^3. The latter expression is used since the parameters in Table (5.1) were fit using Eq. (5.80).

To get an idea of the error in v_2, we will specialize to the $^3S_1$ channel. The Nijmegen phase shift analysis [5] lists two data points for $p < 70\,\mathrm{MeV}$: $p = 21.67\,\mathrm{MeV}$ where $\delta^{(^3S_1)} = 147.747 \pm 0.010\,^\circ$, and $p = 48.45\,\mathrm{MeV}$, where $\delta^{(^3S_1)} = 118.178 \pm 0.021\,^\circ$. Using $a = 5.420 \pm 0.001\,\mathrm{fm}$ and $r_0 = 1.753 \pm 0.002\,\mathrm{fm}$ [165] in the effective range expansion and fitting to the lowest momentum data point, we find $v_2 = -0.50 \pm 0.52\,\mathrm{fm}^3$, where the error in a, r_0, and $p \cot\delta$ have been added in quadrature. This differs by one sigma from both the value predicted by the low-energy theorem, $v_2^{\mathrm{thm}} = -0.95\,\mathrm{fm}^3$, and the value from the fit, $v_2^{\mathrm{fit}} = 0.04\,\mathrm{fm}^3$. Since the range of the pure nucleon theory is 70 MeV, there will also be a $\simeq 0.1\,\mathrm{fm}^3$ error in this extraction from v_3 and higher coefficients. This error was estimated by comparing the theoretical expression for $p \cot\delta$ with the first three terms in its series expansion. If we instead use the higher momentum point we find $v_2 = 0.03 \pm 0.04\,\mathrm{fm}^3$ with $\simeq 0.5\,\mathrm{fm}^3$ theoretical uncertainty. The uncertainty in these values of v_2 is too large to make a definitive test of the low-energy theorems.

Recall that the unnaturally large scattering length a is a fine tuning that was accounted for by demanding that in Eq. (5.75), $C_0(\mu_R)$ is close to its ultraviolet fixed point, and $\gamma \approx 1/a$. Examining the expression for $1/a$ in Eq. (5.74) it may seem that this could be destroyed by chiral corrections. If $D_2(\mu_R) \sim C_0(\mu_R)^2$ then the first term gives $B_0^{(2)} \sim 205\,\mathrm{MeV}$. In fact from Table 5.3, we see that the fit gives $B_0^{(2)} \lesssim 1/a$. The reason for this small value is that since $A^{(0)} \propto (A^{(-1)})^2$ the amplitude has a double pole. Since this pole is spurious (occurring from the perturbative expansion) the residue of the double pole must be small in order to fit the data. This leads to a good fit condition[35] which will be approximately satisfied

$$\frac{A^{(0)}}{[A^{(-1)}]^2}\bigg|_{-ip=\gamma} = 0\,. \tag{5.79}$$

The condition in Eq. (5.79) implies $B_0^{(2)} \simeq 4\pi\gamma^2/M$. In fact this gives the right order of magnitude for the values of $B_0^{(2)}$ determined from the fits in Table 5.3. Similar good fit conditions occur at higher order keeping the coefficients $B_0^{(i)}$ small. The division of $C_0(\mu_R)$ into nonperturbative and perturbative pieces is arbitrary, allowing

	$^1S_0$ Fit				$^3S_1$ Fit			
μ_R(MeV)	γ	$B_0^{(2)}$	$1/a$	r_0	γ	$B_0^{(2)}$	$1/a$	r_0
70	-10.18	2.05	-8.124	0.01468	48.39	-15.82	32.57	0.01101
137	-10.16	2.04	-8.121	0.01480	48.96	-16.76	32.19	0.01098
280	-10.23	2.12	-8.105	0.01484	46.39	-12.64	33.76	0.01111

Table 5.3: Values of γ, $B_0^{(2)}$, $1/a$, and r_0 (in MeV) obtained from our fits. Three values of μ_R are shown to emphasize that the value of the extracted parameters depends weakly on μ_R.

us to set up the theory so that the Q expansion for $1/a$ is well behaved. By imposing conditions like Eq. (5.79), chiral corrections to the location of the pole are absorbed into perturbative pieces of $C_0(\mu_R)$ order by order. Thus, we choose to spoil the short distance nature of C_0 by giving it m_π dependence [166] to keep the pole in the right place.

In Table 5.3 we see that when $B_0^{(2)}$ is added to γ, values of $1/a$ are obtained which are close to the physical values, $1/a(^1S_0) = -8.32\,\text{MeV}$ and $1/a(^3S_1) = 36.4\,\text{MeV}$. It is encouraging that the value of γ found from fits in the $^3S_1$ channel are close to the physical pole in the amplitude which corresponds to the deuteron, $\gamma = 45.7\,\text{MeV}$. Values for r_0 can also be predicted from the fits using Eq. (5.77). Experimentally, $r_0(^1S_0) = 0.0139\,\text{MeV}^{-1}$ and $r_0(^3S_1) = 0.00888\,\text{MeV}^{-1}$, so the values in Table 5.3 agree to the expected accuracy.

5.9 Determining the range Λ_π

Here we will examine the phase shift data to see what it tells us about the range of the effective field theory with perturbative pions. In Ref. [155], a Lepage analysis is performed on the observable $p \cot\delta(p)$ in the $^1S_0$ channel. Near 350 MeV the experimental $^1S_0$ phase shift passes through zero. Therefore, the error $|p\cot\delta^{\text{NPWA}} - p\cot\delta^{\text{EFT}}|$ is greatly exaggerated since $p\cot\delta(p) \to \infty$. To avoid this problem we will use the $^1S_0$ and $^3S_1$ phase shifts as our observables, since $\Delta\delta = |\delta^{\text{NPWA}} - \delta^{\text{EFT}}|$ remains finite for all p. The next-to-leading order amplitudes given in section V will

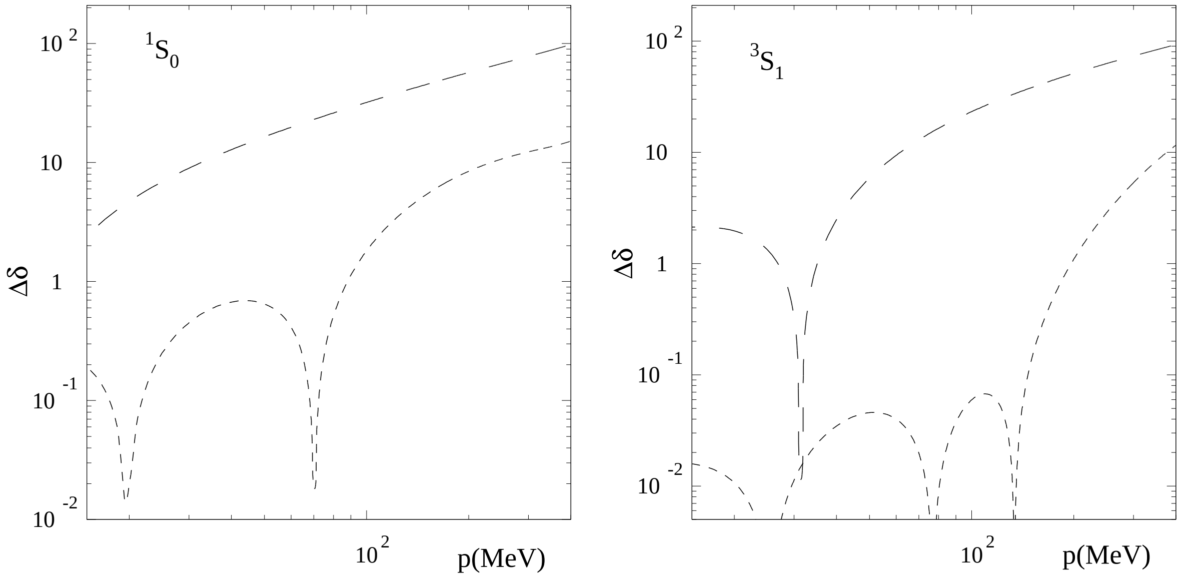

Figure 5.7: Error analysis for the phase shifts in the $^1S_0$ and $^3S_1$ channels. $\Delta\delta$ is the difference between the the effective field theory prediction and the Nijmegen partial wave analysis[2]. The long and short dashed lines use the $\mathcal{O}(Q^0)$ and $\mathcal{O}(Q)$ theoretical phase shifts respectively.

be used. The phase shifts have an expansion of the form $\delta = \delta^{(0)} + \delta^{(1)} + \mathcal{O}(Q^2/^2)$, where [4]

$$\delta^{(0)} = -\frac{i}{2}\ln\left[1 + i\frac{pM}{2\pi}\mathcal{A}^{(-1)}\right], \qquad \delta^{(1)} = \frac{pM}{4\pi}\frac{\mathcal{A}^{(0)}}{1 + i\frac{pM}{2\pi}\mathcal{A}^{(-1)}}\,. \tag{5.80}$$

Recall that a momentum expansion of δ would result in terms with only odd powers of p. However, the expansion for δ in Eq. (5.80) is not simply a momentum expansion, so the next-to-leading order calculation can have errors which scale as p^2/Λ_π^2. For example, once pions are included we can have a term $p^2\tan^{-1}(2p/m_\pi)$ which is odd in p, order Q^2, and scales as p^2 for large momenta.

In Fig. 5.7, we plot $\Delta\delta$ versus p using log-log axes. Note that the sharp dips in Fig. 5.7 are just locations where the theory happens to agree with the data exactly. The Nijmegen data[2] is available up to $p = 405\,\mathrm{MeV}$. In a theory with just a momentum expansion the errors will appear as straight lines on the log-log plot as pointed out by Lepage [30]. In the pion theory the expansion is in both m_π/Λ_π and

p/Λ_π, so this is no longer true. For $p > m_\pi$ we expect the errors to be of the form[8]

$$\begin{aligned} \Delta\delta^{(0)} &\sim \Big(1 + \frac{m_\pi}{\Lambda_\pi} + \ldots\Big)\frac{p}{\Lambda_\pi} + \ldots\,, \\ \Delta\delta^{(1)} &\sim \Big(\frac{m_\pi}{\Lambda_\pi} + \frac{m_\pi^2}{\Lambda_\pi^2} + \ldots\Big)\frac{p}{\Lambda_\pi} + \Big(1 + \frac{m_\pi}{\Lambda_\pi} + \ldots\Big)\frac{p^2}{\Lambda_\pi^2} + \ldots\,. \end{aligned} \tag{5.81}$$

The fact that there is always a p/Λ_π error arises from the fact that, as seen in Eq. (5.74), r_0 is reproduced in the effective field theory as an expansion in m_π/Λ_π. For $p/\Lambda_\pi \gg m_\pi/\Lambda_\pi$ the slope of the lines on the plot should indicate the lowest power of p that has not been included. At low momentum the error in $\Delta\delta^{(n)}$ is dominated by the $p\, m_\pi^n/\Lambda_\pi^{n+1}$ term and the lines should be parallel. From Fig. 5.7 we see that the error is smallest at low momentum and increases as the momentum increases, which is how the theoretical error is expected to behave.

It is clear that even for $p \sim 400\,\mathrm{MeV}$ the next-to-leading order calculations are reducing the error in the phase shift. Because two new parameters are added at next-to-leading order it is always possible to force exact agreement at some value of p. However, if one were to force the data to agree too well at high momentum then this would destroy the agreement at low momentum. Since the improvement of the fit in Fig. 5.7 at high momentum does not come at the expense of the fit at low momentum this is evidence that the error is being reduced in a systematic way. At high momentum one expects that the error is $\sim p^2/\Lambda_\pi^2$. From Fig. 5.7, $\Delta\delta \sim 0.26$ radians for $p = 400\,\mathrm{MeV}$, implying $\Lambda_\pi \sim 800\,\mathrm{MeV}$. This is only a rough estimate for the range because we cannot yet exclude the possibility that the next-to-next-to-leading order phase shift has an anomalously small coefficient. Even though the lines in Fig. 5.7 are not straight they should still cross at approximately the range of the theory since at this point higher order corrections do not improve the agreement with the data. This error analysis is consistent with the possibility that the range is $\gtrsim 500\,\mathrm{MeV}$.

Further information on the range of the effective field theory can be obtained by examining electromagnetic processes involving the deuteron [32, 160, 161, 162, 163], such as the deuteron charge radius, electromagnetic form factors, deuteron polarizability, and deuteron Compton scattering. For these observables errors are typically $\sim 30-40\%$ at leading order and $\sim 10\%$ at next-to-leading order. This is what one would expect if the expansion parameter $m_\pi/\Lambda_\pi \sim 1/3$, implying $\Lambda_\pi \sim 410\,\mathrm{MeV}$. This is consistent with our previous estimate for Λ_π. If the range is this large one should expect that the error in deuteron properties will be at the few percent level once next-to-next-to-leading order calculations are performed[9].

---

[8] At momenta $1/a \ll p \ll m_\pi$ we could have $\Delta\delta^{(0)} \sim B_0^{(2)}/p \sim m_\pi^2/\Lambda_\pi p$. However, as explained in section VI, $B_0^{(2)} \lesssim 1/a$ so this term is very small.

5.10 Summary

In this chapter the structure of the effective field theories of nucleons with and without pions is studied. We discuss a momentum subtraction scheme, the OS scheme, which obeys the KSW power counting. The method of local counterterms is used to obtain the renormalization group equations for the coupling constants in these theories. Using local counterterms defines the OS and PDS renormalization schemes unambiguously. Two-loop graphs with potential pions in the $^3S_1$ channel are computed and shown to have p^2/ϵ poles. The presence of $1/\epsilon$ poles implies that the only model independent piece of pion exchange is the part that can be treated perturbatively. We obtain the renormalized couplings $C_0(\mu_R)$, $C_2(\mu_R)$ and $C_4(\mu_R)$ at order Q in the OS and PDS schemes.

We have emphasized why it is important to have μ_R independent amplitudes order by order in Q. Such amplitudes are obtained automatically in the OS scheme. In PDS μ_R independent amplitudes may be obtained by treating part of $C_0(\mu_R)$ perturbatively. It is also necessary to treat part of $C_0(\mu_R)$ perturbatively if we wish to keep the pole in the amplitude in a fixed location order by order in the chiral expansion. Another result concerns the large μ_R behavior of the couplings in this theory. In the OS scheme the coupling constants obey the KSW power counting for all $\mu_R > 1/a$. In

---

[9] Recently calculations of the deuteron quadrapole moment [167] and the $^1S_0$ phase shift [168, 164] have been carried out at this order.

PDS the breakdown in the power counting for $C_0(\mu_R)$ is avoided if $C_0(\mu_R)$ is split into non-perturbative and perturbative parts. Therefore, the breakdown of the scaling in the coupling constants is artificial.

Next-to-leading order calculations of nucleon-nucleon phase shift data [4] provide fits to data at large momenta which are far more accurate than one would expect if the theory broke down completely at 300 MeV. Of course, this does not mean that nucleon effective theory can be applied at arbitrarily high energies. The scale, $Mg_A^2/(8\pi f^2) \sim 300\,\mathrm{MeV}$, is associated with short distance contributions from pion exchange and provides an order of magnitude estimate for the range. In the S-wave channel, Δ production and ρ exchange become relevant at $\sim 700\,\mathrm{MeV}$, which sets an upper limit on the range of the expansion. To get a better understanding of the range of the nucleon effective theory with perturbative pions one must examine experimental data. An error analysis of the S wave phase shifts with next-to-leading-order calculations seems to be consistent with a range of 500 MeV. Though next-to-next-leading order corrections need to be compared with data and other processes investigated, we remain cautiously optimistic that the range could be as large as 500 MeV.

Chapter 6 Radiation and Soft Pions

In the KSW power counting for nucleon-nucleon interactions, pions are included perturbatively. In evaluating diagrams with pions, three types of contributions can be identified: potential, radiation, and soft. These pion effects differ in size and therefore each have a different power counting. In this chapter the power counting for radiation and soft pions are discussed. The distinction between pion contributions arises because there are several scales associated with two nucleon systems. In this respect the theory is similar to NRQCD and NRQED [19, 22].

In NRQCD there are three mass scales associated with non-relativistic systems containing two heavy quarks: the heavy quark mass M, momenta $\sim Mv$, and kinetic energy $\sim Mv^2$, where v is the relative velocity. QCD effects at the scale M are integrated out and appear as local operators in NRQCD. The remaining low energy contributions can be divided into potential, radiation (sometimes referred to as ultra-soft), and soft pieces [45, 169, 46, 44, 170, 171, 172]. Potential gluons have energy of order Mv^2 and momentum of order Mv, radiation gluons have energy and momentum of order Mv^2, and soft gluons have energy and momentum of order Mv. The power counting for radiation gluons requires the use of a multipole expansion at a quark-gluon vertex [169, 44]. The v power counting of potential and radiation gluons can be implemented in the effective Lagrangian by introducing separate gluon fields and rescaling the coordinates and fields by powers of v [45, 46]. In Ref. [170] the separation of scales was achieved on a diagram by diagram basis using a threshold expansion. The potential, radiation, and soft regimes were shown to correctly reproduce the low energy behavior of relativistic diagrams in a scalar field theory. In Ref. [171, 172] it was pointed out that these effects may be reproduced by an effective Lagrangian in which separate fields are also introduced for the soft regime. Note that soft contributions come from a larger energy scale than potential and radiation effects. The heavy quark system does not have enough energy to radiate a soft gluon, so they only appear in loops. In Ref. [170] it was shown that soft contributions to scattering do not appear until graphs with two or more gluons are considered.

In the nucleon theory there is another scale because the pions are massive. For the purpose of power counting it is still useful to classify pion contributions as potential, radiation, or soft. For a pion with energy q_0 and momentum q, a potential pion has $q_0 \sim q^2/M$ where M is the nucleon mass, while a radiation or soft pion has $q_0 \sim q \geq m_\pi$. In a non-relativistic theory, integrals over loop energy are performed via contour integration. Potential pions come from contributions from the residue of a nucleon pole and give the dominant contribution to pion exchange between two nucleons. For these pions, the energy dependent part of the pion propagator is treated as a perturbation because the loop energy, $q_0 \sim q^2/M \ll q$. The residues of pion propagator poles give radiation or soft pion contributions. The power counting for soft and radiation pions differs. For instance, the coupling of radiation pions to nucleons involves a spatial multipole expansion, while the coupling to soft pions does not.

6.1 Radiation pions

In chiral perturbation theory the expansion is in powers of momenta and the pion mass m_π. For power counting potential pions it is convenient to take the nucleon momentum $p = Mv \sim m_\pi$ [4, 45], so $v = m_\pi/M \sim 0.15$. The situation is different for radiation pions. There is a new scale associated with the threshold for pion production, which occurs at energy $E = m_\pi$ in the center of mass frame. This corresponds to a nucleon momentum $p = Q_r$, where $Q_r \equiv \sqrt{M m_\pi} = 360\,\text{MeV}$. Because the radiation pion fields cannot appear as on-shell degrees of freedom below the threshold $E = m_\pi$, one expects that the radiation pion can be integrated out for $p \ll Q_r$. (Potential pions should be included for $p \gtrsim m_\pi/2$.) Another way to see that radiation pions require $p \sim Q_r$ is to note that in order to simultaneously satisfy $k_0^2 = k^2 + m_\pi^2$ and $k_0 \sim k \sim Mv^2$ requires $v \sim \sqrt{m_\pi/M} \sim 0.38$.

The full theory with pions has operators in the Lagrangian with powers of m_q

which give all the m_π dependence. If the radiation pions are integrated out, then the chiral expansion is no longer manifest because there will be m_π dependence hidden in the coefficients of operators in the Lagrangian. One is still justified in considering the same Lagrangian, but predictive power is lost since it is no longer clear that chiral symmetry relates operators with a different number of pion fields. Also, the m_π dependence induced by the radiation pions may affect the power counting of operators. For example, as shown in Ref. [173, 174, 175], integrating out the pion in the one-nucleon sector induces a nucleon electric polarizability $\alpha_E \propto 1/m_\pi$. Alternatively, one can keep chiral symmetry manifest by working with coefficients in the full theory and including radiation pion graphs. This is the approach we will adopt.

The presence of the scale Q_r modifies the power counting of the theory with radiation pions. In the KSW power counting, one begins by taking external momenta $p \sim m_\pi \sim Q$. The theory is organized as an expansion in powers of Q. To estimate the size of a graph, loop 3-momenta are taken to be of order Q. However, potential loops within graphs with radiation pions can actually be dominated by three momenta of order Q_r. To see how this comes about, consider as an example the graph shown in Fig. 6.1c. Let q be the momentum running through the pion propagator, and let k be the loop momentum running through a nucleon bubble inside the radiation pion loop. The poles from the pion propagator are

$$\frac{i}{q_0^2 - \vec{q}^{\,2} - m_\pi^2 + i\epsilon} = \frac{i}{(q_0 - \sqrt{\vec{q}^{\,2} + m_\pi^2} + i\epsilon)(q_0 + \sqrt{\vec{q}^{\,2} + m_\pi^2} - i\epsilon)}\,, \tag{6.1}$$

so the radiation pion has $|q_0| \geq m_\pi$. This energy also goes into the nucleon bubbles. The k integrand is largest when the nucleons are close to their mass shell. But since the energy going into the loop is $\sim m_\pi$, this occurs when $k^2/M \sim m_\pi$, i.e., $k \sim Q_r$. We will begin by considering the contribution of radiation pions to elastic nucleon scattering at the threshold, $E = m_\pi$. At this energy, external and potential loop momenta are of the same size and power counting is easiest. Because $p \sim Q_r$ it is obvious that we want to count powers of Q_r rather than Q

The power counting rules at the scale Q_r are as follows. A scheme with manifest power counting will be used, so that $C_0(\mu_R) \sim 1/(M\mu_R), C_2(\mu_R) \sim 1/(M\Lambda\mu_R^2)$, etc., where Λ is the range of the theory. We will take $p \sim \mu_R \sim Q_r$. A radiation loop has $q_0 \sim q \sim m_\pi$ so $d^4q \sim Q_r^8/M^4$, where q is the momentum running through the pion propagator. A radiation pion propagator gives a M^2/Q_r^4, while the derivative associated with a pion-nucleon vertex gives Q_r^2/M. A nucleon propagator gives a M/Q_r^2. External energies and momenta are kept in the nucleon propagator since $E \sim p^2/M \sim Q_r^2/M$. Furthermore, it is appropriate to use a multipole expansion for radiation pion-nucleon vertices which is similar to the treatment of radiation gluons in NRQCD [169]. Therefore, radiation pions will not transfer three-momenta to a nucleon. This is usually equivalent to expanding in powers of a loop momentum divided by M before doing the loop integral. The multipole expansion is an expandion in $v = \sqrt{m_\pi/M}$. A potential loop will typically have running through it either an external or radiation loop energy $\sim Q_r^2/M$. Therefore, in these loops the loop energy $k_0 \sim Q_r^2/M$, while the loop three momentum $k \sim Q_r$, so $d^4k \sim Q_r^5/M$. It is not inconsistent for $k \sim Q_r$ while $q \sim Q_r^2/M$, since three momenta are not conserved at the nucleon-radiation pion vertices. At the scale Q_r potential pion propagators may still be treated in the same way, $i/(k_0^2 - k^2 - m_\pi^2) = -i/(k^2 + m_\pi^2) + \mathcal{O}(k_0^2/k^4)$, which has an expansion in Q_r^2/M^2. We will see through explicit examples that this power counting correctly estimates the size of radiation pion graphs.

Note that only the potential loop measure gives an odd power of Q_r, so without potential loops the power counting reduces to power counting in powers of m_π. The power counting here therefore correctly reproduces the usual chiral power counting used in the one nucleon sector[26, 43].

Graphs with one radiation pion and additional higher order contact interactions or potential pions are suppressed by factors of Q_r/Λ relative to graphs with a single radiation pion and C_0 vertices. The Q_r expansion is a chiral expansion about $m_\pi = 0$, so there is a limit of QCD where it is justified. The scale Λ is unknown. One possible estimate is $\Lambda_{\rm NN} = 8\pi f^2/(Mg_A^2) = 300\,\mathrm{MeV}$ since a graph with $m+1$ potential pions is suppressed by $p/300\,\mathrm{MeV}$ relative to a graph with m potential pions. However, this order of magnitude estimate only takes into consideration a partial subset of the

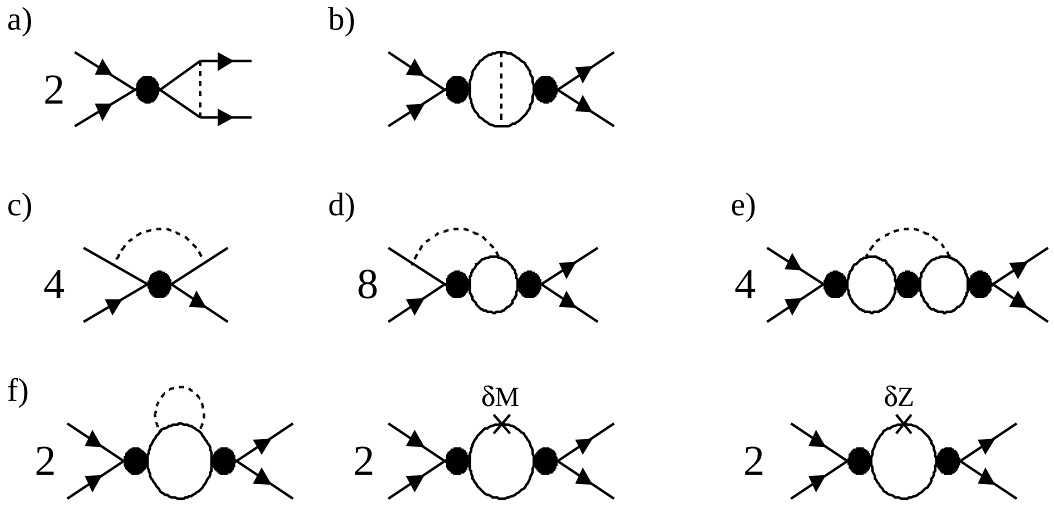

Figure 6.1: Leading order radiation pion graphs for NN scattering. The solid lines are nucleons, the dashed lines are pions and δM, δZ are the mass and field renormalization counterterms. The filled dot denotes the $C_0(\mu_R)$ bubble chain. There is a further field renormalization contribution that is calculated in text, but not shown.

graphs of the theory. As argued in chapter 5, it is possible that the range is of order the scale of short range interactions that are integrated out, implying $\Lambda \sim 500\,\text{MeV}$. In fact, the accuracy of NLO computations of nucleon-nucleon phase shifts is in agreement with this physically motivated estimate of the range. We will assume in this section that an expansion in Q_r/Λ is valid. This hypothesis will be tested further by seeing how well the effective theory makes predictions at $p \sim 300\,\text{MeV}$. For example, processes with external pions could be considered. If the Q_r/Λ expansion is not convergent, then application of the theory is restricted to $p < Q_r$.

The radiation pion graphs that give the leading order contribution to nucleon-nucleon scattering are shown in Fig. 6.1. The filled dot denotes the leading order interaction between nucleons, a $C_0(\mu_R)$ bubble sum. We illustrate the power counting with an example, the graph in Fig. 6.1d. For the moment, replace the C_0 bubble sums with single C_0 vertices. Each C_0 gives a factor of $1/MQ_r$ and each nucleon line gives a factor M/Q_r^2. The derivatives from the pion couplings combine with the radiation pion propagator to give a factor of unity. The radiation loop gives Q_r^8/M^4, while the nucleon bubble loop gives Q_r^5/M. There is also a factor of $1/f^2$ from pion exchange, and two factors of $1/4\pi$ from the radiation loop giving a $1/\Lambda_\chi^2$. ($\Lambda_\chi \sim 1\,\mathrm{GeV}$ is the chiral symmetry breaking scale.) Combining all factors, we find that this graph scales like $Q_r^3/(M^3\Lambda_\chi^2)$. This graph is suppressed relative to the leading order amplitude, $A^{(-1)}$, by a factor of $Q_r^4/(M^2\Lambda_\chi^2) = m_\pi^2/\Lambda_\chi^2$. Note that C_0 bubbles are summed on external nucleon lines as well as in the interior of the radiation loop, and each graph in the sum has the same size. It is straightforward to verify that all graphs in Fig. 6.1 scale the same way. For external bubble sums we can simply use the vertex $iA^{(-1)}$ where $A^{(-1)}$ is the leading order S-wave amplitude,

$$A^{(-1)} = -\frac{4\pi}{M}\frac{1}{\gamma + ip}\,, \tag{6.2}$$

and the pole $\gamma = 4\pi/MC_0(\mu_R) + \mu_R \sim 1/a$. Graphs with two radiation pions are suppressed by at least $Q_r^8/(M^4\Lambda_\chi^4) = m_\pi^4/\Lambda_\chi^4$ and will not be considered.

The first graphs we consider are those in Fig. 6.1a,b. These graphs have contributions from potential and radiation pions, and it may not be obvious that a clean separation occurs. Here the energy integrals will be evaluated without any approximations, after which the graphs split into radiation and potential parts. The graph in Fig. 6.1a gives:

$$iA^{(-1)}\frac{g_A^2}{2f^2}\int\frac{d^dq}{(2\pi)^d}\frac{i}{\frac{E}{2}+q_0-\frac{(\vec{q}-\vec{p})^2}{2M}+i\epsilon}\;\frac{i}{\frac{E}{2}-q_0-\frac{(\vec{q}-\vec{p})^2}{2M}+i\epsilon}\;\frac{i\,\vec{q}^{\,2}}{q_0^2-\vec{q}^{\,2}-m_\pi^2+i\epsilon}\,. \tag{6.3}$$

(Throughout this chapter we will include a factor of $(\mu/2)^{4-d}$ in the loop measures.) Performing the q_0 integral gives a term from the residue of the nucleon pole and a term from the pion pole,

$$-iA^{(-1)}\frac{g_A^2}{2f^2}\int\frac{d^nq}{(2\pi)^n}\frac{M}{(\vec{q}-\vec{p})^2-ME}\;\frac{\vec{q}^{\,2}}{\vec{q}^{\,2}+m_\pi^2-[\frac{E}{2}-\frac{(\vec{q}-\vec{p})^2}{2M}]^2} \tag{6.4}$$

$$-iA^{(-1)}\frac{g_A^2}{4f^2}\int\frac{d^nq}{(2\pi)^n}\frac{\vec{q}^{\,2}}{\sqrt{\vec{q}^{\,2}+m_\pi^2}}\;\frac{1}{\frac{E}{2}+\sqrt{\vec{q}^{\,2}+m_\pi^2}-\frac{(\vec{q}-\vec{p})^2}{2M}}\;\frac{1}{\frac{E}{2}-\sqrt{\vec{q}^{\,2}+m_\pi^2}-\frac{(\vec{q}-\vec{p})^2}{2M}}\,, \tag{6.5}$$

where $n = d - 1$. Eq. (6.4) is the potential pion contribution. Expanding in $[\frac{E}{2} - \frac{(\vec{q}-\vec{p})^2}{2M}]^2 = [\frac{2\vec{q}.\vec{p}-\vec{q}^2}{2M}]^2$ gives the result in Ref. [31, 4]. The subleading terms in this expansion are suppressed by[1] m_π^2/M^2. Eq. (6.5) is the radiation pion contribution. With $|\vec{q}| < M$, we may take $(\vec{q}-\vec{p})^2/M \to p^2/M$ in the last two propagators, which is the same approximation that is made by performing the multipole expansion. Finally, we use the equations of motion to set $E - p^2/M = 0$. It is important to note that we have not neglected E relative to $|\vec{q}|$. For $n = 3 - 2\epsilon$, Eq. (6.5) becomes

$$a) = iA^{(-1)}\frac{g_A^2}{4f^2}\int \frac{d^nq}{(2\pi)^n}\frac{\vec{q}^{\,2}}{(\vec{q}^{\,2}+m_\pi^2)^{3/2}} = -3iA^{(-1)}\frac{g_A^2 m_\pi^2}{(4\pi f)^2}\Big[\frac{1}{\epsilon}+\frac{1}{3}-\ln\Big(\frac{m_\pi^2}{\overline{\mu}^2}\Big)\Big]\,, \tag{6.6}$$

where $\overline{\mu}^2 = \mu^2\pi e^{-\gamma_E}$. Note that this integral is finite in three dimensions ($n = 2$).

The next graph we consider is shown in Fig. 6.1b. We have chosen to route loop momenta so that q runs through the pion and $\pm k$ and $\pm(k+q)$ run through the nucleon lines. The momentum k is potential, while q can be potential or radiation. Doing the k_0 contour integral and combining the two terms gives:

$$\begin{aligned} -2\,[A^{(-1)}]^2\,\frac{g_A^2}{2f^2}\int\frac{d^nk}{(2\pi)^n}\int\frac{d^dq}{(2\pi)^d}\,&\frac{\vec{q}^{\,2}}{q_0^2-\vec{q}^{\,2}-m_\pi^2+i\epsilon}\;\frac{1}{E-\frac{\vec{k}^2}{M}+i\epsilon}\;\frac{1}{E-\frac{(\vec{k}+\vec{q})^2}{M}+i\epsilon} \\ &\times\frac{E-\frac{(\vec{k}+\vec{q})^2}{2M}-\frac{\vec{k}^{\,2}}{2M}}{[E-\frac{(\vec{k}+\vec{q})^2}{2M}-\frac{\vec{k}^{\,2}}{2M}-q_0+i\epsilon][E-\frac{(\vec{k}+\vec{q})^2}{2M}-\frac{\vec{k}^{\,2}}{2M}+q_0+i\epsilon]}\,. \end{aligned} \tag{6.7}$$

Doing the q_0 integral gives two terms, but the radiation and potential contributions are still mixed. Combining these gives

$$\begin{aligned} i\,[A^{(-1)}]^2\,\frac{g_A^2}{2f^2}\int\frac{d^nk\,d^nq}{(2\pi)^{2n}}\,&\frac{\vec{q}^{\,2}}{\sqrt{\vec{q}^{\,2}+m_\pi^2}}\;\frac{1}{E-\frac{\vec{k}^2}{M}}\;\frac{1}{E-\frac{(\vec{k}+\vec{q})^2}{M}} \\ &\times\frac{1}{E-\frac{(\vec{k}+\vec{q})^2}{2M}-\frac{\vec{k}^{\,2}}{2M}-\sqrt{\vec{q}^{\,2}+m_\pi^2}}\,, \end{aligned} \tag{6.8}$$

---

[1] Note that $m_\pi^2/q^2 \sim m_\pi/M$, but we have kept the m_π^2 term in the potential pion propagator in Eq. (6.4). We could consider expanding in m_π/q using the asymptotic expansion techniques discussed in section B, but for $p \sim m_\pi$ these terms would have to be resummed. Unlike the soft and radiation contributions, there is no issue of double counting for potential pions, so for simplicity we will simply keep the m_π^2 in the propagator.

which can be split into potential and radiation parts

$$
\begin{aligned}
&i[A^{(-1)}]^2\,\frac{g_A^2}{2f^2}\int\frac{d^nk}{(2\pi)^n}\int\frac{d^nq}{(2\pi)^n}\frac{\vec{q}^{\,2}}{\sqrt{\vec{q}^{\,2}+m_\pi^2}}\,\frac{1}{E-\frac{\vec{k}^2}{M}}\,\frac{1}{\sqrt{\vec{q}^{\,2}+m_\pi^2}-\frac{(2\vec{k}\cdot\vec{q}+\vec{q}^{\,2})}{2M}} \qquad (6.9)\\
&\qquad\qquad\times\left[\frac{-1}{E-\frac{(\vec{k}+\vec{q})^2}{M}}+\frac{1}{E-\frac{\vec{k}^2}{M}-\frac{(2\vec{k}\cdot\vec{q}+\vec{q}^{\,2})}{2M}-\sqrt{\vec{q}^{\,2}+m_\pi^2}}\right].
\end{aligned}
$$

The first term in Eq. (6.9) is the two-loop potential pion graph evaluated in Ref.[4]. The factors of $(2\vec{k}\cdot\vec{q}+\vec{q}^{\,2})/(2M)$ appearing in the denominators can be dropped because the loop integral is dominated by $k, q \ll M$ and therefore $(2\vec{k}\cdot\vec{q}+\vec{q}^{\,2})/(2M) \ll \sqrt{\vec{q}^{\,2}+m_\pi^2}$. For the second term, which is the radiation pion contribution, this is equivalent to the multipole expansion. Momenta $k \sim \sqrt{M m_\pi}$ and $q \sim m_\pi$ dominate the integrals in the second term. In Ref. [170], the potential and radiation parts of the graph in Fig. 6.1b were evaluated in the limit $m_\pi = 0$, and shown to correctly make up the corresponding part of the fully relativistic calculation. The calculation in Ref. [170] agrees with Eq. (6.9) for $m_\pi = 0$. Note that the radiation part would not agree if we assumed $k \sim m_\pi$ and used static nucleon propagators in the radiation loop[2]. For $n = 3-2\epsilon$ the radiation part of Eq. (6.9) is

$$
\begin{aligned}
b) \;&=\; i[A^{(-1)}]^2\,\frac{g_A^2}{2f^2}\int\frac{d^nk}{(2\pi)^n}\int\frac{d^nq}{(2\pi)^n}\frac{\vec{q}^{\,2}}{\vec{q}^{\,2}+m_\pi^2}\,\frac{1}{E-\frac{\vec{k}^{\,2}}{M}}\,\frac{1}{E-\frac{\vec{k}^{\,2}}{M}-\sqrt{\vec{q}^{\,2}+m_\pi^2}}\\
&=\; [A^{(-1)}]^2\,\frac{g_A^2 M m_\pi^2}{(4\pi f)^2}\left\{\frac{3\,p}{4\pi}\left[\frac{1}{\epsilon}+\frac{7}{3}-2\ln 2-\ln\!\Big(\frac{m_\pi^2}{\overline{\mu}^2}\Big)-\ln\!\Big(\frac{-p^2}{\overline{\mu}^2}\Big)\right]\right.\\
&\qquad\left.+\frac{i\sqrt{M m_\pi}}{4\sqrt{\pi}}\,I_1\!\Big(\frac{E}{m_\pi}\Big)\right\}, \qquad (6.10)
\end{aligned}
$$

where

$$
\begin{aligned}
I_1(x) \;&=\; \frac{3}{2}\frac{\Gamma(-\frac{5}{4})}{\Gamma(\frac{5}{4})}\,{}_3F_2\Big(\{-\frac{5}{4},-\frac{1}{4},\frac{1}{4}\},\{\frac{1}{2},\frac{5}{4}\},x^2\Big)\\
&\quad+\frac{x\Gamma(\frac{1}{4})}{\Gamma(\frac{7}{4})}\,{}_3F_2\Big(\{-\frac{3}{4},\frac{1}{4},\frac{3}{4}\},\{\frac{3}{2},\frac{7}{4}\},x^2\Big)\,. \qquad (6.11)
\end{aligned}
$$

---

[2] Furthermore, if static nucleon propagators are used one obtains a linear divergence requiring a non-analytic counterterm $\propto m_\pi$ [176].

For $n = 2$ the loop integral in Eq. (6.10) is finite, except for the I_1 term which has a $p^2/(n-2)$ pole. In PDS this pole would effect the running of $C_2(\mu_R)$, but as we will see, contributions proportional to I_1 will cancel between graphs. Since $A^{(-1)} \sim 1/(MQ_r)$ the results in Eqs. (6.6, 6.10) are order $Q_r^3/(M^3\Lambda_\chi^2)$ as expected. At one-loop the $1/\epsilon$ pole in Eq. (6.6) is cancelled by a counterterm

$$\delta^{\mathrm{uv},1a} D_2 = -3\, C_0^{\mathrm{finite}} \, \frac{g_A^2}{(4\pi f)^2} \Big[\frac{1}{\epsilon} - \gamma_E + \ln{(\pi)} \Big] \,. \tag{6.12}$$

For higher loops the $1/\epsilon$ poles in Eq. (6.6), Eq. (6.10), and $\delta^{\mathrm{uv},1a} D_2$ dressed with C_0 bubbles cancel. Note that the $O(\epsilon)$ piece of the bubbles give a finite contribution,

$$-\, C_0(\mu_R) \left(\frac{Mp}{4\pi} \right) \left\{ 1 + \epsilon \left[2 - 2\ln 2 - \ln\left(\frac{-p^2 - i\epsilon}{\overline{\mu}^2} \right) \right] \right\} \,. \tag{6.13}$$

The result of combining Figs. 6.1a,b and $\delta^{\mathrm{uv},1a} D_2$ dressed by C_0 bubbles is:

$$\begin{aligned} a) + b) \;\; &= \;\; 3i\, [A^{(-1)}]^2 \, \frac{g_A^2 m_\pi^2}{(4\pi f)^2} \, \frac{M\gamma}{4\pi} \left[\frac{1}{3} - \ln\Big(\frac{m_\pi^2}{\mu^2} \Big) \right] \\ & \quad + i\, [A^{(-1)}]^2 \, \frac{g_A^2 M m_\pi^2}{(4\pi f)^2} \frac{\sqrt{M m_\pi}}{4\sqrt{\pi}} \, I_1\Big(\frac{E}{m_\pi} \Big) \,. \end{aligned} \tag{6.14}$$

Next we consider the graphs in Fig. 6.1c,d,e. The loop integrals in these graphs vanish if the pion pole is not taken so there is no potential pion contribution. As pointed out in Ref. [4], emission of the radiation pion in these graphs changes the spin/isospin of the nucleon pair. Therefore, if the external nucleons are in a spin-triplet(singlet) state, then the coefficients appearing in the internal bubble sum are $C_0^{(^1S_0)}(\mu_R)(C_0^{(^3S_1)}(\mu_R))$. The notation C_0 (C_0') will be used for vertices outside (inside) the radiation pion loop. We begin with Fig. 6.1c. The contribution from the graph with m nucleon bubbles in the internal bubble sum is

$$\begin{aligned} & 4\, \frac{g_A^2}{2f^2} \int \frac{d^dq}{(2\pi)^d} \frac{i}{q_0 - i\epsilon} \, \frac{i}{q_0 - i\epsilon} \, \frac{-i\, \vec{q}^{\,2}}{q_0^2 - \vec{q}^{\,2} - m_\pi^2 + i\epsilon} [-iC_0'(\mu_R)]^{m+1} \\ & \qquad \times \left[\int \frac{d^dk}{(2\pi)^d} \frac{i}{-k_0 + q_0 + \frac{E}{2} - \frac{(\vec{k}-\vec{q})^2}{2M} + i\epsilon} \, \frac{i}{k_0 + \frac{E}{2} - \frac{\vec{k}^2}{2M} + i\epsilon} \right]^m \,, \end{aligned} \tag{6.15}$$

where we used the multipole expansion and then the equations of motion to eliminate E and p from the first two propagators. All nucleon propagators have a q_0 pole above the real axis, while the pion propagator has one pole above and one below. Therefore, the q_0 contour is closed below. The d^dk integrals are also easily performed giving

$$-i\frac{g_A^2 C_0'(\mu_R)}{f^2}\left[\frac{-C_0'(\mu_R)M\Gamma(1-n/2)}{(4\pi)^{n/2}}\right]^m \int \frac{d^nq}{(2\pi)^n}\frac{\vec{q}^{\,2}}{(\vec{q}^{\,2}+m_\pi^2)^{3/2}} \times \left[(-p^2+M\sqrt{\vec{q}^{\,2}+m_\pi^2}\,)^{n/2-1}-\mu_R\right]^m . \tag{6.16}$$

Note that the size of the loop momenta k in the nucleon bubbles is $\sim \sqrt{Mm_\pi}$ even for $p < \sqrt{Mm_\pi}$. The μ_R inside the brackets comes from inclusion of the PDS or OS $\delta^n C_0(\mu_R)$ counterterm graphs for the internal bubble sum. The integral will be dominated by $\vec{q} \sim m_\pi$ so the graph will scale as

$$\frac{1}{\Lambda_\chi^2}\,\frac{m_\pi^2}{M\mu_R}\Big(\frac{\sqrt{Mm_\pi}}{\mu_R}\Big)^m . \tag{6.17}$$

Since $\mu_R \sim \sqrt{Mm_\pi}$, all graphs in the sum are of order $Q_r^3/(M^3\Lambda_\chi^2)$.

For Figs. 6.1c,d,e the sum over bubbles should be done before the radiation loop integral. The reason is that an arbitrary term in the bubble sum has a much different dependence on the energy flowing through it than the sum itself. This can be seen in the $\vec{q}$ dependence in Eq. (6.16). If we integrate over $\vec{q}$ then terms in the sum may diverge whereas the integral of the complete sum is finite. In fact, for $n=3$, Eq. (6.16) has divergences of the form $\Gamma(-1-m/4)\mathrm{F}(E^2/m_\pi^2)$ and $\Gamma(-1/2-m/4)E\,\mathrm{F}(E^2/m_\pi^2)$ where F is a hypergeometric function. These divergences are misleading because for momenta $> 1/a$ we know that the correct form of the leading order four point function falls off as $1/p$. Recall from section 2.3.2 that for $p \sim \mu_R \gg 1/a$ the summation is infrared physics that we have built into our theory. For this reason the summation is performed before introducing counterterms to subtract divergences. (This approach is also taken in the analysis of three body interactions in Ref. [177, 178]). Summing over m, Eq. (6.16) becomes:

$$\begin{aligned} c) &= -i\,\frac{g_A^2}{f^2}\frac{4\pi}{M}\int\frac{d^nq}{(2\pi)^n}\frac{\vec{q}^{\,2}}{(\vec{q}^{\,2}+m_\pi^2)^{3/2}}\,\frac{1}{\gamma'-\left[-p^2+M\sqrt{\vec{q}^{\,2}+m_\pi^2}\right]^{n/2-1}} \\ &= \frac{ig_A^2}{\sqrt{\pi}f^2}\Big(\frac{m_\pi}{M}\Big)^{3/2} I_2\Big(\frac{E}{m_\pi}\Big)\,, \end{aligned} \tag{6.18}$$

where $\gamma' = 4\pi/MC_0'(\mu_R)+\mu_R \sim 1/a$. As expected the graph scales as Q_r^3. In the limit $n\to 3$, I_2 is finite and given by

$$\begin{aligned} I_2(x) = {}&\frac{\Gamma(-\frac{3}{4})}{\Gamma(\frac{3}{4})}\,{}_3F_2\left(\{-\frac{3}{4},\frac{1}{4},\frac{3}{4}\},\{\frac{1}{2},\frac{7}{4}\},x^2\right)-\frac{3x}{2}\frac{\Gamma(\frac{3}{4})}{\Gamma(\frac{9}{4})}\,{}_3F_2\left(\{-\frac{1}{4},\frac{3}{4},\frac{5}{4}\},\{\frac{3}{2},\frac{9}{4}\},x^2\right) \\ &+\mathcal{O}(\gamma'/\sqrt{Mm_\pi})\,. \end{aligned} \tag{6.19}$$

I_2 is manifestly μ_R independent and is also finite as $n\to 2$.

Next we consider the graph in Fig. 6.1d. Integrals are done in the same manner as that of Fig. 6.1c. For $n = 3-2\epsilon$, Fig. 6.1d is

$$\begin{aligned} d) &= -4i\,A^{(-1)}\frac{g_A^2}{2f^2}\frac{\Gamma(n/2-1)}{(4\pi)^{n/2-1}}\int\frac{d^nq}{(2\pi)^n}\frac{\vec{q}^{\,2}}{(\vec{q}^{\,2}+m_\pi^2)^{3/2}} \\ &\qquad\times\frac{\left(-p^2+M\sqrt{\vec{q}^{\,2}+m_\pi^2}\right)^{n/2-1}-(-p^2)^{n/2-1}}{\gamma'-\left(-p^2+M\sqrt{\vec{q}^{\,2}+m_\pi^2}\right)^{n/2-1}} \\ &= -12i\,A^{(-1)}\frac{g_A^2m_\pi^2}{(4\pi f)^2}\Big[\frac{1}{\epsilon}+\frac{1}{3}-\ln\Big(\frac{m_\pi^2}{\bar{\mu}^2}\Big)\Big] \\ &\quad -4\frac{(p-i\gamma')}{\sqrt{\pi}}\frac{MA^{(-1)}}{4\pi}\frac{g_A^2}{2f^2}\Big(\frac{m_\pi}{M}\Big)^{3/2}I_2\Big(\frac{E}{m_\pi}\Big)\,. \end{aligned} \tag{6.20}$$

Fig. 6.1d is finite for $n = 2$. The $1/\epsilon$ pole in Eq. (6.20) is cancelled by a new tree level counterterm $i\delta^{\rm uv,1d}D_2m_\pi^2$ where $\delta^{\rm uv,1d}D_2$ has the same form as Eq. (6.12) except with a -12 instead of a -3.

Evaluation of Fig. 6.1e is also similar to Fig. 6.1c. For $n = 3-2\epsilon$ we find:

$$e) \;=\; -2\,i\,\frac{(p-i\gamma')^2}{\sqrt{\pi}}\Big[\frac{MA^{(-1)}}{4\pi}\Big]^2\frac{g_A^2}{2f^2}\Big(\frac{m_\pi}{M}\Big)^{3/2}I_2\Big(\frac{E}{m_\pi}\Big)$$

$$
\begin{aligned}
&+i[A^{(-1)}]^2\,\frac{g_A^2 M m_\pi^2}{(4\pi f)^2}\,\frac{\sqrt{M m_\pi}}{2\sqrt{\pi}}\,I_1\left(\frac{E}{m_\pi}\right)\\
&+12\,[A^{(-1)}]^2\,\frac{Mp}{4\pi}\,\frac{g_A^2 m_\pi^2}{(4\pi f)^2}\Big[\frac{1}{\epsilon}+\frac{7}{3}-2\ln 2-\ln\Big(\frac{m_\pi^2}{\overline{\mu}^2}\Big)-\ln\Big(\frac{-p^2}{\overline{\mu}^2}\Big)\Big]\\
&-6\,i\,[A^{(-1)}]^2\,\frac{M\gamma'}{4\pi}\,\frac{g_A^2 m_\pi^2}{(4\pi f)^2}\Big[\frac{1}{\epsilon}+\frac{1}{3}-\ln\Big(\frac{m_\pi^2}{\overline{\mu}^2}\Big)\Big]\,. \qquad (6.21)
\end{aligned}
$$

This graph is finite for $n=2$ except for the I_1 term. A D_2 counterterm cancels the divergence in the last line,

$$
\delta^{\mathrm{uv},1e} D_2 = 6\,(C_0^{\mathrm{finite}})^2\,\frac{M\gamma'}{4\pi}\,\frac{g_A^2}{(4\pi f)^2}\Big[\frac{1}{\epsilon}-\gamma_E+\ln(\pi)\Big]\,. \qquad (6.22)
$$

For two and higher loops the remaining $1/\epsilon$ poles cancel between Eqs. (6.20,6.21,6.22) and $\delta^{\mathrm{uv},1d} D_2$ dressed with C_0 bubbles, so no new counterterms need to be introduced. The $O(\epsilon)$ piece of the bubbles again give a finite contribution. Combining Figs. 6.1c,d,e, and $\delta^{\mathrm{uv},1d} D_2$ and $\delta^{\mathrm{uv},1e} D_2$ dressed with C_0 bubbles gives

$$
\begin{aligned}
c)+d)+e) = 2i\,[A^{(-1)}]^2\frac{g_A^2}{(4\pi f)^2}\Big\{&6 m_\pi^2\,\frac{M(\gamma-\gamma'/2)}{4\pi}\Big[\frac{1}{3}-\ln\Big(\frac{m_\pi^2}{\mu^2}\Big)\Big]\\
&+\frac{M^{3/2} m_\pi^{5/2}}{4\sqrt{\pi}} I_1\Big(\frac{E}{m_\pi}\Big)+\frac{(\gamma-\gamma')^2}{2\sqrt{\pi}}\,\frac{(M m_\pi)^{3/2}}{M}\,I_2\Big(\frac{E}{m_\pi}\Big)\Big\}\,. \qquad (6.23)
\end{aligned}
$$

Fig. 6.1f shows a two loop graph with a nucleon self energy on an internal line. It is important to also include graphs with the one-loop wavefunction and mass renormalization counterterms, $\delta Z, \delta M$ inserted on the internal nucleon line. We will use an on-shell renormalization scheme for defining these counterterms, which ensures that the mass, M, appearing in all expressions is the physical nucleon mass. The counterterms are:

$$
\delta M = \frac{3 g_A^2 m_\pi^3}{16\pi f^2}\,, \qquad \delta Z = \frac{9}{2}\frac{g_A^2 m_\pi^2}{(4\pi f)^2}\left(\frac{1}{\epsilon}+\frac{1}{3}-\ln\left(\frac{m_\pi^2}{\overline{\mu}^2}\right)\right)\,. \qquad (6.24)
$$

The result from the graphs in Fig.6.1f is then

$$
f) = -3i[A^{(-1)}]^2\frac{g_A^2}{(4\pi f)^2}\frac{M^{3/2} m_\pi^{5/2}}{4\sqrt{\pi}} I_1\left(\frac{E}{m_\pi}\right)\,. \qquad (6.25)
$$

When Eq. (6.25) is added to Eqs. (6.14,6.23) the terms proportional to I_1 cancel.

To implement PDS we must consider the value of the graphs in Fig. 6.1f using Minimal Subtraction with $n = 2$. For $n = 2 + \epsilon$ we have $\delta M = 3 g_A^2 m_\pi^2 \mu/(16\pi f^2\, \epsilon)$ and $\delta Z = 0$, which makes the sum of graphs in Fig. 6.1f finite except for the I_1 term. Finally, renormalization of the bare nucleon fields in the Lagrangian, $N^{\rm bare} = \sqrt{Z} N$, $Z = 1 + \delta Z$, induces a four-nucleon term

$$\delta\mathcal{L} = -C_0^{(s),{\rm finite}}\, (2\delta Z)\, (N^T P_i^{(s)} N)^\dagger (N^T P_i^{(s)} N)\,. \qquad (6.26)$$

Since $\delta Z \sim Q_r^4 \sim Q^2$ this term is treated perturbatively. A tree level counterterm

$$\delta^{{\rm uv},0} D_2 = 9\, C_0^{\rm finite} \frac{g_A^2}{(4\pi f)^2} \Big[\frac{1}{\epsilon} - \gamma_E + \ln(\pi)\Big] \qquad (6.27)$$

is introduced to cancel the $1/\epsilon$ pole. Dressing the operator in Eq. (6.26) with C_0 bubbles gives

$$-\,9i\, [A^{(-1)}]^2\, \frac{M\gamma}{4\pi}\, \frac{g_A^2 m_\pi^2}{(4\pi f)^2} \Big[\frac{1}{3} + \ln\Big(\frac{\mu^2}{m_\pi^2}\Big)\Big]\,. \qquad (6.28)$$

Again, for $n = 2$ we have $\delta Z = 0$ so no new PDS counterterms were added. Note that if we had instead used bare nucleon fields then there would be no correction of the form in Eq. (6.26). However, Eq. (6.25) would be modified because the last graph in Fig. 6.1f is no longer present. When this is combined with the contribution from the LSZ formula the sum of Eq. (6.25) and Eq. (6.28) is reproduced.

For PDS, the sum of graphs in Figs.6.1a-f are finite for $n = 2$ so no new finite subtractions were introduced. For $n = 3$, counterterms are introduced to renormalize the terms with $\ln(\mu^2)$ in Eqs. (6.14,6.23,6.28) (in PDS $\mu = \mu_R$). In OS only terms analytic in m_π^2 are subtracted [36] (including $m_\pi^2 \ln(\mu^2)$). We find $D_2(\mu_R) \to D_2(\mu_R) + \Delta D_2(\mu_R)$, with

$$\Delta D_2(\mu_R) = 6\, C_0(\mu_R)^2\, \frac{g_A^2}{(4\pi f)^2}\, \frac{M(\gamma - \gamma')}{4\pi} \Big[-\frac{1}{3} + \kappa + \ln\Big(\frac{\mu_R^2}{\mu_0^2}\Big)\Big]\,. \qquad (6.29)$$

Here $\kappa = 1/3$ in PDS and $\kappa = 0$ in OS, and μ_0 is an unknown scale. Note that the logarithm in Eq. (6.29) gives a contribution to the beta function for $D_2(\mu_R)$ of the form

$$\beta_{D_2}^{(rad)} = \frac{3g_A^2}{4\pi^2 f^2}\,\frac{M(\gamma-\gamma')}{4\pi}\,C_0(\mu_R)^2\,. \tag{6.30}$$

This disagrees with the beta function of Ref. [4], because in that paper the beta function was calculated including only the one-loop graphs.

Adding the contributions in Eqs. (6.14,6.23,6.25,6.28) gives the total radiation pion contribution to the amplitude at order Q_r^3:

$$\begin{aligned} iA^{rad} &= 6i\,[A^{(-1)}]^2\frac{g_A^2 m_\pi^2}{(4\pi f)^2}\,\frac{M(\gamma-\gamma')}{4\pi}\left[\kappa+\ln\left(\frac{{\mu_R}^2}{m_\pi^2}\right)\right] - i\,[A^{(-1)}]^2\,\frac{\Delta D_2(\mu_R)\,m_\pi^2}{C_0(\mu_R)^2} \\ &\quad + i\,[A^{(-1)}]^2\left[\frac{M(\gamma-\gamma')}{4\pi}\right]^2\frac{g_A^2}{\sqrt{\pi}f^2}\left(\frac{m_\pi}{M}\right)^{3/2} I_2\left(\frac{E}{m_\pi}\right)\,. \end{aligned} \tag{6.31}$$

The first term here has the same dependence on the external momentum as an insertion of the D_2 operator dressed by C_0 bubbles. Its μ_R dependence is cancelled by μ_R dependence in $\Delta D_2(\mu_R)$. Note that due to cancellations between graphs, this term is actually suppressed by a factor of γ/Q_r relative to what one expects from the power counting. The second term in Eq. (6.31) has a nontrivial dependence on E and is suppressed by an even smaller factor of γ^2/Q_r^2. These cancellations were not anticipated by the power counting. In the next chapter it will be shown that the dependence of Eq. (6.31) on $(\gamma-\gamma')$ follows from the fact that the nucleon theory obeys Wigner's SU(4) symmetry in limit that $\gamma, \gamma' \to 0$. Therefore terms at order Q_r^4 will likely give the leading contribution of radiation pions to NN scattering.

If we now consider momenta $p \sim m_\pi \sim Q \ll Q_r$, we should fix μ_R at the threshold, $\mu_R = \sqrt{M m_\pi}$, and expand in E/m_π giving $I_2(E/m_\pi) = -3.94 + \mathcal{O}(E/m_\pi)$. Therefore, the dominant effect of the graphs that occur at order Q_r^3 is indistinguishable from a shift in $D_2(\mu_R)$. Integrating out the radiation pions amounts to absorbing their effects into the effective D_2 in the low energy theory. The result in Eq. (6.31) is suppressed relative to the NLO contributions in Ref. [4] by a factor of roughly $2(\gamma-\gamma')/M \sim 1/10$.

Since this is smaller than the expansion parameter, $Q/\Lambda \sim 1/3$, it can be neglected at NNLO.

It is useful to consider more closely how the size of a calculation at $p \sim Q_r$ changes when we take $p \sim m_\pi$. At $p \sim Q_r$ the power counting gave contributions of size

$$\frac{Q_r^3}{M^3(4\pi f)^2}\Big(\frac{p}{Q_r}\Big)^k = \frac{1}{(4\pi f)^2}\Big(\frac{m_\pi}{M}\Big)^{3/2}\Big(\frac{p}{Q_r}\Big)^k , \tag{6.32}$$

where k is an integer. Taking $p \sim m_\pi$ gives $p/Qr = \sqrt{M/m_\pi}$, so terms with $k \leq -1$ will grow in size. It is the external bubble sums which are responsible for the factors of momentum in the denominator since $A^{(-1)} \sim 1/p$. The graphs in Fig. 6.1 have either zero, one, or two external bubble sums. Thus, there can be at most two factors of p in the denominator, and the biggest possible enhancement is by M/m_π. Therefore, the Q_r^3 graphs are expected to have terms of order $m_\pi^{1/2}$, m_π, and $m_\pi^{3/2}$ which agrees with what was found above. However, since the terms in Eqs. (6.14) ,(6.23), and (6.25) that are proportional to I_1 cancel, there is no term in the answer proportional to $m_\pi^{1/2}$. There is no obvious reason why this cancellation had to occur. It is interesting to note that the I_1 terms scale as $1/\sqrt{M}$, which is a higher power of M than the leading order amplitude.

Recall, that in evaluating the graphs in Fig. 6.1 a mulitpole expansion was used, which in this case is an expansion in $v = \sqrt{m_\pi/M}$. If the first correction in the multipole series were to multiple a nonzero term of order $m_\pi^{1/2}$ then this would give an order m_π contribution. However, we have checked that for all the graphs in Fig. 6.1 the first correction in the multipole expansion gives a vanishing contribution. This occurs because these terms involve loop integrals with numerators that are odd in the loop momentum.

At order Q_r^4 graphs such as those in Fig. 6.2 will contribute to NN scattering. The graph in Fig. 6.2a includes an insertion of the operator

$$\mathcal{L} = i\, G_2\, [N^T P_i^{(s)} N]^\dagger\, [N^T P_i^{(s)} \sigma_j (\xi \partial_j \xi^\dagger - \xi^\dagger \partial_j \xi) N] + h.c.\,. \tag{6.33}$$

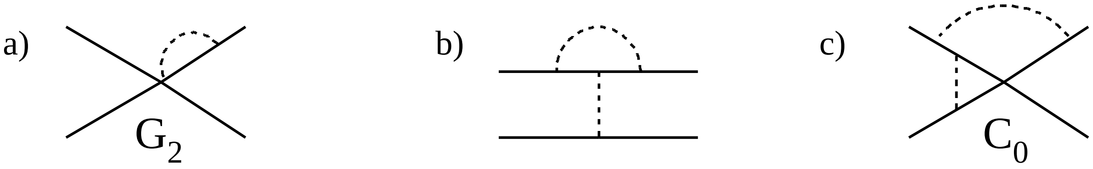

Figure 6.2: Examples of order Q_r^4 radiation pion graphs for NN scattering.

(Note that because of the hermitian conjugate this operator is the same for $s = {}^1S_0$ and $s = {}^3S_1$.) This graph will be dressed with C_0 bubbles inside and outside the radiation pion loop. The renormalization group equation for G_2 gives $G_2(\mu_R) \sim 1/(M\mu_R^2) \sim 1/(MQ_r^2)$. When this is combined with the remaining factors of Q_r, Fig. 6.2a is of order $Q_r^4/(M^4\Lambda_\chi^2)$ and is therefore suppressed by Q_r/M relative to a graph in Fig. 6.1. Power counting the graphs in Fig. 6.2b,c gives $Q_r^4/(M^3\Lambda_{\rm NN}\Lambda_\chi^2)$, yielding a factor of $Q_r/\Lambda_{\rm NN}$ relative to a graph in Fig. 6.1. This provides an example of how graphs with potential pions seem to restrict the range of the effective field theory to $\Lambda_{\rm NN} \sim 300\,{\rm MeV}$. The 300 MeV scale applies only to a subset of graphs and may change once all graphs at this order are included.

A complete NNLO calculation of the NN phase shifts at $p \sim m_\pi$ requires a calculation of terms of order m_π. For graphs with one radiation pion at order Q_r^4, an enhancement by $1/m_\pi$ could give an order m_π contribution. Therefore, it would be interesting to learn if the same cancellation that occurred at order Q_r^3 continues at higher orders. Although terms proportional to $[A^{(-1)}]^3$ will appear at this order, they are factorizable. Therefore, the same cancellation that occured for the order Q_r^3 graphs will occur in these terms.

6.2 Soft pions

In this section soft pion contributions will be discussed. We will see that there are graphs with non-vanishing soft contributions that should be included for $p \gtrsim m_\pi$. In soft loops, two scales appear: m_π and $p = Mv$. It will be shown below that it is necessary to take $p \sim Q_r$ when power counting graphs with soft loops in order to avoid double counting. In other words v should have the same value as in the radiation pion calculation. A soft loop has energy and momentum $q_0 \sim q \sim Q_r$, so $d^4q \sim Q_r^4$. The mass of the soft pion is smaller than its momentum, and is treated perturbatively. Nucleon propagators in a soft loop are static (like in heavy quark effective theory, see Eq. (2.21)) since the loop energy is greater than the nucleon's kinetic energy [171, 172]. Therefore, these propagators count as $1/Q_r$. This power counting is identical to that proposed in Ref. [4] except powers of Q_r are counted rather than Q.

Unlike potential pions, both soft and radiation pion pieces come from taking the pole in a pion propagator. Therefore, care must be taken not to double count when adding these contributions. This is accomplished by taking $p \sim Q_r$ when evaluating both soft and radiation pion graphs. This ensures that the soft and radiation modes have different momenta ($\sim Q_r$ and $\sim m_\pi$ respectively). Integrals involving the scales Q_r and m_π can be separated using the method of asymptotic expansions and dimensional regularization [170, 179, 180, 181, 182, 183]. Consider splitting a loop integral into two regimes by introducing a momentum factorization scale L such that $m_\pi < L < Q_r$. After the pion pole is taken in an energy integral over q_0, the remaining integral is of the form

$$\int d^nq \;=\; \int_0^L d^nq \;(\text{radiation}) + \int_L^\infty d^nq \;(\text{soft})\,, \tag{6.34}$$

which is obviously independent of L. In Eq. (6.34) the power counting dictates that expansions in m_π^2/Q_r^2 should be made so that each integral becomes a sum of integrals involving only one scale (m_π for radiation and Q_r for soft). In dimensional regularization power divergences vanish, while logarithmic divergences show up as $1/\epsilon$ poles. Therefore, after expanding we can take $L \to \infty$ in the radiation integral and $L \to 0$ in the soft integral. Taking the $L \to \infty$ and $L \to 0$ limits may introduce ultraviolet divergences for the radiation integral and infrared divergences for the soft integral. When the radiation and soft contributions are added any superfluous $1/\epsilon$ poles will cancel. This will be illustrated with an explicit example below. The asymptotic ex-

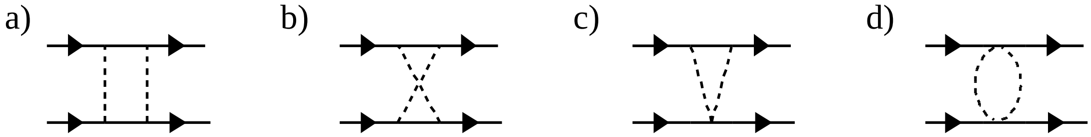

Figure 6.3: Examples of one-loop graphs which have soft pion contributions. Graphs a)-d) also have a radiation pion contribution, while in addition graph a) has a potential pion contribution.

pansion procedure has been rigorously proven for Feynman graphs with large external Euclidean momenta and large masses [184, 185, 186, 187, 188]. It has also been shown to work for the non-relativistic threshold expansion of one and two-loop graphs [170].

Notice that it is crucial to expand the soft pion propagator in powers of m_π^2/Q_r^2, because otherwise the radiation pion contribution may be double counted. As an example, consider the graph in Fig. 6.1a. Taking $p \sim Q_r$ implies $Mv^2 \sim m_\pi$. For the radiation pion contribution $q_0 \sim q \sim Mv^2 \sim m_\pi$, so we keep the m_π^2 in the denominator of Eq. (6.6). When computing the soft contribution, we assume $q_0 \sim q \sim Q_r \gg m_\pi$, and must expand the denominator in powers of m_π^2/Q_r^2. The $\vec{q}$ integration is now scaleless so the soft contribution to Fig. 6.1a vanishes in dimensional regularization. If we did not expand in m_π/Q_r when evaluating the soft contribution, we would have double counted the radiation contribution. The same argument can be applied to all the diagrams in Fig. 6.1. In each case the soft contribution vanishes.

Examples of graphs which have a non-vanishing soft contribution are shown in Fig. 6.3. These diagrams were calculated in Ref. [189] (although the S-wave channels were not analyzed there). In the KSW power counting they must be dressed on the outside with C_0 bubbles. (If Fig. 6.3a or 6.3b are dressed on the inside with C_0 bubbles then the soft contribution vanishes.) To see how these graphs obtain contributions from the soft and radiation regimes consider Fig. 6.3a. Unlike the massless case [170], this graph has a radiation like contribution. In the ${}^1S_0$ channel the loop integral for

Fig. 6.3a is

$$\left(\frac{-ig_A^2}{2f^2}\right)^2 \int \frac{d^dq}{(2\pi)^d} \frac{i}{\frac{E}{2}+q_0-\frac{(\vec{q}+\vec{p})^2}{2M}+i\epsilon} \; \frac{i}{\frac{E}{2}-q_0-\frac{(\vec{q}+\vec{p})^2}{2M}+i\epsilon} \; \frac{\vec{q}^{\,2}}{q_0^2-\vec{q}^{\,2}-m_\pi^2+i\epsilon} \times \frac{(\vec{q}-\vec{t}\,)^2}{q_0^2-(\vec{q}-\vec{t}\,)^2-m_\pi^2+i\epsilon}\,, \tag{6.35}$$

where $\vec{t}=\vec{p}\,'-\vec{p}$ and $\pm\vec{p}$ and $\pm\vec{p}\,'$ are the incoming and outgoing nucleon momenta. Unlike the graphs in Fig. 6.1, we are forced to route an external momentum, $\vec{t}$, through a pion propagator. Taking a nucleon pole in Eq. (6.35) gives the potential pion contribution proportional to Mp. Taking the contribution from the pion poles gives soft and radiation contributions. Our power counting tells us that the leading order soft contribution will be $\sim Q_r^2$, while the leading order radiation contribution will be $\sim Q_r^4/M^2$. In Eq. (6.35) the factors of $E/2-(\vec{q}+\vec{p})^2/(2M)$ can be dropped. In the soft regime the factors of $E/2-(\vec{q}+\vec{p})^2/(2M)$ are order Q_r^2/M, and are dropped relative to $q_0\sim Q_r$ leaving static nucleon propagators. In the radiation regime $E/2-(\vec{q}+\vec{p})^2/(2M)\to 0$ after using the multipole expansion and equations of motion. This leaves

$$\begin{aligned} &\frac{i}{2}\left(\frac{g_A^2}{2f^2}\right)^2 \int \frac{d^nq}{(2\pi)^n} \frac{\vec{q}^{\,2}(\vec{q}-\vec{t}\,)^2}{\vec{q}^{\,2}-(\vec{q}-\vec{t}\,)^2} \left\{ \frac{1}{[\vec{q}^{\,2}+m_\pi^2]^{3/2}} - \frac{1}{[(\vec{q}-\vec{t}\,)^2+m_\pi^2]^{3/2}} \right\} \\ &= \frac{i}{2}\left(\frac{g_A^2}{2f^2}\right)^2 \int \frac{d^nq}{(2\pi)^n} \frac{\vec{q}^{\,2}(\vec{q}-\vec{t}\,)^2}{[\vec{q}^{\,2}+m_\pi^2]^{3/2}} \left\{ \frac{1}{\vec{q}^{\,2}-(\vec{q}-\vec{t}\,)^2+i\epsilon} + \frac{1}{\vec{q}^{\,2}-(\vec{q}-\vec{t}\,)^2-i\epsilon} \right\}, \end{aligned} \tag{6.36}$$

where $n=d-1$. The singularity at $\vec{q}^{\,2}=(\vec{q}-\vec{t}\,)^2$ is cancelled only in the sum of terms in the first line of Eq. (6.36). These terms can be calculated separately by introducing an $i\epsilon$ in this denominator [170], giving an average over $\pm i\epsilon$ as indicated[3]. The factor of $(\vec{q}-\vec{t}\,)^2$ in the numerator can be removed by partial fractioning. For the soft contribution the scale of the loop momentum is set by the external momentum,

---

[3] The second line of Eq. (6.36) is more easily split into soft and radiation contributions. If we had used the integrand on the first line we would also have to consider $(\vec{q}-\vec{t}\,)^{\,2}\sim m_\pi^2$.

$q_0 \sim |\vec{q}| \sim |\vec{t}| \sim Q_r$. Expanding Eq. (6.36) in $m_\pi^2/\vec{q}^{\,2}$ gives

$$
\begin{aligned}
& i\Big(\frac{g_A^2}{2f^2}\Big)^2 \int \frac{d^n q}{(2\pi)^n}\, \frac{|\vec{q}|}{(2\vec{q}\cdot\vec{t}-\vec{t}^{\,2}\pm i\epsilon)} \sum_{m=0}^{\infty} \frac{\Gamma(-1/2)}{\Gamma(-1/2-m)\Gamma(m+1)}\Big(\frac{m_\pi^2}{\vec{q}^{\,2}}\Big)^m \\
&= \frac{-i}{192\pi^2}\Big(\frac{g_A^2}{2f^2}\Big)^2 \bigg\{ \Big[\frac{1}{\epsilon} + \ln\Big(\frac{\bar{\mu}^2}{t^2}\Big)\Big]\Big(t^2 - 18\, m_\pi^2\Big) \\
& -\Big[\frac{1}{\epsilon} + \ln\Big(\frac{\bar{\mu}^2}{t^2}\Big)\Big]\Big(90\,\frac{m_\pi^4}{t^2} - 140\,\frac{m_\pi^6}{t^4} + \ldots\Big) + \frac{8}{3}\,t^2 - 36\, m_\pi^2 + 280\,\frac{m_\pi^6}{t^4} + \ldots \bigg\},
\end{aligned}
\tag{6.37}
$$

where we have kept the first few terms in the expansion. The soft contribution starts at order Q_r^2 as expected. The first $1/\epsilon$ pole in Eq. (6.37) is an ultraviolet divergence, while the second is an infrared divergence. For the radiation contribution $q_0 \sim |\vec{q}| \sim m_\pi \ll |\vec{t}|$. Expanding in $(2\vec{t}\cdot\vec{q})/\vec{t}^{\,2}$ gives

$$
\begin{aligned}
& -i\Big(\frac{g_A^2}{2f^2}\Big)^2 \int \frac{d^n q}{(2\pi)^n}\, \frac{1}{[\vec{q}^{\,2}+m_\pi^2]^{3/2}} \bigg[\, \vec{q}^{\,2} + \frac{\vec{q}^{\,4}}{\vec{t}^{\,2}} \sum_{m=0}^{\infty} \Big(\frac{2\vec{q}\cdot\vec{t}}{\vec{t}^{\,2}\pm i\epsilon}\Big)^m \,\bigg] \\
&= \frac{-i}{192\pi^2}\Big(\frac{g_A^2}{2f^2}\Big)^2 \bigg\{ -72\, m_\pi^2 \Big[\frac{1}{\epsilon} + \ln\Big(\frac{\bar{\mu}^2}{m_\pi^2}\Big)\Big] \\
& +\Big[\frac{1}{\epsilon} + \ln\Big(\frac{\bar{\mu}^2}{m_\pi^2}\Big)\Big]\Big(90\,\frac{m_\pi^4}{t^2} - 140\,\frac{m_\pi^6}{t^4} + \ldots\Big) - 24\, m_\pi^2 + 39\,\frac{m_\pi^4}{t^2} - \frac{482}{3}\,\frac{m_\pi^6}{t^4} + \ldots \bigg\}.
\end{aligned}
\tag{6.38}
$$

The radiation contribution starts out as order Q_r^4/M^2 as expected. Note that only powers of $m_\pi = Q_r^2/M$ appear. The $1/\epsilon$ poles in Eq. (6.38) are ultraviolet divergences. When the soft and radiation contributions are added the infrared poles in Eq. (6.37) cancel a subset of the ultraviolet poles in Eq. (6.38). Adding Eq. (6.37) and Eq. (6.38) we find

$$
\begin{aligned}
& \frac{-i}{192\pi^2}\Big(\frac{g_A^2}{2f^2}\Big)^2 \bigg\{ t^2\Big[\frac{1}{\epsilon} + \ln\Big(\frac{\bar{\mu}^2}{t^2}\Big)\Big] + \frac{8}{3}\,t^2 - m_\pi^2\Big[\frac{90}{\epsilon} + 18\ln\Big(\frac{\bar{\mu}^2}{t^2}\Big) + 72\ln\Big(\frac{\bar{\mu}^2}{{m_\pi}^2}\Big)\Big] \\
& -60\, m_\pi^2 + \ln\Big(\frac{t^2}{m_\pi^2}\Big)\Big(90\,\frac{m_\pi^4}{t^2} - 140\,\frac{m_\pi^6}{t^4} + \ldots\Big) + 39\,\frac{m_\pi^4}{t^2} + \frac{358}{3}\,\frac{m_\pi^6}{t^4} + \ldots \bigg\},
\end{aligned}
\tag{6.39}
$$

where the remaining ultraviolet $1/\epsilon$ poles are cancelled by counterterms for C_2 and D_2.

If we are interested in making predictions for $p \sim m_\pi$, then powers of m_π^2/t^2 must be summed up. Summing the series in Eq. (6.39) gives

$$3a) = \frac{-i}{192\pi^2}\Big(\frac{g_A^2}{2f^2}\Big)^2\bigg\{\Big(t^2 - 90\, m_\pi^2\Big)\Big[\frac{1}{\epsilon} + \ln\Big(\frac{\bar{\mu}^2}{m_\pi{}^2}\Big)\Big] + \frac{8}{3}\,t^2 - 58 m_\pi^2 \\ - \frac{(128 m_\pi^4 + 16 m_\pi^2 t^2 - t^4)}{t\sqrt{t^2+4m_\pi^2}}\ln\Big(\frac{\sqrt{t^2+4m_\pi^2}-t}{\sqrt{t^2+4m_\pi^2}+t}\Big)\bigg\}. \qquad (6.40)$$

Since the coefficients in the series in Eqs. (6.37,6.38) diverge for $\vec{p}\,' = \vec{p}$, Eq. (6.40) should be used when integrating over dt to obtain the ${}^1S_0$ partial wave amplitude (even for $p \sim Q_r$). Eq. (6.40) agrees with the result of evaluating Eq. (6.36) exactly. Although the asymptotic expansion is not necessary for evaluating Fig. 6.3a, it allows us to identify the radiation and soft contributions to this graph and verify that the power counting for each regime works. We also see that adding soft and radiation pions reproduces the correct answer without double counting. Recall that power counting with $p \sim Q_r$ was necessary to avoid double counting for graphs like those in Fig. 6.1.

For $p \sim Q_r$ the diagrams in Fig. 6.3 are order $Q_r^2/(f^2\Lambda_\chi^2)$, and are larger than the order Q_r^3 graphs with a single radiation pion in Fig. 6.1. Decreasing p to $p \sim m_\pi$ the graphs in Fig. 6.3 give contributions of the form

$$\frac{\vec{t}^{\,2}}{f^2\,(4\pi f)^2}\; F\Big(\vec{t}^{\,2}/m_\pi^2\Big)\,, \qquad (6.41)$$

where F is a function. For $p \sim m_\pi$ the graphs in Fig. 6.3 are order m_π^2 which is smaller than the graphs in Fig. 6.1 which include order $m_\pi^{1/2}$, m_π, and $m_\pi^{3/2}$ terms. It is interesting to note that the relative importance of these graphs changes with p. The graphs in Fig. 6.3 dressed by C_0 bubbles give a contribution that is the same size as a four nucleon operator with 6 derivatives, $C_6(\mu_R)p^6$, and are N^{3}LO in the KSW power counting. Note that dressing these graphs with C_0 bubbles does not result in enhanced terms for $p \sim m_\pi$, unlike the graphs in the previous section.

It would be nice to see the expansion used in evaluating the radiation contribution to Fig. 6.3a implemented at the level of the Lagrangian. It is not clear to us how to do this at the present time. In the radiation regime, the pion whose pole is taken can be thought of as a radiation pion. However, the other propagator gives factors of $1/t^2$, $\vec{q}\cdot\vec{t}/t^4$, etc., which look more like insertions of non-local operators than the propagator of a field. Also, since in general $\vec{p} \neq \vec{p}\,'$, the couplings for this second propagator change the nucleon momenta and therefore do not involve a multipole expansion. Finally, the result in Eq. (6.40) does not have an expansion in E/m_π. So unlike the radiation pion contribution computed in section A, this contribution cannot be integrated out for $p < \sqrt{Mm_\pi}$. For these reasons, the use of the term radiation for this contribution differs somewhat from the usage in section A.

To summarize, a power counting in factors of $Q_r = \sqrt{Mm_\pi}$ has been introduced which is appropriate for graphs with radiation pions. The order Q_r^3 radiation contributions to NN scattering were computed and found to be suppressed by inverse powers of the scattering length. Soft pion contributions also have a power counting in Q_r. For $p \sim Q_r$ they are $\sim Q_r^2$, but are higher order than the radiation contributions for $p \sim m_\pi$. Higher order corrections are suppressed by factors of Q_r/Λ, and whether or not this expansion is convergent is an open question. If the range of the two-nucleon effective field theory with perturbative pions is really 300 MeV, then contributions from radiation pions induce an incalculable error of order m_π^2/Λ_χ^2 to the NN scattering amplitude in this theory. The validity of the Q_r/Λ expansion can be tested by examining processes at $p \sim 300\,\text{MeV}$ such as those with external pions.

Chapter 7 Wigner's SU(4) Symmetry from Effective Field Theory

In this chapter it is shown that in the limit where the NN ${}^1S_0$ and ${}^3S_1$ scattering lengths, $a^{({}^1S_0)}$ and $a^{({}^3S_1)}$, go to infinity, the leading terms in the effective field theory for strong NN interactions are invariant under Wigner's SU(4) spin-isospin symmetry. This explains why the leading effects of radiation pions on the S-wave NN scattering amplitudes, calculated in the chapter 6, vanish as $a^{({}^1S_0)}$ and $a^{({}^3S_1)}$ go to infinity. The implications of Wigner symmetry for $NN \to NN$ axion and $\gamma\, d \to n\, p$ are also considered.

Wigner's SU(4) spin-isospin transformations are [190, 191]

$$\delta N = i\alpha_{\mu\nu}\, \sigma^\mu\, \tau^\nu\, N\,, \qquad N = \begin{pmatrix} p \\ n \end{pmatrix}. \tag{7.1}$$

In Eq. (7.1), $\sigma^\mu = (1, \vec{\sigma})$, $\tau^\nu = (1, \vec{\tau})$, and $\alpha_{\mu\nu}$ are infinitesimal group parameters (the notation here is that greek indices run over $\{0, 1, 2, 3\}$, while roman indices run over $\{1, 2, 3\}$). The σ matrices act on the spin degrees of freedom, and the τ matrices act on the isospin degrees of freedom. (Actually the transformations in Eq. (7.1) correspond to the group SU(4)×U(1). The additional U(1) is baryon number and corresponds to the α_{00} term.)

Consider first the effective field theory for nucleon strong interactions with the pion degrees of freedom integrated out. The Lagrange density is composed of nucleon fields and has the form $\mathcal{L} = \mathcal{L}_1 + \mathcal{L}_2 + \ldots$, where $\mathcal{L}_n$ denotes the n-body terms. We have

$$\mathcal{L}_1 \;=\; N^\dagger \Big[i\partial_t + \overrightarrow{\nabla}^2/(2M) \Big] N + \ldots\,,$$

$$
\begin{aligned}
\mathcal{L}_2 &= -\sum_s C_0^{(s)} (N^T P_i^{(s)} N)^\dagger (N^T P_i^{(s)} N) + \dots \,, \\
\mathcal{L}_3 &= -\frac{D_0}{6} (N^\dagger N)^3 + \dots \,, \\
\mathcal{L}_4 &= E_0 \, (N^\dagger N)^4 + \dots \,,
\end{aligned}
\tag{7.2}
$$

where the ellipses denote higher derivative terms and $P_i^{(s)}$ was defined in Eq. (2.31) for $s = {}^1S_0, {}^3S_1$. Without derivatives, higher body contact interactions vanish because of Fermi statistics. Fermi statistics also implies that there is only one four body term, which is invariant under Wigner symmetry. Furthermore, there is only one term in $\mathcal{L}_3$ which is also invariant[1]. To count operators it is useful to classify them by their transformation properties under SU(4). The three nucleon and anti-nucleon fields must be combined in an antisymmetric way, so the three N's ($N^\dagger$'s) combine to a $\bar{4}$ (4) of SU(4). Combining the 4 and $\bar{4}$ gives $1 \oplus 15$. However, the 15 does not contain a singlet under the spin and isospin SU(2) subgroups so there is only one three body operator with no derivatives. A group theory argument can also be used to show that there are only two two-body operators. Combining two N's in an antisymmetric manner gives a $\bar{6}$, while combining two $N^\dagger$'s gives a 6. Then $6 \times \bar{6} = 1 \oplus 15 \oplus 20$, and only the 1 and 20 contain singlets under the spin and isospin subgroups. The Lagrange density $\mathcal{L}_2$ can also be written in a different operator basis:

$$
\mathcal{L}_2 = -\frac{1}{2}\Big[C_0^S (N^\dagger N)^2 + C_0^T (N^\dagger \vec{\sigma} N)^2 \Big] + \dots \,, \tag{7.3}
$$

where $C_0^{({}^1S_0)} = C_0^S - 3C_0^T$ and $C_0^{({}^3S_1)} = C_0^S + C_0^T$. In this basis it is the C_0^T term that breaks the SU(4) symmetry (as well as some of the higher derivative terms). The Lagrangian in Eq. 7.2 will be SU(4) symmetric at leading order if $C_0^T = 0$ in the two-body sector and if higher derivative operators are suppressed in the three and four body sectors.

In the $\overline{\text{MS}}$ scheme, neglecting two derivative operators the NN scattering amplitude is

---

[1] P.F. Bedaque, H.W. Hammer, and U. van Kolck, private communication and Ref. [192].

$$\mathcal{A}^{(s)} = \frac{-\bar{C_0}^{(s)}}{1 + i\frac{Mp}{4\pi}\,\bar{C_0}^{(s)}}\,, \tag{7.4}$$

where

$$\bar{C_0}^{(s)} = \frac{4\pi a^{(s)}}{M}\,, \tag{7.5}$$

as was discussed section 2.3.2. The scattering lengths are very large: $a^{({}^1S_0)} = -23.714 \pm 0.013\,\mathrm{fm}$ and $a^{({}^3S_1)} = 5.425 \pm 0.001\,\mathrm{fm}$ [63], and even have the opposite sign. Therefore, the value of $\bar{C_0}^{({}^1S_0)}$ and $\bar{C_0}^{({}^3S_1)}$ are very different. In this scheme the Lagrangian in Eq. (7.3) does not have Wigner symmetry. Nonetheless, for $p \gg 1/a^{(s)}$ the amplitudes become, $\mathcal{A}^{(s)} = 4\pi i/(Mp)$. The equality of the ${}^1S_0$ and ${}^3S_1$ amplitudes is consistent with expectations based on Wigner symmetry. The p-dependence is consistent with expectations based on scale invariance[2], since the cross section $\sigma^{(s)} = 4\pi/p^2$.

Recall from section 2.3.2 that in the $\overline{\mathrm{MS}}$ scheme each term in the bubble sum in Fig. 2.1 gives a factor of $a\,p$, so for $p > 1/a$ the series diverges. For these momenta minimal subtraction is not natural from a power counting perspective. In natural schemes like PDS and OS, each term in the bubble sum is of the same order as the sum. It is in these "natural" schemes that the fixed point structure of the theory and Wigner spin-isospin symmetry are manifest in the Lagrangian. In PDS or OS the coefficients depend on the renormalization point μ_R and for $a^{(s)} \to \infty$ we have

$$C_0^{(s)}(\mu_R) = -\frac{4\pi}{M}\frac{1}{\mu_R - 1/a^{(s)}} \;\to\; -\frac{4\pi}{M\mu_R}\,, \tag{7.6}$$

which is the same in both channels. In this limit

$$C_0^T(\mu_R) = [C_0^{({}^3S_1)}(\mu_R) - C_0^{({}^1S_0)}(\mu_R)]/4 = 0\,, \tag{7.7}$$

---

[2] The scale transformations appropriate for the non-relativistic theory are $x \to \lambda x$, $t \to \lambda^2 t$, and $N \to \lambda^{-3/2} N$.

and

$$\mathcal{L}_2 = -\frac{2\pi}{M\mu_R}(N^\dagger N)^2 + \dots . \tag{7.8}$$

The first term in Eq. (7.8) is invariant under the Wigner spin-isospin transformations in Eq. (7.1). The ellipses in Eq. (7.8) denote terms with derivatives which will not be invariant under Wigner symmetry even in the limit $a^{(s)} \to \infty$. However, these terms are corrections to the leading order Lagrange density and their effects are suppressed by powers of p/Λ (where Λ is a scale determined by the pion mass and $\Lambda_{\rm QCD}$). In the region $1/a^{(s)} \ll p \ll \Lambda$ Wigner spin-isospin symmetry is a useful approximation and deviations from this symmetry are suppressed by

$$C_0^T(\mu_R) \propto (1/a^{(^1S_0)} - 1/a^{(^3S_1)})\,, \tag{7.9}$$

and by powers of p/Λ. The measured effective ranges are $r_0^{(^1S_0)} = 2.73 \pm 0.03\,{\rm fm}$ and $r_0^{(^3S_1)} = 1.749 \pm 0.008\,{\rm fm}$ [63]. A rough estimate of the scale is $1/\Lambda \sim [r_0^{(^1S_0)} - r_0^{(^3S_1)}]/2 = 0.49\,{\rm fm}$, or $\Lambda \sim 400\,{\rm MeV}$. In PDS or OS, the limit $a^{(s)} \to \infty$ is clearly a fixed point of $C_0^{(s)}(\mu_R)$ since $\mu_R\,\partial/\partial\mu_R\,[\mu_R\,C_0^{(s)}(\mu_R)] = 0$. Also, scale invariance is manifest since $\mu_R \to \mu_R/\lambda$ under scale transformations.

In the KSW power counting potential pion exchange is order Q^0 and is treated perturbatively. Thus, pion exchange is higher order than the iterated C_0 bubbles and the theory still has Wigner symmetry at leading order.

Wigner symmetry is useful in the two-body sector even though $a^{(^1S_0)}$ and $a^{(^3S_1)}$ are very different. This is because for $1/a^{(s)} \ll p \ll \Lambda$ corrections to the symmetry limit go as $(1/a^{(^1S_0)} - 1/a^{(^3S_1)})$ rather than $(a^{(^1S_0)} - a^{(^3S_1)})$. This is similar to the heavy quark spin-flavor symmetry of QCD [20, 21], which occurs in the $m_Q \to \infty$ limit. Heavy quark symmetry is a useful approximation for charm and bottom quarks even though $m_b/m_c \simeq 3$.

As an application of the symmetry consider $NN \to NN$ axion, which is relevant for astrophysical bounds on the axion coupling [193]. The axion is essentially massless.

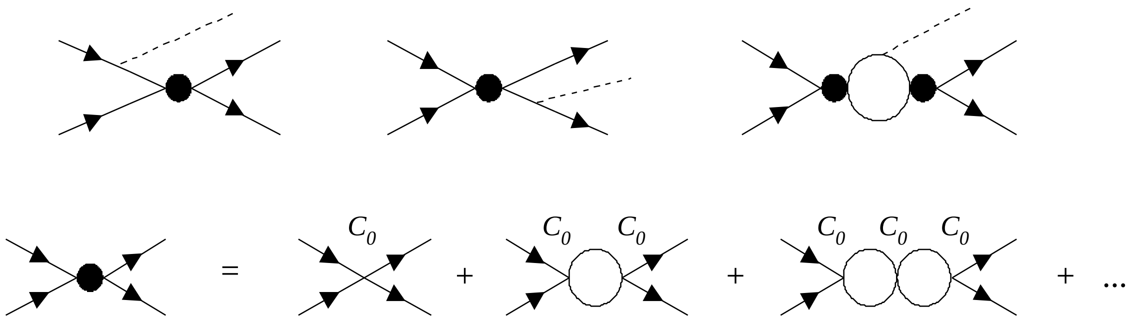

Figure 7.1: Graphs contributing to $NN \to NN\,$axion at leading order. The solid lines denote nucleons and the dashed lines are axions.

If the axion has momentum $\vec{k}$, and the initial nucleons have momenta $\vec{p}$ and $-\vec{p}$ then the final state nucleons have momenta $\vec{q} - \vec{k}/2$ and $-\vec{q} - \vec{k}/2$. Energy conservation implies that $p^2/M = q^2/M + k^2/(4M) + k$ where $p = |\vec{p}|, q = |\vec{q}|$, and $k = |\vec{k}|$. In the kinematic region we consider $q, p \gg k$, and the axion momentum can be neglected in comparison with the nucleon momenta. Again, this is just a multipole expansion (see chapter 6). In this limit the terms in the Lagrange density which couple the axion to nucleons take the form

$$\mathcal{L}_{int} \;=\; g_0\Big(\nabla^j X^0\Big)\Big|_{\vec{x}=0} N^\dagger \sigma^j N + g_1 \Big(\nabla^j X^0\Big)\Big|_{\vec{x}=0} N^\dagger \sigma^j \, \tau^3 N \,, \tag{7.10}$$

where X^0 is the axion field and g_0, g_1 are the axion-nucleon isosinglet and isovector coupling constants. Associated with spin-isospin symmetry are the conserved charges

$$Q^{\mu\nu} = \int d^3x N^\dagger \sigma^\mu \tau^\nu N \,, \tag{7.11}$$

and the axion terms in the action are proportional to these charges

$$S_{int} \;=\; g_0 \int dt \Big(\nabla^j X^0\Big)\Big|_{\vec{x}=0} Q^{j0} + g_1 \int dt \Big(\nabla^j X^0\Big)\Big|_{\vec{x}=0} Q^{j3} \,. \tag{7.12}$$

The charge Q^{j0} is the total spin of the nucleons which is conserved even without taking the $a^{(s)} \to \infty$ limit, however Q^{j3} is only conserved in the $a^{(s)} \to \infty$ limit (and also in the limit $a^{({}^1S_0)} \to a^{({}^3S_1)}$). Since conserved charges are time independent, only a zero energy axion couples in Eq. (7.12), and these terms will not contribute to the scattering amplitude. We conclude that $NN({}^1S_0) \to NN({}^3S_1)X^0$ vanishes in the limit $a^{(s)} \to \infty$ and that $NN({}^3S_1) \to NN({}^3S_1)X^0$ vanishes for all scattering lengths[3]. Calculation of the Feynman diagrams in Fig. 7.1 shows that the leading order ${}^3S_1 \to {}^3S_1$ scattering amplitude does indeed vanish, and the $NN({}^1S_0) \to NN({}^3S_1)X^0$ amplitude is

$$\mathcal{A} \;=\; g_1 \frac{4\pi}{M} \frac{\vec{k}\cdot\vec{\epsilon}^{\,*}}{k} \bigg[\frac{1}{a^{({}^1S_0)}} - \frac{1}{a^{({}^3S_1)}}\bigg] \bigg[\frac{1}{1/a^{({}^1S_0)} + i\,p}\bigg] \bigg[\frac{1}{1/a^{({}^3S_1)} + i\,q}\bigg] , \tag{7.13}$$

where $\vec{\epsilon}$ is the polarization of the final ${}^3S_1$ NN state. This is proportional to $(1/a^{({}^1S_0)} - 1/a^{({}^3S_1)})$ and is consistent with our expectations based on the Wigner symmetry. The fact that the graphs in Fig. 7.1 vanish as $a^{(s)} \to \infty$ lends some support to statements in the literature [194] which claim that one-pion exchange is sufficiently accurate to describe the matrix element for $NN \to NN$ axion (at least for momenta $\gg 1/a$ such as in neutron stars). This process has contributions from different partial waves, and in all but the S-wave a single perturbative pion exchange is the leading order contribution in the KSW power counting. For the ${}^1S_0 \to {}^3S_1$ transition the graphs in Fig. 7.1 are small, so the first sizeable S-wave contribution occurs at NLO (the same order as the other partial waves). It involves one-pion exchange and insertions of $C_2^{(s)}$ dressed by C_0 bubbles. Besides tree level pion exchange these NLO contributions to $NN \to NN$ axion have not been considered in the axion literature. Note that to properly treat the S-wave contribution in neutron stars Pauli blocking effects would have to be incorporated in the calculation of the loop graphs.

Coupling of photons to nucleons occurs by gauging the strong effective field theory and by adding terms involving the field strengths $\vec{E}$ and $\vec{B}$. In the kinematic regime where the photon's momentum is small compared to the nucleons' momentum the part of the action involving the field strengths is

---

[3] $NN({}^1S_0) \to NN({}^1S_0)X^0$ vanishes due to angular momentum conservation since the axion is emitted in a P-wave.

$$S_{int} = \frac{e}{2M} \int dt\, B^j \Big|_{\vec{x}=0} \left(\kappa_0 Q^{j0} + \kappa_1 Q^{j3} \right) + \ldots\, , \tag{7.14}$$

where κ_0 and κ_1 are the isosinglet and isovector nucleon magnetic moments in nuclear magnetons, and the ellipses denote subdominant terms. The term proportional to κ_1 in Eq. (7.14) gives the lowest order contribution to the amplitude for $\gamma d \rightarrow np(^1S_0)$. The form of the coupling above implies that like the axion case, this amplitude is proportional to $(1/a^{(^1S_0)} - 1/a^{(^3S_1)})$.

As our last example, we discuss the corrections to NN scattering due to radiation pions discussed in chapter 6. As pointed out in chapter 6, one should perform a multipole expansion on the coupling of radiation pions to nucleons. The first term in the multipole expansion is:

$$S_{int} = -\frac{g_A}{\sqrt{2} f} \int dt \left(\nabla^i \pi^j \right) \Big|_{\vec{x}=0} Q^{ij}\, , \tag{7.15}$$

where $g_A \simeq 1.25$ is the axial coupling and $f \simeq 131\,\mathrm{MeV}$ is the pion decay constant. Radiation pions also couple to a conserved charge of the Wigner symmetry in the large scattering length limit. (A multipole expansion is not performed on the coupling to potential pions so they do not couple to a conserved charge.) This implies that only a radiation pion with $k^0 = 0$ will couple, which is incompatible with the condition $k^0 \sim \sqrt{k^2 + m_\pi^2}$, so in the symmetry limit radiation pions do not contribute to the scattering matrix element. In Eq. (6.31) we saw by explicit computation that graphs with one radiation pion and any number of $C_0^{(s)}$'s give a contribution that is suppressed by at least one power of $1/a^{(^3S_1)} - 1/a^{(^1S_0)}$. This suppression was the result of cancellations between the Feynman diagrams shown in Fig. 6.1. Wigner symmetry guarantees that the leading contribution of graphs with an arbitrary number of radiation pions are suppressed by inverse powers of the scattering lengths.

It has also been shown that Wigner symmetry is obtained in the large number of colors limit of QCD [195, 196]. The implications of Wigner symmetry in nuclear physics were studied in Ref. [197, 198, 199, 200, 201, 202, 203]. So far the applications in this chapter have been specific to the two-nucleon sector, however Wigner symmetry is observed in some nuclei with many nucleons. Recent progress [204, 205, 177, 178] in the three body sector suggests that the $(N^\dagger N)^3$ contact interaction is not subleading compared with the effects of the first two body term in Eq. (7.8). (This conclusion is not uncontroversial, see Ref. [206].) If the higher body operators with derivatives can be treated as perturbations, then the above discussion shows that approximate Wigner symmetry in nuclear physics is a consequence of the large NN scattering lengths.

Chapter 8 Predictions for the $^3S_1 -^3 D_1$ Mixing Parameter, ϵ_1

This chapter briefly discusses results for the $NN \to NN$ $^3S_1 -^3 D_1$ mixing parameter, ϵ_1, at next-to-leading order (NLO) in the theory with pions. A number of observables have been computed at NLO in the KSW power counting. These include, nucleon-nucleon phase shifts [31, 4, 207, 168, 6], coulomb corrections to proton-proton scattering [208, 209], proton-proton fusion [210, 211], electromagnetic form factors for the deuteron [32, 6], deuteron polarizabilities [160, 6], $np \to d\gamma$ [212, 6, 213], Compton deuteron scattering [162, 214], and parity violating effects [163, 161]. Typically errors of order 30%-40% are found at LO and of order 10% at NLO. As mentioned in chapter 5, this is consistent with an expansion parameter $Q/\Lambda \sim 1/3$. Since the expansion parameter is fairly large, calculations at next-to-next-to-leading order (NNLO) are useful. In the theory without pions, calculations at this order can be carried out in a straightforward manner [6]. With pions, the loop graphs become more difficult, but even two and three loop graphs can be evaluated analytically[1]. To truly test the convergence and range of the theory with pions, the above observables need to be calculated to NNLO. The phase shift in the $^1S_0$ channel has been calculated at this order [168] (and independently in Ref. [164]), while work in the $^3S_1$, $^3D_1 -^3 S_1$, and $^3D_1$ channels is near completion [215]. In this chapter a presentation of the prediction for ϵ_1 at order Q is given[2].

At order $1/Q$ there is no contribution to ϵ_1, which is consistent with the fact that this angle is much smaller than the $^3S_1$ phase shift. At order Q^0 the graphs for ϵ_1 include single potential pion exchange and pion exchange dressed on one side by $C_0^{(^3S_1)}$ bubbles as shown in Fig. 8.1 [4]. This prediction does not involve any free

---

[1] The basic reason that loops in three dimensions are simpler, is that the integrals can be done in position space where the Bessel functions reduce to exponentials.

[2] The material in this chapter appears in Ref. [216] with a more detailed discussion

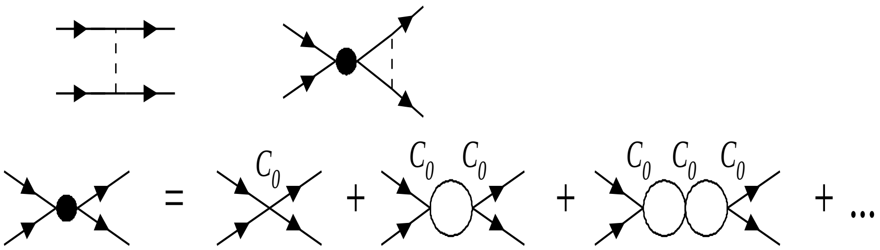

Figure 8.1: The two order Q^0 diagrams that contribute to ϵ_1 [4]. The solid lines are nucleons and the dashed lines are potential pions.

parameters. The order Q calculation includes a two derivative operator which causes transitions from ${}^3S_1$ to ${}^3D_1$ with coefficient $C_2^{(SD)}$. This operator is normalized so that on-shell in the center of mass frame the Feynman rule is

$$ {}^3S_1 \overset{C_2^{(SD)}}{\times} {}^3D_1 \quad = \quad -i\, C_2^{(SD)}\, p^2 \,, \tag{8.1} $$

where p is the center of mass momentum. In this section the PDS renormalization scheme will be used. It was shown in chapter 5, that in the PDS scheme $C_2^{(SD)}(\mu_R) \sim 1/\mu_R$, so this operator enters at order Q. The Feynman diagrams that can contribute to ϵ_1 at order Q include:

$$ \begin{array}{rl} i) & \text{one } C_2^{(SD)} \text{ and any number of } C_0^{({}^3S_1)}\text{'s} \\ ii) & \text{one } C_2^{({}^3S_1)}, \text{ one potential pion and any number of } C_0^{({}^3S_1)}\text{'s} \\ iii) & \text{one } D_2^{({}^3S_1)}, \text{ one potential pion and any number of } C_0^{({}^3S_1)}\text{'s} \\ iv) & \text{two potential pions and any number of } C_0^{({}^3S_1)}\text{'s} \\ v) & \text{radiation pion corrections}\,. \end{array} \tag{8.2} $$

The graphs for i) through iv) are shown in Fig. 8.2. It can be shown that there are no radiation pion contributions to the mixing parameter at this order.

The value of $C_2^{({}^3S_1)}$, $D_2^{({}^3S_1)}$, $C_0^{({}^3S_1)}$ and $C_0^{p\,({}^3S_1)}$ are fixed from the ${}^3S_1$ phase shift calculation at order Q^0. The only free parameter is $C_2^{(SD)}(\mu_R)$, which is varied to give

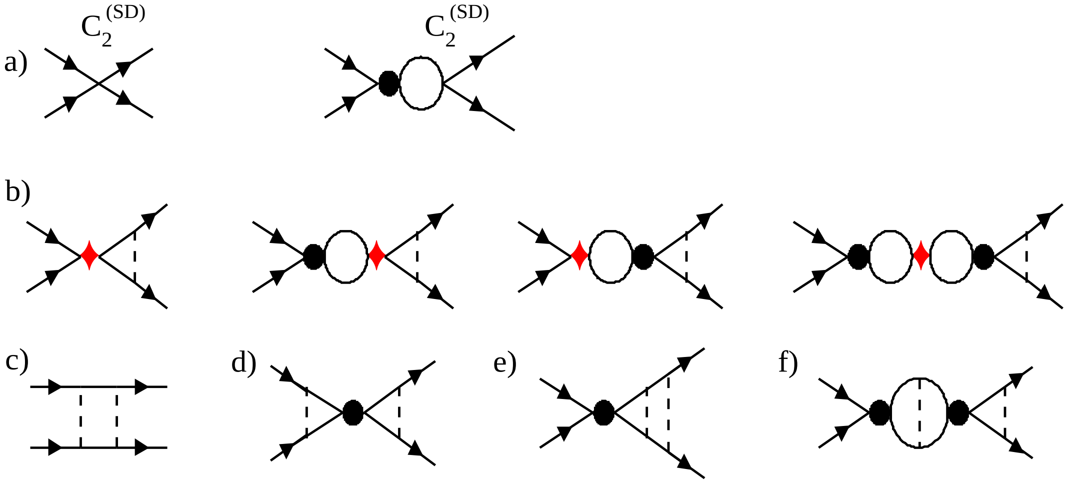

Figure 8.2: Order Q diagrams for ϵ_1. The filled circle is defined in Fig. 8.1, and the diamonds in c) denote insertions of the ${}^3S_1$ operators with $C_0^{(0)}$, C_2 or D_2 coefficients.

a reasonable fit. The result of the ϵ_1 calculation at order Q in the theory with pions is given by the dot-dashed line in Fig. 8.3. The order Q^0 result in the theory with pions [4] is shown by the dotted line. The stars in Fig. 8.3 are data from Virginia Tech [7]. The open circles are the Nijmegen single energy fit to the data [5] whose quoted errors are invisible on the scale shown. The solid line is the Nijmegen multi-energy partial wave analysis [5]. The value of $C_2^{(SD)}(\mu_R)$ corresponding to the fit in Fig. 8.3 is not given since we have not specified what constants are subtracted along with a p^2/ϵ pole that appears in one of the graphs with two potential pions.

For comparison results have been shown for the theory without pions [6]. The long dashed line is the LO result and involves a one parameter fit. The smaller dashed line is the NLO result and involves fitting two free parameters. With fewer free parameters, the theory with pions does better than the theory without pions for $p > 60\,\text{MeV}$. In fact the theory without pions breaks down around $m_\pi/2$, which is where we expect it to since this is where the pion cut begins (see chapter 5). It has been noted in the literature [217] that many observables do not test the power counting for perturbative pions. As can be seen from Fig. 8.3, the mixing parameter provides an example in which perturbative pions clearly give improved agreement with the data.

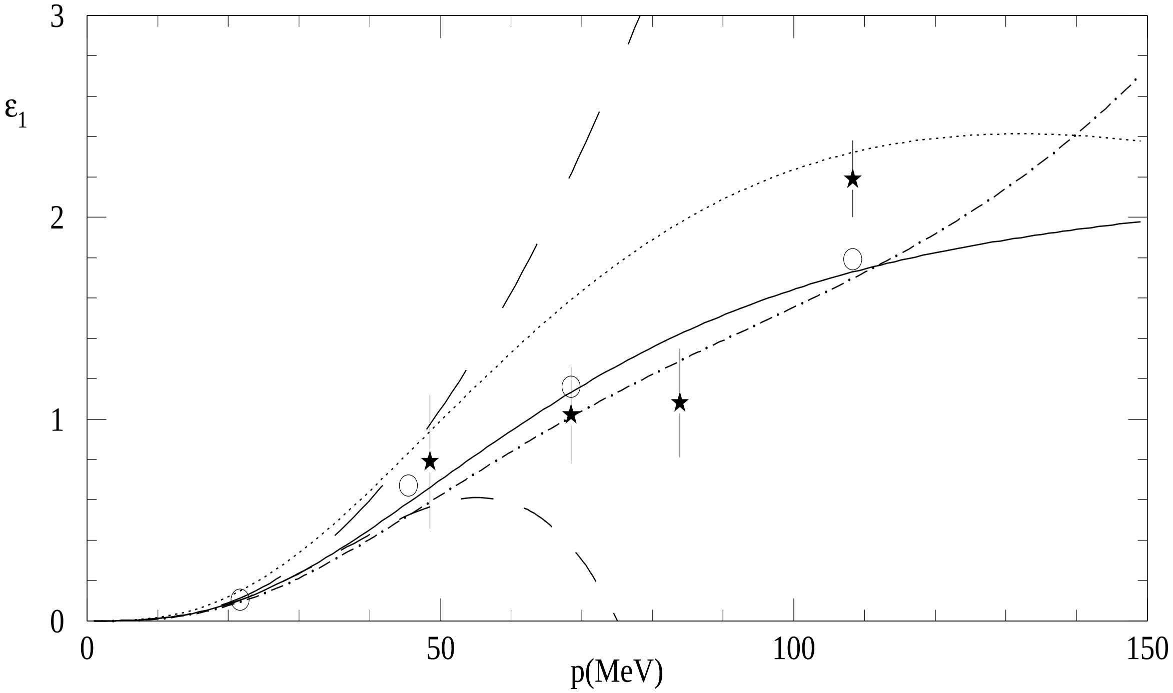

Figure 8.3: Predictions for the ${}^3S_1 - {}^3D_1$ mixing parameter ϵ_1 in degrees. The solid line is the multi-energy Nijmegen partial wave analysis [5]. The long and short dashed lines are the LO and NLO predictions in the theory without pions [6]. The dotted line is the LO prediction in the theory with pions from Ref. [4]. The dash-dotted line is the NLO prediction in the theory with pions. The stars are data from Virginia Tech [7] and the open circles are Nijmegen single energy data [5] whose quoted errors are invisible on the scale shown.

The dot-dashed line in Fig. 8.3 improves over the order Q^0 result for $p < 140\,\mathrm{MeV}$. For larger values of p, the order Q prediction grows, while the Nijmegen partial wave analysis has $\epsilon_1(p) \leq 3^\circ$ for $p \leq 300\,\mathrm{MeV}$. In Ref. [148] the mixing angle was calculated using Weinberg's power counting and solving with a potential. In this approach graphs with potential pions are summed up. A direct comparison with this calculation is difficult since graphs with Δ's were included, and more parameters were varied in the fit. When the potential method is used there is cutoff dependence in the result which cannot be cancelled by cutoff dependence in the coefficients. This is because contributions that are formally higher order are included in the answer. Since the results are numerical these can not be thrown away. For a cutoff of order m_ρ, the prediction in Ref. [148] also grows with p. In the potential approach the cutoff dependence gives a measure of the uncertainty due to higher order corrections. Varying the cutoff from $0.6\,m_\rho$ to $1.3\,m_\rho$ the prediction varies by $\sim 1.0^\circ$ at $p = 150\,\mathrm{MeV}$. Therefore, at $150\,\mathrm{MeV}$ the theory with perturbative pions seems to be doing no worse than a calculation where the pions are treated non-perturbatively.

Chapter 9 Conclusion

In this thesis effective field theory techniques are used to describe the interaction of heavy particles at low momentum in a model independent way. The focus has been on interactions with pions, described using chiral perturbation theory techniques. Chapter 2 gives an overview of the formalism for describing interactions of one or two heavy particles.

In chapter 3, the decays $D^* \to D\pi$ and $D^* \to D\gamma$ are studied using heavy meson chiral perturbation theory. With the recent measurement of $\mathcal{B}(D^{*+} \to D^+\gamma)$, the D^{*0}, D^{*+}, and D_s^* branching fractions can be used to extract the $D^*D\pi$ and $D^*D\gamma$ couplings g and β. The $D^* \to D\gamma$ decays receive important corrections at order $\sqrt{m_q}$ and, from the heavy quark magnetic moment, at order $1/m_c$. Here all the decay rates are computed to one-loop, to first order in m_q and $1/m_c$, including the effect of heavy meson mass splittings, and the counterterms at order m_q. A fit to the experimental data gives two possible solutions, $g = 0.27\,^{+.04}_{-.02}\,^{+.05}_{-.02}$, $\beta = 0.85^{+.2}_{-.1}\,^{+.3}_{-.1}\,\mathrm{GeV}^{-1}$ or $g = 0.76\,^{+.03}_{-.03}\,^{+.2}_{-.1}$, $\beta = 4.90^{+.3}_{-.3}\,^{+5.0}_{-.7}\,\mathrm{GeV}^{-1}$. The first errors are experimental, while the second are estimates of the uncertainty induced by the counterterms. (The experimental limit $\Gamma_{D^{*+}} < 0.13\,\mathrm{MeV}$ excludes the $g = 0.76$ solution.) Predictions for the D^* and B^* widths are given.

In chapter 4, the prospects for determining $|V_{ub}|$ from exclusive B semileptonic decay are discussed. The double ratio of form factors

$$\frac{f^{(B\to\rho)}/f^{(B\to K^*)}}{f^{(D\to\rho)}/f^{(D\to K^*)}} \tag{9.1}$$

is calculated using chiral perturbation theory. Its deviation from unity due to contributions that are non-analytic in the symmetry breaking parameters is very small. It is concluded that combining experimental data obtainable from $B \to \rho\,\ell\,\bar\nu_\ell$, $B \to K^*\ell\,\bar\ell$ and $D \to \rho\,\bar\ell\,\nu_\ell$ can lead to a model independent determination of $|V_{ub}|$ with an uncertainty from theory of about 10%.

In chapter 5, an effective field theory description of nucleon nucleon interactions is investigated. A momentum subtraction scheme (OS) is introduced which obeys the power counting of Kaplan, Savage, and Wise (KSW). The KSW power counting was developed for systems with large scattering lengths, a. Unlike the power divergence subtraction scheme (PDS), coupling constants in this scheme obey the KSW scaling for all $\mu_R > 1/a$. This chapter explains in detail how the renormalization in the OS and PDS schemes is implemented using local counterterms. The main complication is the need to include an infinite number of counterterms since the leading order result includes an infinite number of loop graphs. Fits to the NN scattering data are performed in the ${}^1S_0$ and ${}^3S_1$ channels. An error analysis indicates that the range of the theory with perturbative pions is consistent with 500 MeV, so it can be concluded that there is no obstruction to using perturbative pions for momenta $p > m_\pi$. Some comments are made on the low-energy theorems derived by Cohen and Hansen[3].

In chapter 6, radiative pion interactions are investigated. For interactions involving two or more nucleons it is useful to divide pions into three classes: potential, radiation, and soft. The momentum threshold for the production of radiation pions is $Q_r = \sqrt{M_N m_\pi}$. It is shown that radiation pions can be included systematically with a power counting in Q_r. The leading order radiation pion graphs which contribute to NN scattering are evaluated using the the PDS and OS renormalization schemes and are found to give a small contribution which vanishes as the singlet and triplet scattering lengths go to infinity. The power counting for soft pion contributions is also discussed.

Chapter 7 shows that in the limit where the NN ${}^1S_0$ and ${}^3S_1$ scattering lengths, $a^{({}^1S_0)}$ and $a^{({}^3S_1)}$, go to infinity, the leading terms in the effective field theory for strong NN interactions are invariant under Wigner's SU(4) spin-isospin symmetry. This explains why the leading effects of radiation pions on the S-wave NN scattering amplitudes vanish as $a^{({}^1S_0)}$ and $a^{({}^3S_1)}$ go to infinity. The implications of Wigner symmetry for $NN \to NN$ axion and $\gamma\, d \to n\, p$ are also considered.

Finally, in chapter 8 results for the ${}^3S_1 -{}^3 D_1$ mixing parameter, ϵ_1 are presented.

This observable provides an example where the theory with perturbative pions gives better agreement with the data at $p \sim m_\pi$ with fewer parameters than the theory without pions.

Bibliography

[1] ACCMOR, S. Barlag *et al.*, Phys. Lett. **B278**, 480 (1992),

[2] V. G. J. Stoks, R. A. M. Klomp, C. P. F. Terheggen, and J. J. de Swart, Phys. Rev. **C49**, 2950 (1994), nucl-th/9406039,

[3] T. D. Cohen and J. M. Hansen, Phys. Rev. **C59**, 13 (1999), nucl-th/9808038,

[4] D. B. Kaplan, M. J. Savage, and M. B. Wise, Nucl. Phys. **B534**, 329 (1998), nucl-th/9802075,

[5] V. G. J. Stoks, R. A. M. Kompl, M. C. M. Rentmeester, and J. J. de Swart, Phys. Rev. **C48**, 792 (1993),

[6] J.-W. Chen, G. Rupak, and M. J. Savage, (1999), nucl-th/9902056,

[7] R. A. Arndt and R. L. Workman, Few Body Syst. Suppl. **7**, 64 (1994), Data from: http://said.phys.vt.edu/.

[8] D. R. Yennie, In *Steamboat Springs 1984, Proceedings, Intersections Between Particle and Nuclear Physics*, 468-476.

[9] T. Kinoshita, In *Erice 1981, Proceedings, Quantum Metrology and Fundamental Physical Constants*, 423-441.

[10] M. Martinez, R. Miquel, L. Rolandi, and R. Tenchini, (1998), CERN-EP-98-027.

[11] Y. K. Kim, In *Hamburg 1997, Lepton photon interactions* 493-514.

[12] W. de Boer, Invited Talk at the Topical Conference of the 18th SLAC Summer Inst. on Particle Physics, Stanford, CA, Jul 16-27, 1990.

[13] D0 and CDF, N. A. Graf, In *Stanford 1997, The physics of leptons* 443-461.

[14] J. F. Verdu, In *Formigal 1997, Fundamental physics* 46-64.

[15] H. D. Politzer, Phys. Rev. Lett. **30**, 1346 (1973),

[16] D. J. Gross and F. Wilczek, Phys. Rev. Lett. **30**, 1343 (1973),

[17] K. G. Wilson, Phys. Rev. **179**, 1499 (1969),

[18] G. Buchalla, A. J. Buras, and M. E. Lautenbacher, Rev. Mod. Phys. **68**, 1125 (1996), hep-ph/9512380,

[19] W. E. Caswell and G. P. Lepage, Phys. Lett. **167B**, 437 (1986),

[20] N. Isgur and M. B. Wise, Phys. Lett. **B232**, 113 (1989),

[21] N. Isgur and M. B. Wise, Phys. Lett. **B237**, 527 (1990),

[22] G. T. Bodwin, E. Braaten, and G. P. Lepage, Phys. Rev. **D51**, 1125 (1995), hep-ph/9407339, Erratum-ibid.D55:5853,1997,

[23] M. B. Wise, Phys. Rev. **D45**, 2188 (1992),

[24] G. Burdman and J. F. Donoghue, Phys. Lett. **B280**, 287 (1992),

[25] T.-M. Yan *et al.*, Phys. Rev. **D46**, 1148 (1992),

[26] E. Jenkins and A. V. Manohar, Phys. Lett. **B255**, 558 (1991),

[27] S. Weinberg, Phys. Lett. **B251**, 288 (1990).

[28] S. Weinberg, Nucl. Phys. **B363**, 3 (1991),

[29] U. van Kolck, (1999), nucl-th/9902015,

[30] G. P. Lepage, (1997), nucl-th/9706029,

[31] D. B. Kaplan, M. J. Savage, and M. B. Wise, Phys. Lett. **B424**, 390 (1998), nucl-th/9801034,

[32] D. B. Kaplan, M. J. Savage, and M. B. Wise, Phys. Rev. **C59**, 617 (1999), nucl-th/9804032,

[33] I. W. Stewart, Nucl. Phys. **B529**, 62 (1998), hep-ph/9803227,

[34] Z. Ligeti, I. W. Stewart, and M. B. Wise, Phys. Lett. **B420**, 359 (1998), hep-ph/9711248,

[35] T. Mehen and I. W. Stewart, Phys. Lett. **B445**, 378 (1999), nucl-th/9809071,

[36] T. Mehen and I. W. Stewart, (1998), nucl-th/9809095,

[37] T. Mehen and I. W. Stewart, (1999), nucl-th/9901064,

[38] T. Mehen, I. W. Stewart, and M. B. Wise, (1999), hep-ph/9902370,

[39] P. G. Harris *et al.*, Phys. Rev. Lett. **82**, 904 (1999),

[40] H. Georgi, Phys. Lett. **B240**, 447 (1990),

[41] A. Manohar and M. B. Wise, *Heavy Quark Physics* (in press, 1999).

[42] A. V. Manohar, (1996), hep-ph/9606222,

[43] V. Bernard, N. Kaiser, and U.-G. Meissner, Int. J. Mod. Phys. **E4**, 193 (1995), hep-ph/9501384,

[44] P. Labelle, Phys. Rev. **D58**, 093013 (1998), hep-ph/9608491,

[45] M. Luke and A. V. Manohar, Phys. Rev. **D55**, 4129 (1997), hep-ph/9610534,

[46] M. Luke and M. J. Savage, Phys. Rev. **D57**, 413 (1998), hep-ph/9707313,

[47] H. D. Politzer, Nucl. Phys. **B172**, 349 (1980),

[48] H. Georgi, Nucl. Phys. **B361**, 339 (1991),

[49] C. Arzt, Phys. Lett. **B342**, 189 (1995), hep-ph/9304230,

[50] J. Gasser and H. Leutwyler, Phys. Rept. **87**, 77 (1982),

[51] J. Gasser and H. Leutwyler, Nucl. Phys. **B250**, 465 (1985),

[52] J. Gasser and H. Leutwyler, Nucl. Phys. **B250**, 465 (1985),

[53] S. Weinberg, Physica **96A**, 327 (1979),

[54] J. Collins, *Renormalization* (Cambridge University Press, Cambridge, 1984).

[55] A. Manohar and H. Georgi, Nucl. Phys. **B234**, 189 (1984),

[56] N. Isgur and M. B. Wise, Phys. Rev. Lett. **66**, 1130 (1991),

[57] R. M. Barnett *et al.*, Phys. Rev. **D54**, 1 (1996),

[58] E. Jenkins, A. V. Manohar, and M. B. Wise, Phys. Rev. Lett. **75**, 2272 (1995), hep-ph/9506356,

[59] G. 't Hooft, Nucl. Phys. **B72**, 461 (1974),

[60] U. van Kolck, Nucl. Phys. **A645**, 273 (1999), nucl-th/9808007,

[61] D. B. Kaplan, M. J. Savage, and M. B. Wise, Nucl. Phys. **B478**, 629 (1996), nucl-th/9605002,

[62] J. Blatt and J. Jackson, Phys. Rev. **76**, 18 (1949).

[63] W.E.Burcham, *Elements of Nuclear Physics* (John Wiley and Sons, Inc., New York, 1979).

[64] J. Gegelia, (1998), nucl-th/9802038,

[65] M. C. Birse, J. A. McGovern, and K. G. Richardson, (1998), hep-ph/9807302,

[66] M. J. Savage, K. A. Scaldeferri, and M. B. Wise, (1998), nucl-th/9811029,

[67] C. L. Y. Lee, M. Lu, and M. B. Wise, Phys. Rev. **D46**, 5040 (1992),

[68] H.-Y. Cheng *et al.*, Phys. Rev. **D48**, 3204 (1993), hep-ph/9305340,

[69] G. Kramer and W. F. Palmer, Phys. Lett. **B298**, 437 (1993),

[70] C. L. Y. Lee, Phys. Rev. **D48**, 2121 (1993), hep-ph/9212205,

[71] J. L. Goity and W. Roberts, Phys. Rev. **D51**, 3459 (1995), hep-ph/9406236,

[72] N. Isgur and M. B. Wise, Phys. Rev. **D41**, 151 (1990),

[73] G. Burdman, Z. Ligeti, M. Neubert, and Y. Nir, Phys. Rev. **D49**, 2331 (1994), hep-ph/9309272,

[74] R. Fleischer, Phys. Lett. **B303**, 147 (1993),

[75] R. Casalbuoni *et al.*, Phys. Lett. **B294**, 106 (1992), hep-ph/9209247,

[76] Q. P. Xu, Phys. Lett. **B306**, 363 (1993),

[77] A. F. Falk and B. Grinstein, Nucl. Phys. **B416**, 771 (1994), hep-ph/9306310,

[78] J. L. Goity, Phys. Rev. **D46**, 3929 (1992), hep-ph/9206230,

[79] B. Grinstein, E. Jenkins, A. V. Manohar, M. J. Savage, and M. B. Wise, Nucl. Phys. **B380**, 369 (1992), hep-ph/9204207,

[80] M. Neubert, Phys. Rev. **D46**, 1076 (1992),

[81] B. Grinstein, Phys. Rev. Lett. **71**, 3067 (1993), hep-ph/9308226,

[82] C. G. Boyd and B. Grinstein, Nucl. Phys. **B442**, 205 (1995), hep-ph/9402340,

[83] H. Davoudiasl, Phys. Rev. **D54**, 6830 (1996), hep-ph/9604418,

[84] L. Randall and M. B. Wise, Phys. Lett. **B303**, 135 (1993), hep-ph/9212315,

[85] C.-K. Chow and M. B. Wise, Phys. Rev. **D48**, 5202 (1993), hep-ph/9305229,

[86] C. G. Boyd and B. Grinstein, Nucl. Phys. **B451**, 177 (1995), hep-ph/9502311,

[87] J. L. Rosner and M. B. Wise, Phys. Rev. **D47**, 343 (1993),

[88] L. Randall and E. Sather, Phys. Lett. **B303**, 345 (1993), hep-ph/9211267,

[89] E. Jenkins, Nucl. Phys. **B412**, 181 (1994), hep-ph/9212295,

[90] R. Casalbuoni *et al.*, Phys. Rept. **281**, 145 (1997), hep-ph/9605342,

[91] CLEO, J. Bartelt *et al.*, Phys. Rev. Lett. **80**, 3919 (1998), hep-ex/9711011,

[92] J. L. Rosner, (1988), EFI-88-37-CHICAGO.

[93] L. Angelos and G. P. Lepage, Phys. Rev. **D45**, 3021 (1992),

[94] P. Colangelo, F. D. Fazio, and G. Nardulli, Phys. Lett. **B334**, 175 (1994), hep-ph/9406320,

[95] P. Colangelo, G. Nardulli, and M. Pietroni, Phys. Rev. **D43**, 3002 (1991),

[96] V. M. Belyaev, V. M. Braun, A. Khodjamirian, and R. Ruckl, Phys. Rev. **D51**, 6177 (1995), hep-ph/9410280,

[97] P. Colangelo *et al.*, Phys. Lett. **B339**, 151 (1994), hep-ph/9406295,

[98] T. M. Aliev, D. A. Demir, E. Iltan, and N. K. Pak, Phys. Lett. **B351**, 339 (1995),

[99] J. F. Amundson *et al.*, Phys. Lett. **B296**, 415 (1992), hep-ph/9209241,

[100] P. Cho and H. Georgi, Phys. Lett. **B296**, 408 (1992), hep-ph/9209239, Erratum-ibid.B300:410,1993,

[101] H.-Y. Cheng *et al.*, Phys. Rev. **D49**, 5857 (1994), hep-ph/9312304,

[102] P. Cho and M. B. Wise, Phys. Rev. **D49**, 6228 (1994), hep-ph/9401301,

[103] M. Luke and A. V. Manohar, Phys. Lett. **B286**, 348 (1992), hep-ph/9205228,

[104] H.-Y. Cheng *et al.*, Phys. Rev. **D49**, 2490 (1994), hep-ph/9308283,

[105] E. Jenkins and A. V. Manohar, Talk presented at the Workshop on Effective Field Theories of the Standard Model, Dobogoko, Hungary, Aug 1991.

[106] H.-Y. Cheng *et al.*, Phys. Rev. **D47**, 1030 (1993), hep-ph/9209262,

[107] M. Gremm, A. Kapustin, Z. Ligeti, and M. B. Wise, Phys. Rev. Lett. **77**, 20 (1996), hep-ph/9603314,

[108] M. Gremm and I. Stewart, Phys. Rev. **D55**, 1226 (1997), hep-ph/9609341,

[109] A. F. Falk, Phys. Lett. **B305**, 268 (1993), hep-ph/9302265,

[110] A. F. Falk and T. Mehen, Phys. Rev. **D53**, 231 (1996), hep-ph/9507311,

[111] U. Kilian, J. G. Korner, and D. Pirjol, Phys. Lett. **B288**, 360 (1992),

[112] CLEO, M. Artuso *et al.*, Phys. Rev. Lett. **75**, 785 (1995),

[113] P. Colangelo, F. D. Fazio, and G. Nardulli, Phys. Lett. **B372**, 331 (1996), hep-ph/9506332,

[114] G. Eilam, I. Halperin, and R. R. Mendel, Phys. Lett. **B361**, 137 (1995), hep-ph/9506264,

[115] C. G. Boyd, B. Grinstein, and R. F. Lebed, Phys. Rev. Lett. **74**, 4603 (1995), hep-ph/9412324,

[116] A. X. El-Khadra, A. S. Kronfeld, P. B. Mackenzie, S. M. Ryan, and J. N. Simone, Phys. Rev. **D58**, 014506 (1998), hep-ph/9711426,

[117] JLQCD, S. Aoki *et al.*, (1997), hep-lat/9711041,

[118] C. Bernard, (1997), hep-ph/9709460,

[119] K.-I. Ishikawa, H. Matsufuru, T. Onogi, N. Yamada, and S. Hashimoto, Phys. Rev. **D56**, 7028 (1997), hep-lat/9706008,

[120] C. R. Allton *et al.*, Phys. Lett. **B405**, 133 (1997), hep-lat/9703002,

[121] UKQCD, R. M. Baxter *et al.*, Phys. Rev. **D49**, 1594 (1994), hep-lat/9308020,

[122] C. W. Bernard, J. N. Labrenz, and A. Soni, Phys. Rev. **D49**, 2536 (1994), hep-lat/9306009,

[123] CLEO, J. Bartelt *et al.*, Phys. Rev. Lett. **71**, 4111 (1993),

[124] CLEO, J. P. Alexander *et al.*, Phys. Rev. Lett. **77**, 5000 (1996),

[125] N. Isgur and M. B. Wise, Phys. Rev. **D42**, 2388 (1990),

[126] Z. Ligeti and M. B. Wise, Phys. Rev. **D53**, 4937 (1996), hep-ph/9512225,

[127] Fermilab E791, E. M. Aitala *et al.*, Phys. Rev. Lett. **80**, 1393 (1998), hep-ph/9710216,

[128] Fermilab E791, E. M. Aitala *et al.*, Phys. Lett. **B397**, 325 (1997), hep-ex/9611002,

[129] CDF II Collaboration, T. C. I. Collaboration, (1996), Fermilab-Pub-96/390-E.

[130] H. Davoudiasl and M. B. Wise, Phys. Rev. **D53**, 2523 (1996), hep-ph/9509414,

[131] A. I. Sanda and A. Yamada, Phys. Rev. Lett. **75**, 2807 (1995), hep-ph/9507283,

[132] A. J. Buras and M. Munz, Phys. Rev. **D52**, 186 (1995), hep-ph/9501281,

[133] M. Misiak, Nucl. Phys. **B393**, 23 (1993),

[134] C. S. Lim, T. Morozumi, and A. I. Sanda, Phys. Lett. **B218**, 343 (1989),

[135] N. G. Deshpande, J. Trampetic, and K. Panose, Phys. Lett. **B214**, 467 (1988),

[136] N. G. Deshpande, J. Trampetic, and K. Panose, Phys. Rev. **D39**, 1461 (1989),

[137] P. J. O'Donnell and H. K. K. Tung, Phys. Rev. **D43**, 2067 (1991),

[138] M. Neubert and B. Stech, (1997), hep-ph/9705292,

[139] T. E. Browder, K. Honscheid, and D. Pedrini, (1996), hep-ph/9606354,

[140] N. Isgur, Phys. Rev. **D43**, 810 (1991),

[141] L. Wolfenstein, Phys. Lett. **B291**, 177 (1992),

[142] Z. Ligeti and M. B. Wise, (1999), hep-ph/9905277,

[143] A. F. Falk, Z. Ligeti, and M. B. Wise, Phys. Lett. **B406**, 225 (1997), hep-ph/9705235,

[144] R. D. Dikeman and N. G. Uraltsev, Nucl. Phys. **B509**, 378 (1998), hep-ph/9703437,

[145] J. M. Flynn and C. T. Sachrajda, (1997), hep-lat/9710057,

[146] C. Ordonez and U. van Kolck, Phys. Lett. **B291**, 459 (1992),

[147] C. Ordonez, L. Ray, and U. van Kolck, Phys. Rev. Lett. **72**, 1982 (1994),

[148] C. Ordonez, L. Ray, and U. van Kolck, Phys. Rev. **C53**, 2086 (1996), hep-ph/9511380,

[149] U. van Kolck, Phys. Rev. **C49**, 2932 (1994),

[150] T.-S. Park, K. Kubodera, D.-P. Min, and M. Rho, Nucl. Phys. **A646**, 83 (1999), nucl-th/9807054,

[151] J. V. Steele and R. J. Furnstahl, Nucl. Phys. **A637**, 46 (1998), nucl-th/9802069,

[152] T. D. Cohen and J. M. Hansen, Phys. Lett. **B440**, 233 (1998), nucl-th/9808006,

[153] M. J. Savage, (1998), nucl-th/9804034,

[154] J. Gegelia, (1998), nucl-th/9806028,

[155] J. V. Steele and R. J. Furnstahl, Nucl. Phys. **A645**, 439 (1999), nucl-th/9808022,

[156] M. J. Savage, Phys. Rev. **C55**, 2185 (1997), nucl-th/9611022,

[157] H. Georgi, Phys. Lett. **B298**, 187 (1993), hep-ph/9207278,

[158] H. Georgi, *Weak Interactions and Modern Particle Physics* (Benjamin /Cummings Publishing Company, Inc., Menlo Park, USA, 1984).

[159] D. B. Kaplan, (1998), nucl-th/9901003,

[160] J.-W. Chen, H. W. Griesshammer, M. J. Savage, and R. P. Springer, Nucl. Phys. **A644**, 221 (1998), nucl-th/9806080,

[161] M. J. Savage and R. P. Springer, Nucl. Phys. **A644**, 235 (1998), nucl-th/9807014,

[162] J.-W. Chen, H. W. Griesshammer, M. J. Savage, and R. P. Springer, Nucl. Phys. **A644**, 245 (1998), nucl-th/9809023,

[163] D. B. Kaplan, M. J. Savage, R. P. Springer, and M. B. Wise, Phys. Lett. **B449**, 1 (1999), nucl-th/9807081,

[164] T. Mehen and I. W. Stewart, (1999), nucl-th/9906010,

[165] J. J. de Swart, C. P. F. Terheggen, and V. G. J. Stoks, (1995), nucl-th/9509032,

[166] D. B. Kaplan and J. V. Steele, (1999), nucl-th/9905027,

[167] M. Binger, (1999), nucl-th/9901012,

[168] G. Rupak and N. Shoresh, (1999), nucl-th/9902077,

[169] B. Grinstein and I. Z. Rothstein, Phys. Rev. **D57**, 78 (1998), hep-ph/9703298,

[170] M. Beneke and V. A. Smirnov, Nucl. Phys. **B522**, 321 (1998), hep-ph/9711391,

[171] H. W. Griesshammer, Phys. Rev. **D58**, 094027 (1998), hep-ph/9712467,

[172] H. W. Griesshammer, (1998), hep-ph/9810235,

[173] V. Bernard, N. Kaiser, and U. G. Meissner, Phys. Rev. Lett. **67**, 1515 (1991),

[174] V. Bernard, N. Kaiser, and U. G. Meissner, Nucl. Phys. **B373**, 346 (1992),

[175] V. Bernard, N. Kaiser, A. Schmidt, and U. G. Meissner, Phys. Lett. **B319**, 269 (1993), hep-ph/9309211,

[176] N. Shoresh and G. Rupak, private communication.

[177] P. F. Bedaque, H. W. Hammer, and U. van Kolck, Phys. Rev. Lett. **82**, 463 (1999), nucl-th/9809025,

[178] P. F. Bedaque, H. W. Hammer, and U. van Kolck, Nucl. Phys. **A646**, 444 (1999), nucl-th/9811046,

[179] S. G. Gorishnii, Nucl. Phys. **B319**, 633 (1989),

[180] G. B. Pivovarov and F. V. Tkachev, Int. J. Mod. Phys. **A8**, 2241 (1993), hep-ph/9612287,

[181] V. A. Smirnov, Phys. Lett. **B394**, 205 (1997), hep-th/9608151,

[182] A. Czarnecki and V. A. Smirnov, Phys. Lett. **B394**, 211 (1997), hep-ph/9608407,

[183] V. A. Smirnov and E. R. Rakhmetov, (1998), hep-ph/9812529,

[184] K. Chetyrkin, Teor. Mat. Fiz. **75**, 26 (1998).

[185] K. Chetyrkin, Teor. Mat. Fiz. **76**, 207 (1998).

[186] K. G. Chetyrkin and V. A. Smirnov, Phys. Lett. **144B**, 419 (1984),

[187] V. A. Smirnov, Commun. Math. Phys. **134**, 109 (1990),

[188] V. A. Smirnov, Basel, Switzerland: Birkhaeuser (1991) 380 p. (Progress in physics, 14).

[189] N. Kaiser, R. Brockmann, and W. Weise, Nucl. Phys. **A625**, 758 (1997), nucl-th/9706045,

[190] E. Wigner, Phys. Rev. **51**, 106, 947 (1937).

[191] E. Wigner, Phys. Rev. **56**, 519 (1937).

[192] P. F. Bedaque, H. W. Hammer, and U. van Kolck, (1999), nucl-th/9906032,

[193] G. Raffelt, *Stars as Laboratories for Fundamental Physics* (The University of Chicago Press, Chicago, 1996).

[194] M. S. Turner, H.-S. Kang, and G. Steigman, Phys. Rev. D. **40**, 299 (1989).

[195] D. B. Kaplan and M. J. Savage, Phys. Lett. **B365**, 244 (1996), hep-ph/9509371,

[196] D. B. Kaplan and A. V. Manohar, Phys. Rev. **C56**, 76 (1997), nucl-th/9612021,

[197] J. Parikh, *Group Symmetries in Nuclear Structure* (Plenum press, 1978).

[198] T. Donnelly and G. Walker, Ann. of Phys. **60**, 209 (1970).

[199] J. Walecka, *Theoretical Nuclear Physics and Subnuclear Physics* (Oxford University Press, 1995).

[200] J. E. in, *Isospin in Nuclear Physics* (North Holland Publishing, 1969).

[201] P. Vogel and M. Zirnbauer, Phys. Rev. Lett. **57**, 3148 (1986).

[202] P. Vogel and W. Ormand, Phys. Rev. C **47**, 623 (1993).

[203] Y. Gaponov, N. Shulgina, and D. Vladimirov, Nucl. Phys. A **391**, 93 (1982).

[204] P. F. Bedaque and U. van Kolck, Phys. Lett. **B428**, 221 (1998), nucl-th/9710073,

[205] P. F. Bedaque, H. W. Hammer, and U. van Kolck, Phys. Rev. **C58**, R641 (1998), nucl-th/9802057,

[206] J. Gegelia, (1999), nucl-th/9903030,

[207] E. Epelbaum and U.-G. Meissner, (1999), nucl-th/9903046,

[208] X. Kong and F. Ravndal, (1999), hep-ph/9903523,

[209] X. Kong and F. Ravndal, Phys. Lett. **B450**, 320 (1999), nucl-th/9811076,

[210] X. Kong and F. Ravndal, (1999), nucl-th/9902064,

[211] X. wei Kong and F. Ravndal, (1999), nucl-th/9904066,

[212] M. J. Savage, K. A. Scaldeferri, and M. B. Wise, (1998), nucl-th/9811029,

[213] J.-W. Chen, G. Rupak, and M. J. Savage, (1999), nucl-th/9905002,

[214] J.-W. Chen, (1998), nucl-th/9810021,

[215] S. Fleming, T. Mehen, and I. W. Stewart, (1999), In preparation.

[216] S. Fleming, T. Mehen, and I. W. Stewart, (1999), nucl-th/9906056,

[217] T. D. Cohen and J. M. Hansen, (1999), nucl-th/9901065,